

**GEOLOGY OF THE JACKSONS GAP, ALABAMA, QUADRANGLE AND
STRUCTURAL IMPLICATIONS FOR THE BREVARD FAULT ZONE**

by

Joshua Dorsey Poole

A thesis submitted to the Graduate Faculty of
Auburn University
in partial fulfillment of the
requirements for the Degree of
Master of Science

Auburn, Alabama
May 9, 2015

Brevard Zone, Structural Geology, Fault, Shear, Ductile, Appalachian, Alabama,
Southeast, Tallasse Synform, Jacksons Gap, Eastern Blue Ridge, Inner Piedmont

Copyright © 2015 by Joshua Dorsey Poole

Approved by

Mark G. Steltenpohl, Chair, Professor of Geosciences
Willis E. Hames, Professor of Geosciences
Haibo Zou, Professor of Geosciences
Randy L. Kath, Professor of Geosciences (University of West Georgia)

ABSTRACT

The Brevard fault zone is a major Appalachian structure that marks the boundary between the eastern Blue Ridge (EBR) and the Dadeville Complex (DC) of the Inner Piedmont (IP) terrane in Alabama. Despite over a century of geologic scrutiny, it remains an enigmatic structure with more than forty interpretations having been suggested. The southernmost exposures of the zone in Alabama contain several poorly understood features that are unique to the zone of deformation, requiring detailed 1:24,000-scale geologic mapping to clarify their significance. In the study area, the Brevard zone is lithologically defined by the Jacksons Gap Group (JGG), a distinctive group with uncertain affinities. Apparent repetition of strata within portions of the JGG implies contractional duplexing, folding, primary sedimentary repetitions, or a combination of these. The Brevard zone is folded by the late-stage Tallassee synform, providing an unusual structural setting to investigate its geometry. The JGG is fault bounded, the Abanda fault separating it from the underlying eastern Blue Ridge, and the Katy Creek fault marking the boundary with the overlying the DC. Tabular, curvilinear cataclastic zones splay out from the Abanda fault to merge westward with the Alexander City fault zone (ACFZ), which occurs in locally intense distributed ductile shears. The Abanda and ACFZ are kinematically similar, with ductile oblique, predominantly dextral, movement. The Katy Creek fault is cryptic where studied, with no recognized post-metamorphic (retrogressive) fabric disruption, implying a pre- or syn-metamorphic origin. $^{40}\text{Ar}/^{39}\text{Ar}$

isotopic analyses on muscovite from phyllonites of the Abanda fault and ACFZ are interpreted to constrain the timing of their movement histories to a mean age of ~317.5 Ma.

Two-dimensional graphical methods and a simple cut-and-staple-paper model are described to help students visualize and understand complex three-dimensional fault-rock structures/fabrics such as those of the Brevard zone. Lower hemisphere, equal-area, stereographic projections are used to resolve problems recognized while mapping oblique-slip shears, and the methods explained have a general applicability for characterizing movement in ductile shear zones containing S-C composite planar fabrics. The technique allows for the solving of movement direction as dip-slip (reverse/normal), strike-slip (dextral/sinistral), or oblique-slip motion based on plots of the S and C relative to the center of the stereonet. The method is transportable for field use since it only requires one to understand and measure the outcrop relationship(s) of penetrative mylonitic fabric(s) in the rock, and then to plot and analyze the measurements on a stereogram. Digital models and a simple paper physical model provide tools to help advanced undergraduate and graduate students to better understand and grasp S-C fabrics and their applications for solving movement sense along natural fault/shear zones.

ACKNOWLEDGEMENTS

I would like to thank the faculty and staff of the Department of Geosciences at Auburn University for their patience, encouragement, and guidance to mold me into a well-polished geologist through challenging course work, dynamic field studies, and research opportunities. Specifically, I am thankful for my mentor and friend, Dr. Mark Steltenpohl, for his support, discussions, advice, and many reviews/revisions of manuscripts and maps. Dr. Randy Kath was also an integral part of molding me into the geologist I am today; without his mentoring, friendship, and support, I would not have made it to this point, so I would also like to thank him. The Department of Geosciences at the University of West Georgia prepared and equipped me with the knowledge and tools to succeed with, so to them I am forever indebted. I would like to thank Amanda Reynolds for the opportunity and permission to report isotopic data and analysis that she collected. Thanks should also be given to Joel Abrahams, Mike Mason, and John Hawkins for the valued discussions and communal scientific findings. Finally, I express my infinite thanks and gratitude to my friends and family for their unwavering support, and to my wife, Amanda Poole, for her patience, encouragement, and love. I have a strong support network for which I am very lucky and appreciative.

Funding for portions of this project was provided by the National Cooperative Geologic Mapping Program and the USGS for EdMap No. G12A20461 to Dr. Mark Steltenpohl, Auburn University. I am very appreciative of this support.

Style manuals used:

Manuscript I: Bulletin of the Geological Society of America

Manuscript II: Journal of Geological Education

Computer software used: Microsoft Office Suite 2010/2013, ArcGIS 10.2, Adobe

Illustrator CS2, Adobe Photoshop CS2, Sketchup, and Stereonet 9

TABLE OF CONTENTS

Abstract.....	ii
Acknowledgements.....	iv
Table of Contents.....	vi
List of Tables.....	viii
List of Figures.....	ix
List of Plates.....	xvi
List of Abbreviations.....	xvii
Introduction.....	1
I. Geology of the Jacksons Gap, Alabama, 7.5-Minute Quadrangle: Implications for the Evolution of the Brevard Fault Zone.....	3
Introduction.....	3
Geologic Setting.....	7
Lithostratigraphic Units.....	15
Structural and Metamorphic Analysis.....	55
⁴⁰ Ar/ ³⁹ Ar Isotopic Analyses and Interpretations.....	72
Conclusions.....	91
References.....	94

Ii. Graphical Tools for Teaching Geometries and Kinematics of Fault Zones	101
Abstract	101
Introduction	102
S-C Fabrics and their Geometries	103
Determining Direction of Movement from Stereograms	107
Dip-Slip	108
Strike-Slip	108
Oblique-Slip	109
Problems with Steep and Shallow Dip Angles	110
Estimating Relative Degree of Shear	110
A Three-Dimensional S-C Model	111
Conclusions	112
References	115
Conclusions	132
Combined References	136
Appendix	147

LIST OF TABLES

Table 1. Summary of deformational phases in rocks of the study area.	56
Table 2. Summary of isotopic analyses of samples (n=10)	75

LIST OF FIGURES

1. Figure 1. Alabama Piedmont (black area representing Fig. 2) and the southern Appalachian orogen (from Steltenpohl, 1988). Gray sub-Coastal Plain geophysical lineaments from Horton et al. (1984); ACFZ = Alexander City fault zone. 4
2. Figure 2. Geologic map of part of the Alabama Piedmont (from Osborne et al., 1988, and Steltenpohl, 2005) illustrating the location of the Jacksons Gap Quadrangle (red rectangle) and Horseshoe Bend National Military Park (HBNMP) (green polygon). Dashed gray lines are geophysical lineaments from Horton et al. (1984). EDMAP Quadrangle abbreviations: TS = Tallassee (White, 2008); CV = Carrville; NO = Notasulga; LO = Loachapoka; AU = Auburn; PX = Parker’s Crossroads; BK = Bleeker; SS = Smith’s Station; RH = Red Hill (Sterling, 2008); WA = Waverly; OW = Opelika; OE = Opelika East; BU = Beulah; OT = Our Town (Hawkins, 2013); DV = Dadeville (Abrahams, 2014); and JG = Jacksons Gap (red box, current author). 4
3. Figure 3. Geologic map and cross section of east-central Alabama (modified after Osborne et al., 1988; Hatcher et al., 1990; Steltenpohl, 2005). 9
4. Figure 4. Graphite-muscovite-biotite-quartz-chlorite phyllonite of the Wedowee Group with shear fabrics associated with the Alexander City fault zone. A) S-C fabrics/phacoids. B) S-C fabric and a thin quartz vein/ribbon marking a transposed fold nose (scale on the pencil is one centimeter per block). C) Thin quartz ribbons highlighting shear structures, such as S-C fabrics, shear bands, asymmetric porphyroclasts, and anastomosing/boudinaged layers (see structure section). 17
5. Figure 5. Photomicrograph mosaic in cross-polarized light of graphite-muscovite-biotite-quartz-chlorite phyllonite of the Wedowee Group, Alexander City fault zone, displaying retrogressive alteration to sericite and chlorite. A) Muscovite phacoids help to outline S-C fabrics, with kinks and undulatory extinction in muscovites as well as folds and transposed fold noses. B) S-C fabric and NSC shear. Pre- and syn-kinematic garnet (extinct). 18
6. Figure 6. Emuckfaw Group lithologies. A1) Outcrop of garnetiferous schist. A2) Photomicrograph in cross-polarized light of Emuckfaw schist muscovite phacoids and NSC shear bands. B1) Mineral elongation lineation within a metagraywacke layer; pencil highlights lineation trend. B2) Photomicrograph in cross-polarized

- light of sheared metagraywacke with recrystallized quartz (see text). S-C and NSC fabric are highlighted by biotite, muscovite, sericite, and chlorite. C) Photomicrographs of amphibolite from the Emuckfaw Group. Foliation is defined by elongate hornblende and interstitial quartz, plagioclase, epidote, and trace titanite. C1) Plane-polarized light. C2) Cross-polarized light. 19
7. Figure 7. Kowaliga Gneiss (32° 58' 35.26" N, 85° 51' 10.17" W). A) Megacrysts (upwards of 5 cm in length) of potassium feldspar. B) Asymmetric potassium feldspar augens. C) Large feldspar augen within S-C-NSC fabric. D) Zoned, minimally sheared euhedral to subhedral potassium feldspar grain adjacent to asymmetric augens and intensely developed shear fabric. E) Photomicrograph mosaic in cross-polarized light displaying S-C-NSC structures..... 22
 8. Figure 8. Greenstone pod within the Kowaliga Gneiss. A) Amphibolite/greenstone and quartzo-feldspathic (meta-rhyolite/dacite protolith?) with high-angle brittle fault offsets (see text). B1) Photomicrograph in plane-polarized light and B2) in cross-polarized light of lepidoblastic foliation defined by aligned pyroxenes and elongated amphiboles. C1) Photomicrograph in plane-polarized light and C2) in cross-polarized light of pyroxenes having altered to amphibole..... 23
 9. Figure 9. Type I cataclastic rock. A1. and B1) slabbed and polished hand samples. Note the variance in colors and the separation of individual clasts by the vein quartz. A2) Photomicrograph in cross-polarized light of A1. B2) Photomicrograph in plane-polarized light and B3) in cross-polarized light of B1. showing a wide variance in grain size of polycrystalline quartz. 26
 10. Figure 10. Type II cataclastic rock. A. and B) slabbed and polished and samples. C1) Photomicrograph in plane-polarized light and C2) in cross-polarized light of C1.; relict breccia clasts separated by the vein quartz; however, nearly everything has been completely replaced by silica..... 27
 11. Figure 11. Type III cataclastic rock. A. and B) Hand samples. C1) Photomicrograph in plane-polarized light and C2) in cross-polarized light of C1.; relict breccia clasts that are matrix supported with rounded clasts and effectively complete silica replacement..... 28
 12. Figure 12. Garnetiferous phyllite of the Jacksons Gap Group. A) Outcrop photo of phyllonite displaying S-C fabric. View slightly oblique to S-C intersection. B) Photomicrograph in plane-polarized light; micro-scale z-folds, kinking, and stacking within micaceous phacoids, highlighted by minor graphite. C) Photomicrograph mosaic in cross-polarized light. Muscovite phacoids and composite phacoids duplexed/stacked atop one another. 30
 13. Figure 13. Photomicrograph in cross-polarized light of the flaggy, “clean,” mylonitic quartzite interlayered within the garnetiferous phyllite..... 32

14. Figure 14. Photomicrograph of micaceous quartzite in cross-polarized light. Muscovite and sericite outline micro-shear structures and also form phacoids indicative of dextral shearing in this unoriented view.	33
15. Figure 15. Interlayering within the Jacksons Gap Group. A) Interlayered micaceous/phyllitic quartzite, graphitic phyllite, and garnetiferous quartz schist (32° 55' 2.90" N, 85° 47' 17.09" W). B) Outcrop of the Jacksons Gap Group with interlayering of units that is too fine-scale to differentiate at map-scale (32° 52' 57.36" N, 85° 49' 6.10" W). C) Fabric deforming z-folds, view is down-dip of foliation and down-plunge of hinge lines.	35
16. Figure 16. Outcrop of the garnetiferous graphitic phyllite displaying S-C fabrics and z-folds.	36
17. Figure 17. Photomicrographs of garnetiferous graphitic phyllite of the Jacksons Gap Group (1. plane-polarized, 2. cross-polarized light). A) Quartz and muscovite inclusion trails within syn-kinematic “snowballed” garnet, with asymmetric pressure shadows indicating dextral-shear. B) Crenulations highlighted by micas. C) Z-folds marked by micas.	37
18. Figure 18. Garnetiferous quartz schist. A) Cut hand sample. Horizontal lines mark abrupt contacts of layers and arrows denote the fining upward direction. B. C. and D) photomicrographs (1. plane-polarized light and 2. cross-polarized light). B) Cross-polarized light with arrow indicating fining-upwards direction. C) Cross-polarized light, weak crenulations with associated muscovite, sericite, and retrograde chlorite. D) M-folds, view is slightly oblique to down-dip.	39
19. Figure 19. Carbonaceous phyllite. A) Cut and polished hand sample with S-C and NSC fabric and crenulations, indicative of oblique dextral shear. View is oblique to strike and dip. B) Relict bedding (S_0) (yellow) contact oblique to metamorphic/mylonitic foliation (S_1) (red). C) Photomicrograph in plane-polarized light showing high abundance of graphite present and a pre-kinematic garnet with asymmetrical pressure shadows symbolizing dextral shear, and retrogressive alteration around the grain boundary. View is oblique to strike and dip.	41
20. Figure 20. Massive quartzite in cross-polarized light. Micas highlight dextral S-C fabrics and discrete shear bands. View is perpendicular to lineations and down the S-C intersection.	42
21. Figure 21. Outcrop of the massive quartzite showing relict cross-bedding. View is down-dip of foliation.	43
22. Figure 22. Hand sample of the sericite-chlorite phyllite. The conspicuously green sheen is chlorite and a well-developed S-C fabric is evident.	45
23. Figure 23. Photomicrographs of porphyroclastic mylonitic conglomerate. A) Plane-polarized light and B) cross-polarized light.	47

24. Figure 24. Photomicrograph in cross-polarized light of the Waresville Schist. ...	50
25. Figure 25. Mafic-ultramafic complex lithologies. A) Outcrop photo of pyroxenite displaying a layered cumulate texture. B) Photomicrographs of the pyroxenite. B1) plane-polarized light and B2) cross-polarized light showing a relict cumulate texture and a weakly developed foliation. Pyroxenes are altered to amphiboles, and secondary quartz is present. C) Amphibole-actinolite-pyroxene-biotite-chlorite schist. D) Lineated metanorite.....	52
26. Figure 26. Agricola schist. A) Fresh hand sample showing strongly developed mylonitic fabric with stretched, anastomosing felsic bands interspersed with asymmetric porphyroclasts, indicating dextral shear. Note reddish orange color of weathered sample (upper left). B1) Photomicrograph in plane-polarized light and B2) photomicrograph in cross-polarized light; representative fabric with syn-kinematic garnet.....	54
27. Figure 27. Metamorphic conditions suggested for the peak metamorphism. Eastern Blue Ridge = purple, Jacksons Gap Group = green, and Dadeville Complex = orange (modified from Hawkins, 2013). Grid univariant reaction curves and facies boundaries are from Richardson (1968), Hoschek (1969), Holdaway (1971), and Ernst (1973).....	58
28. Figure 28: Lower-hemisphere stereographic projections and compilation of structural data from the three terranes within the Jacksons Gap Quadrangle. A) Eastern Blue Ridge (n=415). B) Jacksons Gap Group (n=268). C) Dadeville Complex (n=57). Orange projected great circle and pole represents the average strike and dip of the terrane.	60
29. Figure 29. Contoured lower-hemisphere stereographic projection of poles to S_1 measured regionally across the Tallassee synform (Plate 3) with the plane of best fit and its pole (compiled from Dr. Steltenpohl's unpublished data base). (n=2236). β =beta fold axis. Contour interval is 2% and counting area is 0.4% of net area.	61
30. Figure 30: Photomicrographs of M_2 retrograde (graphite-muscovite-biotite-quartz-chlorite phyllite of the Wedowee Group) shear fabrics of the Alexander City fault zone. A1. Plane-polarized light and A2. cross-polarized light of syn-kinematic snowballed garnets with asymmetric pressure shadows. Retrograde chlorite is visible within the fabric. B1. Plane-polarized light and B2. cross-polarized light, F_2 z-folds produced during shear with retrograde chlorite within the noses of some folds.....	63
31. Figure 31: Fabric deforming F_2 asymmetric folds. A. Outcrop-scale fold in the Alexander City fault zone ($32^\circ 59' 12.22''$ N, $85^\circ 51' 35.61''$ W) with tick marks marking the direction of dip. B. Small z-fold of the Kowaliga Gneiss.	67
32. Figure 32: Lower hemisphere stereographic projections of D_2 S-C fabric observations. A. Abanda fault (n=19). B Alexander City fault (n=18). Arcs	

connect the poles of S-C planes with arrows at poles of S-planes. Green arrows = slip-lines.....	69
33. Figure 33. Distribution of thermochronological dates (n=11) reported in this study (yellow boxes, Amanda Reynolds; orange boxes, current author). Red dots indicate sample localities. (Inset map modified from Steltenpohl, 2005).	73
34. Figure 34. Tallassee Quadrangle reduced Plate 1 of White (2008), showing muscovite sample locations (n=6).	74
35. Figure 35. A) The ANIMAL facility, Auburn University. B) The author separating muscovites from samples to be analyzed. C) Dr. Zeki Billor loading muscovites into irradiation discs before being sent to the USGS TRIGA reactor to be irradiated.	77
36. Figure 36. Microscopic photograph of muscovites extracted from samples. A) Relatively coarse, euhedral muscovites that are free from inclusions (JP-ACF-1). B) Finer muscovite grains with hematite staining and graphite, biotite, and chlorite inclusions (Sample JP-AF-1). Squares in background are 1mm ²	78
37. Figure 37. Photomicrographs in cross-polarized light of samples dated (left side) and their correlative measured dates plotted (right side). JP-ACF-1 (A1 and A2), JP-ACF-2 (B1 and B2), JP-KG (C1 and C2), and JP-AF-1 (D1 and D2).	81
38. Figure 38. Laser single crystal ⁴⁰ Ar/ ³⁹ Ar incremental heating spectra and plateau ages for two different muscovite crystals of sample JP-KG.....	82
39. Figure 39. Density probability plots of 6 muscovite grains from Reynold's samples: TA-28 (A), TA-13(B), and TA-35 (C) with photomicrographs of respective thin sections in cross-polarized light. (Continued on next page). Figure 39 (continued). Density probability plots of 6 muscovite grains from samples TA-44 (D), TA-49 (E), and TA-71 (F) with photomicrographs of respective thin sections in cross-polarized light.....	83
40. Figure 40. Collage of all 10 probability density plots illustrating where the dates obtained correlate the most (Reynolds' density plots in green and author's plots in red).	90
41. Figure 1. Tectonostratigraphic map of the Blue Ridge in east central Alabama (AL) and part of Georgia (GA) with major tectonic features, such as the ACF and the Abanda fault (in AL) of the BFZ, highlighted in red (modified after Tull, 1984; McClellan et al., 2007). (Cross section modified from Thomas et al., in Hatcher et al., 1989; Thomas, 1991; Steltenpohl, 2005; and Steltenpohl et al., 2008.) ACF—Alexander City fault; BFZ—Brevard fault zone; EBR—Eastern Blue Ridge; GEF—Goodwater-Enitachopco fault; HLF—Hollins Line fault; IP—Inner Piedmont; TFC Talladega Cartersville fault; TSB—Talladega slate belt; V&R—Valley and Ridge; Ordo-Dev—Ordovician–Devonian (modified from Steltenpohl, 2005; Steltenpohl et al., 2013).....	120

42. Figure 2. Stereonet showing slip-lines plotted on the C-plane's great circle representing dip-slip, strike-slip, and oblique-slip. Highlighted areas define degree of error. 121
43. Figure 3. Dip-slip faults. A) S- and C-planes share the same strike but vary in dip magnitude. With true dip-slip, the slip-line lies at the maximum dip of the C-plane's great circle (green circle). B) Poles to S-C planes plot near the center of stereonet, and slip-line aligns along the same geometric line containing the arc angle (see text). S-C intercept lies along the primitive of the stereonet (see A.). C) Dip-slip motion is based on the poles of S-C planes' proximity to center of stereonet. S-plane's pole is more proximal to the center of the stereonet than is the C-plane's pole. Correspondingly, C-plane's dip > S-plane's dip = normal-slip. 122
44. Figure 4. Reverse dip-slip faults. A) S- and C-planes share the same strike but vary in dip magnitude. B) Slip-line lies at the maximum dip of the C-plane's great circle and the poles to S-C planes, the center of stereonet, and slip-line aligns along the same line. The C-plane's pole is more proximal to the center of the stereonet than that of the S-plane. Correspondingly, C-plane's dip > S-plane's dip = reverse-slip..... 123
45. Figure 5. Normal dip-slip motion. A) Three-dimensional block diagram for normal dip-slip motion. B) Three-dimensional, cross-section perspective view (ideal view parallel to S-C intersections and along strike) of S-C fabrics illustrating normal dip-slip motion. 124
46. Figure 6. Outcrop photo looking parallel to the S-C planes' intersection, which is horizontal. Garnetiferous graphitic phyllonite/button schist from the Jacksons Gap Group within the Abanda fault, the basal fault of the Brevard fault zone. C-plane's dip > S-plane's = normal-slip. 124
47. Figure 7. Reverse dip-slip motion. A) Three-dimensional block diagram for reverse dip-slip motion. B) Three-dimensional, cross-sectional perspective view (ideal view parallel to S-C intersections) of S-C fabrics showing reverse dip-slip motion. 125
48. Figure 8. Outcrop photo with view parallel to horizontal S-C intersection lineation within a graphitic phyllonite of the Jacksons Gap Group proximal to the Abanda fault. C-plane's dip < S-plane's = reverse-slip. 125
49. Figure 9. Strike-slip faults. S- and C-planes have different strikes but share the same strike dip magnitude. Slip-line (green circle) lies at the intersection of the C-plane's great circle and the primitive of the stereonet. S-C intercept lies near the maximum dip of the C-plane. A) C-plane's great circle and pole are more clockwise than that of the S-plane, indicative of dextral strike-slip motion. B) S-plane's great circle and pole are more clockwise than that of the C-plane, indicating sinistral strike-slip motion..... 126

50. Figure 10. Dextral strike-slip motion. A) Three-dimensional block diagram illustrating dextral strike-slip motion. B) Three-dimensional, map-perspective view (ideal view parallel to S-C intersections) of S-C fabrics showing dextral strike-slip motion. 126
51. Figure 11. Outcrop photo looking down-dip of a button schist from the Jacksons Gap Group proximal to the Abanda fault. Viewed down-plunge of the S-C intersection with C-plane displaying a more clockwise orientation than that of the S-plane, demonstrating dextral slip..... 127
52. Figure 12. Sinistral strike-slip motion. A) Three-dimensional block diagram for sinistral strike-slip motion. B) Three-dimensional, map-perspective view (ideal view parallel to S-C intersections) of S-C fabrics showing sinistral strike-slip motion. 127
53. Figure 13. Dextral-normal-oblique-slip faults. A) S- and C-plane will have different strikes and dip magnitudes. Slip-line (green circle) does not lie near the maximum dip of the C-plane's great circle or at the intersection of the C-plane's great circle and the primitive, but somewhere in-between. B) Strike-slip is based on clockwise rotation of the S-C pair's great circles and poles relative to one another. C-plane's great circle and pole are more clockwise than that of the S-plane, indicating dextral strike-slip motion. The dip-slip component is based on the S-C planes' poles' proximity to center of stereonet. S-plane's pole is more proximal to the center of the stereonet than that of the C-plane, demonstrating normal slip (B.). 128
54. Figure 14. Dextral strike-slip motion. A) Three-dimensional block diagram showing oblique components of both a dextral strike-slip and normal dip-slip motion. B) Three-dimensional perspective view (ideal view parallel to S-C intersections) of S-C fabrics..... 128
55. Figure 15. Countered lower hemisphere stereographic projection of slip vectors as determined from a set of paired S-C plane measurements made on the Abanda fault (n=9). The red great circle is best visual fit and represents the average C-plane orientation. Arcs connecting the poles of paired S-C planes indicate both oblique-dextral-normal- (southwest plunging maximum) -reverse-slip (northeast plunging maximum) movement. All of the C-planes' poles are more clockwise than that of the S-planes' poles, documenting the dextral component. Contour interval is 2% and counting area is 1% of net area. 129
56. Figure 16. Arc-angle as a proxy for angular shear strains. A1. and A2) Lower magnitude of relative angular shear is reflected in a larger arc angle between S-C planes. B1. and B2) Smaller arc angles reflect higher degrees of angular shear strain..... 130
57. Figure 17. Constructing a three-dimensional S-C model out of basic office supplies. See text..... 131

LIST OF PLATES

1. Detailed Geologic Map of the Jacksons Gap, AL, 7.5-Minute Quadrangle
2. Cross-Sections Dissecting the Jacksons Gap, AL, 7.5-Minute Quadrangle

LIST OF ABBREVIATIONS

A	amps
ADEM	Alabama Department of Environmental Management
AL	Alabama
ANIMAL	Auburn Noble Gas Isotopic Mass Analysis Laboratory
ca	circa
COCORP	Consortium for Continental Reflection Profiling
DC	Dadeville Complex
EBR	eastern Blue Ridge
Fig	Figure
GIS	Geographic Information System
GPS	Global Positioning System
HNMP	Horseshoe Bend National Military Park
IP	Inner Piedmont
JGG	Jacksons Gap Group
LOI	Loss of Ignition
Ma	million years ago
MSWD	mean square weighted deviation
Mt	Mount
NE	northeast

NW	northwest
ppm	parts per million
S-C	schistosity and cisaillement
SE	southeast
s.e.	standard error
SW	southwest
REE	Rare Earth Elements
USGS	United States Geological Survey
V	volts

MINERAL ABBREVIATIONS

amp	amphibole
bt	biotite
ep	epidote
kspar	potassium feldspar
ky	kyanite
grt	garnet
hbl	hornblende
musc	muscovite
plag	plagioclase
px	pyroxene
qtz	quartz

INTRODUCTION

The format followed herein is a manuscript-style thesis composed of two papers that have been prepared for journal submission. The first paper, Geology of the Jacksons Gap, Alabama, 7.5-minute Quadrangle: Implications for the Evolution of the Brevard Fault Zone, was prepared as a geologic technical report for submission to the Geological Survey of Alabama using their manuscript guidelines. The second paper, Graphical Tools for Teaching Geometries and Kinematics of Fault Zones, has been prepared according to the manuscript guidelines for the Journal of Geological Education.

The first manuscript is the product of 1:24,000-scale detailed geologic field investigation of approximately 90 km² within the Jacksons Gap, Alabama, 7.5-minute Quadrangle. The Jacksons Gap Quadrangle centers around one of the largest fault systems of the Appalachians, the Brevard fault zone, which marks the boundary between the eastern Blue Ridge and the Inner Piedmont terranes in Alabama. The Alexander City fault zone, a major shear zone internal to the eastern Blue Ridge, also occurs in the quadrangle. The purpose of this first manuscript is to describe the lithologic units, metamorphic features, isotopic ages, and structural development of rocks found in the quadrangle (Plate 1), and also to document the polyphase deformation and movement history of the Brevard and Alexander City fault zones. Detailed geologic mapping was performed throughout 2012-2014 using traditional mapping techniques. The final geologic map was combined with the growing compilation of 1:24,000-scale maps of Dr.

Steltenpohl and his graduate students. Laboratory work included the following: petrographic analysis of over thirty thin sections to characterize mineral assemblages, microstructures, fabrics, and lithologies; $^{40}\text{Ar}/^{39}\text{Ar}$ isotopic age-dating analyses; and lower-hemisphere, equal-area, stereographic structural analyses.

The objective of the second paper is to present graphical methods for analyzing fault/shear zone geometries and kinematics that have general applications. Rock fabrics as a result of ductile shear (e.g. Schistosity [S] and Cisaillement [C] planes) were studied along the Brevard and Alexander City fault/shear zones. Data were plotted on a lower-hemisphere, equal-area, Schmidt stereonet. The sense of shear and slip direction, and relative angular shear strain can be resolved based on the geometric relationships of S- and C-planes plotted on a stereogram. This method allows a reader to study and understand fault/shear geometries based simply on the stereogram. Digital and simple paper physical models provide three-dimensional tools to help advanced undergraduate and graduate students better visualize and understand S-C fabrics and to graphically solve for movement geometries in natural fault systems.

**I. GEOLOGY OF THE JACKSONS GAP, ALABAMA, 7.5-MINUTE
QUADRANGLE: IMPLICATIONS FOR THE EVOLUTION OF THE BREVARD
FAULT ZONE**

INTRODUCTION

The geologic history of rocks underlying the Jacksons Gap, Alabama, 7.5-minute Quadrangle of Tallapoosa County, east-central Alabama, provides important insight to how the southernmost Appalachian Mountains evolved (Figs. 1 and 2). Metasedimentary, metaplutonic, and metavolcanic complexes of undetermined tectonic affinity are bounded by two major Appalachian fault zones that occur within the quadrangle, the Brevard and Alexander City fault zones (Bentley and Neathery, 1970; Steltenpohl, 2005) (Fig. 2). These fault zones separate three terranes, from northwest to southeast, the eastern Blue Ridge, the Brevard zone/Jacksons Gap Group, and the Inner Piedmont (Figs. 1 and 2). The eastern Blue Ridge is thought to represent the distal slope-rise facies of the ancient Laurentian margin (Hatcher, 1987; Drummond et al., 1994), whereas the Brevard zone/Jacksons Gap Group and the Inner Piedmont have uncertain affinities that need to be clarified. Rocks and structures in the Jacksons Gap Quadrangle have not been previously mapped at 1:24,000-scale and this investigation presents the results of detailed, 1:24,000-scale geologic mapping. Interpretation of the results have implications for a working synthesis of the tectonic evolution of the southernmost Appalachians.

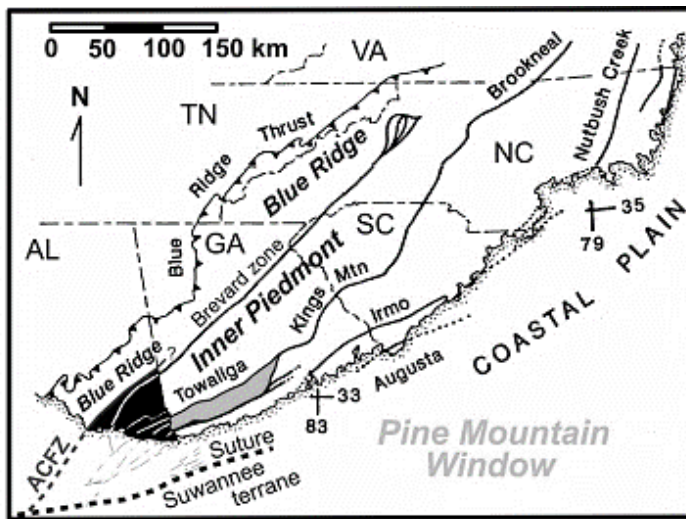


Figure 1. Alabama Piedmont (black area representing Fig. 2) and the southern Appalachian orogen (from Steltenpohl, 1988). Gray sub-Coastal Plain geophysical lineaments from Horton et al. (1984); ACFZ = Alexander City fault zone.

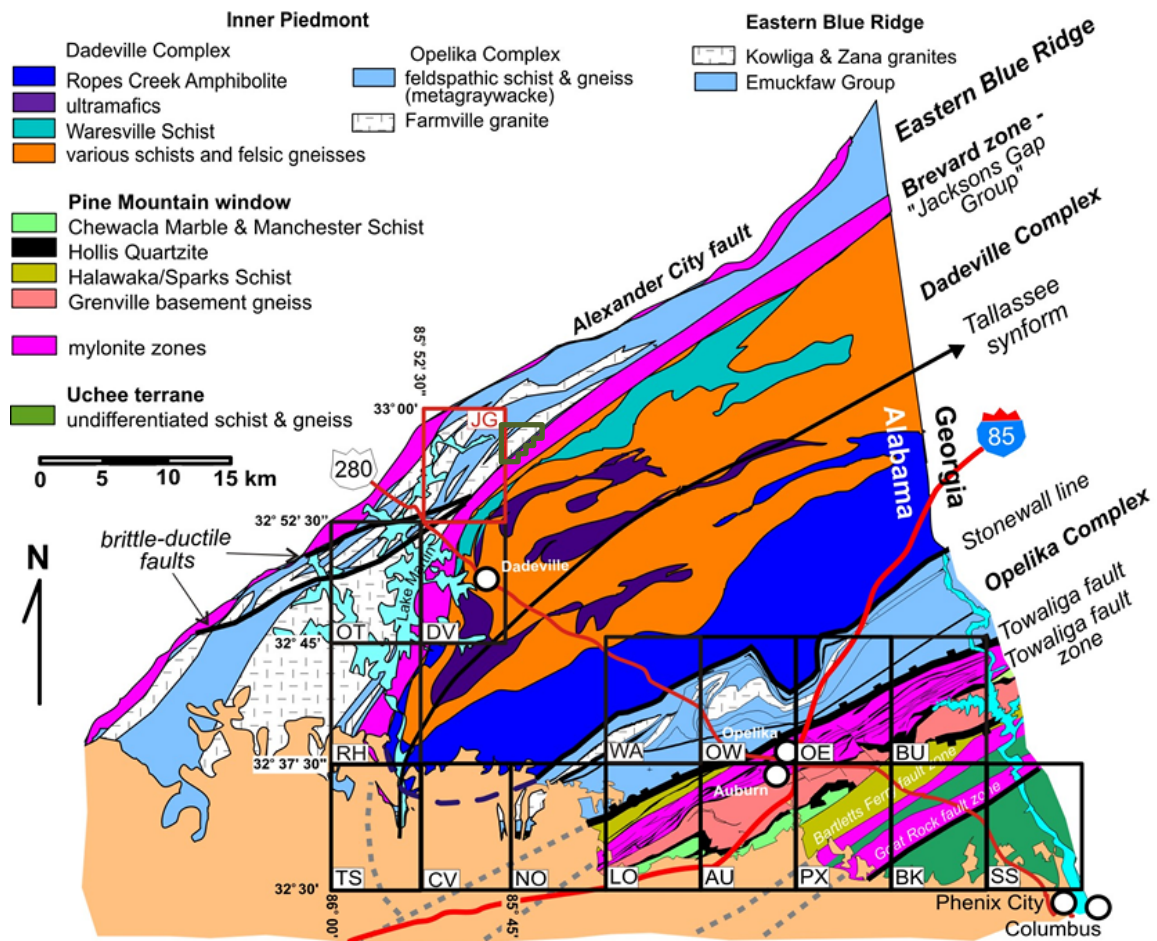


Figure 2. Geologic map of part of the Alabama Piedmont (from Osborne et al., 1988, and Steltenpohl, 2005) illustrating the location of the Jacksons Gap Quadrangle (red rectangle) and Horseshoe Bend National Military Park (HBNMP) (green polygon). Dashed gray lines are geophysical lineaments from Horton et al. (1984). EDMAQ Quadrangle abbreviations: TS = Tallassee (White, 2008); CV = Carrville; NO = Notasulga; LO = Loachapoka; AU = Auburn; PX = Parker's Crossroads; BK = Bleeker; SS = Smith's Station; RH = Red Hill (Sterling, 2008); WA = Waverly; OW = Opelika; OE = Opelika East; BU = Beulah; OT = Our Town (Hawkins, 2013); DV = Dadeville (Abrahams, 2014); and JG = Jacksons Gap (red box, current author).

There are four overarching objectives to this research project: 1) to characterize lithologies and define the tectonostratigraphic sequence of the Jacksons Gap Group; 2) to describe and analyze the kinematics of micro- and macro-structures; 3) to constrain timing of shear zone movements; and 4) to synthesize the geologic history of this part of the southernmost Appalachians.

Detailed geologic mapping was performed using traditional mapping techniques. Mapping stations were recorded in a field notebook and keyed to the 7.5-minute topographic quadrangle map using GPS readings for latitude-longitude/Universal Transverse Mercator (UTM) coordinates. Attitudes of structures and fabrics were measured using a Brunton Pocket Transit compass. Lithologies, mineral resources, and environmentally sensitive or hazardous features were noted, and representative samples were collected for laboratory analysis. The geologic field map was digitized using Esri ArcGIS, specifically ArcMap, and was combined with the growing set of 1:24,000-scale geologic maps mapped and compiled by Dr. Steltenpohl and his graduate students (Fig. 2). Laboratory work included the following: petrographic analysis of over thirty thin sections to characterize mineral assemblages, microstructures, fabrics, and lithologies; $^{40}\text{Ar}/^{39}\text{Ar}$ isotopic age-dating analyses; and lower-hemisphere, equal-area, stereographic structural analyses.

Geologic work on rocks and structures in the Jacksons Gap Quadrangle is important on both applied and basic research grounds. First, Horseshoe Bend National Military Park is one of our National Parks that had not yet been geologically evaluated when the current project was initiated. For that reason it was given a high priority by the National Parks Service, Geologic Resource Division, for detailed geologic mapping.

Horseshoe Bend National Military Park (Fig. 2) lies adjacent to the Jacksons Gap Quadrangle, east of its boundary with the Buttston 7.5-Minute Quadrangle, Alabama. Second, the Jacksons Gap Quadrangle was determined to have the second highest mapping priority in the state by the Geological Survey of Alabama's Geologic Mapping Advisory Board due to four reasons: 1) rapid development along the US-280 Corridor; 2) Lake Martin is a major recreational area, reservoir, and hydroelectric generating facility on the Tallapoosa River; 3) the Alabama Department of Environmental Management (ADEM) needs basic bedrock information for Source Water Protection studies; and 4) there is a need to delineate granitic aggregate and precious metal/mineral resources in the area.

GEOLOGIC SETTING

The Brevard zone is a complex, polyphase deformation zone that has been studied for over 100 years, and has over forty-two, and growing, interpretations (as summarized by Bobyarchick, 1999). It is a major, Appalachian fault zone that in segments is up to 6 km wide and it extends in surface exposures for approximately 650 km from Mt. Airy, North Carolina, southwest to the Coastal Plain onlap in Tallassee, Alabama (Figs. 1 and 2). The origin of the Brevard zone remains a classic, but fundamental, problem in Appalachian evolution. Workers mostly agree that it contains an early, northwest-directed crystal-plastic thrust history (Devonian/Acadian?) that predated broadly Carboniferous (Alleghanian), dextral strike-slip brittle-plastic overprinting that imparted its remarkably linear, approximately N55°E-S55°W trend throughout most of its surface trace (Hatcher, 1972, 1987; Steltenpohl, 2005). In its northeastern most extent in North Carolina, the Brevard zone is a brittle fault. At Rosman, North Carolina, near its type locality, the zone is principally a plastic mylonite zone that rests upon a brittle fault, the Rosman fault. These mylonites, and locally associated brittle faults, continue to its southernmost extent where it is covered by the Coastal Plain onlap in Alabama (see Medlin and Crawford, 1973, for a summary). Medlin and Crawford (1973) worked on the Brevard zone in eastern Alabama and western Georgia and provided a thorough report of the history of early investigations.

The Brevard zone generally marks the boundary between the eastern Blue Ridge and the overlying Inner Piedmont in eastern Alabama and western Georgia. Studies of the Brevard fault zone near the Alabama-Georgia line and to the northeast define a structural zone of intense and discrete deformation (Bentley and Neathery, 1970; Medlin and Crawford, 1973). Southwest of the Alabama-Georgia state line, the zone appears to bifurcate into two distinct, but kinematically and rheologically different, fault zones that completely encapsulate a distinct lithologic group called the Jacksons Gap Group. In the Jacksons Gap Quadrangle, however, lithologies and structures of the Brevard zone make an uncharacteristic bend to nearly due south (Fig. 2, Plate 1, and Plate 2). Northeast of Horseshoe Bend National Military Park (Fig. 2), mylonitic fabric (shear foliation) in the Brevard zone generally has moderate-to-steep eastward dips (Bentley and Neathery, 1970; Medlin and Crawford, 1973; Hatcher, 1987). Recent EdMap-funded geologic mapping work of Dr. Steltenpohl and his students document dips becoming progressively shallower along strike southward through the Jacksons Gap, Dadeville, Our Town, Red Hill, and Tallassee Quadrangles (Figs. 2 and 3, and Plates 1 and 2), interpreted to reflect the west-limb of the Tallassee synform.

The Jacksons Gap Quadrangle (latitudes $32^{\circ} 52' 30''$ N and $33^{\circ} 00'$ N; longitudes $85^{\circ} 52' 30''$ W and $85^{\circ} 45'$ W) is located in Tallapoosa County, east-central Alabama, approximately thirty miles north-northwest of Auburn, Alabama (Fig. 2). The quadrangle is situated between Lake Martin and Horseshoe Bend National Military Park, along the Tallapoosa River. Highway 280, a major corridor connecting Columbus, Georgia, to Birmingham, Alabama, passes through the southwestern corner of the quadrangle. The Jacksons Gap Quadrangle is underlain by three geologic terranes, from northwest to

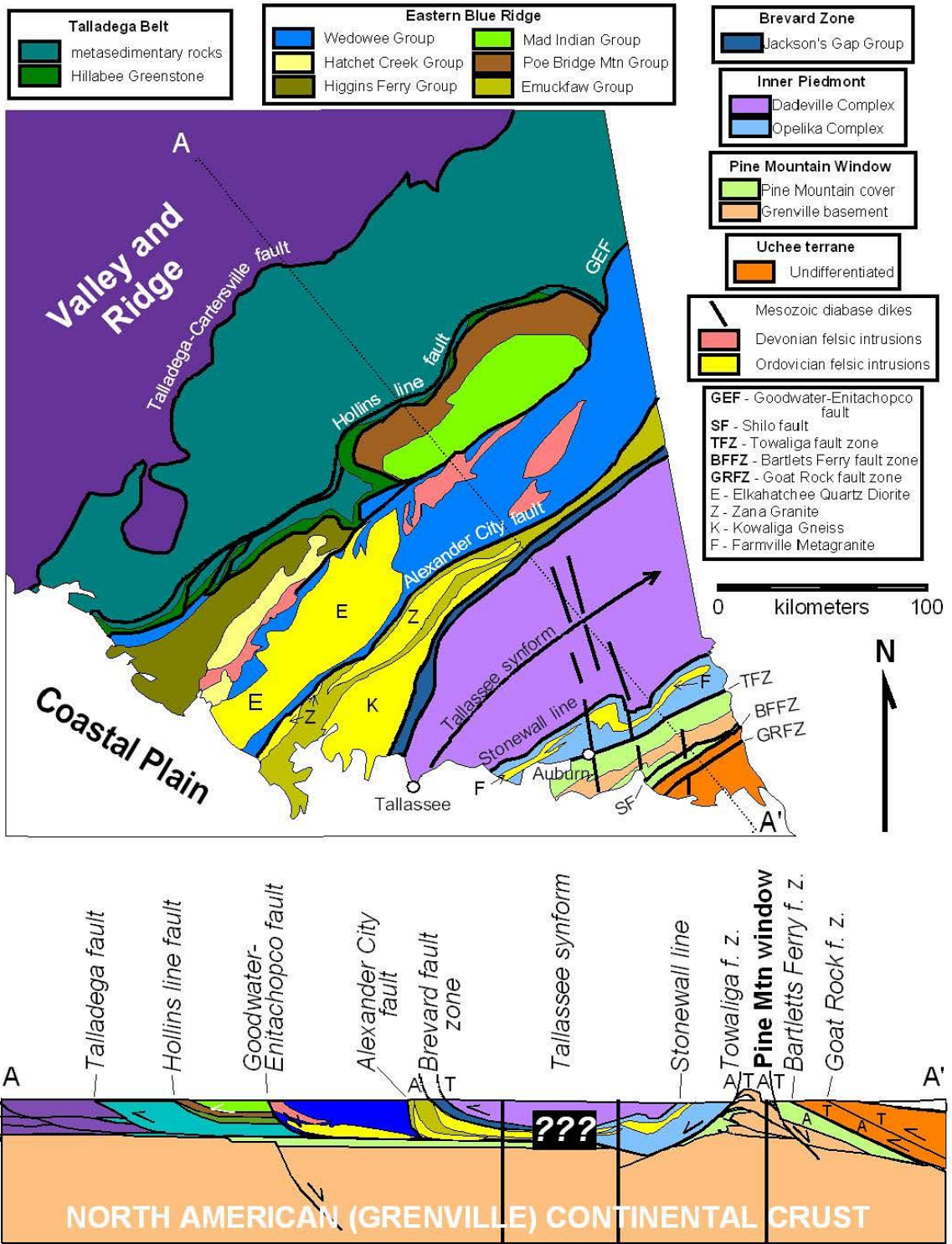


Figure 3. Geologic map and cross section of east-central Alabama (modified after Osborne et al., 1988; Hatcher et al., 1990; Steltenpohl, 2005).

southeast, the eastern Blue Ridge, the Brevard fault zone/Jacksons Gap Group, and the Inner Piedmont/Dadeville Complex. The eastern Blue Ridge is situated in the northwestern half of the quadrangle and contains lower- to middle-amphibolite facies metasedimentary rocks of the Wedowee Group, which is generally in fault contact with the Emuckfaw Group and its sill-like granitic plutons, the Kowaliga Gneiss and Zana Granite (Plates 1 and 2). The eastern Blue Ridge is separated from the Jacksons Gap Group by the Abanda fault, the basal and northwestern most fault of the Brevard zone in Alabama (Plates 1 and 2). The Jacksons Gap Group spans approximately one-third of the quadrangle and contains greenschist- to amphibolite-facies metasedimentary rocks (Plates 1 and 2). The southeastern corner of the quadrangle is underlain by middle- to upper-amphibolite facies rocks of the Dadeville Complex, which are in fault contact with the Jacksons Gap Group along the cryptic Katy Creek fault (Plates 1 and 2) (Bentley and Neathery, 1970).

The metasedimentary units of the eastern Blue Ridge are interpreted to have been deposited off of the passive Laurentian margin following the breakup of the Rodinian supercontinent, and represent the distal slope-rise facies (Tull, 1978; Hatcher, 1987; Drummond et al. 1994). More recently, workers have suggested that the uppermost eastern Blue Ridge units in Alabama and Georgia may reflect back-arc basin affinities (Neilson and Stow, 1986; Tull et al., 2014). The Jacksons Gap Group has shallow marine affinities that could potentially be the uppermost portion of a back-arc basin or the fringe of an arc. The rocks within the Inner Piedmont/Dadeville Complex have been variably interpreted as a back-arc basin, rift basin, or island-arc complex, with most recent

workers supporting the latter (Bentley and Neathery, 1970; Sears et al., 1981; Nielson and Stow, 1986; Hawkins, 2014; Tull et al., 2014).

Rocks of the Wedowee and Emuckfaw Groups, the Jacksons Gap Group, and the Dadeville Complex are polydeformed, and generally dip to the southeast in the study area. The Wedowee and Emuckfaw Groups of the eastern Blue Ridge and Dadeville Complex were metamorphosed to middle- to upper-amphibolite facies conditions, and subsequently all three terranes were retrograded under upper-greenschist to lower-amphibolite facies conditions along shear zones (Bentley and Neathery, 1970; Steltenpohl, 2005).

In Alabama, three lithologic complexes compose the eastern Blue Ridge, from tectonostratigraphic bottom to top (from northwest to southeast), the Ashland Supergroup, the Wedowee Group, and the Emuckfaw Group (Fig. 3) (Bentley and Neathery, 1970; Neathery and Reynolds, 1973; Neathery, 1975). The Ashland Supergroup lies in the immediate hanging wall of the Hollins Line fault (Tull, 1978; Steltenpohl, 2005; Steltenpohl et al., 2013). West of the retrogressive, oblique-dextral-normal-slip Goodwater-Enitachopco fault, rocks of the Wedowee Group comprise locally graphitic and garnetiferous schist and phyllite with intercalated quartzite and local amphibolite (Bentley and Neathery, 1970; Johnson, 1987; Steltenpohl, 2013). It is intruded by the Elkahatchee Quartz Diorite Gneiss batholith (Bentley and Neathery, 1970; Neathery and Reynolds, 1975). The intrusive age of the Elkahatchee Quartz Diorite is uncertain; Russell (1987) reported an Early Ordovician age (490 Ma) but Mueller et al. (2011) reported an Early Devonian age (388 Ma).

The retrogressive, oblique-dextral-normal-and-minor-reverse-slip Alexander City fault zone generally separates the Wedowee and Emuckfaw Groups (Plates 1 and 2) (Steltenpohl et al., 2013). The Emuckfaw Group, previously known as the Heard Group and the Emuckfaw formation, was named for exposures along Emuckfaw Creek, Tallapoosa County, Alabama (Bentley and Neathery, 1970; Neathery and Reynolds, 1975). Bieler and Deininger (1987) informally split the group into two lithologic units based on apparent compositional variations, the lower Josie Leg and upper Timbergut formations, named for creeks in Tallapoosa County, Alabama. The Emuckfaw Group contains mainly mica schist and metagraywacke with less abundant interlayers of quartzite, amphibolite, and calc-silicate (Bentley and Neathery, 1970; Neathery and Reynolds, 1973; Johnson, 1988). It is intruded by the Zana Granite and Kowaliga Gneiss (Figs. 2 and 3). The Zana Granite is a highly sheared, medium- to coarse-grained, meta-granite to meta-quartz-monzonite that typically has a strongly lineated fabric. The Kowaliga Gneiss is a coarse-grained, sheared, meta-granite to quartz monzonite augen-gneiss with a strongly sheared fabric (Bentley and Neathery, 1970; Raymond et al., 1988; Johnson, 1988). The Zana Granite has been determined to be a highly sheared derivative of the Kowaliga Gneiss (Hawkins, 2013). The intrusive ages of the Zana Granite and Kowaliga Gneiss were originally interpreted to be Middle Ordovician to Devonian by Russell (1987). Recent U-Pb dating of zircons from the Kowaliga Gneiss and Zana Granite indicate that the two have roughly the same intrusive age, 441 ± 6.6 Ma (Hawkins, 2013) and ~ 439 Ma (Tull et al., 2013), respectively.

The Emuckfaw Group is separated from the structurally overlying Jacksons Gap Group by the Abanda fault. The Jacksons Gap Group has a distinctly lower metamorphic

grade than the eastern Blue Ridge and Inner Piedmont. Metasiliciclastic units (graphitic phyllite/schist, sericite-rich phyllite, graphitic metaquartzite, quartzite) and their phyllonitized/mylonitized derivatives characterize the Jacksons Gap Group, and, notably, it is devoid of granitic intrusives that typify the underlying eastern Blue Ridge units (Bentley and Neathery, 1970; Wielchowsky, 1986; Johnson, 1988; Steltenpohl 2005; Sterling, 2005). Distinctive orthoquartzite units (e.g., Devils Backbone and Tallassee quartzite) are common in the Jacksons Gap Group, whereas the only other major, clean orthoquartzite in this region is the Hollis Quartzite that forms part of the cover sequence to the Grenville Pine Mountain basement massif (Figs. 1 and 2). Some units within the Jacksons Gap Group locally contain gold that has been historically mined.

The internal structure of the Brevard fault zone in Alabama has yet to be resolved, but recent interpretations evoke tectonic repetition due to duplexing and imbricate faulting (e.g. the Tallassee imbricate zone of Keefer, 1992, and the Lake Martin imbricate zone of Sterling, 2005). Alternatively, some workers variably interpret the lithologic repetitions as due to folding (Wielchowsky, 1986), or primary sedimentary facies variations (Bentley and Neathery, 1970). Medlin and Crawford (1973), Wielchowsky (1986), Johnson (1988), Keefer (1992), and Sterling (2006) each suggested a general stratigraphic order of the Jacksons Gap Group; however, detailed geologic mapping has demonstrated that these units are discontinuous along strike (Plate 1).

The Katy Creek fault separates the distinctively lower metamorphic grade rocks of the Jacksons Gap Group from the higher metamorphic grade units of the Inner Piedmont (Fig. 2). Traditionally, rocks of the Inner Piedmont in Alabama are divided into two tectonometamorphic complexes, the metavolcanic and metaplutonic Dadeville

Complex, and the underlying, mostly metasedimentary Opelika Complex, which lie in the core of the gently northeast-plunging Tallassee synform (Bentley and Neathery, 1970; Osborne et al., 1988; Steltenpohl et al., 1990). The Dadeville Complex contains the Ropes Creek Amphibolite, Waresville Formation, undifferentiated mafic-ultramafic complexes, Agricola Schist, Camp Hill Gneiss, Rock Mills Granite, and Waverly Gneiss (Bentley and Neathery, 1970; Sears et al., 1981; Wielchowsky, 1983; Nielson and Stow, 1986; Osborne, 1988; Johnson, 1988; Steltenpohl, 1990; McClellan et al., 2007; and Abrahams, 2014). Peak metamorphic conditions recorded by Dadeville Complex units are in the amphibolite facies, but these assemblages were locally retrograded to greenschist facies along ductile shears (Steltenpohl and Moore, 1988). The timing of the tectonic assembly and metamorphism of the Inner Piedmont in Alabama is poorly constrained (Steltenpohl and Moore, 1988; Steltenpohl and Kunk; 1993; Steltenpohl, 2005). For a detailed synthesis of previous investigations on the geology of the area, see Abrahams (2014).

LITHOSTRATIGRAPHIC UNITS

The lithologic units of the Jacksons Gap Quadrangle (Plates 1 and 2) are herein described based on field and petrographic thin section observations. Photographs and photomicrographs and shear fabrics (S-C planes, phacoids, and asymmetric folds [e.g. z-folds]), are viewed oblique to strike and dip and down plunge of the S-C intersection and fold hinge lines, unless otherwise noted. Figures with labels such as A1, A2, etc. are associated as the same sample, either a hand sample (A1) with its thin section (A2), or a thin section in plane polarized light (A1) and cross-polarized light (A2), unless otherwise stated. Minerals are listed in order, from left to right, from most abundant to least abundant. Lithologic units are described in tectonostratigraphic order from bottom to top (from the northwest corner to the southeast of the quadrangle) (Plates 1 and 2). Mapping units are represented at 1:24,000-scale; however, some lithologies described do not appear on the map due to their being too thin to be shown. Lithologic symbols for these units on Plate 1 are indicated parenthetically below.

EASTERN BLUE RIDGE

Parts of two lithologic complexes of the eastern Blue Ridge of Alabama are exposed in the Jacksons Gap Quadrangle: the Wedowee and Emuckfaw Groups (Bentley and Neathery, 1970; Neathery and Reynolds, 1973; Neathery 1975) (Fig. 2 and Plate 1).

Wedowee Group (Ewd)

The Wedowee Group comprises varyingly sheared, locally graphitic and garnetiferous muscovite-biotite-quartz-feldspar-chlorite phyllite, schist, and phyllonite (i.e., button-schist) that have a silvery-gray sheen in fresh outcrop. These units may be intercalated with locally graphitic, muscovite-biotite quartzite and local, discontinuous layers/lenses of amphibolite (Figs. 4 and 5). Only the phyllite, phyllonite, and schist were observed to crop-out in the study area. Grain size is typically fine grained (less than 0.5 mm) but ranges up to medium grained (0.5 mm to 2 mm) in the phyllite and schist. Nearly all of the Wedowee Group outcropping within the quadrangle records a relatively high-degree of right-slip shear strain as indicated by S-C-NSC fabrics, asymmetric z-folds, rotated pre- and syn-kinematic garnets, and extended phacoid-shaped veins of quartz (Figs. 4 and 5). Chlorite and sericite are modally abundant in some discrete shear zones (Fig. 5). These rocks weather to an olive-tan color, with an orange tinge, and locally they are conspicuously blueish-gray.

Emuckfaw Group (Eem)

The Emuckfaw Group occupies a significant portion of the eastern Blue Ridge in the study area. The topography of rolling hills reflects variable weathering of the interlayered schists and quartzites with metagranitic intrusions and mafic pods (Fig. 6). Nomenclature of Bieler and Deininger (1987) and Tull and Barineau (2012) are suggested to be abandoned as applied to the current study area because the Emuckfaw Group is composed of gradational, not starkly differing, packages of schist, with varying abundances of garnet, graphite, quartz, biotite, chlorite, kyanite, staurolite, and varying

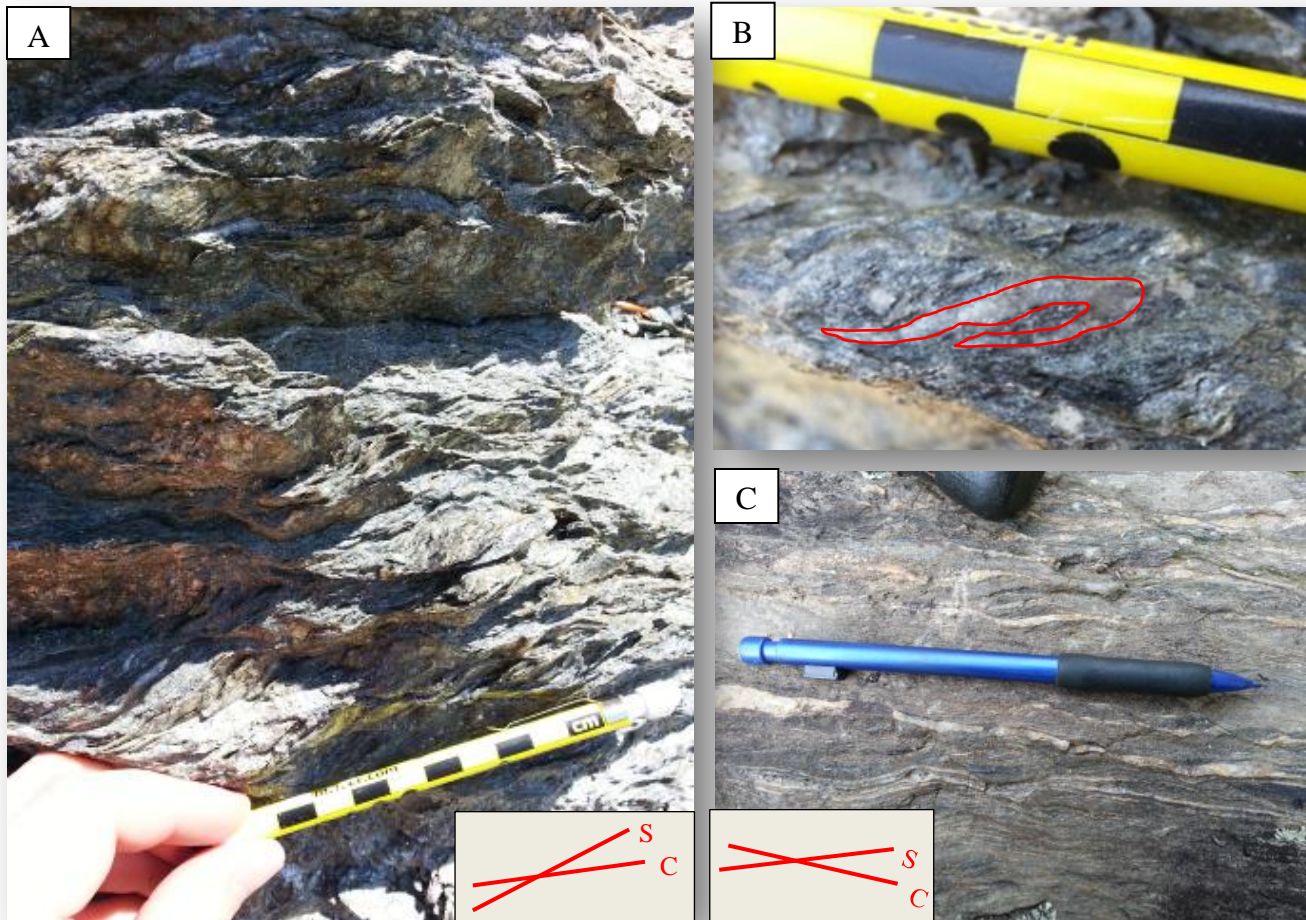


Figure 4. Graphite-muscovite-biotite-quartz-chlorite phyllonite of the Wedowee Group with shear fabrics associated with the Alexander City fault zone. A) S-C fabrics/phacoids. B) S-C fabric and a thin quartz vein/ribbon marking a transposed fold nose (scale on the pencil is one centimeter per block). C) Thin quartz ribbons highlighting shear structures, such as S-C fabrics, shear bands, asymmetric porphyroclasts, and anastomosing/boudinaged layers (see structure section).

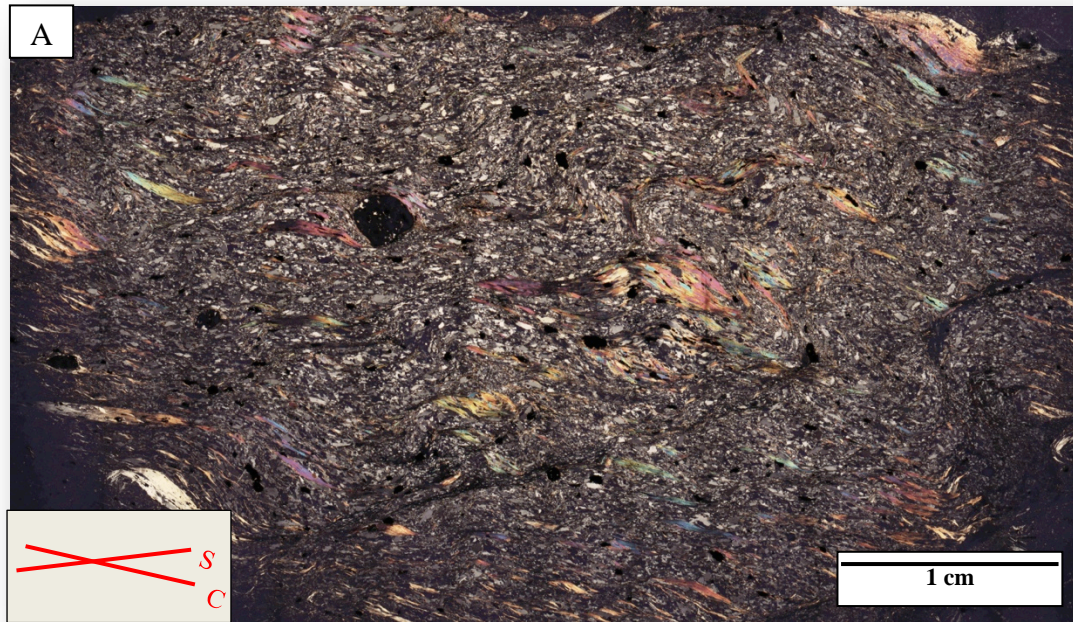


Figure 5. Photomicrograph mosaic in cross-polarized light of graphite-muscovite-biotite-quartz-chlorite phyllonite of the Wedowee Group, Alexander City fault zone, displaying retrogressive alteration to sericite and chlorite. A) Muscovite phacoids help to outline S-C fabrics, with kinks and undulatory extinction in muscovites as well as folds and transposed fold noses. B) S-C fabric and NSC shear. Pre- and syn-kinematic garnet (extinct).

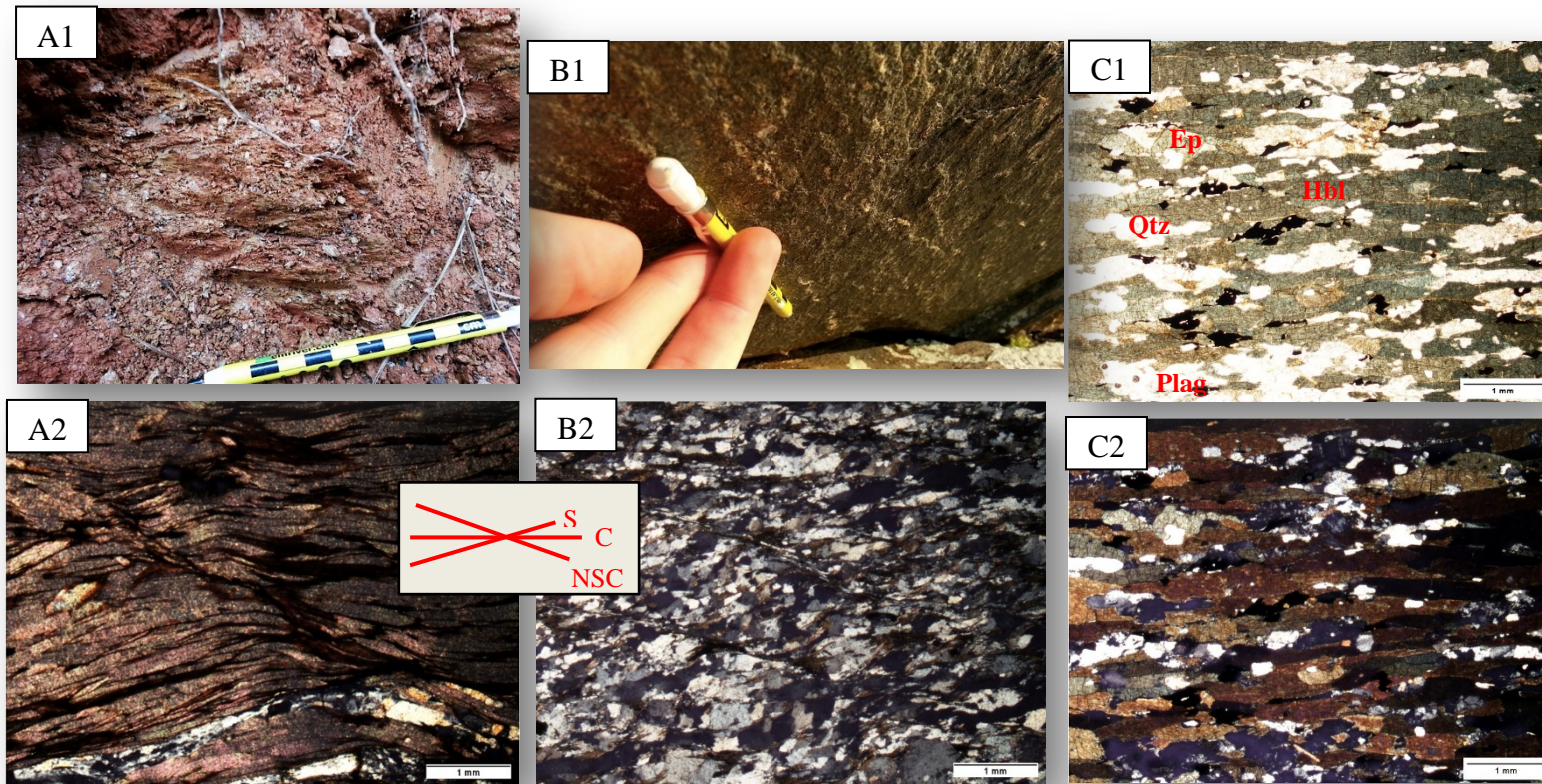


Figure 6. Emuckfaw Group lithologies. A1) Outcrop of garnetiferous schist. A2) Photomicrograph in cross-polarized light of Emuckfaw schist muscovite phacoids and NSC shear bands. B1) Mineral elongation lineation within a metagraywacke layer; pencil highlights lineation trend. B2) Photomicrograph in cross-polarized light of sheared metagraywacke with recrystallized quartz (see text). S-C and NSC fabric are highlighted by biotite, muscovite, sericite, and chlorite. C) Photomicrographs of amphibolite from the Emuckfaw Group. Foliation is defined by elongate hornblende and interstitial quartz, plagioclase, epidote, and trace titanite. C1) Plane-polarized light. C2) Cross-polarized light.

grain-size distributions. Hawkins (2013) differentiated three different types of schist within the Emuckfaw Group on the subjacent (to the southwest) Our Town Quadrangle; the current study, however, does not separate these out as individual units. Primary compositional differences are gradational, typically across two-to-three meters of section between the varying schists.

Pre- and syn-kinematic anhedral to euhedral garnets up to 1 cm in diameter occur locally throughout portions of the muscovite schist. Muscovite is typically coarse-grained (up to 2.5 mm) and varies from gray, occasionally with a silvery sheen, tan, to bronze in color (Figs. 6A1 and A2). Many of the exposures weather to a deep red-maroon saprolite color with a glittery shimmer due to the micas; garnets have been oxidized to dark brown splotches (Fig. 6A1).

In the study area, the Emuckfaw Group commonly contains interlayered metaquartzite, amphibolite, and metagranite. Metagraywacke is relatively resistant to weathering and contain S-C and NSC fabrics and strongly developed mineral elongation lineations (Fig. 6B1 and B2). These medium-grained rocks comprise recrystallized, polycrystalline quartz, muscovite, biotite, sericite, and retrogressive chlorite (Fig. 6B1 and B2). Amphibolites are medium- to coarse-grained, are well foliated, and contain elongated hornblende, interstitial quartz, plagioclase, epidote group minerals, chlorite, and trace titanite which display radiation damage (Fig. 6C1 and C2).

Kowaliga Gneiss (Ekg) and Zana Granite

Intruding the lithologies of the Emuckfaw Group, and interleaved over approximately 5 m near contacts, are the Kowaliga Gneiss and Zana Granite. Hawkins

(2013) concluded that the Zana Granite and Kowaliga Gneiss are chemically similar and share nearly identical intrusive ages, with differences being their shear fabrics and geographical occurrence. Based in these similarities, Hawkins (2013) and Bentley and Neathery (1970) suggested that the two be consolidated into the same lithostratigraphic unit. Only the Kowaliga Gneiss was observed within the study area where it is characterized as a medium- to coarse-grained (greater than 2 mm), augen gneiss with quartz, potassium feldspar, plagioclase, biotite, muscovite, and chlorite, with accessory clinozoisite and epidote (Fig. 7). The dominant gneissosity is defined by the alignment of biotite, muscovite, and quartz ribbons that drape augens of larger more competent, primarily potassium feldspar augens (Fig. 7). Feldspar megacrysts can be randomly oriented but are most often aligned within the foliation (Fig. 7). Composite S-C and NSC fabrics and asymmetric z-folds indicate oblique-dextral-normal-slip movement. Stretched biotite and quartz grains lie within the gneissic foliation, defining the elongation lineation. Northwest trending, late-stage, discontinuous brittle faults are near perpendicular to strike of the unit (Fig. 8A). Saprolitized outcrops of the Kowaliga Gneiss are a light creamy to brick-orange color and commonly retain the metamorphic foliation.

Portions of the Kowaliga Gneiss contain volumes of interlayered amphibolite and quartzo-feldspathic layers that are xenoliths of greenstone and meta-rhyolites/dacites, respectively (Fig. 8). These typically occur as small, discontinuous pods (measuring ~ 3.5 m by 3 m), and thus not large enough to depict at the 1:24,000 map-scale of Plate 1. They appear to occur along a generally consistent horizon that trends into similarly described rocks in the Our Town Quadrangle (Hawkins, 2013). The greenstone/amphibolite layers

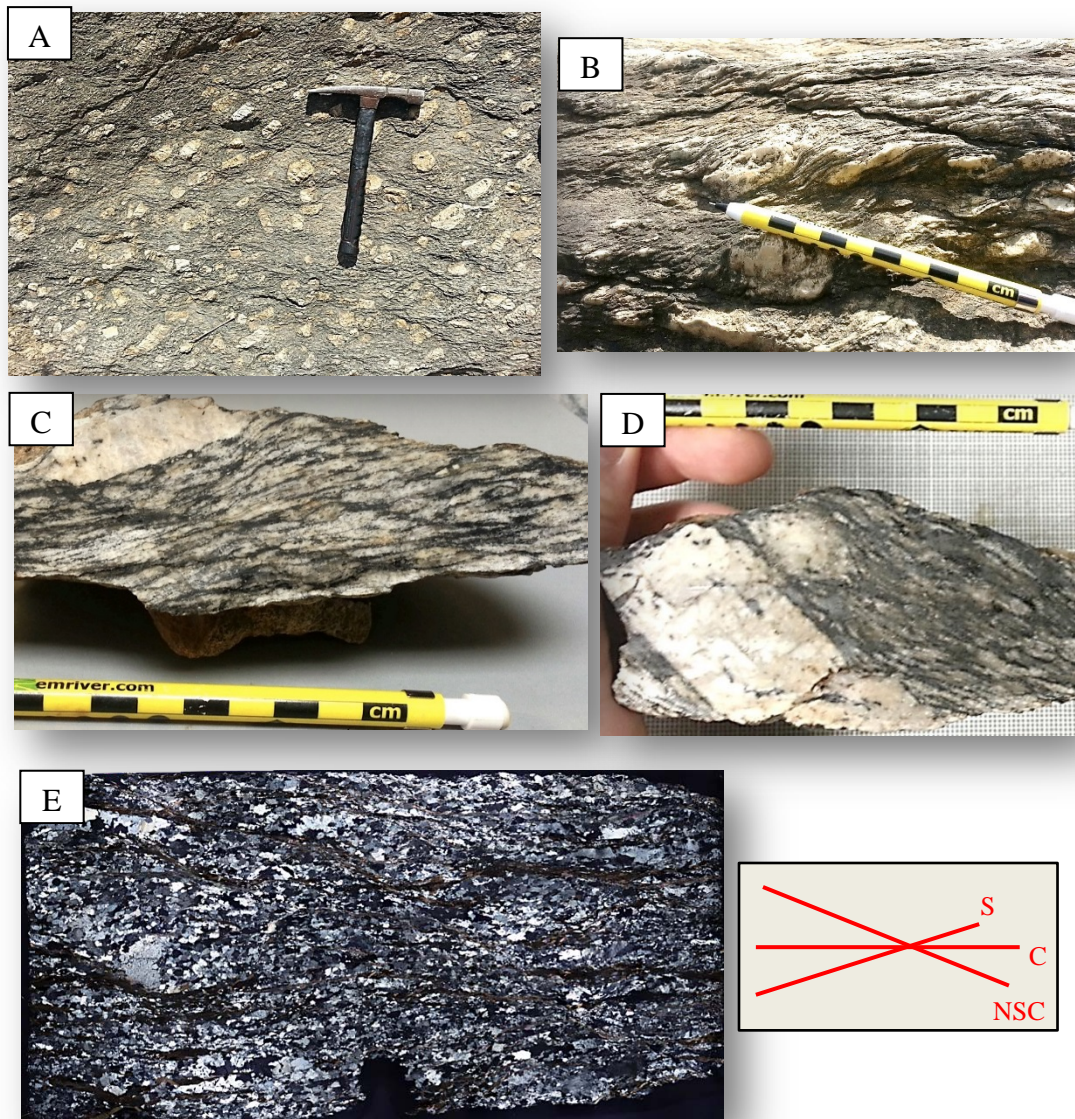


Figure 7. Kowaliga Gneiss (32° 58' 35.26" N, 85° 51' 10.17" W). A) Megacrysts (upwards of 5 cm in length) of potassium feldspar. B) Asymmetric potassium feldspar augens. C) Large feldspar augen within S-C-NSC fabric. D) Zoned, minimally sheared euhedral to subhedral potassium feldspar grain adjacent to asymmetric augens and intensely developed shear fabric. E) Photomicrograph mosaic in cross-polarized light displaying S-C-NSC structures.

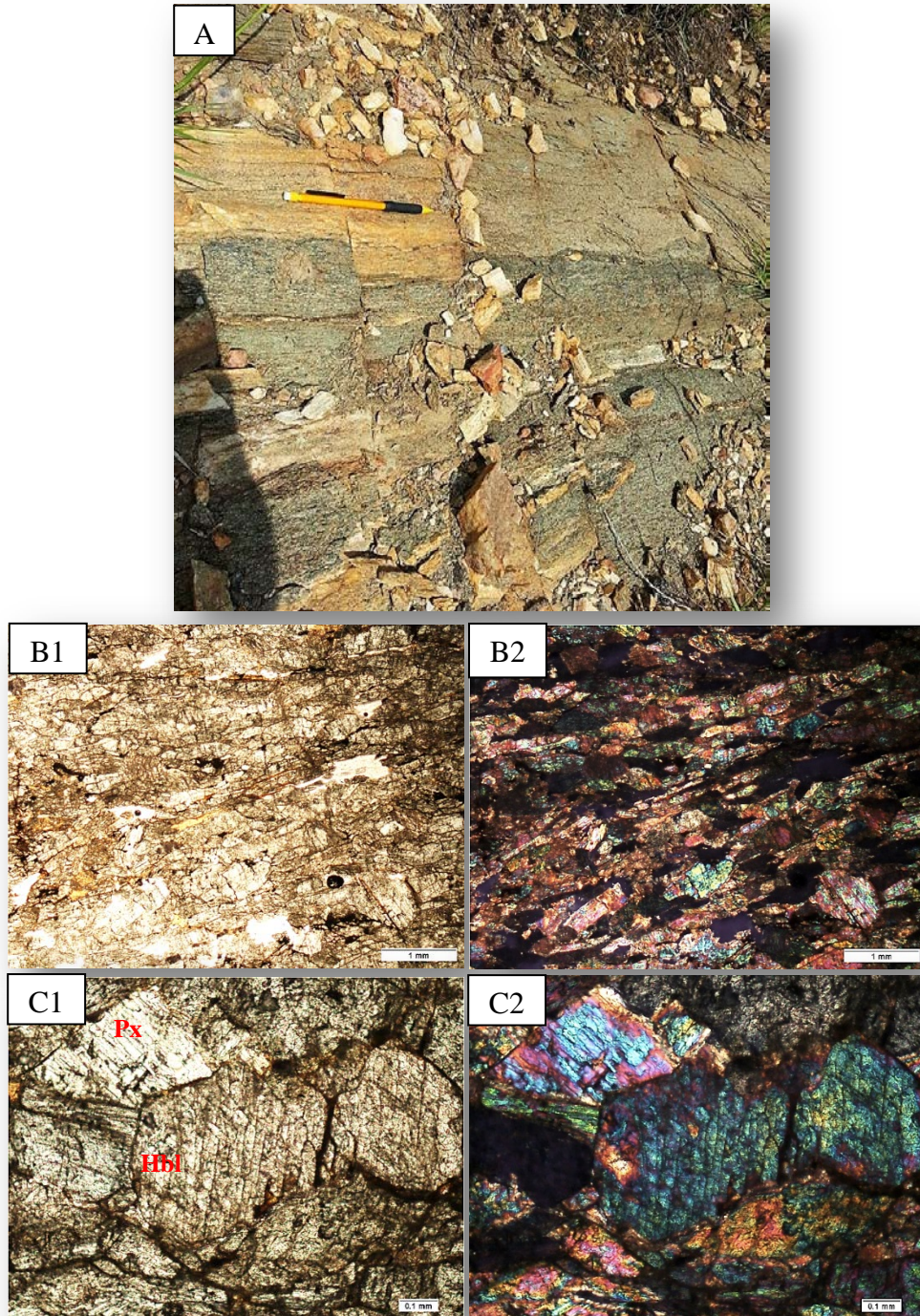


Figure 8. Greenstone pod within the Kowaliga Gneiss. A) Amphibolite/greenstone and quartzo-feldspathic (meta-rhyolite/dacite protolith?) with high-angle brittle fault offsets (see text). B1) Photomicrograph in plane-polarized light and B2) in cross-polarized light of lepidoblastic foliation defined by aligned pyroxenes and elongated amphiboles. C1) Photomicrograph in plane-polarized light and C2) in cross-polarized light of pyroxenes having altered to amphibole.

are medium-grained and vary from massive to foliated with the lepidoblastic foliation defined by elongated amphibole, pyroxene, and plagioclase (Fig. 8B1 and B2). The more felsic meta-rhyolite/dacite layers are fine- to medium-grained, strongly lineated, and contain quartz, muscovite, and feldspar. Xenoliths of meta-rhyolites and greenstones within the Kowaliga Gneiss are no younger than 440 Ma (intrusive of Kowaliga Gneiss). These, therefore, could be a similar age as the 470 Ma Hillabee and Pumpkinvine Creek volcanics to the northeast and further down-section (McClelland et al., 2007).

Pods of a felsic granitic gneiss occur near the core of the Emuckfaw Group that contrastingly contain few biotite grains compared to the Kowaliga Gneiss, and they also have abundant muscovite. These gneissic pods have a weak foliation and strong lineation and they are more evenly grained than typical Kowaliga Gneiss, but are interpreted to be part of the same lithostratigraphic unit.

Cataclastic Zone (CZ)

A cataclastic zone coincides with the Abanda fault, separating the eastern Blue Ridge from the Jacksons Gap Group throughout most of the quadrangle (Plate 1). They occur in multiple splays primarily trending NE-SW (Hawkins, 2013; Steltenpohl et al., 2013; Abrahams, 2014). Cataclastic rocks defining these tabular bodies contain subrounded to angular, randomly oriented clasts of varying sizes (from 1 mm to 2.5 cm) and compositions that are well cemented. There are varying types of cataclastic rocks containing clasts of mostly quartz, feldspar, and rare lithic material; however, some contain clasts of other cataclastics/breccias. The agent of cementation also varies from predominantly vascular silica-rich fluids, to a fine-grained, fault-gouge matrix.

At least three types of cataclastic rocks are observed within these zones. Type I has colorful clasts ranging from a light tan, bright brick-red, to brown (Fig. 9). These are riddled with interstitial quartz veins that completely isolate individual clasts, and in thin section, the quartz displays a wide-range of grain sizes (Fig. 9). Type II has a very dull, earthy-tan color with small interstitial quartz veins (Fig. 10). These are typically clast supported, with quartz veins separating individual clasts in only few cases (Fig. 10). Type III has a colorful matrix and clasts, ranging from yellow, light-orange, brick-red, to brown (Fig. 11). The clasts contained in this type are matrix supported and are conspicuously rounded, showing evidence for a polyphase history, with clasts including brecciated and veined clasts from an earlier event (Fig. 11).

Although there are at least three types of cataclastic rocks (described above), these types are not unique to any particular outcrop, and occur together within the same outcrop. No preference or order has yet been established to the different types. Although there are varying types of cataclastics rocks, all are siliceous, appearing to have been almost entirely flushed with fluid causing silica replacement, except for sparse feldspars and some fine-grained muscovite and sericite. In addition to the cross-cutting quartz-filled fractures, other microstructures include undulatory, polycrystalline quartz, and in some samples, significant volumes of microcrystalline quartz filling interstitial spaces between the larger grains.

Generally, the cataclastic zones form narrow, erosionally resistant ridges that locally have been quarried for road metal, “borrow pits.” Their origin is not exactly understood. They appear to be subvertical to vertical based on their topographic relief and curvilinear to linear trend in map view. In-situ measurements prove difficult to acquire

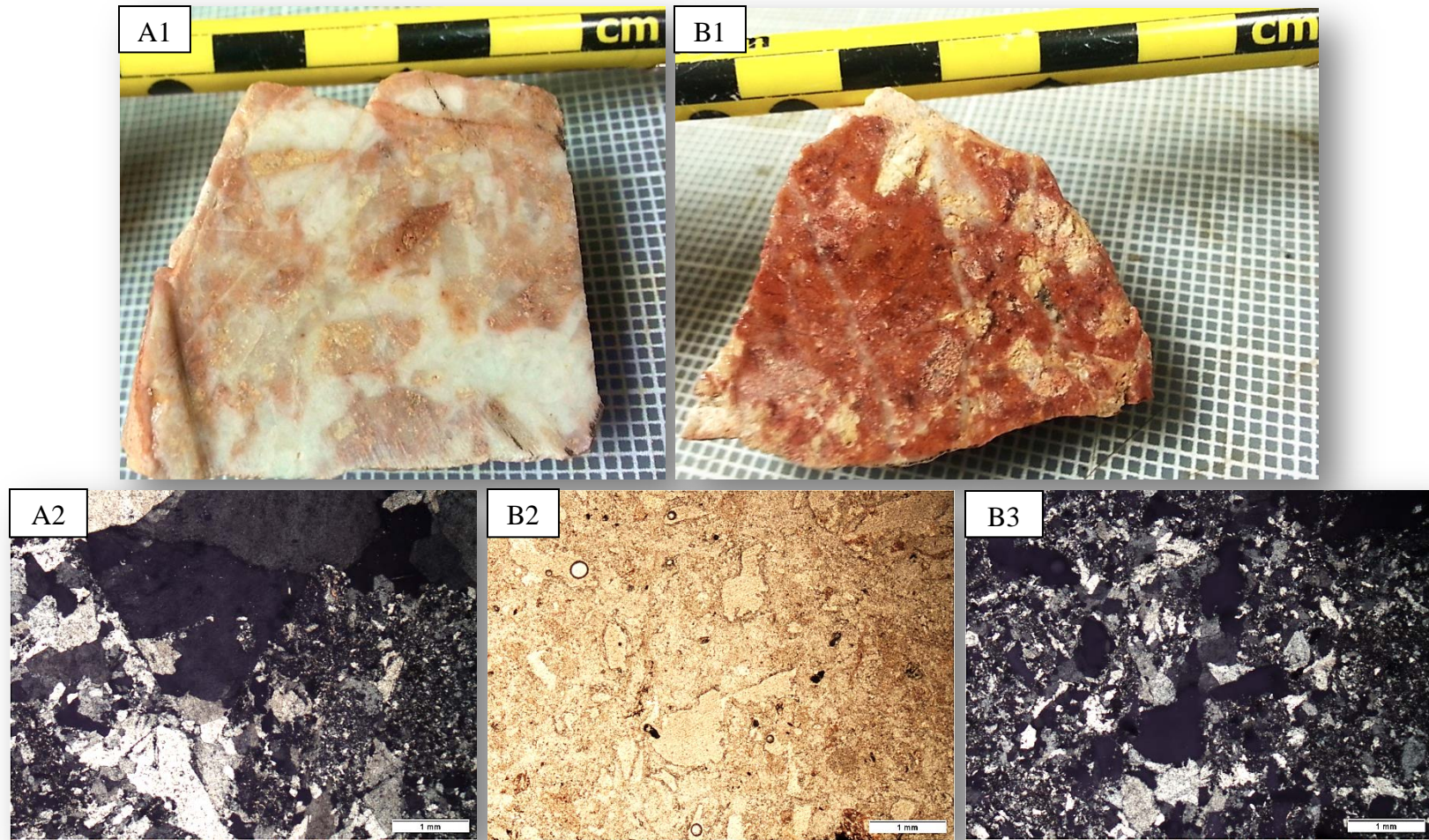


Figure 9. Type I cataclastic rock. A1. and B1) slabbed and polished hand samples. Note the variance in colors and the separation of individual clasts by the vein quartz. A2) Photomicrograph in cross-polarized light of A1. B2) Photomicrograph in plane-polarized light and B3) in cross-polarized light of B1. showing a wide variance in grain size of polycrystalline quartz.

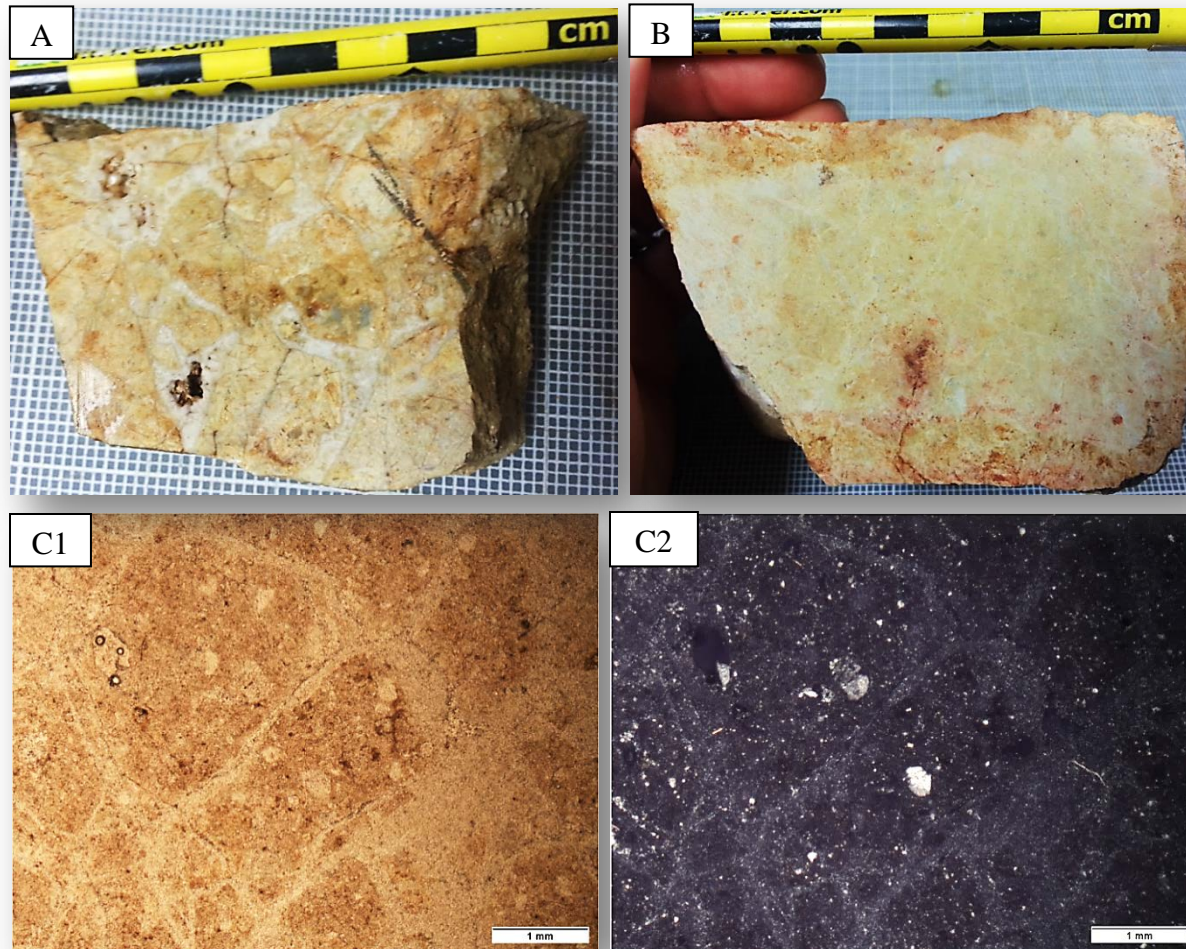


Figure 10. Type II cataclastic rock. A. and B) slabbed and polished and samples. C1) Photomicrograph in plane-polarized light and C2) in cross-polarized light of C1.; relict breccia clasts separated by the vein quartz; however, nearly everything has been completely replaced by silica.

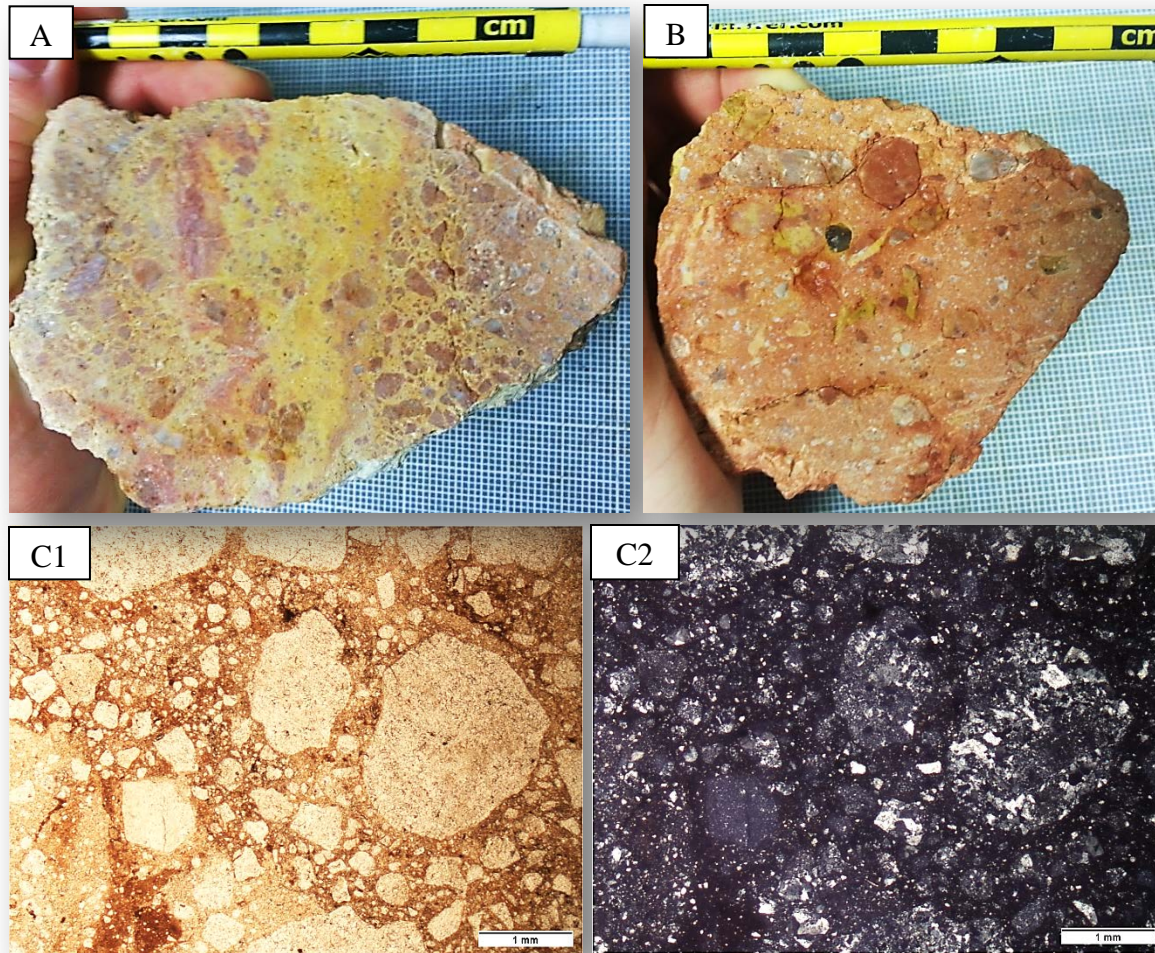


Figure 11. Type III cataclastic rock. A. and B) Hand samples. C1) Photomicrograph in plane-polarized light and C2) in cross-polarized light of C1.; relict breccia clasts that are matrix supported with rounded clasts and effectively complete silica replacement.

due to the lack of any planar penetrative fabrics. They are tabular zones but do not appear to truncate recognizable or displace units that they cut. In general, the zones weather to a light creamy pink/tan color with tinges of orange and maroon.

JACKSONS GAP GROUP

Within the study area, the Jacksons Gap Group is informally divided into, at least, seven mappable units: garnetiferous phyllite; micaceous quartzite; garnetiferous graphitic phyllite; garnetiferous quartz schist; carbonaceous phyllite; massive quartzite; sericite-chlorite phyllite; and porphyroclastic mylonite. The group contains polydeformed phyllonitic and mylonitic units that pinch and swell along strike, and are stretched, faulted, and folded, so no stratigraphic order is intended in the text below (Raymond et al., 1988). The following descriptions are in structural order from bottom to top.

Garnetiferous Phyllite (JGgp)

The garnetiferous phyllite is the most common basal unit of the Jacksons Gap Group, and is typically phyllonitized along the Abanda fault. This unit is a fine- to medium-grained, well-foliated, garnetiferous (with garnets 1-5 mm) quartz-biotite-chlorite-muscovite phyllite with strongly developed phyllonitic textures and minor graphite, unidentified opaque minerals, and trace epidote (Fig. 12). It is locally graphitic (up to ~15% modal abundances). In outcrop, the unit is tan to dark olive-green/brown, with a locally gray graphitic sheen (Fig. 12A). Light olive-gray to light gray-orange phyllonite contains 1-5 mm pre- and syn-kinematic garnets, S-C composite-planar fabrics, and asymmetric z-folds of the phyllitic cleavage recording oblique-dextral

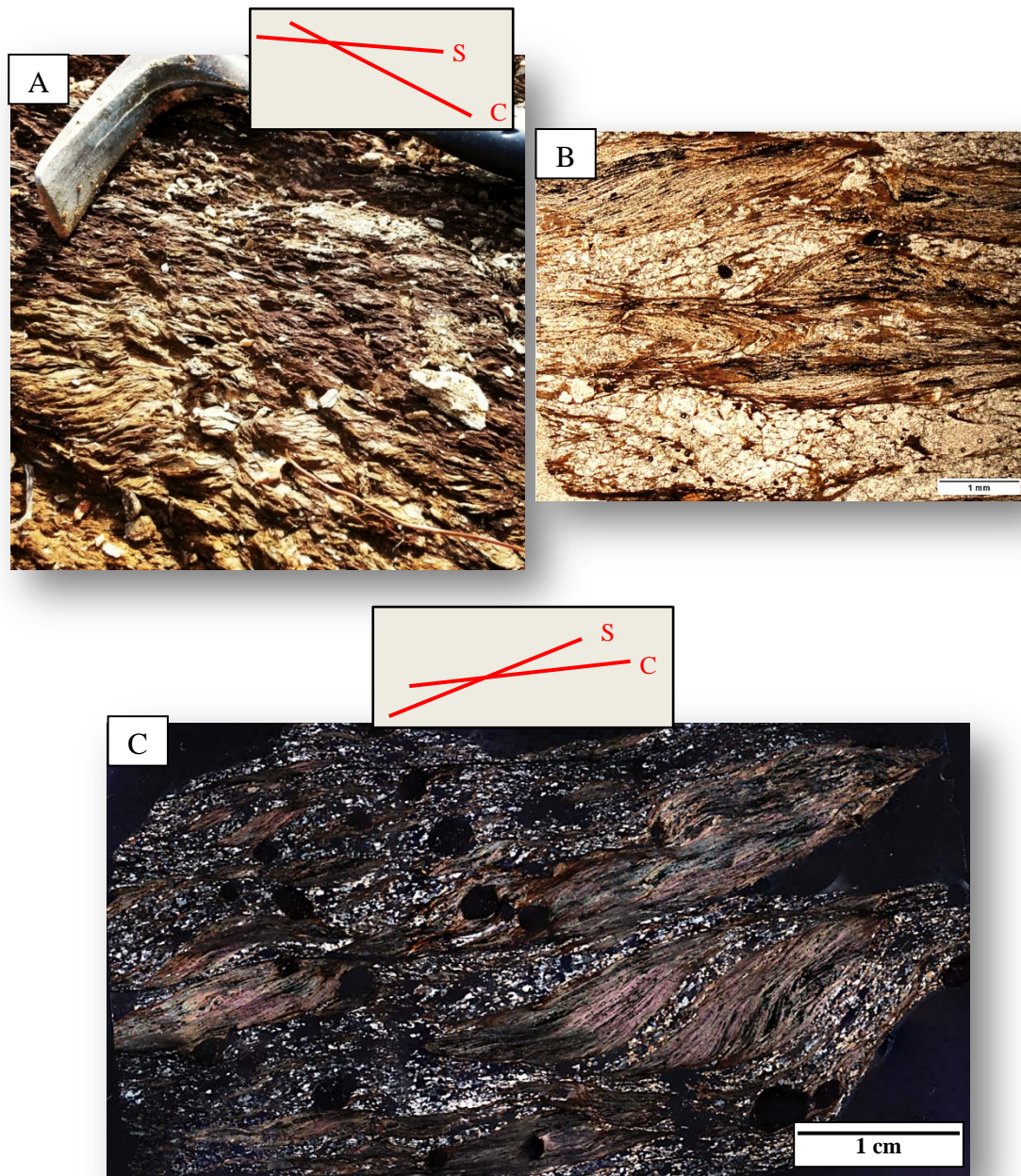


Figure 12. Garnetiferous phyllite of the Jacksons Gap Group. A) Outcrop photo of phyllonite displaying S-C fabric. View slightly oblique to S-C intersection. B) Photomicrograph in plane-polarized light; micro-scale z-folds, kinking, and stacking within micaceous phacoids, highlighted by minor graphite. C) Photomicrograph mosaic in cross-polarized light. Muscovite phacoids and composite phacoids duplexed/stacked atop one another.

normal-slip movement with local reverse-slip components (Figs. 12B and C). Quartz-rich pressure shadows around garnets have sigmoidal tails in thin-section that further support dextral shear (Fig. 12). Composite muscovite phacoids outline S-C fabrics and contain internal deformation features such as polycrystalline quartz, undulatory muscovite, and kinked, folded, and duplexing/stacking of grains (Fig. 12C). The phyllonite weathers into small (~1-3 cm), phacoidal shaped chips (buttons) that litter the outcrop (Fig. 12A).

Thinly laminated, tabular/flaggy metaquartzites (Fig. 13) are commonly interlayered within the garnetiferous phyllite. Quartzite layers are locally medium- to coarse-grained, conglomeratic, and micaceous (Fig. 13). The contact between the garnetiferous phyllite of the Jacksons Gap Group and the underlying Emuckfaw Group and Kowaliga Gneiss is defined by the Abanda fault, which is paralleled by a cataclastic zone throughout the entire quadrangle, as shown on Plate 1.

Micaceous Quartzite (JGpq)

Overlying the garnetiferous phyllite is micaceous quartzite, which is a fine- to coarse-grained, well-foliated, moderately mature, mylonitic quartzite with varying amounts of muscovite, sericite, chlorite, and accessory feldspar, epidote, biotite, graphite, and unidentified opaques (Fig. 14). A phyllitic cleavage is defined by parallel muscovite and sericite, and grain size varies with elongation in the C-plane. Micaceous quartzite commonly forms distinct, sharp ridges of relatively higher relief making them easily mappable throughout the study area. The unit is very light creamy-tan in color and has a phyllitic, papery texture, weathering to blade-like chips.

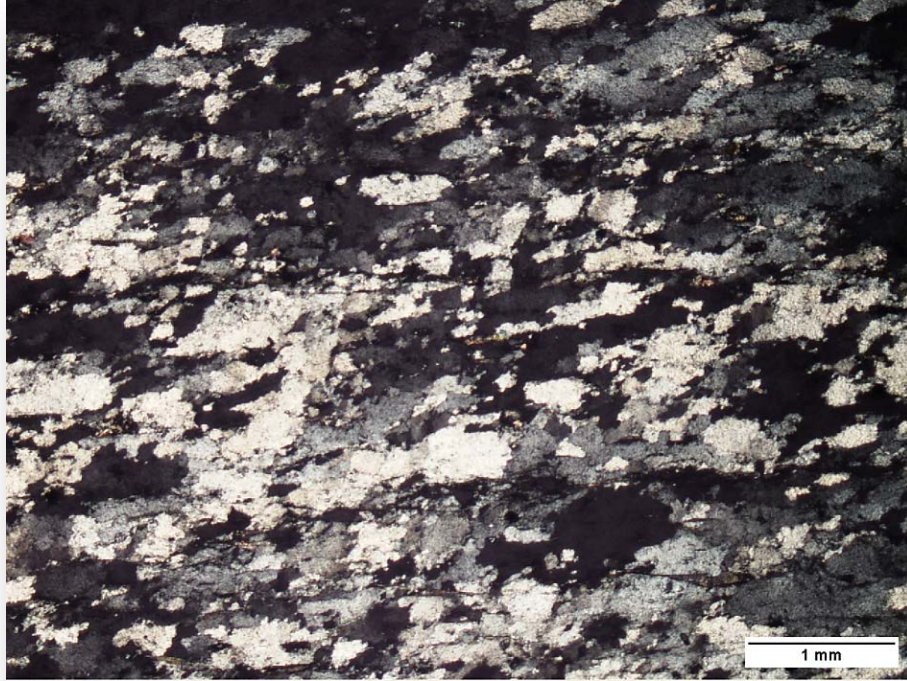


Figure 13. Photomicrograph in cross-polarized light of the flaggy, “clean,” mylonitic quartzite interlayered within the garnetiferous phyllite.

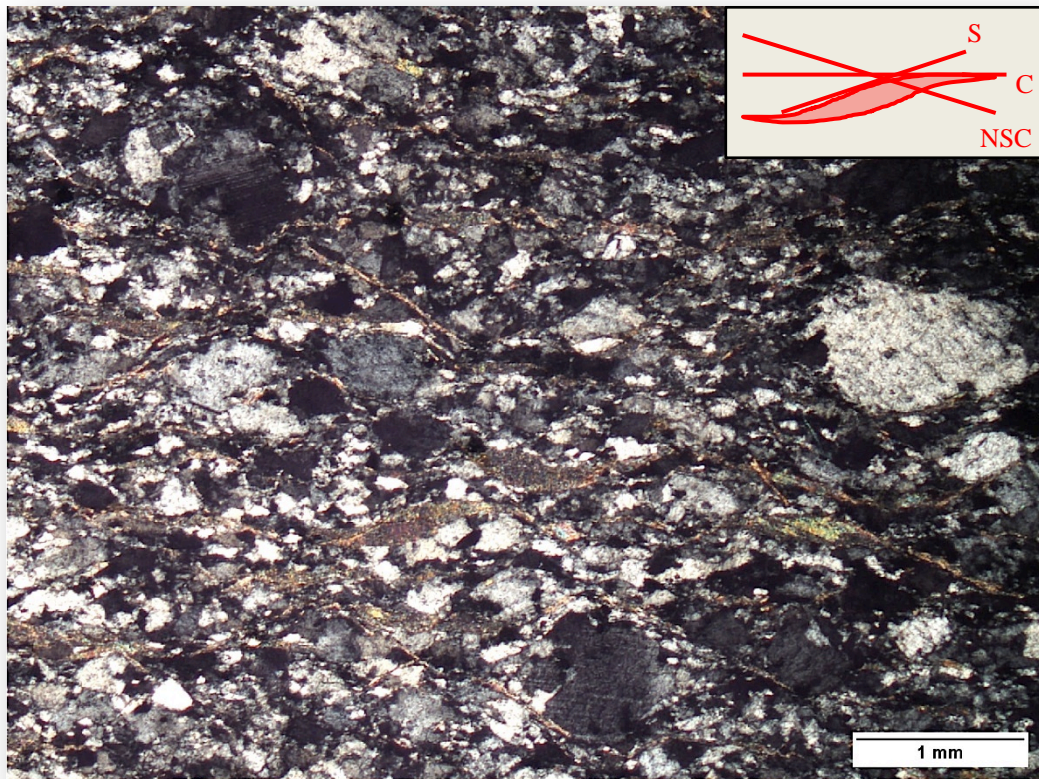


Figure 14. Photomicrograph of micaceous quartzite in cross-polarized light. Muscovite and sericite outline micro-shear structures and also form phacoids indicative of dextral shearing in this unoriented view.

The contact between the micaceous quartzite and the enveloping phyllitic units is generally gradational over ~3 cm and is marked by resistant, sheared phyllitic quartzites (Fig. 15A), which was noted by Abrahams (2014) on the Dadeville Quadrangle (Fig. 2). Further up structural section, the micaceous quartzite reappears and is interlayered with locally graphitic phyllites/phyllonites and schists (Fig. 15B). Alternating layers of fine- to medium-grained quartzite and graphite-muscovite phyllite are locally folded into sharp-hinged and straight-limbed z-folds (Fig. 15C). Phyllites within micaceous quartzite vary in quartz content (from ~30-45%) and locally contain high amounts of graphite (up to 50%). These graphitic phyllites resemble the garnetiferous graphitic phyllite, and if graphite exceeds ~40%, also the carbonaceous phyllite. Due to fine-scale interlayering (from 2 cm to upwards of 1 m) of these units, they are not always separable at map-scale, so in these cases, the more abundant lithology is represented on the map (Plate 1).

Garnetiferous Graphitic Phyllite (JGgpp)

Overlying and locally interlayered with the micaceous quartzite is garnetiferous graphitic phyllite, which constitutes the majority of phyllites in the middle portions of the Jacksons Gap Group. The garnetiferous graphitic phyllite is typically fine-grained, locally phyllonitized, locally garnetiferous, well foliated, and interlayered with sericitic quartzite (Figs. 16 and 17). Mineral constituents include muscovite, quartz, graphite, sericite, chlorite, biotite, and small (2-3 mm) garnets (Figs. 16 and 17). Locally the unit contains coarser micas such that it becomes a schist rather than a phyllite. Fresh outcrops are typically light-gray to brown, with a lustrous, bluish-colored, graphitic sheen (Fig. 16).

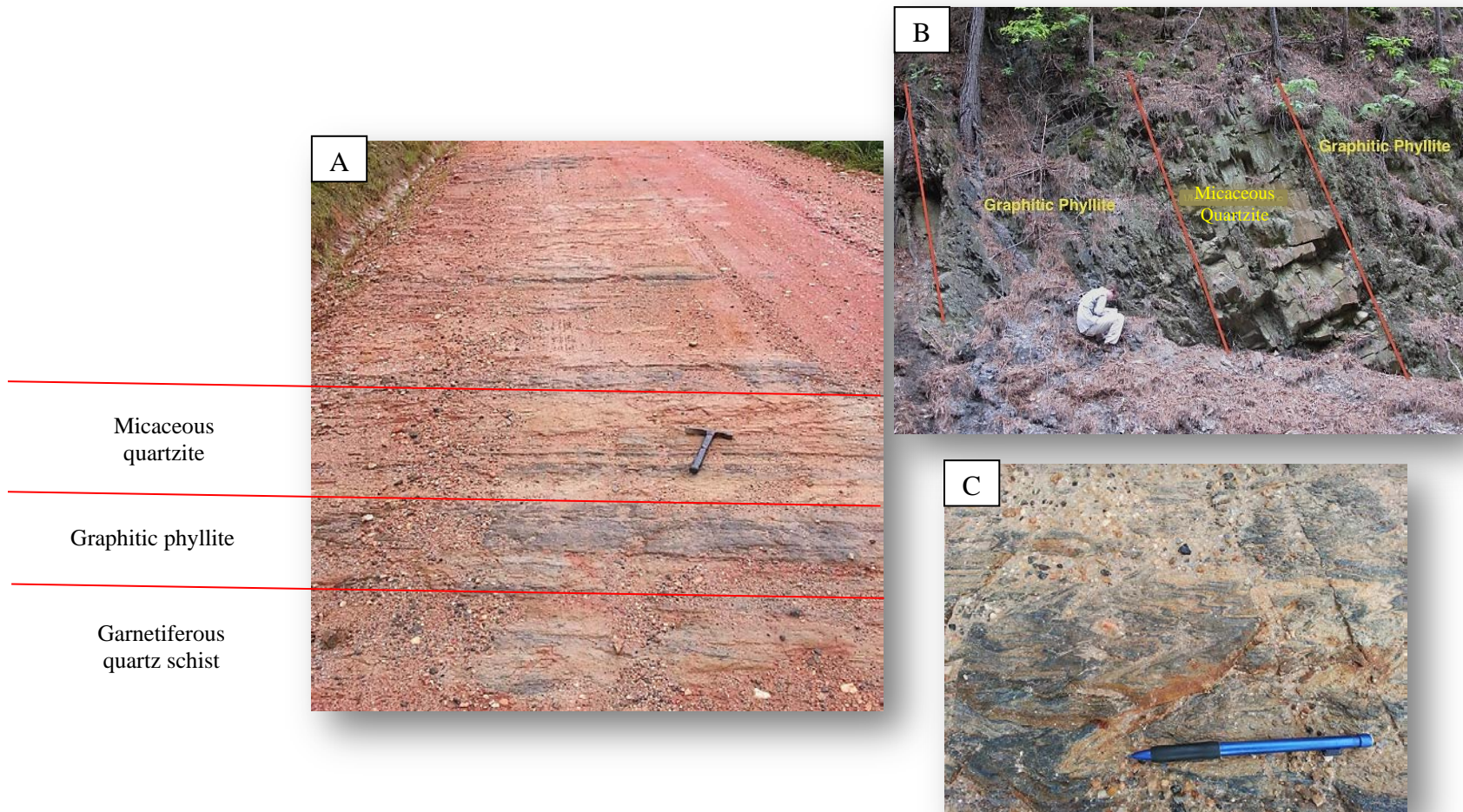


Figure 15. Interlayering within the Jacksons Gap Group. A) Interlayered micaceous/phyllitic quartzite, graphitic phyllite, and garnetiferous quartz schist ($32^{\circ} 55' 2.90''$ N, $85^{\circ} 47' 17.09''$ W). B) Outcrop of the Jacksons Gap Group with interlayering of units that is too fine-scale to differentiate at map-scale ($32^{\circ} 52' 57.36''$ N, $85^{\circ} 49' 6.10''$ W). C) Fabric deforming z-folds, view is down-dip of foliation and down-plunge of hinge lines.



Figure 16. Outcrop of the garnetiferous graphitic phyllite displaying S-C fabrics and z-folds.

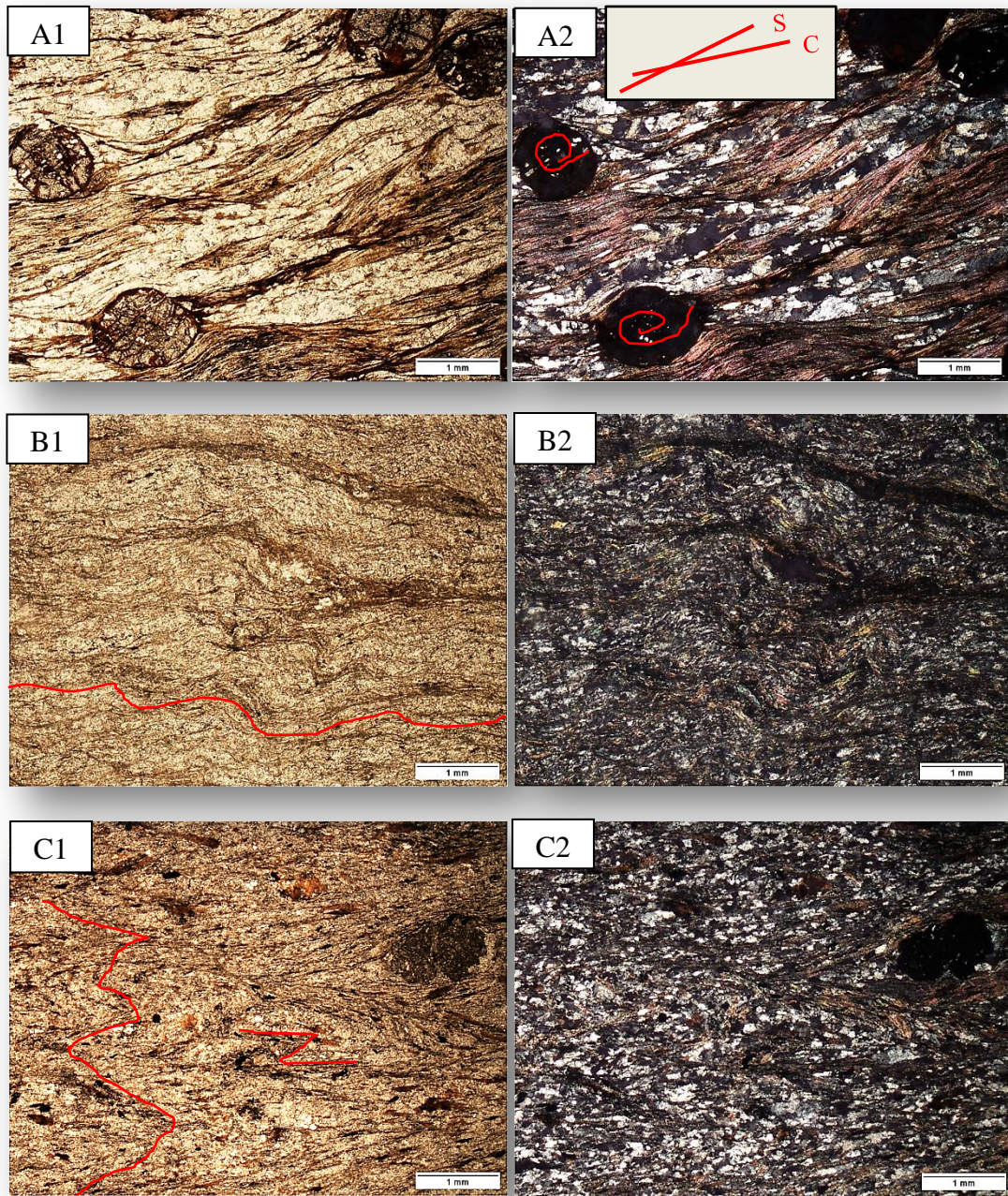


Figure 17. Photomicrographs of garnetiferous graphitic phyllite of the Jacksons Gap Group (1. plane-polarized, 2. cross-polarized light). A) Quartz and muscovite inclusion trails within syn-kinematic “snowballed” garnet, with asymmetric pressure shadows indicating dextral-shear. B) Crenulations highlighted by micas. C) Z-folds marked by micas.

This unit is dextrally sheared, locally well lineated, with highly crenulated portions. Other portions have strong z-fold development, when viewed slightly obliqueto down-dip, verging closely along strike and contain pre- to syn-kinematic garnets (Fig. 17), and some portions are more of a button-schist. Thin (less than 10 cm), asymmetrically folded quartzite ribbons/layers anastomose along strike causing them to appear and disappear, forming phacoidal boudins. The phyllite weathers to an olive-brown, gray, to brick-red-orange color with a glittery shimmer from abundant micas.

Garnetiferous Quartz Schist (JGgqs)

Adjacent to and locally interlayered with the garnetiferous graphitic phyllite and micaceous quartzite is garnetiferous quartz schist, which comprises a significant volume of the central part of the Jacksons Gap Group. The garnet-quartz schist is fine-grained, well-foliated, and conspicuously planar/flaggy layered. It is a garnetiferous, quartz-rich muscovite and sericite schist that is typically gray, olive-brown, to light-orange in color in relatively fresh sample (Figs. 18). Its primary mineral constituents are fine-grained muscovite, sericite, and quartz, with accessory garnet, biotite, graphite, and chlorite. Thin (~3 cm thick), relict, fining-upward, graded beds are common, with the base of beds a lighter color due to a higher, generally coarser-grained, quartz content that grades into more abundant finer-grained material, mostly micas (clay protoliths), as the color darkens (Figs. 18A and B). Micro S-C fabrics, thin (up to 2 mm thick) graphitic lenses, crenulations (Fig. 18C), and m-type folds (Fig. 18D) are locally present. This unit weathers to a light olive-orange, sandy, saprolite with a glittery shimmer due to the high concentrations of micas.

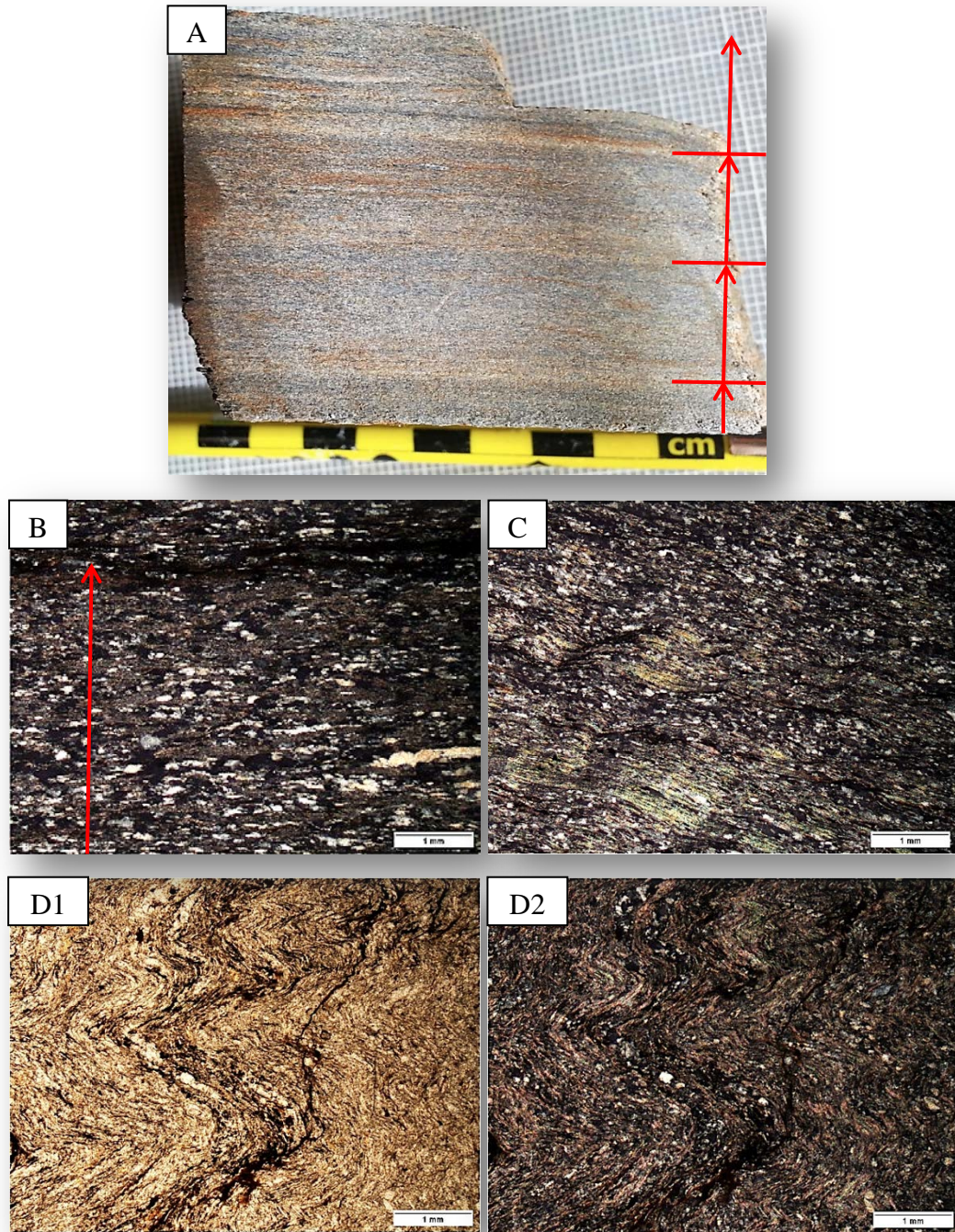


Figure 18. Garnetiferous quartz schist. A) Cut hand sample. Horizontal lines mark abrupt contacts of layers and arrows denote the fining upward direction. B. C. and D) photomicrographs (1. plane-polarized light and 2. cross-polarized light). B) Cross-polarized light with arrow indicating fining-upwards direction. C) Cross-polarized light, weak crenulations with associated muscovite, sericite, and retrograde chlorite. D) M-folds, view is slightly oblique to down-dip.

Carbonaceous Phyllite (JGcp)

Interlayered with garnetiferous graphitic phyllite is the carbonaceous phyllite. This unit is a fine-grained, well-foliated phyllite that is dusky-blue-maroon-black in color with a distinctive graphitic sheen in fresh outcrop (Fig. 19). The unit contains very fine- to fine-grained graphite, quartz, and muscovite with accessory biotite, chlorite, unidentified opaques, and is locally garnetiferous (up to 15%). Highly carbonaceous varieties (upwards of 50% graphite) are very distinct. Due to the remarkably high amount of graphite present, this unit is structurally weak and has accommodated a great deal of the strain within in the Jacksons Gap Group. The carbonaceous/graphitic phyllite anastomoses along strike, with shearing forming lenticular layers.

The overall fabric of the rock is predominantly defined by S-C-NSC fabrics (Fig. 19) and z-folds. Along with S-C, NSC, and z-folds, this unit contains pre- and syn-kinematic garnets, and thin (up to ~10 cm) anastomosing quartzite layers. Locally, relict bedding is oblique to the metamorphic/mylonitic fabric (Fig. 19B).

Massive Quartzite (JGmq)

Also interlayered with phyllitic units of the Jacksons Gap Group are massive quartzites. These quartzites are thick-bedded, massive, white-to-tannish-yellow, fine- to medium-grained, and weakly-to moderately-foliated (Figs. 20 and 21). They contain quartz and minor muscovite, chlorite, sericite, biotite, kyanite, staurolite, and garnet (Fig. 20). Massive quartzite is a prominent ridge former with sharp boundaries against adjacent phyllites, but the units are discontinuous along strike due to a combination of structural and facies changes. This unit preserves cross-beds (Fig. 21), documenting stratigraphic

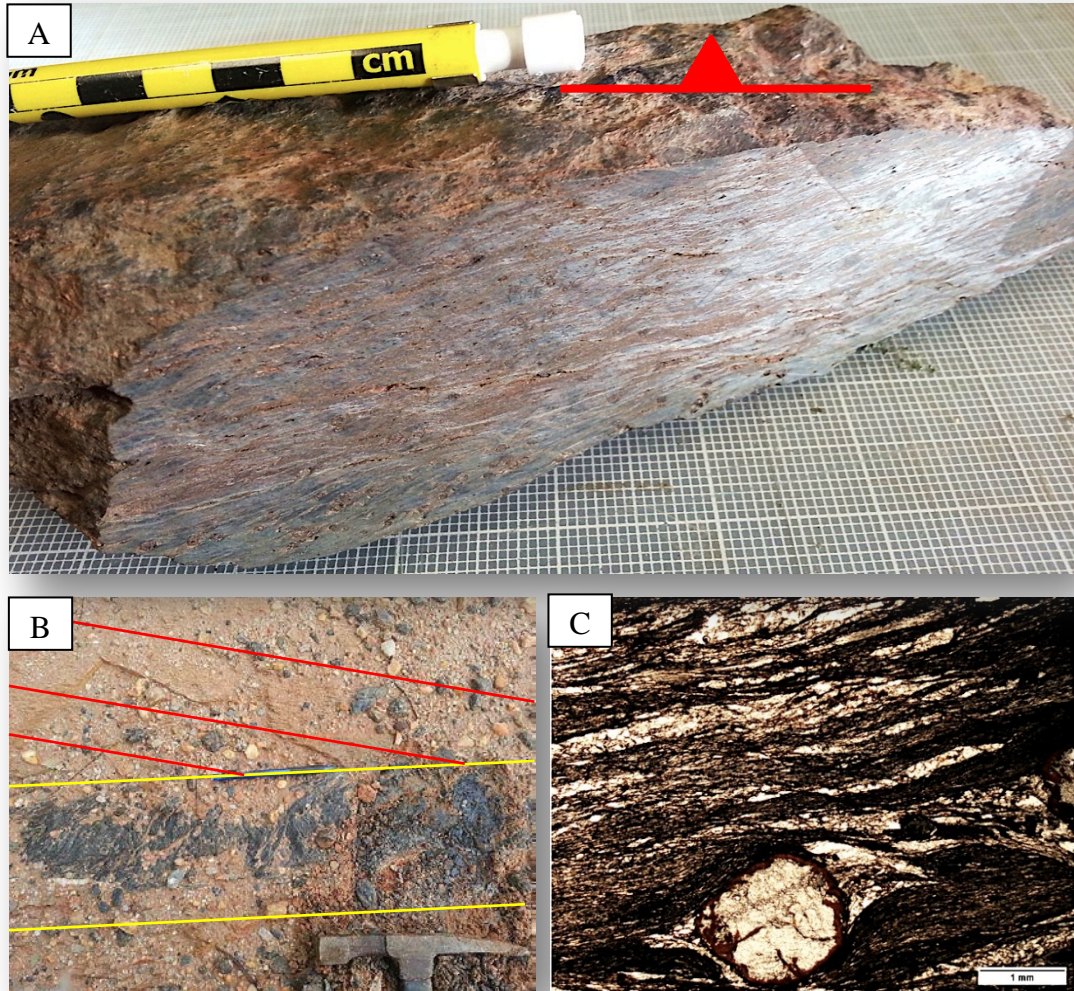


Figure 19. Carbonaceous phyllite. A) Cut and polished hand sample with S-C and NSC fabric and crenulations, indicative of oblique dextral shear. View is oblique to strike and dip. B) Relict bedding (S_0) (yellow) contact oblique to metamorphic/mylonitic foliation (S_1) (red). C) Photomicrograph in plane-polarized light showing high abundance of graphite present and a pre-kinematic garnet with asymmetrical pressure shadows symbolizing dextral shear, and retrogressive alteration around the grain boundary. View is oblique to strike and dip.

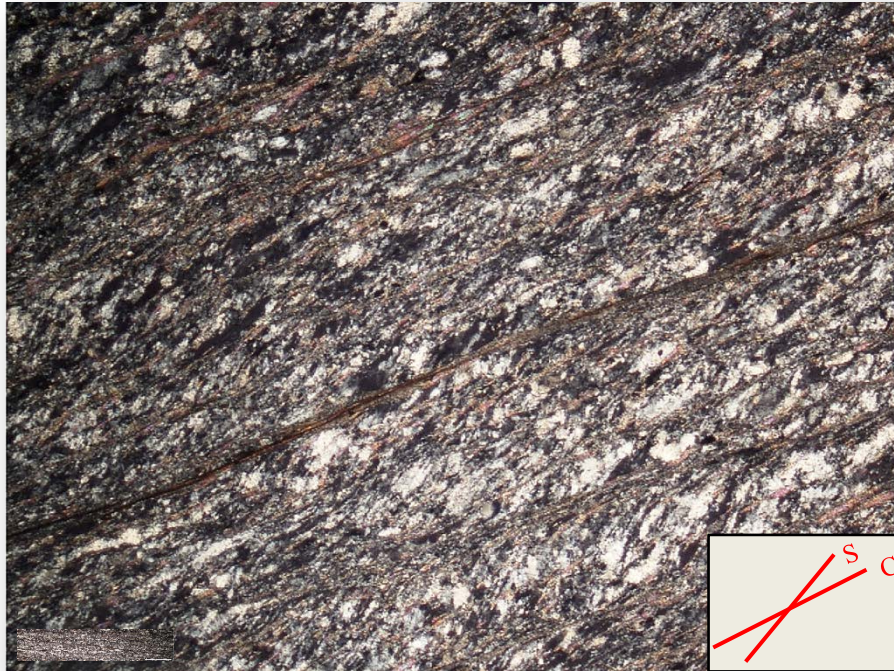


Figure 20. Massive quartzite in cross-polarized light. Micas highlight dextral S-C fabrics and discrete shear bands. View is perpendicular to lineations and down the S-C intersection.

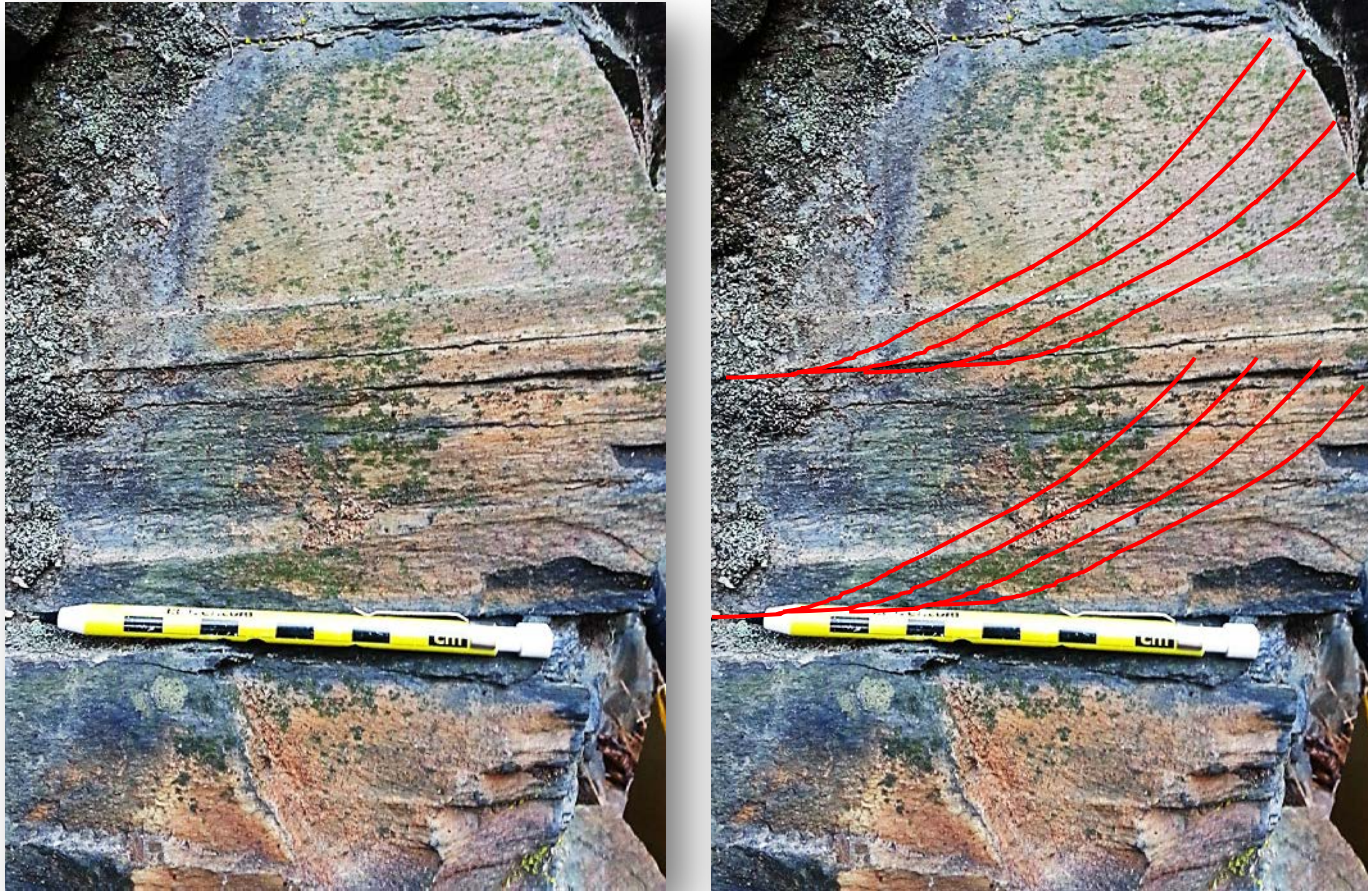


Figure 21. Outcrop of the massive quartzite showing relict cross-bedding. View is down-dip of foliation.

“up” direction, which indicate that the rocks are upright where observed. The unit tends to be coarser and “dirtier” (i.e., metagraywacke) on the margins and grades to a finer-grained, relatively “cleaner” and well-lineated metagraywacke towards the core of the unit (Fig. 20). Composite S-C fabrics are observable in thin section with composite phacoids of subgranular quartz highlighted by muscovite, sericite, and chlorite (Fig. 20). This unit weathers to a creamy, light-tan to orange color.

Sericite-Chlorite Phyllite (JGscp)

Structurally overlying and interlayered with the packages of the phyllites and quartzites, sericite-chlorite phyllite locally forms the upper-half of Jacksons Gap Group. The phyllite is fine-grained, well-foliated, lustrous, and locally phyllonitized with a conspicuous green tinge. It contains muscovite, sericite, chlorite, quartz, garnet, and chloritoid, and is locally graphitic (see also Abrahams, 2014). S-C fabrics, z-folds, and transposed crenulations are common in the phyllite (Fig. 22). In fresh outcrops, the unit tends to be a light olive-green-silvery gray to dark yellowish-green, and it weathers to a dusky brick-red saprolite with a glittery shimmer from its high mica content. Button-shaped chips litter the base of outcrops.

Porphyroclastic Mylonite

Near the top of the Jacksons Gap Group lies a porphyroclastic mylonite too thin (< 5 m) to depict on Plates 1 and 2. Slightly weathered exposures are dark-black-brown to orange-tan in color and are medium- to coarse-grained with biotite, muscovite, quartz, plagioclase, potassium feldspar, amphibole, kyanite, chlorite, chloritoid, and epidote (Fig.



Figure 22. Hand sample of the sericite-chlorite phyllite. The conspicuously green sheen is chlorite and a well-developed S-C fabric is evident.

23). The rock displays a gneissosity with dark bands of medium-grained minerals such as biotite and amphibole, with splotches of large, creamy white (less than ~ 1cm) feldspars, and thin (~1 mm) quartz ribbons. The unit is strongly mylonitized with a banded mylonitic foliation, asymmetric feldspar sigma and delta porphyroclasts, anastomosing quartz ribbons, muscovite and/or kyanite fish (some of which are kinked and stacked) with pressure shadows, and feldspars that are commonly zoned and display strain-related myrmekite growths (Fig. 23). The unit also appears to have undergone multiphase alteration and mineral growth phases with feldspars showing perthitic and antiperthitic textures, quartz replacement, large grains being replaced by clays, and later replacement by goethite. The rock weathers to a brown-olive to orange color, has a low-density, and is pitted, appearing to be highly altered. The occurrence of numerous, zoned feldspar porphyroclasts, varying grain sizes, rounded clasts, and intermediate mineral assemblage is interpreted as evidence for a volcanoclastic origin for the protolith.

Depositional Environment

The volume of quartzites enveloped gradationally by phyllites of varying graphite content may indicate that the Jacksons Gap Group was deposited in a shallow near-shore environment, such as a barrier island system with reducing/anoxic tidal (possibly volcanic) muds, or a submarine fan system. It most likely represents a back-arc basin deposited atop the Emuckfaw Group.

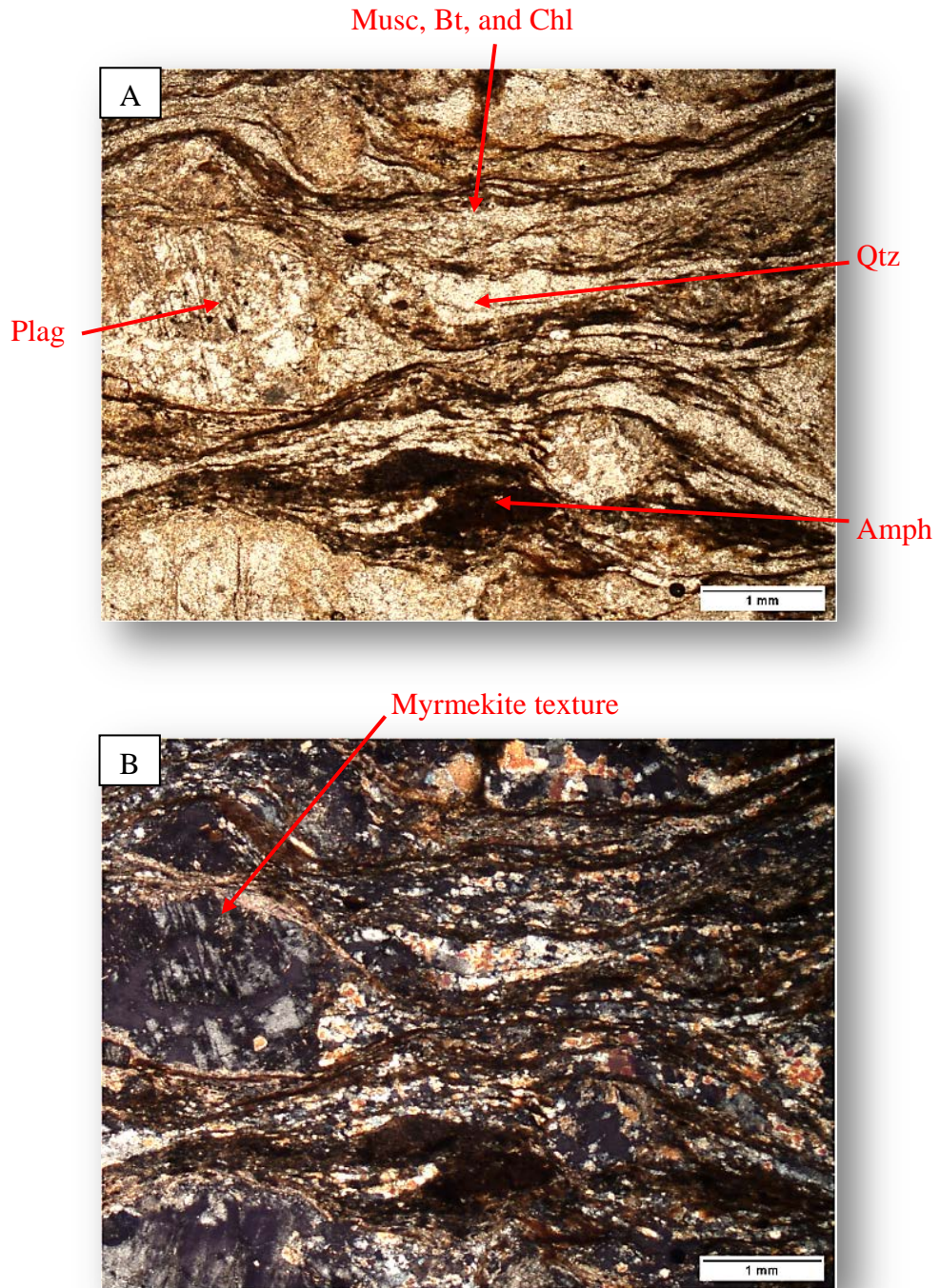


Figure 23. Photomicrographs of porphyroclastic mylonitic conglomerate. A) Plane-polarized light and B) cross-polarized light.

INNER PIEDMONT/DADEVILLE COMPLEX

The Dadeville Complex was emplaced atop of the Jacksons Gap Group along the Katy Creek fault. The structural order, from bottom to top, of Dadeville Complex units in the study area can be generalized into the Ropes Creek Amphibolite, Waresville Schist, undifferentiated mafic-ultramafic complexes, and the Agricola Schist (Raymond et al., 1988).

Ropes Creek Amphibolite (IDrc)

The Ropes Creek Amphibolite is the basal unit of the Dadeville Complex in the study area, typically in direct contact with the Jacksons Gap Group along the Katy Creek fault. It is a distinctive black in fresh outcrop, and is a medium-grained, well-foliated, and lineated amphibolite with varying amounts of hornblende, plagioclase, biotite, quartz, subhedral epidote, garnet, chlorite, unidentifiable opaques, sphene, and apatite. Local tonalitic layers are white-to-tan and are composed of feldspar, quartz, muscovite, biotite, amphibole, and sericite. The unit is locally cataclastic and/or mylonitic. Fresh exposures of this unit are uncommon within the study area. Most exposures are a reddish-orange to ochre saprolite that may retain measurable fabrics. The Ropes Creek Amphibolite is interpreted to have originally been lavas of an island-arc

Waresville Schist (IDws)

The Waresville Schist of the Waresville Formation most commonly occurs sheared together with rocks of the Ropes Creek Amphibolite, suggesting structural alteration of the Ropes Creek amphibolite into the Waresville schist. Compared to the Ropes Creek Amphibolite, the Waresville Schist is finer-grained, is greener colored in its weathered

form, and it has a more schistose rather than gneissic fabric. It is generally composed of muscovite, biotite, plagioclase, quartz, potassium feldspar, chlorite, and sericite with accessory opaques (Fig. 24). There are alteration halos present around the more mafic minerals along with secondary quartz. It is interlayered on a decimeter scale with a variety of amphibole-bearing schists, banded amphibolite with chlorite schist, chlorite amphibolite, chlorite-actinolite schist, chlorite-magnetite quartzite, and actinolite quartzite, and small (up to ~4 m wide) local ultramafic pods near the boundary with the mafic-ultramafic complex and Agricola Schist. The interlayered mafic and felsic schists are typically moderate-to-deeply weathered resulting in a light greenish-maroon-orange-tan to white, low-density, saprolite with micas retaining the rock fabric. The Waresville Schist is interpreted to be intermixed volcanics and volcanoclastics of felsic to mafic compositions and may be fringe deposits of an island arc.

Mafic-Ultramafic Complex (IDmum)

Small (less than ~0.75 km wide) mafic-ultramafic complexes occur generally at a consistent, predictable horizon near the contact between the Waresville Schist and the Agricola Schist. Rocks constituting mafic-ultramafic complexes generally are coarse-grained, dense, and peculiarly resistant to weathering, commonly forming clusters of boulders strewn about the topographic surface. The mafic-ultramafic complexes may comprise any of the following: enstatite metapyroxenite; hornblendite; garnet hornblendite; garnet-amphibole-pyroxene-actinolite-chlorite schist; layered actinolite-tremolite amphibolite altered locally to serpentine, anthophyllite, and talc; talc-actinolite schist; metanorite; metagabbro; and massive amphibolite. They are generally

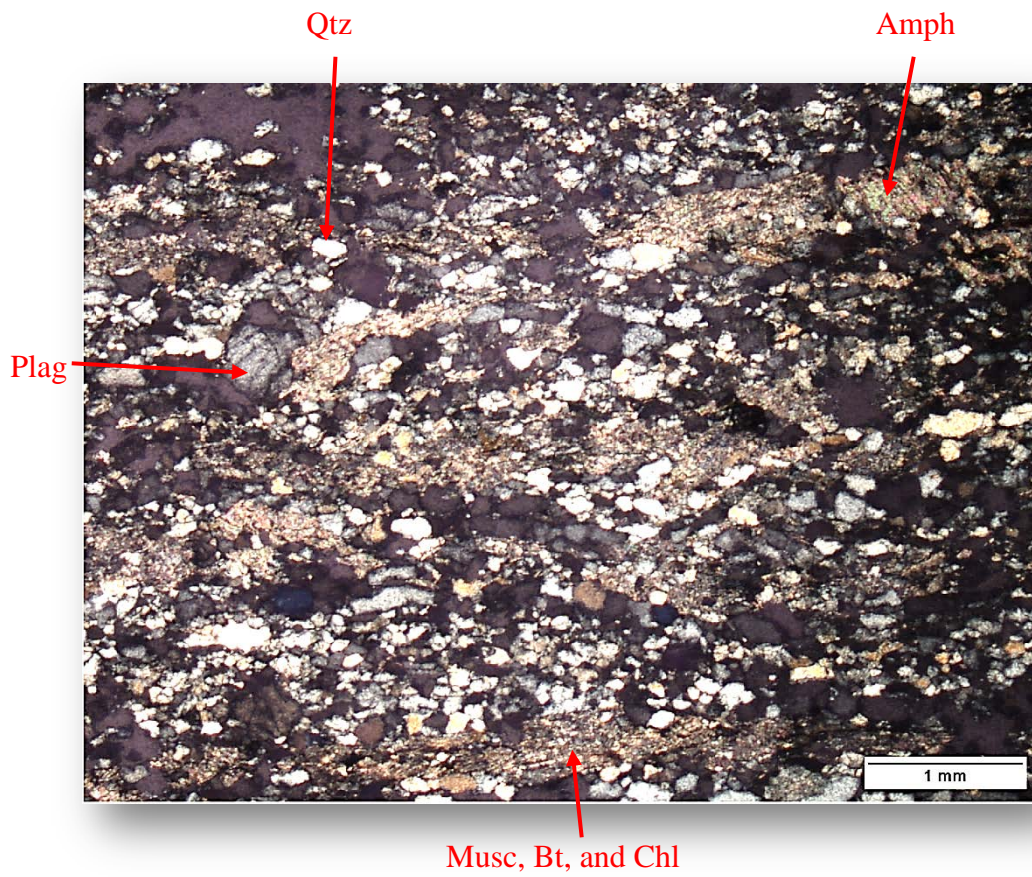


Figure 24. Photomicrograph in cross-polarized light of the Waresville Schist.

characterized by dark green-black, medium- to coarse-grained amphibole, clinopyroxene, orthopyroxene, actinolite, epidote, chlorite, biotite, and plagioclase, with minor amounts of garnet, sphene, chromite, magnetite, and opaques. The cores of the mafic-ultramafic complexes are predominantly composed of the metapyroxenite to peridotite, which is very coarse-grained and lacks evidence for strain and retains primary igneous textures (Fig. 25A). In this rock type, primary pyroxene defines a relict, layered cumulate texture with alteration to amphibole, chlorite, epidote, and actinolite; plagioclase occupies interstitial areas (Fig. 25B).

The margins of the complex are variably altered, due to the effects of shearing and metamorphic fluid activity. From the core of the complex towards the margins, the grain-size decreases and the cumulate pyroxenite/peridotite grades into either a moderately foliated and lineated amphibole-actinolite-pyroxene-biotite-chlorite schist (Fig. 25C), or a weakly foliated but strongly lineated metanorite/metagabbro/amphibolite (Fig. 25D). Both types of rim rocks show the effects of shear, such as retrogressive mineral alterations (pyroxenes to amphibole and biotite), bulging grain contacts between amphibole grains, plagioclase grains, and secondary quartz grains, weak S-C fabric development, and mineral elongation lineations. There is also an increase in deformed, disharmonically folded and ptygmatic quartz veins and sweat-outs closer to the margins. The ultramafic bodies within the Dadeville Complex contain platinum-group metal (PGM) deposits that are being investigated for their potential economic viability as this report was written. The mafic-ultramafic complex may have been the core of an island-arc.

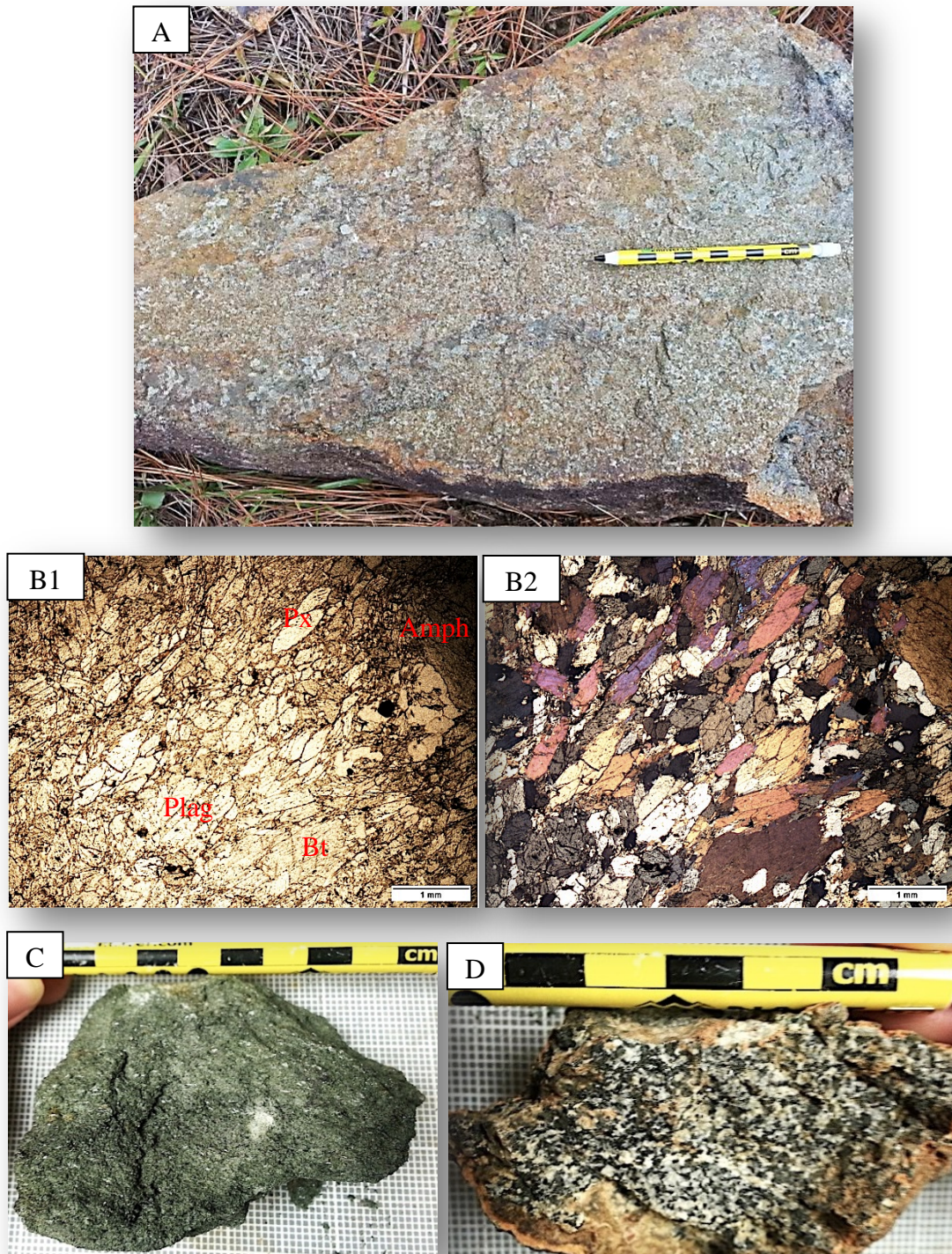


Figure 25. Mafic-ultramafic complex lithologies. A) Outcrop photo of pyroxenite displaying a layered cumulate texture. B) Photomicrographs of the pyroxenite. B1) plane-polarized light and B2) cross-polarized light showing a relict cumulate texture and a weakly developed foliation. Pyroxenes are altered to amphiboles, and secondary quartz is present. C) Amphibole-actinolite-pyroxene-biotite-chlorite schist. D) Lineated metanorite.

Agricola Schist (IDas)

The Agricola Schist is considered one of the structurally highest units of the Dadeville Complex, forming the core of the Tallassee synform. Fresh exposures are not common in the study area, but where exposed, fresh rocks occur as highly mylonitized and migmatized gneisses and schist (Fig. 26). Mylonitic foliation is defined by anastomosing thin (less than ~2 cm thick) felsic layers containing asymmetric porphyroclasts (Fig. 26). The predominant rock is fine- to medium-grained with biotite, muscovite, feldspar, quartz, chlorite, and pre- and syn-garnet with accessory sillimanite, staurolite, kyanite, chloritoid, and unidentified opaques. Syn-kinematic garnets contain rotational inclusion trails and both pre- and syn-kinematic garnets have asymmetric pressure shadows. The mylonitic schists are interleaved with thinly layered (up to ~1 m) mylonitic feldspar-hornblende amphibolite/gneiss and rare pegmatite pods/lenses. Generally, it weathers to an interlayered, light colored, reddish-brown-maroon saprolite. The Agricola Schist may represent the intermixing of lava and ash of an island-arc.

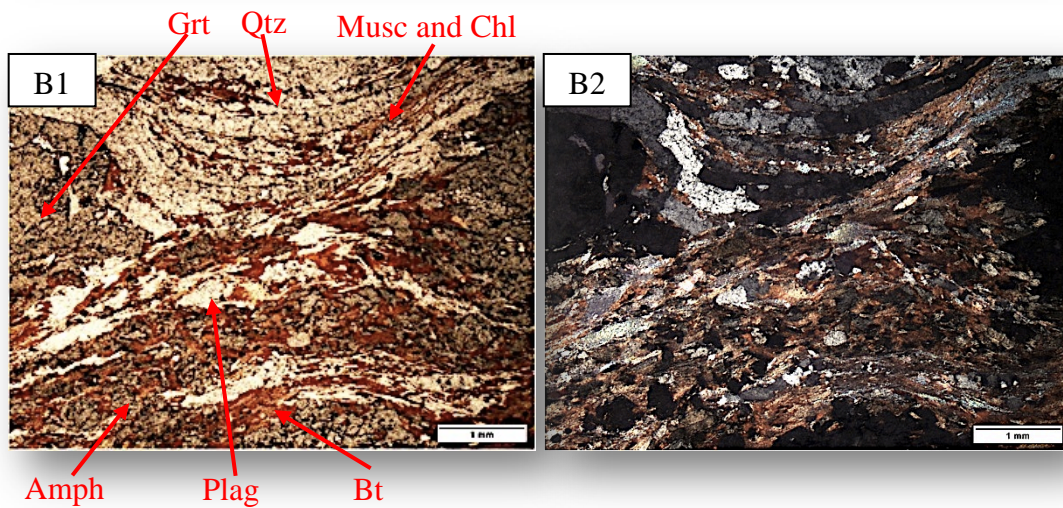


Figure 26. Agricola schist. A) Fresh hand sample showing strongly developed mylonitic fabric with stretched, anastomosing felsic bands interspersed with asymmetric porphyroclasts, indicating dextral shear. Note reddish orange color of weathered sample (upper left). B1) Photomicrograph in plane-polarized light and B2) photomicrograph in cross-polarized light; representative fabric with syn-kinematic garnet.

STRUCTURAL AND METAMORPHIC ANALYSIS

Rocks of the Jacksons Gap Quadrangle exhibit evidence for a complex polydeformational history comprising at least four deformational events (Table 1) recognized on the basis of structural style, geometry, deformational fabrics, paragenesis, and their mutual cross-cutting relationships. In addition to lithological differences, the eastern Blue Ridge, Jacksons Gap Group, and Dadeville Complexes contain structural differences unique to each terrane.

The eastern Blue Ridge comprises nearly equal volumes of sheared metasedimentary and metaplutonic units in the study area. The Jacksons Gap Group contains sheared metasedimentary units with some that are discontinuous along strike due to plastic shearing, stretching, internal faults, and tight-to-isoclinal doubly-plunging folds; some units, however, retain relict sedimentary structures. The Dadeville Complex contains sheared metavolcanic and metaplutonic rocks that range from mylonitized felsic- to mafic-schists and gneisses to mafic/ultramafic complexes retaining original igneous textures. The area, therefore, was divided into three subareas for structural analysis, A) eastern Blue Ridge, B) Jacksons Gap Group, and C) Dadeville Complex. Structural nomenclature used herein is based on the convention that structural phases produced during a deformational event are numbered the same (e.g., F_1 and S_1 formed during D_1 ; F_2 and S_2 formed during D_2 ; and so on). There are also prograde metamorphic differences between the terranes, with the Jacksons Gap Group appearing to have experienced lower

Table 1. Summary of deformational phases in rocks of the study area.

Deformational Phases	Structural Elements	Description
D ₁	M ₁	Regional amphibolite-facies dynamothermal metamorphism of EBR, JGG, and DC
	S ₁	Regional foliation (schistosity and gneissosity)
	L ₁	Early movement along the BZ Pre- or syn-peak metamorphic Katy Creek fault, Early movement along the Agricola/Dadeville shear zones
	F ₁	Internal folding of JGG
D _{1L}	M _{1L}	Retrograde shearing as the M ₁ peak waned Reactivation of the Agricola/Dadeville shear zones Movement along Abanda and ACFZ
	S _{1L}	Composite S-C mylonitic fabric indicating right-slip transpression
	L _{1L}	Elongation lineation within mylonitized gneisses
	F _{1L}	Isoclinal, intrafolial folds of S ₀ /S ₁ and thin-skinned faults within the JGG
D ₂	M ₂	Upper greenschist-facies reactivation Abanda fault and ACFZ
	S ₂	Local transposition of S ₁ into S ₂ in the Jacksons Gap Group Further composite S-C-NSC mylonitic fabric development indicating oblique-dextral-normal movement
	L ₂	Mineral elongation lineation within mylonitized gneisses, quartzites, and mafic units
	F ₂	Asymmetric shear folds along Abanda fault and ACFZ
D ₃	F ₃	Late regional folding (Tallasse synform phase)
D ₄		Reactivation of BZ and ACFZ under BDT to supra-BDT conditions Brittle faults characterized by siliceous cataclasites splaying from Abanda fault to ACFZ

* Abbreviations are: Alexander City fault zone (ACFZ); Brevard fault zone (BZ); Brittle-Ductile Transition (BDT); cisaillement (C); Dadeville Complex (DC); eastern Blue Ridge (EBR); Jacksons Gap Group (JGG); normal slip crenulations (NSC); schistosity (S). Subscript “L” = late.

grade conditions than the encapsulating eastern Blue Ridge and Dadeville Complex. The three terranes are interpreted as having been amalgamated during the first deformational event (D_1) and afterward were deformed together.

D_1

The first deformational event (D_1) occurred in association with the peak dynamothermal metamorphic event, M_1 . Rocks of the eastern Blue Ridge reached a peak of metamorphism at middle-amphibolite-facies conditions based pelitic assemblages containing staurolite, kyanite, or sillimanite; estimated conditions depicted in Figure 27 and noted by Bentley and Neathery (1970), Hawkins (2013), and Abrahams (2014). Jacksons Gap Group metapelite assemblages locally include chloritoid, staurolite, kyanite, or sillimanite indicating a lower-amphibolite facies peak (Fig. 27). The Dadeville Complex reached a peak of metamorphism at upper-amphibolite-facies conditions based garnet + sillimanite and garnet-kyanite pelitic assemblages and metamorphic amphibole in mafic rocks (Fig. 27). In ultramafic rocks, pyroxenes show alteration to amphiboles in the rims of grains.

The principal foliation (schistosity and gneissosity) found in each terrane, S_1 , is defined by the peak- M_1 mineral phases. Concordant with the dominant metamorphic schistosity found in the surrounding country rocks, the Kowaliga Gneiss likely intruded either prior to or synchronous with peak metamorphism. Within the Jacksons Gap Group, local primary bedding, S_0 , is preserved and is locally subparallel to or transposed into the S_1 foliation. A nematoblastic mineral lineation found within the gneissic banding or schistosity is assigned to L_1 . Tight-to-isoclinal folds of compositional layering transposed

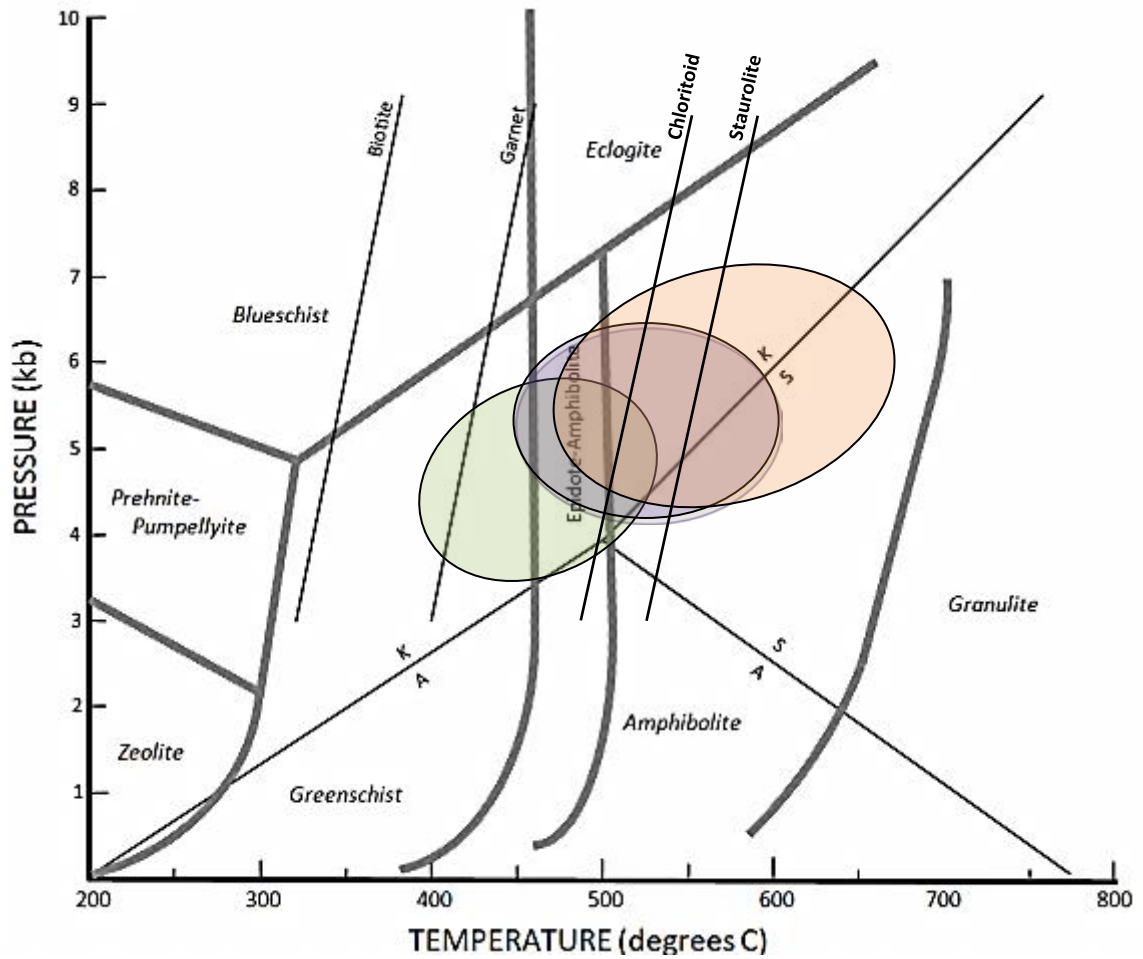


Figure 27. Metamorphic conditions suggested for the peak metamorphism. Eastern Blue Ridge = purple, Jacksons Gap Group = green, and Dadeville Complex = orange (modified from Hawkins, 2013). Grid univariant reaction curves and facies boundaries are from Richardson (1968), Hoschek (1969), Holdaway (1971), and Ernst (1973).

into, and axial-planar with S_1 are assigned to F_1 , and within the Jacksons Gap Group these folds occur at the scale of the geologic map (Plates 1 and 2).

Early movement along the Brevard fault, recorded by the Katy Creek fault, and possibly the Agricola/Dadeville shear zones (internal fault/shear zones internal to the Dadeville Complex; see Steltenpohl et al., 1990), may reflect pre-, syn-, and/or late metamorphic-peak (M_{IL} , see below) movement. The Katy Creek fault juxtaposes higher-grade Dadeville Complex rocks atop distinctly lower-grade Jacksons Gap Group, with structures and lithologies in the hanging wall truncated along the fault but no persistent zone of intense retrogressive fabric disruption has been observed (Plate 2). L_1 mineral lineations commonly are found paralleling stretched M_1 prograde mineral grains and are described further below (see L_{1L}).

For mapping and structural analysis, the S_1 foliation was the primary plane of foliation that was measured, as it is the most penetrative and consistent. Commonly, however, particularly within the metaplutonic units, composite-planar S-C fabrics with very small angles between them parallel and transpose the S_1 foliation, and the high-temperature, slightly sub-peak (M_1) rheologies of the former make them essentially inseparable in outcrops and in hand specimens (e.g., Fig. 7). Because of these difficulties, fabric plots in Figure 28 lump together these high-temperature S-C fabrics with S_1 . The average attitude of S_1 in the eastern Blue Ridge is $N30^\circ E, 60^\circ SE$ (Fig. 28A); in the Jacksons Gap Group is $N40^\circ E, 45^\circ SE$ (Fig. 28B); and in the Dadeville Complex is $N40^\circ E, 45^\circ SE$ (Fig. 28C). Lineations such as mineral elongation and stretching lineations tend to be oblique to strike and dip, but trend closer to strike and are represented by blue boxes in Figure 28. Figure 29 plots S_1 measured regionally across the Tallassee synform

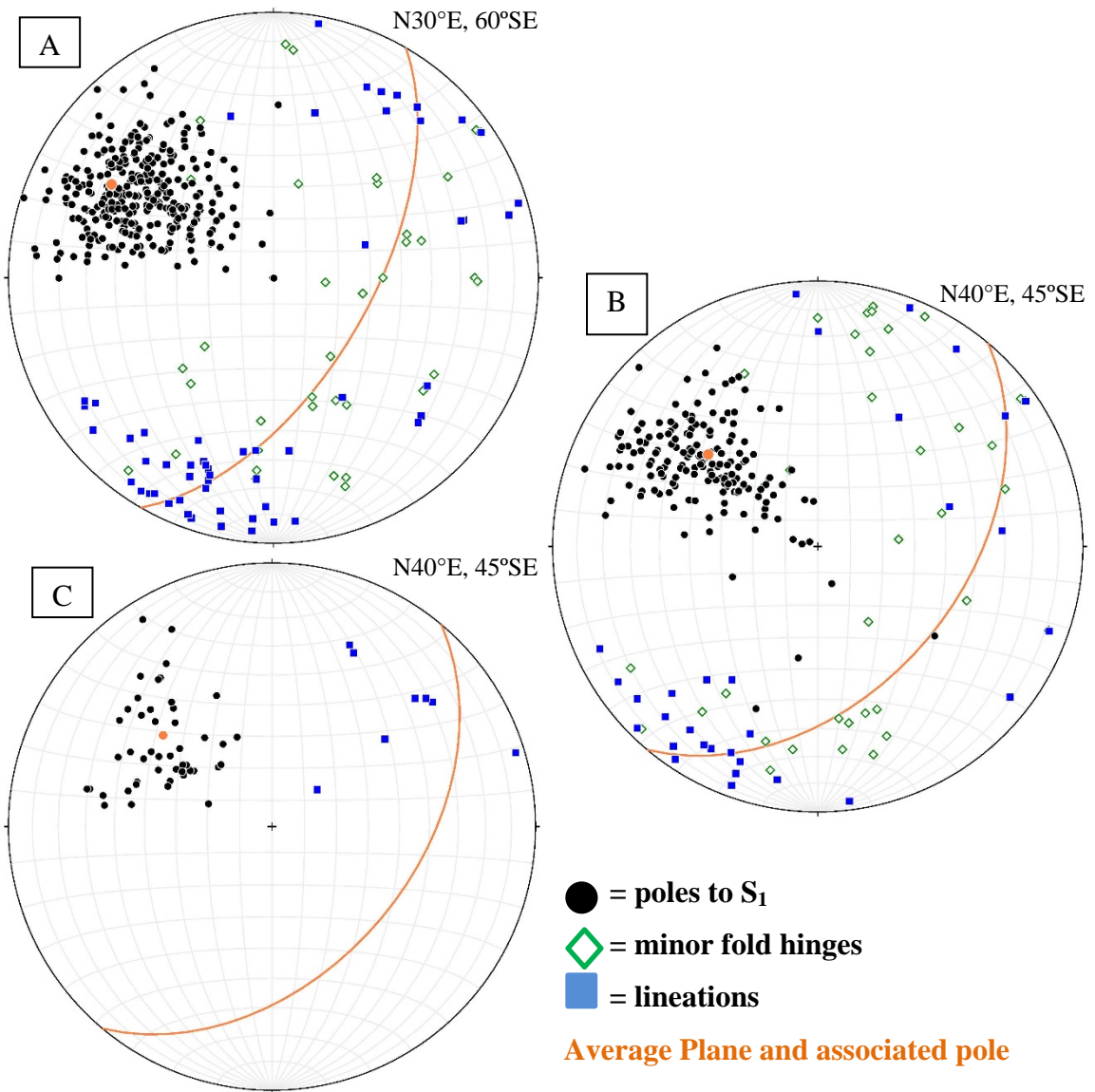


Figure 28: Lower-hemisphere stereographic projections and compilation of structural data from the three terranes within the Jacksons Gap Quadrangle. A) Eastern Blue Ridge (n=415). B) Jacksons Gap Group (n=268). C) Dadeville Complex (n=57). Orange projected great circle and pole represents the average strike and dip of the terrane.

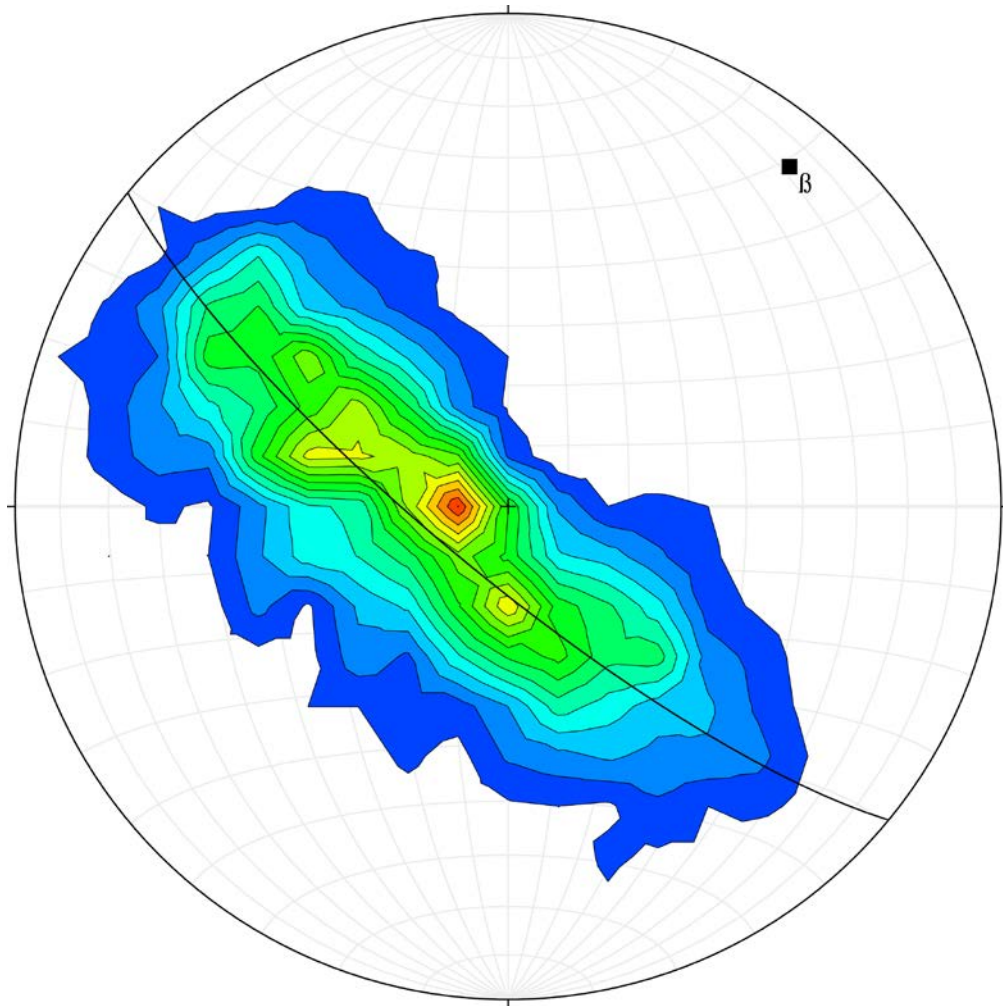


Figure 29. Contoured lower-hemisphere stereographic projection of poles to S_1 measured regionally across the Tallasse synform (Plate 3) with the plane of best fit and its pole (compiled from Dr. Steltenpohl's unpublished data base). ($n=2236$). β =beta fold axis. Contour interval is 2% and counting area is 0.4% of net area.

documenting conformity with S_1 of the northwest limb measured in the current study (Fig. 28).

D_{IL}

D_1 deformation associated with conditions reflective of the initial waning of the M_1 peak is assigned to D_{IL} . S_{IL} composite-planar S-C fabrics with very small angles between them parallel and transpose the S_1 foliation and the high-temperature, slightly sub-peak (M_1) rheologies of the former make them essentially inseparable in outcrops and in hand specimens. Because of these difficulties, fabric plots in Figure 28 lump together these high-temperature S-C fabrics with S_1 . These sub-to-peak M_1 minerals and microstructures occur in sheared rocks from each terrane and include stretched and rotated M_1 minerals such as garnet and kyanite (Figs. 17 and 30) (see Steltenpohl et al., 1990), asymmetric microfolds of sillimanite and muscovite layers and quartzo-feldspathic migmatitic veins, dynamically-recrystallized asymmetric potassium and plagioclase feldspar augens, and dynamically-recrystallized polycrystalline ribbons of quartz. Similar sub-peak microstructures are reported in mylonites along the flanks of the Alexander City fault zone (Steltenpohl et al., 2013) and in the Agricola and Dadeville shear zones (Steltenpohl et al., 1990). Internal, early-formed, intrafolial isoclinal folds of S_0/S_1 (i.e., F_{IL}) have an axial planar relationship to S_{IL} indicating that they formed during D_{IL} . Thin-skinned faults and ductile shear zones exploiting graphitic units within the Jacksons Gap Group also are interpreted as D_{IL} structures.

S_{IL} sufficiently transposed S_1 to produce a regionally penetrative, high-temperature mylonitic foliation recorded by sub-parallel composite S-C fabrics. L_{IL} is a

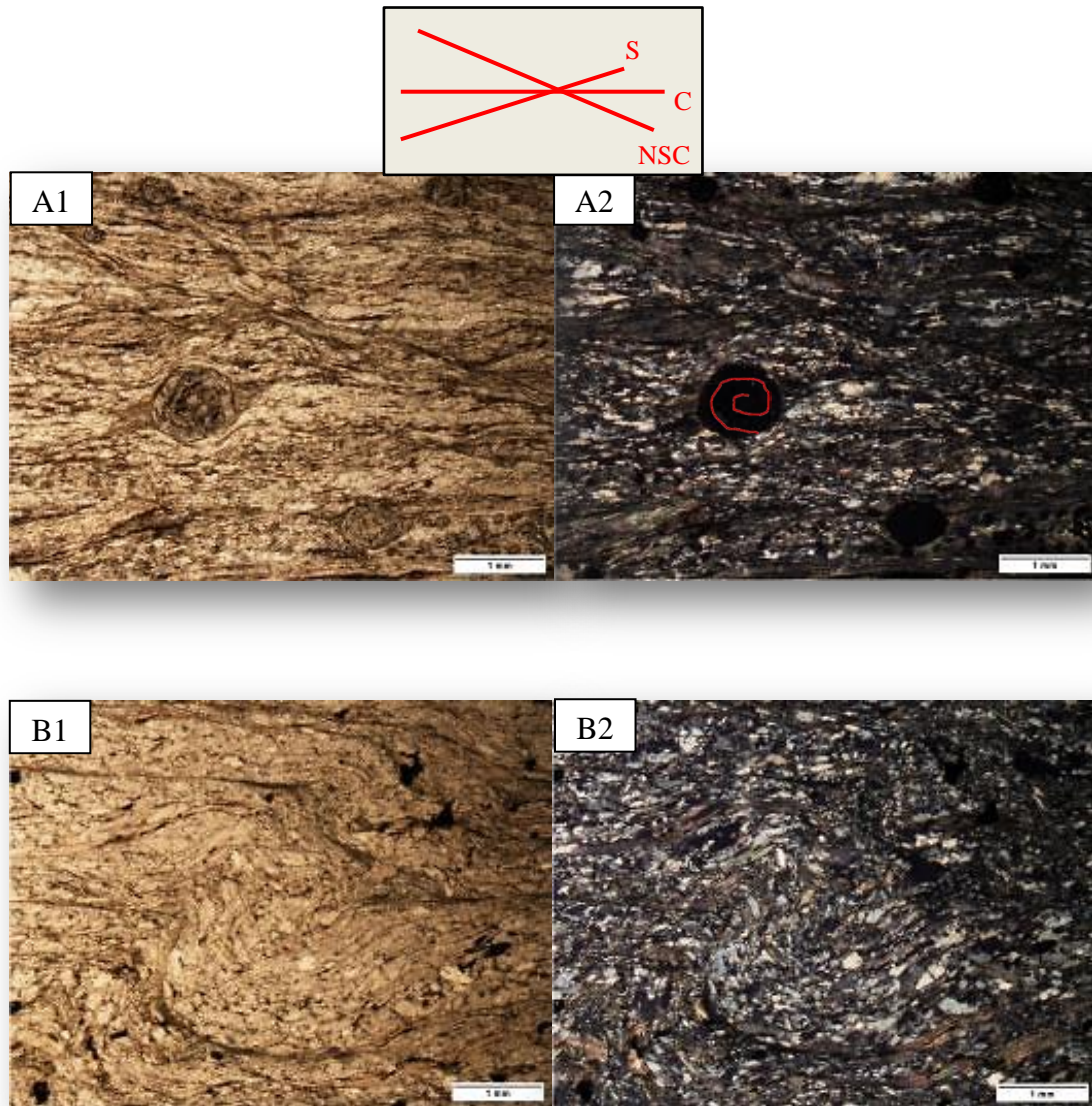


Figure 30: Photomicrographs of M_2 retrograde (graphite-muscovite-biotite-quartz-chlorite phyllite of the Wedowee Group) shear fabrics of the Alexander City fault zone. A1. Plane-polarized light and A2. cross-polarized light of syn-kinematic snowballed garnets with asymmetric pressure shadows. Retrograde chlorite is visible within the fabric. B1. Plane-polarized light and B2. cross-polarized light, F_2 z-folds produced during shear with retrograde chlorite within the noses of some folds.

mineral stretching lineation defined by elongated phyllosilicates and tectosilicates that plunges shallowly to the northeast and southwest within the C-plane. Petrographic studies indicate that quartz microstructures include lobate to bulging grain contacts suggesting that subgrain rotation and grain boundary migration were the predominant recrystallization mechanisms of Regime 2 or 3 of Hirth and Tullis (1992) suggesting temperatures of deformation above 500 °C. Feldspar microstructures include subhedral to anhedral asymmetric grains and core-mantle structures, indicating rotational recrystallization with some showing perthitic and antiperthitic textures. Crystal-plastic deformation indicates temperatures of deformation greater than ~450° C and potentially up to peak metamorphic conditions within sub-ductile-brittle-transition conditions for mylonitization (Passchier and Trouw, 1996).

Along its trace through North Carolina and Georgia, the Brevard fault zone is reported to have had an early movement history (Late Devonian) that formed under middle- to upper-amphibolite facies metamorphic conditions coming off of the peak of metamorphism (Vauchez, 1987; Bobyarchick et al., 1988; Davis 1993; Vauchez et al., 1993; Hatcher 2001; Mershcat et al., 2005; Hatcher and Mershcat; 2006; Abrahams, 2014), and the S_{1L} mylonitic fabric in the current study is interpreted to reflect this movement. Late Devonian dextral shearing during early-Brevard fault zone movement reported in the more northern parts of the fault zone correspond to that recorded by D_{1L} structures and fabrics in the current study). Similar, syn- to late-amphibolite-facies, Devonian (~388-369 Ma), right-lateral strike-slip shearing also is documented in the Elkahatchee Quartz Diorite adjacent to the Alexander City fault zone (Steltenpohl et al., 2013).

*D*₂

Structures associated with deformation event *D*₂ are easily distinguished because they deform and retrograde all *D*₁ and *D*_{1L} structures, minerals, and fabrics. *D*₂ mylonites and phyllonites record the retrogressive reactivation of the Abanda fault and Alexander City fault zone under upper-greenschist facies metamorphic conditions. *D*₂ structures and fabrics include anastomosing shears defined by composite S-C fabrics and spottily developed NSC (C') shear bands (modified from Dennis and Secor, 1987) that attenuate earlier-developed S-C fabrics (Figs. 5B, 6A2, 7, and 30A) (*S*₂), boudins or lenses of relatively low-strained rocks encapsulated by ductile shears, an elongation lineation (*L*₂) defined by quartz, biotite, and/or chlorite, and ductile, tight-to-isoclinal phase of folding (*F*₂) that almost exclusively display a dextral-oblique shear sense.

Microstructures observed within the mylonitic shears are mica phacoids with internal phacoid deformations (e.g., phacoid stacking, kinking, and folding) (Figs. 5, 6A2, and 12C), asymmetric porphyroclasts and rotated grains (sometimes with inclusion trails) with asymmetric pressure shadows (Fig. 30A), displaced grains, strung out, and broken grains, late brittle stacking of more competent grains, transposition structures (such as disconnected fold noses), undulatory, polycrystalline and subgranular grains with bulging grain contacts (Figs. 7E, 13, and 14), and retrograde growths of minerals (e.g., chlorite after biotite and garnet). *M*₂ is a regional retrograde metamorphism under upper-greenschist to lower-amphibolite facies, more readily observable in the eastern Blue Ridge and Jacksons Gap Group rocks based on the presence of syn-kinematic garnets, chlorite, biotite, and sericite bearing *M*₂ assemblages. Feldspars show multiphase

alteration and mineral growths with strain-related myrmekite growths (Fig. 23) and replacement by quartz and mica.

Asymmetric F_2 folds and crenulations associated with movement of Abanda and Alexander City faults have a dextral (z-fold) sense of rotation when viewed down-dip of the mylonitic foliation (Figs. 30B and 31). Small F_2 folds are displayed on stereograms as green diamonds representing fold hinges and have a vergence oblique to dip, trending closer to strike (Fig. 28). The minor folds are most often easily viewed looking down-dip of foliation, and lineations when viewed close to along strike (Fig. 28). This aids in interpreting oblique movement with major strike-slip and minor dip-slip components. F_2 folds may reflect reverse-slip crenulations (RSC) of Dennis and Secor (1987).

Discrete D_2 ductile shear zones are recognized at micro- to macro-scales along the Brevard fault zone and the Alexander City shear zone. The Jacksons Gap Group is almost wholly mylonitized although lenses and boudins may record remarkably low degrees of strain. Quartzites and quartz-rich schists preserve relict sedimentary structures such as fining-upward sequences and cross-bedding that record stratigraphic way-up (Figs. 18A and B, and 21). Highly graphitic units appear to have accommodated the highest amount of strain based on low angles between S-C planes, extensive NSC's, and common strung out minerals such as quartz and micas. Some units within the Jacksons Gap Group are discontinuous along strike and are structurally repeated. Mirrored repetitions are interpreted to be due to doubly-plunging, isoclinal folds that are transposed along tectonic ramp-style shears exploiting incompetent graphitic phyllite layers (F_1 , F_{1L} , and F_2) (Fig. 19, and Plates 1 and 2).

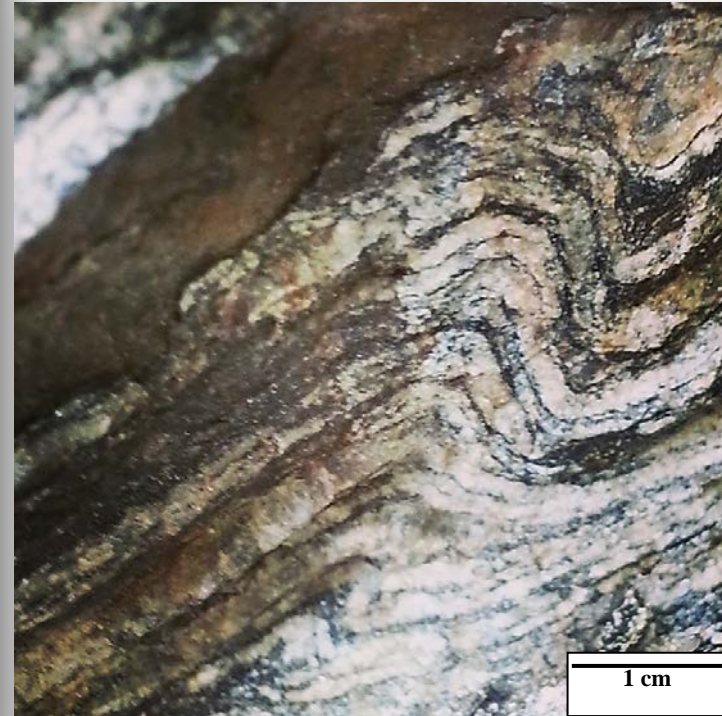
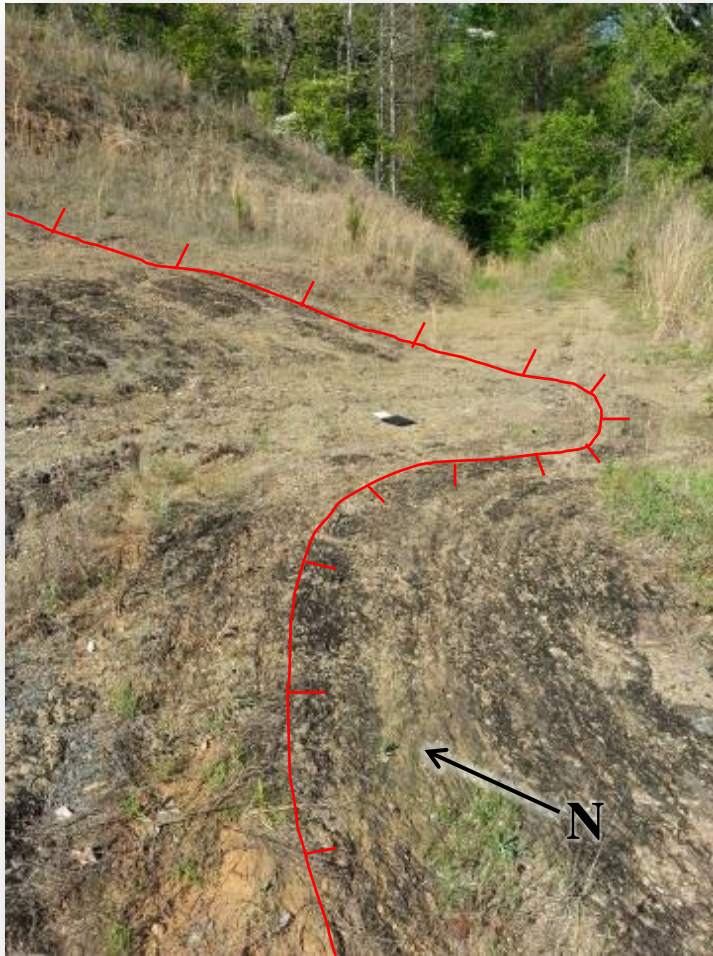


Figure 31: Fabric deforming F_2 asymmetric folds. A. Outcrop-scale fold in the Alexander City fault zone ($32^{\circ} 59' 12.22''$ N, $85^{\circ} 51' 35.61''$ W) with tick marks marking the direction of dip. B. Small z-fold of the Kowaliga Gneiss.

The eastern Blue Ridge and Dadeville Complex also display wide variations in degree of strain, which is to be expected in distributed simple shear deformation. In the eastern Blue Ridge, the Emuckfaw Schist and the Kowaliga Gneiss is strongly sheared; however, in the middle of the Emuckfaw Group, distal from the fault zones, the Kowaliga Gneiss appears less sheared. Potassium feldspar grains, upwards of 5 cm in length, range from zoned and euhedral to subhedral and unaffected from shear, to asymmetrically sheared augens completely consumed by the effects of dynamic recrystallization (Fig. 7). The mafic/ultramafic unit of the Dadeville Complex shows evidence for retrogressive alteration on the margins of the unit, but appears relatively unaffected by retrograde metamorphism and shear strain in the core of the unit, preserving the original igneous cumulate texture and mineralogy.

Figure 32 shows S-C plane and related measurements for the Abanda fault (A) and the Alexander City fault (B) zones in the study area. Net slip vectors (green arrows) were determined by a 90° rotation from the acute bisectrix of paired S-C planes along the C-plane, connected by arcs, in the direction of slip (Abanda fault, $n=19$; Alexander City fault, $n=18$). Arcs connect the poles of S-C planes (arrowhead at pole of S-plane). The average C-plane (red great circle) for the Abanda fault has a strike of $N35^\circ E$ with a 57° dip to the southeast, and a strike of $N46^\circ E$ with a 46° dip to the southeast for the Alexander City fault. Both faults record oblique dextral-slip as well as normal- or reverse-slip movement. Portions containing both normal and reverse components may be explained in multiple ways: 1) sheared volumes of rock may have been rotated while being transported along strike; 2) small step-overs or flower structures may occur along the fault plane; or 3) they may record different episodes of movement.

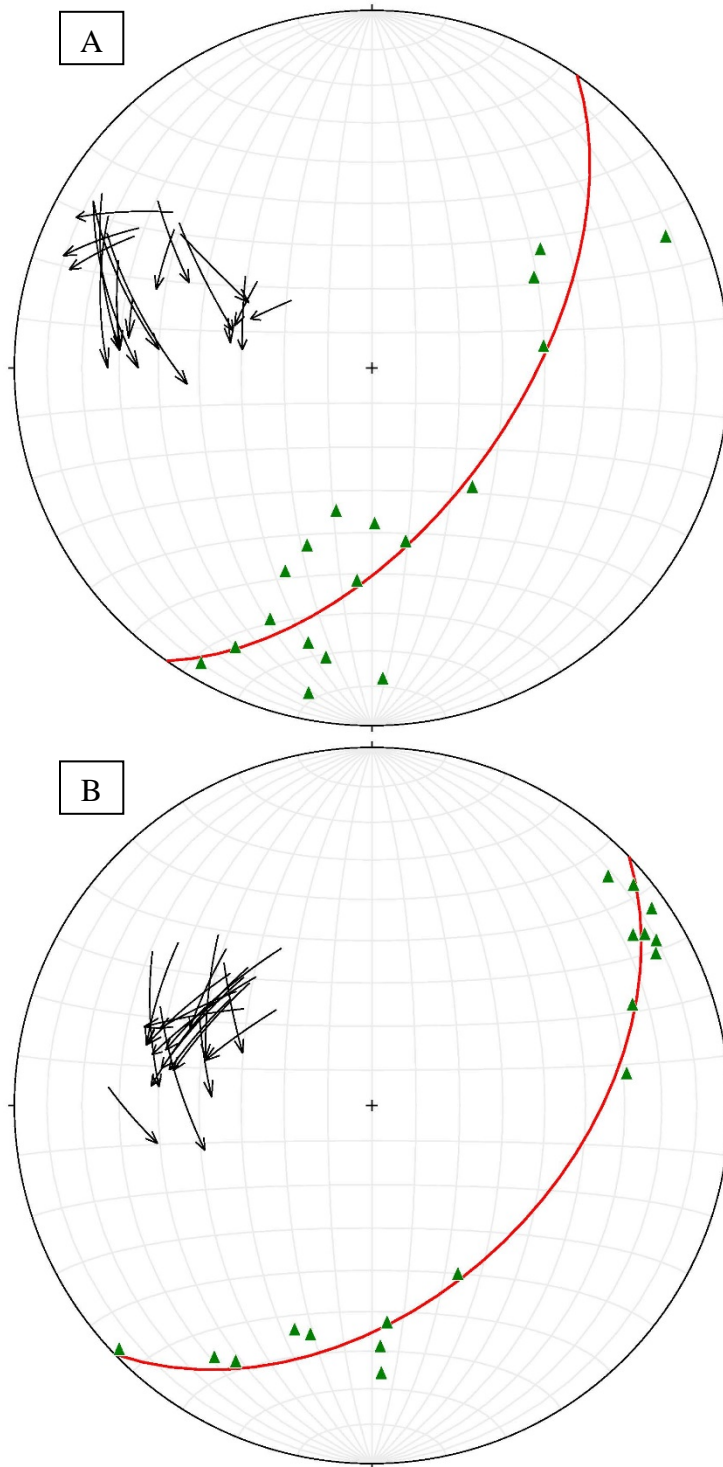


Figure 32: Lower hemisphere stereographic projections of D_2 S-C fabric observations. A. Abanda fault (n=19). B Alexander City fault (n=18). Arcs connect the poles of S-C planes with arrows at poles of S-planes. Green arrows = slip-lines.

D₃

Regional folding of schistosity by the late-stage Tallassee synform (F_3) marks deformational event D_3 . Figure 29 is a compilation of S_0/S_1 poles (from Poole, 2013; Abrahams, 2012; Hawkins, 2011; Davis, 2010; Reynolds, 2009; Key, 2008; White, 2007; Robinson, 2006; Buchan et al., 2005; Steltenpohl, 2004; Kassos, 2003; Carter, 2002; Moore, 2001; Mager, 2000; Zeltner, 1999; Steltenpohl, 1996) (Fig. 2) documenting a $N40^\circ E$ trend (π -girdle) and a plunge of 12° for axes of the Tallassee synform.

D₄

Reactivation of Brevard fault zone and Alexander City fault zone at the brittle ductile transition to supra-brittle ductile transition characterize D_4 . Brittle faults characterized by siliceous cataclasites splaying from Abanda fault to Alexander City fault record deformation related to D_4 . These supra-ductile-brittle transition faults are generally narrow (< 50 m wide), brittle deformation zones as described above in the Cataclastic Zone of the Lithostratigraphic Units section) There are varying degrees of cataclastics, with some containing clasts of previous cataclastics/breccias.

Silica replacement entirely consumes the zone except for sparse feldspars and some fine-grained micas. In outcrops, cross-cutting quartz veins indicate polyphase fracturing events with the latest veins lacking evidence for attrition. The latest-formed quartz veins are coarsest grained (up to $500 \mu\text{m}$) with curved, well-equilibrated triple-point grain boundaries and tend to be tabular and more continuous (Abrahams, 2014). Internal veins of quartz also cut across clasts. Some thin sections contain multiple optical growth zones of quartz marked by varying concentrations of mineral and/or fluid

inclusions, with zones commonly having differing densities and orientations of fractures occurring in roughly subparallel sets, as noted by Abrahams (2014).

⁴⁰Ar/³⁹Ar ISOTOPIC ANALYSES AND INTERPRETATIONS

Isotopic analyses are reported for ten samples collected from ten locations and eight lithologies from the Jacksons Gap, Alexander City/ Our Town, and Tallassee, Alabama Quadrangles (Figs. 33 and 34, Table 2). Six samples (see Table 2) were collected and prepared by Ms. Amanda Reynolds and analyzed under the direction of Dr. Hames (personal communication to Dr. Steltenpohl, 2014). These muscovite dates were targeted to constrain the timing of regional cooling. The current author's samples and analyses (Table 2) were aimed at constraining the timing of movement along the Brevard (Abanda fault) and Alexander City fault/shear zones and also the post-shearing cooling of the Kowaliga Gneiss. The difference between the sampling strategies is that the author collected samples from within the highest-strained mylonitic/phyllonitic portions of shear zones, where Reynolds' samples were collected from metamorphic rocks away from the shear zones.

The nominal closure temperature for argon in muscovite for a wide range of plausible cooling rates and grain sizes, is ca. 350°C (Robbins, 1972; Harrison and McDougall, 1981; Dodson and McClelland-Brown, 1985; Hodges, 1991; and Hames and Hodges, 1993). Careful petrographic characterization of this phase and its relationships with mylonitic and metamorphic fabrics help to constrain the timing of fault movement and ductile shearing. This method of dating has been employed by Dr. Steltenpohl and his students in the past to help characterize broad cooling trends for these terranes, but

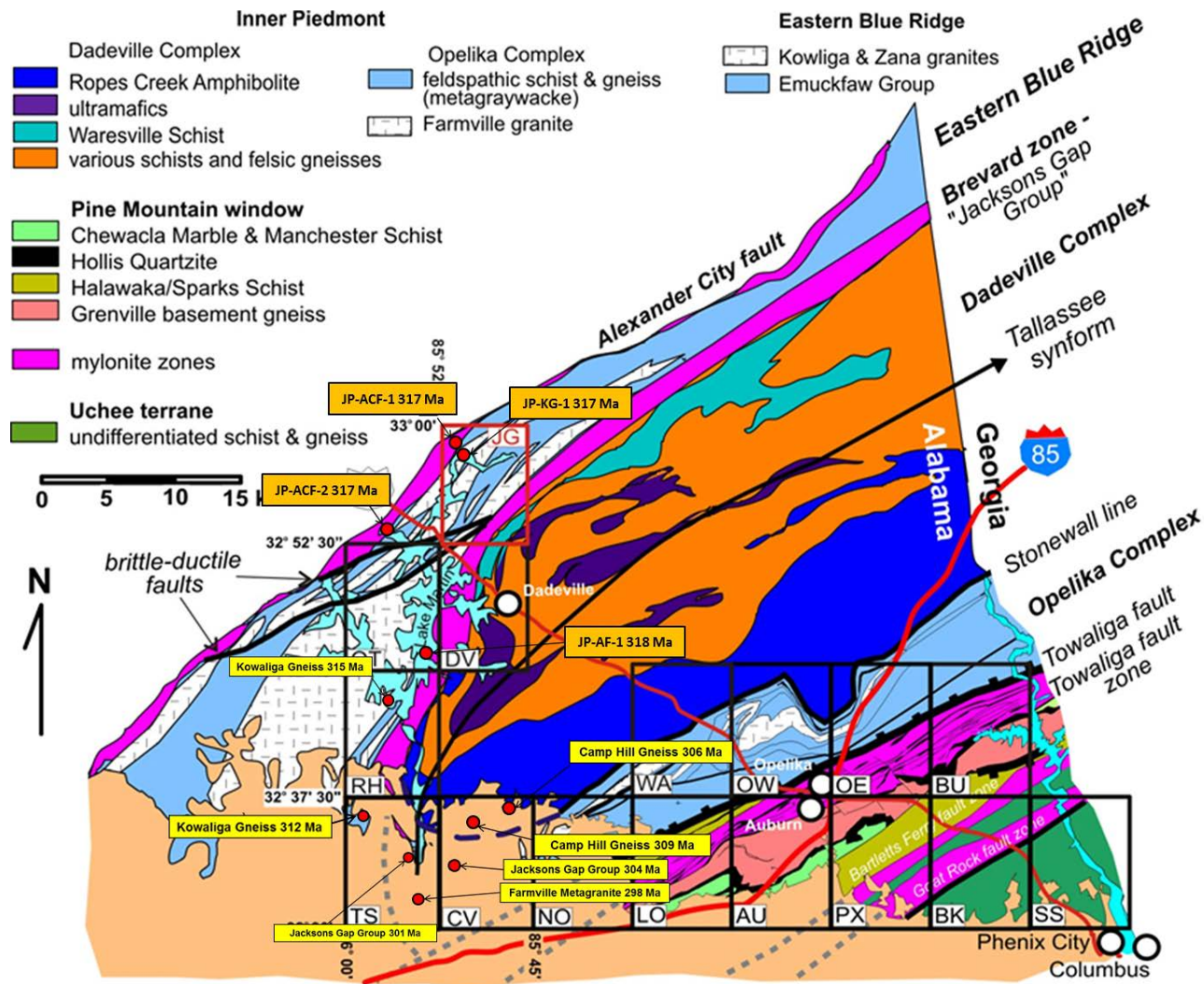


Figure 33. Distribution of thermochronological dates (n=11) reported in this study (yellow boxes, Amanda Reynolds; orange boxes, current author). Red dots indicate sample localities. (Inset map modified from Steltenpohl, 2005).

**GEOLOGIC MAP OF THE TALLASSEE QUADRANGLE
ELMORE AND TALLAPOOSA COUNTIES, ALABAMA**
West White and Mark Steltenpohl, Auburn University

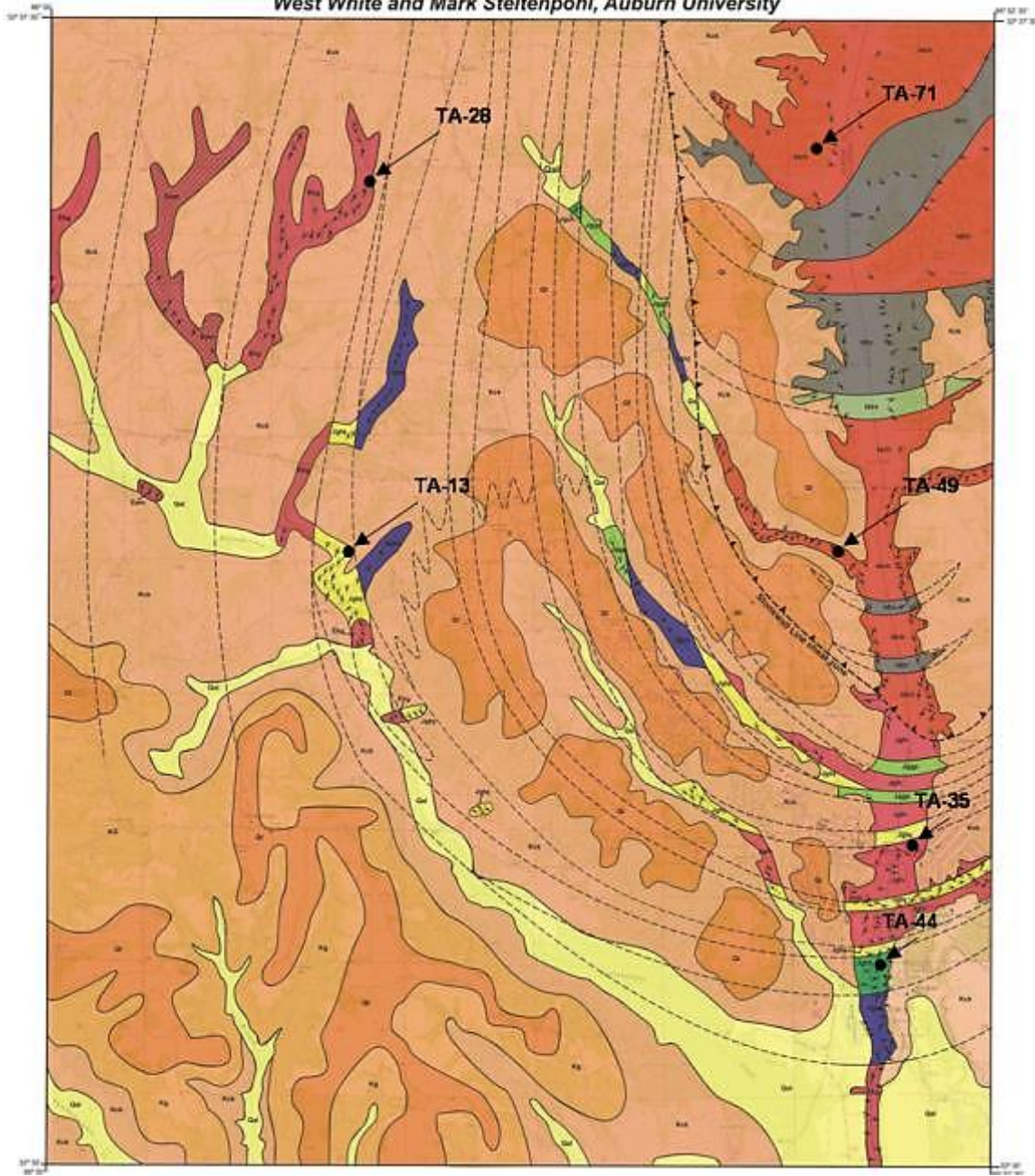


Figure 34. Tallassee Quadrangle reduced Plate 1 of White (2008), showing muscovite sample locations (n=6).

Table 2. Summary of isotopic analyses of samples (n=10)

$^{40}\text{Ar}/^{39}\text{Ar}$ dating samples for ANIMAL						
Sample	Lithologic Unit	Isotopic Date	Analysis Type	Collector	Lat. Long.	Comments
JP-ACF-1	Wedowee Group	317.22 ± 0.61 Ma	single crystal total fusion	Josh Poole	32°59'5.61"N, 85°51'35.90"W	Relatively homogeneous, inclusion free, easy to pick, some grains have yellow tinge and inclusions. Seived twice.
JP-ACF-2	Wedowee Group	317.31 ± 0.45 Ma	single crystal total fusion	Josh Poole	32°52'27.70"N, 85°57'57.56"W	Graphite on/within grains, biotite and/or chlorite inclusions. Some yellow tinge. Seived twice.
JP-KG	Kowaliga Gneiss	317.38 ± 0.50 Ma	single crystal total fusion & laser single crystal incremental heating	Josh Poole	32°58'24.51"N, 85°51'1.59"W	Some yellow tinge and biotite inclusions. Seived three times and magnetically separated.
JP-AF-1	garnetiferous phyllite of JGG	318.09 ± 0.91 Ma	single crystal total fusion	Josh Poole	32°45'13.45"N, 85°53'17.00"W	Graphite on/within grains. Some yellow tinge. Seived three times.
TA-28	Kowaliga Gneiss	311.8 ± 1.20 Ma	single crystal total fusion	Amanda Reynolds	32°36'26.3"N, 85°57'26"W	N/A
TA-13	Tallassee Quartzite of JGG	301.4 ± 1.30 Ma	single crystal total fusion	Amanda Reynolds	32°33'59.3"N, 85°57'38.9"W	N/A
TA-35	Farmville Metagranite	297.7 ± 0.90 Ma	single crystal total fusion	Amanda Reynolds	32°32'04.7"N, 85°53'08.1"W	N/A
TA-44	chlorite-hornblende-biotite schist of JGG	303.6 ± 1.00 Ma	single crystal total fusion	Amanda Reynolds	32°31'21"N, 85°53'16.9"W	N/A
TA-49	Camp Hill Gneiss	309.1 ± 1.30 Ma	single crystal total fusion	Amanda Reynolds	32°34'01.6"N, 85°53'42.6"W	N/A
TA-71	Camp Hill Gneiss	305.8 ± 1.30 Ma	single crystal total fusion	Amanda Reynolds	32°36'46.5"N, 85°54'03.3"W	N/A

not within the fault rocks that may contain evidence for the timing of movement (Fig. 32).

ANALYTICAL TECHNIQUES

These analyses were conducted at the Auburn Noble Gas Isotopic Mass Analysis Laboratory (ANIMAL) at Auburn University under the supervision of Dr. Willis Hames (Fig. 35A). The preparation for the isotopic analysis of the muscovite samples is a multi-step process. The muscovites must be separated from individual samples via crushing using a hand mortar and pestle with attention to minimize comminuting the size of individual grains. The crushed samples were thoroughly sieved to size fractions 30-40 and 40-60 mesh sieves. These two size fractions were then passed through a Frantz Magnetic Separator as an additional means to increase the proportion of muscovite. Approximately 75-100 muscovite grains per sample were then selected by hand under a binocular microscope, (Figs. 35 and 36). The grains were packed into irradiation discs and sent to the USGS TRIGA reactor in Denver, Colorado to be irradiated (Fig. 35C). After irradiation, the discs were returned to ANIMAL for laser single-crystal total muscovite fusion, and laser single-crystal $^{40}\text{Ar}/^{39}\text{Ar}$ incremental heating spectra.

The ANIMAL facility is equipped with an ultra-high vacuum, 90° sector, 10 cm radius spectrometer. The spectrometer employs second-order focusing (Cross, 1951), and is fitted with a high sensitivity electron-impact source and a single ETP electron multiplier. Typically analyses are made using a filament current of 2.75 A, and potentials for the source and multiplier of 2000 V and 1300 V, respectively. Measurements of atmospheric argon passed through an air pipette monitor sensitivity, which was measured

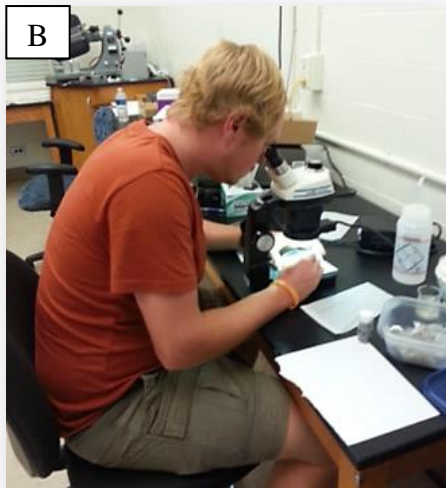


Figure 35. A) The ANIMAL facility, Auburn University. B) The author separating muscovites from samples to be analyzed. C) Dr. Zeki Billor loading muscovites into irradiation discs before being sent to the USGS TRIGA reactor to be irradiated.

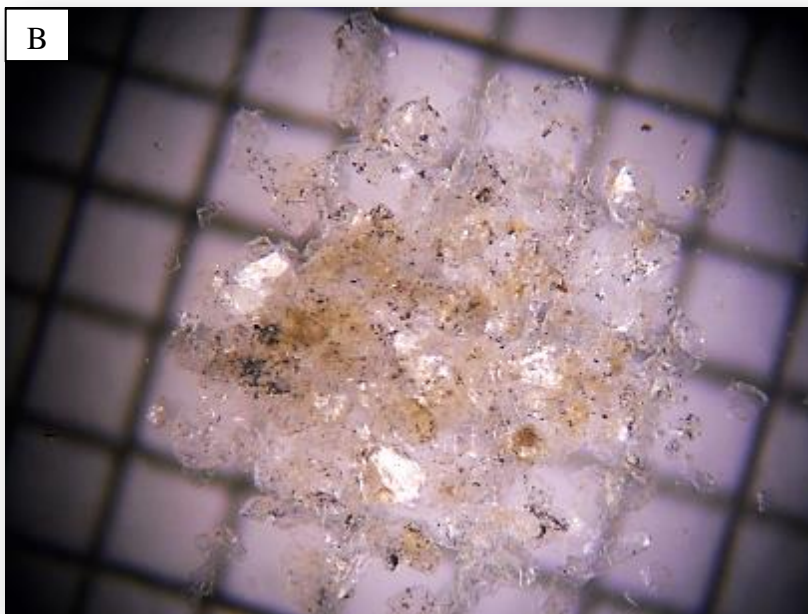


Figure 36. Microscopic photograph of muscovites extracted from samples. A) Relatively coarse, euhedral muscovites that are free from inclusions (JP-ACF-1). B) Finer muscovite grains with hematite staining and graphite, biotite, and chlorite inclusions (Sample JP-AF-1). Squares in background are 1mm^2 .

at 8.06×10^{-15} moles/V. The high sensitivity and low blank of the instruments permits measurement of 10-14 mole samples to within 0.2% precision. The standards used were GA-1550, a 98.79 ± 0.96 Ma biotite sample, and FC, a 28.02 ± 0.28 Ma Fish Canyon sanidine (Renne et al., 1998). Ten irradiated grains for each sample were placed in a copper holding disc and analyzed using single crystal total fusion and two analyzed using single-crystal $^{40}\text{Ar}/^{39}\text{Ar}$ incremental heating. Data were reduced using Microsoft® Excel and Isoplot 3 (Ludwig, 2003; Appendix 1). All samples were corrected for background measurements of atmospheric argon contamination. Ca and K interferences were corrected for using ^{37}Ar . Mass spectrometer sensitivity was measured by running air samples daily and blank samples interspersed among every five unknown samples.

SAMPLE LOCATIONS

Eastern Blue Ridge/Alexander City Fault Zone

Three samples from the eastern Blue Ridge were collected and analyzed (JP-ACF-1, JP-ACF-2, and JP-KG). JP-ACF-1 and JP-ACF-2 were from similar Wedowee Group phyllonites of the Alexander City fault zone (see lithologic description above). JP-ACF-1 (Table 2) contained muscovites less than 1 mm in diameter that were easy to pick and separate; some grains had minor staining of hematite along with graphite, biotite, and chlorite inclusions (Fig. 35A). Twenty-four single crystal total fusion analyses yielded a mean age of 317.22 ± 0.61 Ma at the 95% confidence level; a mean square weighted deviation (MSWD) of 1.7, and a relatively low probability of fit (2.7%) suggests variation in age beyond analytical precision (Figs. 36A, 37A1 and A2) (Appendix).

JP-ACF-2 (Table 2) contained muscovites with graphite occurring as a coating and as inclusions along with biotite and/or chlorite. Some grains also displayed hematite staining. Twenty-five single crystal total fusion analyses yielded a mean age of 317.31 ± 0.45 Ma at the 95% confidence level, and a MSWD of 0.88 with a relatively high probability of fit (64%) (Figs. 37B1 and B2) (Appendix).

JP-KG (Table 2) muscovites were separated out of an outcrop of highly-sheared Kowaliga Gneiss that is proximal to the Alexander City fault zone. These muscovites were similar in character to the two samples previously described (see Table 2). Twenty-five single crystal total fusion analyses yielded a mean age of 317.38 ± 0.50 Ma at the 95% confidence level, with a MSWD of 1.7, and a relatively low probability of fit (1.7%) that suggests variation in age beyond analytical precision (Figs. 37C1 and C2) (Appendix). Two different muscovite crystals from sample JP-KG also were also used for laser single crystal $^{40}\text{Ar}/^{39}\text{Ar}$ incremental heating analyses. The first analysis yielded a plateau age of 319.01 ± 1.04 Ma (2σ), MSWD of 0.99, probability of 0.43, and included 100% of the ^{39}Ar (Fig. 38A) (Appendix). The second analysis yielded a plateau age of 315.79 ± 0.76 Ma (2σ), MSWD of 0.84, probability of 0.64, and included 100% of the ^{39}Ar (Fig. 38B) (Appendix).

Muscovite sample TA-28 (Table 2) is one of Reynolds' samples from the Kowaliga Gneiss ~2 km away from the closest ductile shear zone (i.e., the Abanda fault). Muscovite age dates in this sample range from 303.1 ± 1.2 Ma to 333.0 ± 1.2 Ma with a mean age of 311.8 ± 1.2 Ma (Figs. 39A1 and A2).

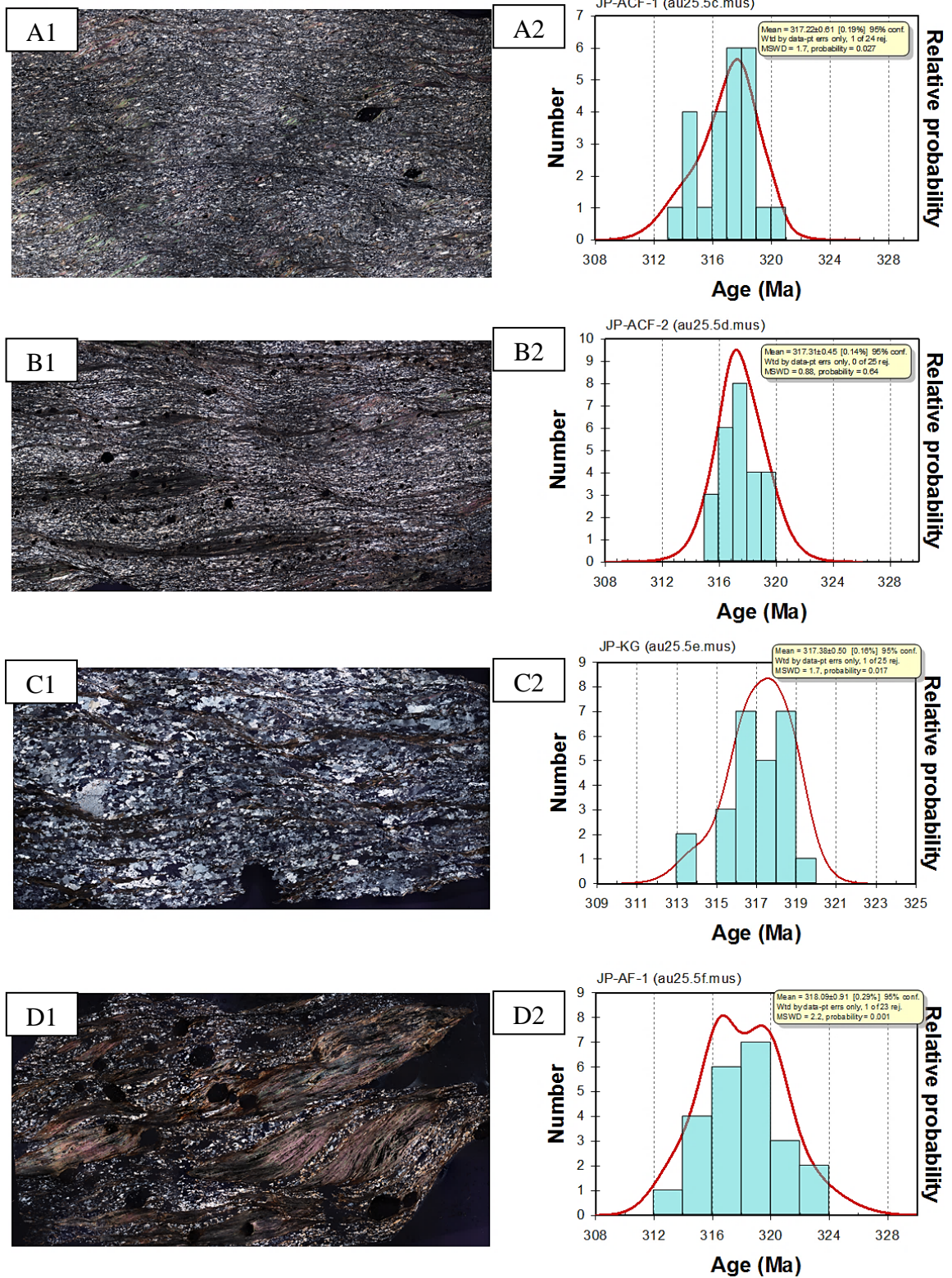


Figure 37. Photomicrographs in cross-polarized light of samples dated (left side) and their correlative measured dates plotted (right side). JP-ACF-1 (A1 and A2), JP-ACF-2 (B1 and B2), JP-KG (C1 and C2), and JP-AF-1 (D1 and D2).

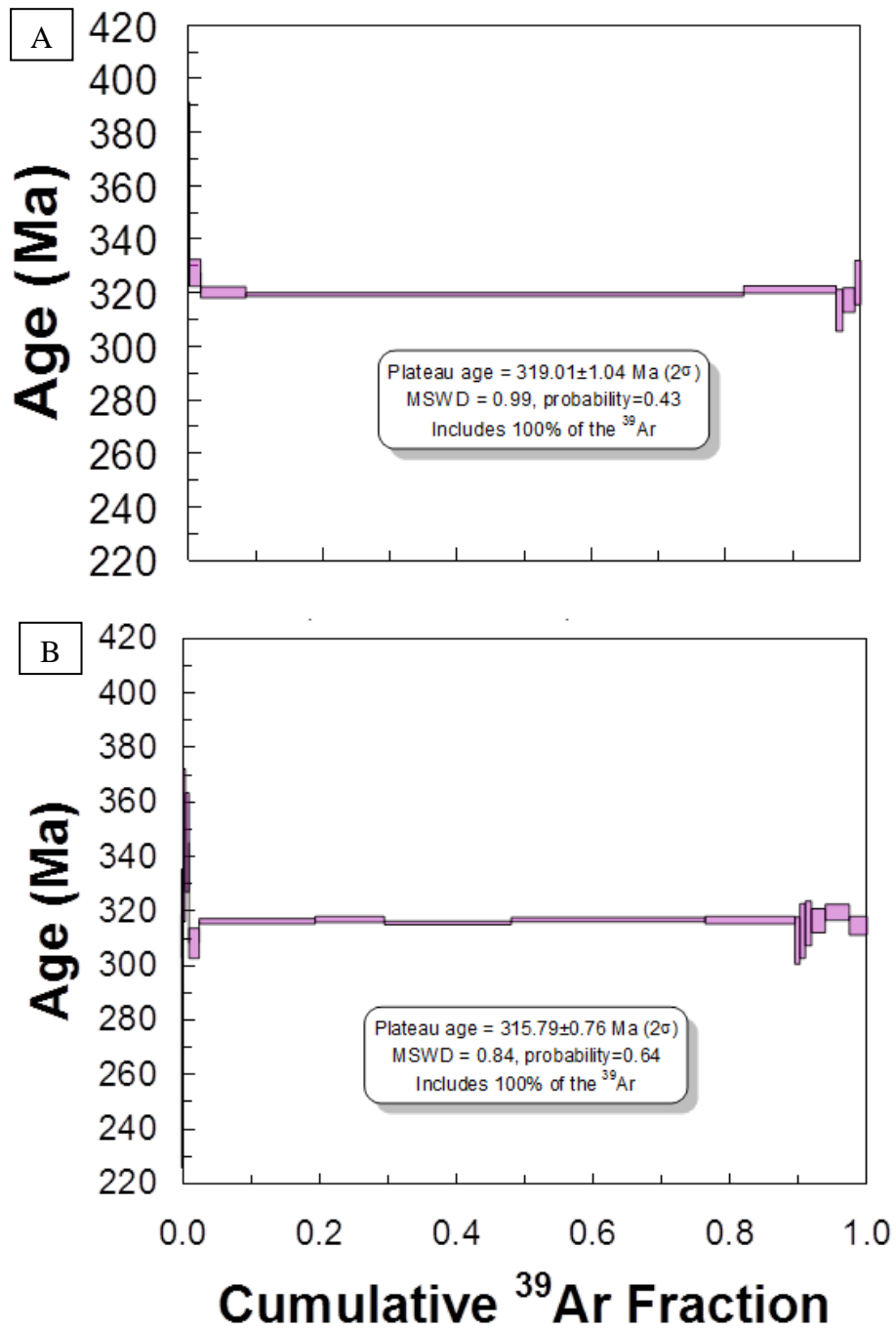


Figure 38. Laser single crystal ⁴⁰Ar/³⁹Ar incremental heating spectra and plateau ages for two different muscovite crystals of sample JP-KG.

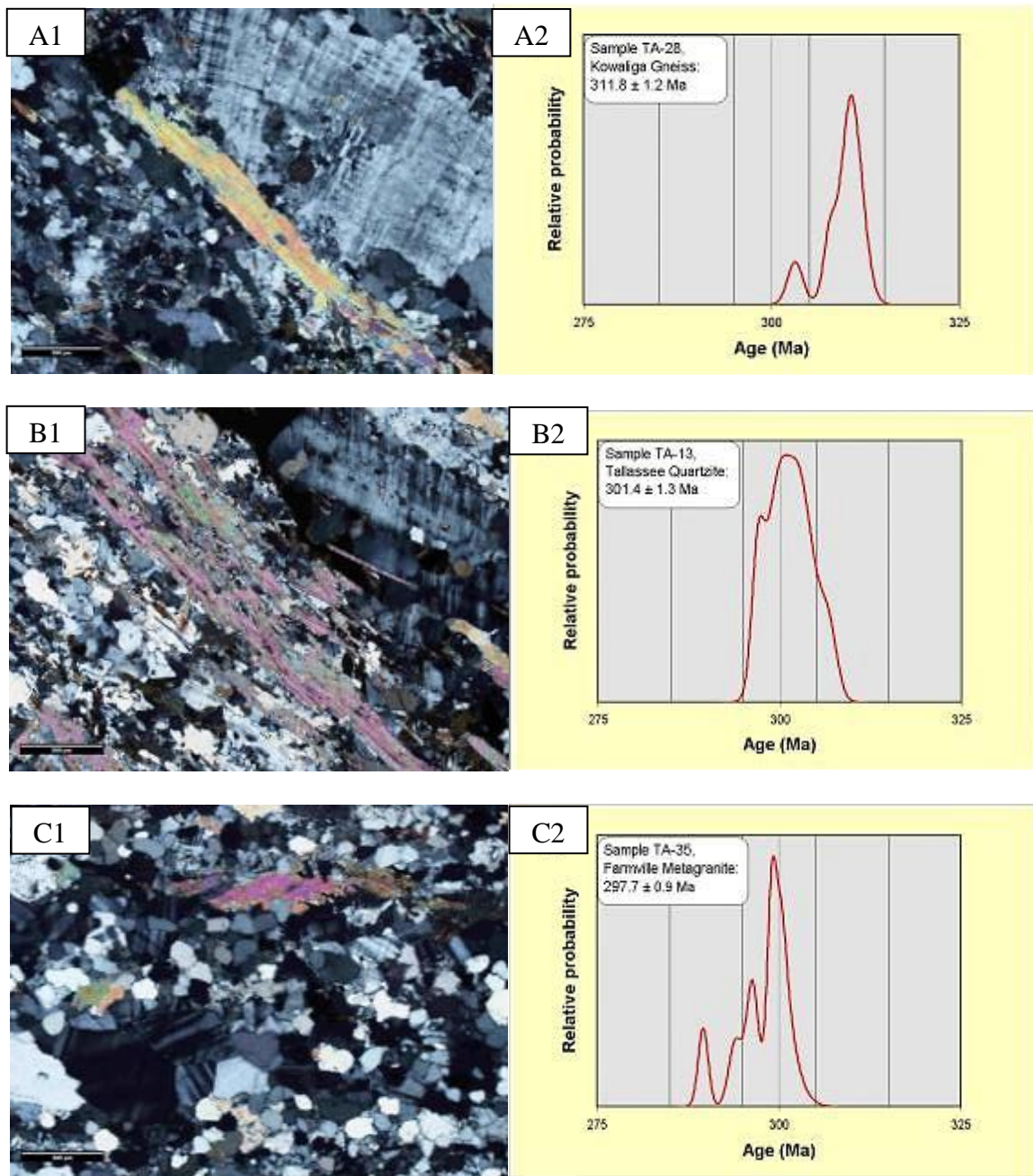


Figure 39. Density probability plots of 6 muscovite grains from Reynold's samples: TA-28 (A), TA-13(B), and TA-35 (C) with photomicrographs of respective thin sections in cross-polarized light. (Continued on next page).

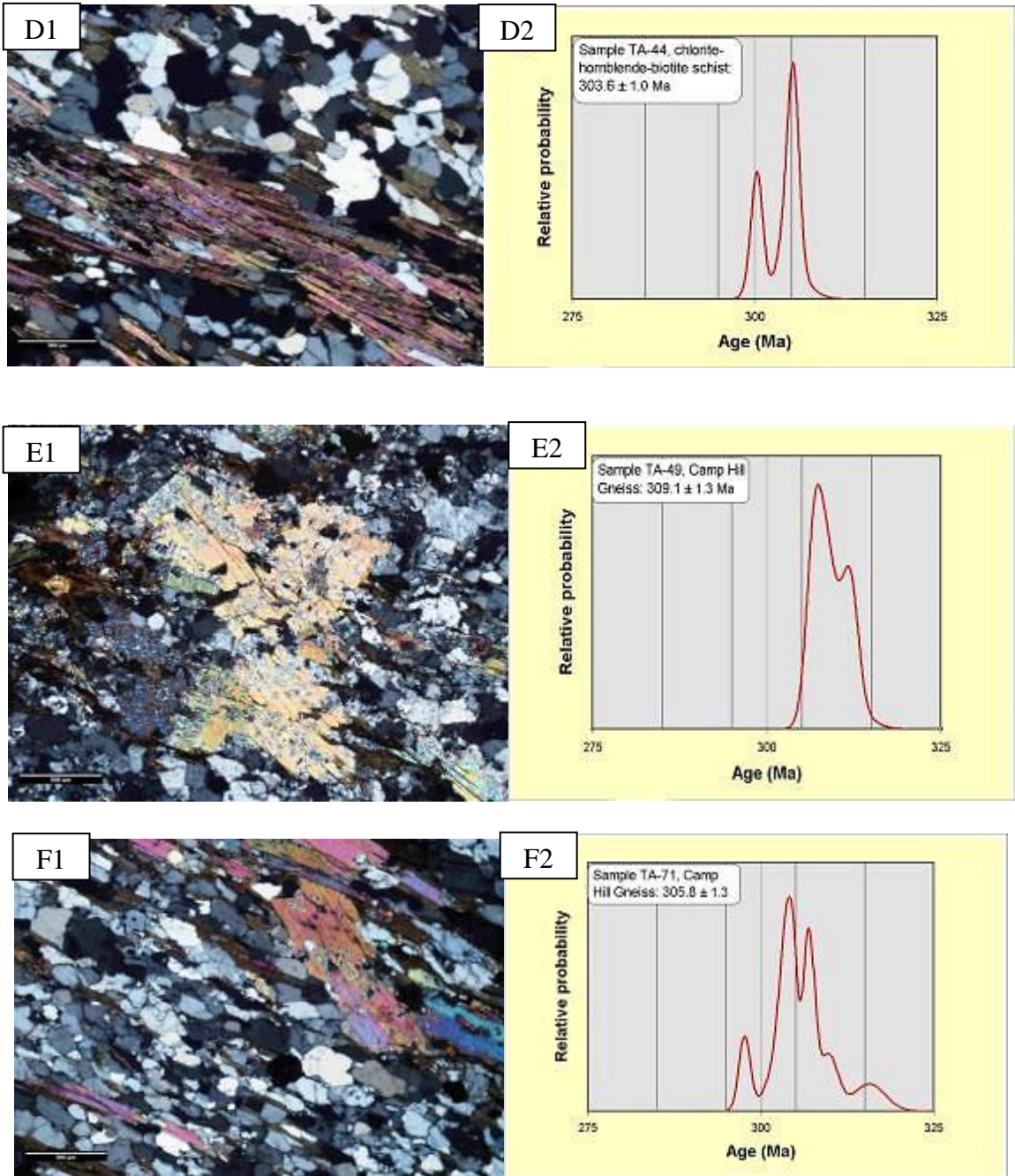


Figure 39 (continued). Density probability plots of 6 muscovite grains from Reynold's samples: TA-44 (D), TA-49 (E), and TA-71 (F) with photomicrographs of respective thin sections in cross-polarized light.

Jacksons Gap Group/Brevard fault zone (Abanda fault)

Sample JP-AF-1 (Table 2) is from the Abanda fault and basal unit of the Jacksons Gap Group, the garnetiferous graphitic phyllite/phyllonite. The muscovites in this sample also appeared to have graphite occurring as a coating and as inclusions with some grains also displayed staining of hematite (Table 2 and Fig. 36B). Twenty-three single crystal total fusion analyses yielded a mean age of 318.09 ± 0.91 Ma [0.29%] with 95% confidence, MSWD of 2.2, and a low probability of fit (~0.1%) suggests variation in age beyond analytical precision (Figs. 37D1 and D2) (Appendix).

Reynolds collected three muscovite samples from metamorphic rocks of the Jacksons Gap Group. Sample TA-13 (Table 2) was taken from the Tallassee Quartzite. Muscovite dates for this sample range from 298.1 Ma to 306.1.2 Ma with a mean age of 301.4 ± 1.3 Ma (Figs. 39B1 and B2).

Sample TA-35 (32° 32' 04.7" N, 85° 53' 08.1" W) was taken from the Farmville Metagranite of the Opelika Complex in the hinge zone to the Tallassee synform. White (2008) placed this unit within the Jacksons Gap Group, although it does not extend north of the Tallassee Quadrangle. Muscovite dates from this sample range from 289.6 ± 0.7 Ma to 301.6 ± 1.8 Ma with a mean age of 297.7 ± 0.9 Ma (Figs. 39C1 and C2). Sample TA-44 (Table 2) from the chlorite-hornblende-biotite schist of the Jacksons Gap Group dates range from 300.1 ± 1.0 Ma to 305.9 ± 2.1 Ma with a mean age of 303.6 ± 1.00 Ma (Fig. 39D1 and D2).

Inner Piedmont

Reynolds' muscovite samples TA-49 (Table 2) and TA-71 (Table 2) were collected from the Camp Hill Gneiss of the Dadeville Complex. Muscovite dates for sample TA-49 range from 306.6 ± 1.2 Ma to 312.2 ± 1.1 Ma with a mean age of 309.1 ± 1.3 Ma (Figs. 39 E1 and E2). Muscovite dates for sample TA-71 range from 297.7 ± 0.8 Ma to 315.7 ± 2.3 Ma with a mean age of 305.8 ± 1.3 Ma (Figs. 39F1 and F2).

ISOTOPIC INTERPRETATIONS

The author's $^{40}\text{Ar}/^{39}\text{Ar}$ analyses of muscovite cooling ages from samples JP-ACF-1, JP-ACF-2, JP-KG, and JP-AF-1 yielded an Early to Middle Pennsylvanian (Alleghanian) mean age of 317.5 Ma, with 95% confidence; probability density diagrams (Figs. 37A2, B2, C2, and D2) show strong peaks that imply minimal influence by later thermal events. $^{40}\text{Ar}/^{39}\text{Ar}$ muscovite ages for the fault/shear zones indicate that the muscovites recorded the timing of the last, mid-crustal level deformation due to movement. The Alexander City and the Abanda faults, therefore, appear to have been emplaced and cooled at about the same time based on geologic and isotopic analysis. That the isotopic dates record timing for the latest movement rather than regional cooling is based on the fact that the muscovites have been recrystallized and internally deformed along with the development of retrogressive chlorite and yielded approximately the same age regardless of crystal size.

These four samples (JP-ACF-1, JP-ACF-2, JP-KG, and JP-AF-1) experienced conditions allowing for the lattice to be altered and grains to recrystallize at mid-crustal levels due to deformation during shear zone movement. Since it appears that almost a

total recrystallization occurred, then it is probable that these dates reflect the timing of the last deformation. This suggests that the latest metamorphic conditions experienced by these samples were positioned in the crust below, but near, the brittle-ductile transition of Sibson (1977). This seems reasonable considering that a nominal $\sim 350^\circ\text{C}$ temperature of closure for muscovite corresponds roughly to the typical brittle-ductile transition levels in continental crust ($\sim 15\text{ km}$ depth).

Micas' inherent rheologies allow them to accommodate much of the overall internal deformation in rocks during orogenic deformation (Cosca et al., 2011). Shearing of rocks and the associated dynamic recrystallization of grains occurs at the lattice scale by means of multiple mechanisms of internal migration of lattice defects: partial dislocations, unit dislocations, line dislocations, edge/screw dislocations, and dislocation creep causing progressive subgrain rotation, basal slip, folding, kinking, stack faulting, and grain boundary migration (Etheridge, 1973; Etheridge and Hobbs, 1974; Wilson and Bell, 1979; Lister and Snoke, 1984; Meike, 1989; Kronenberg et al., 1990; Dunlap et al., 1991; Passchier and Trouw, 2005; and Cosca et al., 2011). Cosca et al. (2011) explain that, "Reduction in the effective diffusion length scale in naturally deformed samples occurs most probably through production of mesoscopic and submicroscopic defects such as, e.g., stacking faults. A network of interconnected defects, continuously forming and annealing during dynamic deformation, likely plays an important role in controlling both ^{40}Ar retention and intragrain distribution in deformed mica." Argon is chemically inert and resides within a mineral's lattice defects, defects such as point defects (vacancies and interstitials) or line defects (dislocations and partial dislocations) (Cosca et al., 2011). Loss of radiogenic argon, from white micas in particular, is dependent upon lattice

defects, the temperature reached during deformation, residence time at those temperatures, the degree of recrystallization, the degree of internal deformation, and grain boundary migration (Dunlap et al., 1991; Cosca et al., 2011). The distance for grain size diffusion and diffusion length scale decreases with increasing deformation (Kelley, 1988; Goodwin and Renne, 1991; Hess et al., 1993; Markley et al., 2002; and Cosca et al., 2011). Cosca et al. (2011) reported that if minerals, specifically micas, remain at relatively lower temperatures (near the brittle-ductile transition) over the period of deformation then they may preserve intracrystalline deformation features, and shear zones lying within polymetamorphic terranes containing recrystallized mica shear bands and/or mica fish could preserve and record $^{40}\text{Ar}/^{39}\text{Ar}$ protracted time-temperature histories.

Deformation under greenschist/amphibolite facies conditions typically causes a reduction in grain size, dissolution of old grains, and recrystallization into new grains; however, the “breakdown of micas during deformation is a complex process driven by both stored energy and chemical free energy,” which generally deform by disaggregation along cleavage, kinking, folding, and fracturing (Etheridge and Hobbs, 1974; Dunlap et al., 1991). Although this deformation and shearing/mylonitization causes a grain size reduction partially by mechanical disaggregation, dissolution, and recrystallization, recrystallization appears to also cause grains to grow. So, as old grains are reducing in size, the “new” grains appear to grow due to both static and dynamic recrystallization. The strain observed in samples dated as a result of these stresses is evident. However, there appears to be no consistent crystallization rate versus strain rate, but as shear ceased, so did diffusion. Hence, ~317.5 Ma is interpreted to represent a deformation age.

Amanda Reynolds' muscovite dates were obtained from metamorphic rocks distant from throughgoing shear zones and they generally record isotopic closure between ~312 to 298 Ma based on the mean dates for each sample. This is consistent with the interpreted time frame of 315 Ma to 300 Ma (Alleghanian) for cooling of the regional metamorphic event. There appears to be a trend among the three terranes with rocks of the Jacksons Gap group having younger cooling ages (303.6 Ma to 297.7 Ma) overall, indicating that rocks of these units were the last among the terranes to reach closure. Samples from the Dadeville Complex have closure dates somewhat earlier than those of the Jacksons Gap and the sample of the Kowaliga Gneiss of the eastern Blue Ridge has the oldest closure date.

Rocks deformed and metamorphosed during the Alleghanian orogenic event within shear zones appear to have cooled earlier than that of rocks away from shear zones, suggesting that shear deformation ceased just prior to regional cooling. Figure 40 is a collage of all ten relative probability plots to summarize and illustrate where obtained ages overlap and the probability density is the strongest, between 319 and 315 Ma and 310 and 300 Ma. Lithologies tracing around the Tallasse synform to the southeast show progressively younger ages of cooling. This may suggest that normal fault movement caused tectonostratigraphically lower footwall blocks, to the northwest, to be exhumed and cooled prior to hanging wall blocks. Folding by the late-stage Tallasse synform may have also tilted the fault blocks, placing older and younger muscovite ages at the same erosional horizon. Previous isotopic studies support this trend of later cooling towards the southeast, with some rocks in the region maintaining temperatures above 300° C as late as 290 Ma (Wampler, 1970; Steltenpohl and Kunk, 1993; and Cook and Thompson, 1995).

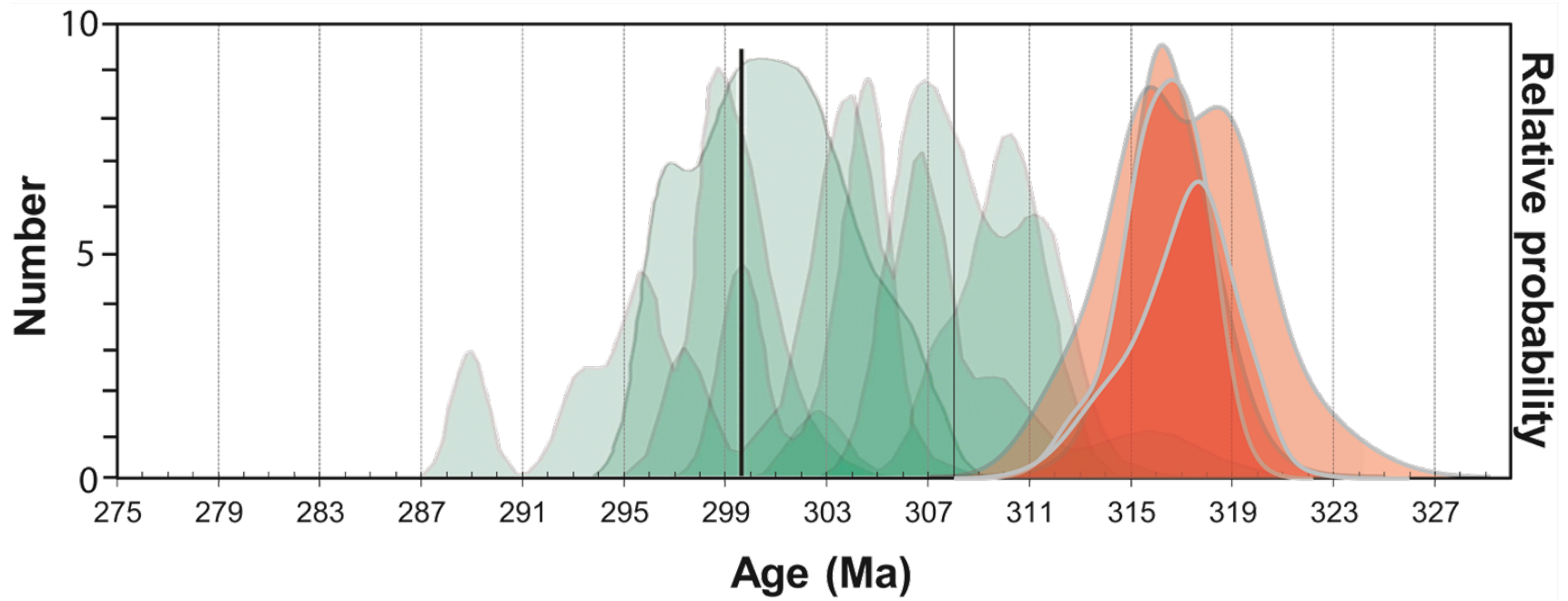


Figure 40. Collage of all 10 probability density plots illustrating where the dates obtained correlate the most (Reynolds' density plots in green and author's plots in red).

CONCLUSIONS

The oldest units on the Jacksons Gap Quadrangle likely are those of the eastern Blue Ridge. These rocks reflect the Neoproterozoic to Cambrian slope-rise of the eastern Laurentian margin that evolved into a back-arc basin with time. During the Late Ordovician to Early Silurian, this package was intruded by the Kowaliga granite, which engulfed mafic and tonalitic lavas that likely correspond to metamorphosed Early Ordovician volcanics exposed elsewhere in the Blue Ridge (e.g., the 470 Ma Hillabee Greenstone; McClellan et al., 2007). Next, the Jacksons Gap Group probably records the shallowing of the back-arc basin to include clean sands (barrier islands or submarine fans?) infused with felsic and mafic volcanics and lavas at the top, recording the approach of the colliding Dadeville Complex island-arc.

The Jacksons Gap Group contains greenschist- to lower-amphibolite-facies assemblages and is sandwiched between the relatively high-grade eastern Blue Ridge and Dadeville Complex. Down-heating during syn-metamorphic movement along the Katy Creek fault to emplace the Dadeville Complex arc accounts for its cryptic nature. The contact between the top of the Emuckfaw Group and the base of the Jacksons Gap Group may have originally been an unconformity or stratigraphic boundary later exploited by the Abanda fault. Low-strain units contain relict sedimentary structures that generally indicate that the units remain stratigraphically upright. Repetition and excision of strata along strike is due to a combination of doubly-plunging folds and shearing/faulting that

imbricated along highly graphitic units. Zones of mylonitization appear to anastomose, leaving lenses of rock with relatively low-strain.

The Brevard zone in Alabama has unique qualities that have important implications for the tectonic development of this controversial Appalachian structure. The Katy Creek is a cryptic pre- to syn-peak metamorphic fault marking the boundary with the Dadeville Complex-arc suture. The Abanda fault, on the contrary, is a retrograde fault with kinematic and rheologic characteristics almost identical to that of the Alexander City fault/shear zone. The two zones, and associated fabrics and structures, are interpreted to represent regionally, reactivated (polyphase), mid-crustal level, Alleghanian, ductile shear zones with a major right-slip component. Minor normal and reverse-slip components are interpreted to reflect dynamic motion along the fault plane.

Based on isotopic $^{40}\text{Ar}/^{39}\text{Ar}$ muscovite dating analyses, it is concluded that shearing and regional cooling are not synchronous. The author's dates were obtained from phyllonites and mylonites within and proximal to the Abanda and Alexander City fault zones and the resulting ~318-316 Ma ages are interpreted to represent the time of the latest ductile movement. Isotopic dates reported for muscovites from metamorphic rocks distal to major shear zones range from ~312 to 298 Ma and are interpreted to reflect regional cooling following faulting at ~317.5 Ma. That muscovites from the shear zones are statistically older than the average metamorphic cooling dates is interpreted to indicate exhumation due to normal faulting and later tilting of fault blocks by the late-stage Tallasse synform.

The cataclastic zones that parallel to the Abanda fault and also splay off towards the Alexander City fault zone may reflect one or a combination of the following: 1.) they

may be small, not discernable, displacement faults; 2.) displacement within them may have been synchronous with nearby ductile shear zones but siliceous fluids that flushed the zones was not hot enough to allow for diffusion and resetting of argon isotopes within muscovites (Hawkins, 2013); 3.) rounding of clasts may indicate tensile opening of zones where a fluidized environment caused clasts to periodically be rounded; or 4.) they may reflect Mesozoic tensional relay zones between Triassic and Jurassic extensional faults.

REFERENCES

- Abrahams, J.B., 2014, Geology of the Dadeville Quadrangle and the Tallassee synform in characterizing the Dog River window, [unpublished M.S. thesis]: Auburn University, Auburn, Alabama, p. 126.
- Beiler, D.B., and Deininger, R.W., 1987, Geologic setting of the Kowaliga Augen Gneiss and the Zana Granite, northern Alabama Piedmont: in Drummond, M.S., and Green, N.L., eds., *Granites of Alabama: Geological Survey of Alabama*, p. 57-72.
- Bentley, R.D., and Neathery, T.L., 1970, Geology of the Brevard zone and Related Rocks of the Inner Piedmont of Alabama: Tuscaloosa, AL, Alabama Geological Society 8th Annual Field Trip Guidebook, 119 p.
- Bobyarchick, A.R., Edelman, S.H., and Horton, J.W., Jr., 1988, The role of dextral strike-slip in the displacement history of the Brevard fault zone, in Secor, D.T., Jr., ed., *Southeastern Geological Excursions: Geological Society of America 1988 Annual Meeting Field Trip Guidebook*, p. 53-104.
- Bobyarchick, A.R., 1999, The history of investigation of the Brevard fault zone and evolving concepts in tectonics: *Southeastern Geology*, v. 38, no. 3, p. 223-238.
- Coker-Dewey, J., Steltenpohl, M.G., and Andresen, A., 2000, Geology of western Ullfjord, North Norway, with emphasis on the development of an inverted metamorphic gradient at the Top of the Lyngen Nappe Complex: *Norsk Geologisk Tidsskrift*, v. 80.2, p. 111-127.
- Cook, F.A., Albuagh, D.S., Brown, L.D., Kaufman, S., Oliver, J.E., and Hatcher, R.D., Jr., 1979, Thin-skinned tectonics in the crystalline southern Appalachians; COCORP seismic-reflection profiling of the Blue Ridge and Piedmont: *Geology*, v. 7, p. 563-567.
- Davis, T.L., 1993, Lithostratigraphy, structure, and metamorphism of a crystalline thrust terrane, western Inner Piedmont, North Carolina [PhD dissertation]: University of Tennessee, 245 p.
- Dennis, A.J., and Secor, D.T., 1987, A model for the development of crenulations in shear zones with the applications from the southern Appalachian Piedmont: *Journal of Structural Geology*, v. 9, no. 7, p. 807-817.

- Dodson, M.H., and McClelland-Brown, E., 1985, Isotopic and palaeomagnetic evidence for rates of cooling, uplift, and erosion, *in* Snelling, N.J., ed., *The chronology of the geologic record: Geological Society of London Memoir 10*, p. 315-325.
- Drummond, M.S., Allison, D.T., and Wesolowski, D.J., 1994, Igneous petrogenesis and tectonic setting of the Elkahatchee Quartz Diorite, Alabama Appalachians: Implications for the Penobscotian Magmatism in the eastern Blue Ridge: *American Journal of Science*, v. 294, p.173-236.
- Duebendorfer, E.M., 1988, Evidence for an inverted metamorphic gradient associated with a Precambrian suture, southern Wyoming: *Journal of Metamorphic Geology*, v. 6, p. 41-63.
- Dunlap, W.J., Teyssier, C., McDougall, I., and Balwin, S., 1991, Ages of deformation from K/Ar and $^{40}\text{Ar}/^{39}\text{Ar}$ dating of white micas: *Geology*, v. 19, p. 1213-1216.
- Etheridge, M.A., and Hobbs, B.E., 1974, Chemical and deformational controls on recrystallization of mica: *Contributions to Mineralogy and Petrology*, v. 43, p. 111-124.
- Hames W.E., and Hodges K. V., 1993, Laser $^{40}\text{Ar}/^{39}\text{Ar}$ evaluation of slow cooling and episodic loss of ^{40}Ar from a sample of polymetamorphic muscovite: *Science* 261, p.1721-1723.
- Harrison T.M., and McDougall I., 1981, Excess ^{40}Ar in metamorphic rocks from Broken Hill, New South Wales: Implications for $^{40}\text{Ar}/^{39}\text{Ar}$ age spectra and the thermal history of the region; *Earth and Planetary Science Letters*, v. 55, p.123–149
- Hatcher, R.D., Jr., 1972, Developmental model for the southern Appalachians: *Geological Society of America Bulletin*, v. 83, p. 2735-2760.
- Hatcher, R.D., Jr., 1987, Tectonics of the southern and central Appalachian internides: *Annual Review of Earth and Planetary Sciences*, v. 15, p. 337-362.
- Hatcher, R.D., Jr., Osberg, P.H., Drake, A.A., Jr., Robinson, P., and Thomas, W.A., 1990, Tectonic Map of the U.S. Appalachians: The Appalachian-Ouachita Orogen in the United States, v. F-2 of *The Geology of North America (GNA-F2)*.
- Hatcher, R.D., Jr., 2001, Rheological partitioning during multiple reactivation of the Paleozoic Brevard fault zone, southern Appalachians, USA, *in* Holdsworth, R.E., et al., eds., *The Nature and Tectonic Significance of Fault Zone Weakening: Geological Society of London Special Publication 186*, p. 255–269.

- Hatcher, R.D., Jr., and Merschat, A.J., 2006, The Appalachian Inner Piedmont: An exhumed strike-parallel, tectonically forced orogenic channel, *in* Law, R.D., Searle, M.P., and Godin, L., eds., Channel Flow, Ductile Extrusion and Exhumation in Continental Collision Zones: Geological Society of London Special Paper 268, p. 517–541.
- Hatcher, R.D., Jr., 2010, The Appalachian orogen: A brief summary, in Tollo, R.P., Bartholomew, M.J., Hibbard, J.P., and Karabinos, P.M., eds., From Rodina to Pangea: The Lithotectonic Record of the Appalachian Region: Geological Society of America Memoir 206, p. 1-19.
- Hawkins, J.F., Steltenpohl, M.G., Zou, H., Mueller, P.A., and Schwartz, J.J., 2013, New constraints on Ordovician magmatism in the southernmost exposures of the eastern Blue Ridge in Alabama: Geological Society of America Abstracts with Programs, v. 45, p. 62.
- Hawkins, J.F., 2013, Geology, petrology, and geochronology of rock in Our Town, Alabama quadrangle [M.S. thesis]: Auburn, Auburn University, 118p.
- Hirth, G., and Tullis, J., 1992, Dislocation Creep Regimes in Quartz Aggregates: Journal of Structural Geology, v. 14.2, p. 145-59.
- Hodges, K.V. 1991, Pressure-temperature-time paths: Annual Review of Earth and Planetary Sciences, v. 19, p. 207-236.
- Holdaway, M.J., 1971, Stability of andalusite and the aluminosilicate phase diagram: American Journal of Science, v. 271, p. 97-131.
- Hopson, J.L. and Hatcher, R.D., Jr., 1988, Structural and stratigraphic setting of the Alto allochthon, northeast Georgia: Geological Society of America Bulletin, v. 100, p. 339-350.
- Horton, J.W., Jr., Avery, A.D., Jr., and Rankin, D.W., 1989, Tectonostratigraphic terranes and their Paleozoic boundaries in the central and southern Appalachians: Geological Society of America Special Paper 230, p. 213-245.
- Hoschek, G., 1969, The Stability of Staurolite and Chloritoid and their Significance in Metamorphism of Pelitic Rocks: Contributions to Mineralogy and Petrology, v. 22.3, p. 208-32.
- Hubbard, M.S., 1989, thermobarometric constraints on the thermal history of the Main Central Thrust zone and Tibetan Slab, eastern Nepal Himalaya: Journal of Metamorphic Geology 7, p. 19-30.
- Johnson, M.J., 1988, Geology of the gold occurrences near Jackson's Gap, Tallapoosa County, Alabama, [M.S. thesis]: Auburn University, Auburn, Alabama, 156 p.

- Keefer, W.D., 1992, Geology of the Tallassee Synform hinge zone and its relationship to the Brevard zone, Tallapoosa and Elmore Counties, Alabama [M.S. thesis]: Auburn, Auburn University, 195 p.
- McClellan, E.A., Steltenpohl, M.G., Thomas, C., and Miller, C.F., 2007, Isotopic Constraints and Metamorphic History of the Talladega Belt: New Evidence for Timing of Arc Magmatism and Terrane Emplacement Along the Southern Laurentian Margin: *The Journal of Geology*, v. 115, p. 541–561.
- Medlin, J.H., and Crawford, T.J., 1973, Stratigraphy and structure along the Brevard fault zone in western Georgia and Alabama: *American Journal of Science*, v. 273-A, p. 89-104.
- Merschat, A.H., Hatcher, R.D., Jr., and Davis, T.L., 2005, The northern Inner Piedmont, southern Appalachians, USA: Kinematics of transpression and SW-directed mid-crustal flow: *Journal of Structural Geology*, v. 27, p. 1252–1281.
- Muangnoicharoen, N., 1975, The geology and structure of a portion of the northern piedmont, east-central Alabama [M.S. thesis]: Tuscaloosa, University of Alabama, p. 72.
- Mueller, P. A., Wooden, J.L., Mogk, D.W., and Foster, D.A., 2011, Paleoproterozoic evolution of the Farmington zone: Implications for terrane accretion in southwestern Laurentia: *Lithosphere*, v. 3, p. 401-408.
- Neathery, T.L., and Reynolds, J.W., 1973, Stratigraphy and metamorphism of the Wedowee Group, a reconnaissance: *American Journal of Science Alabama*, v. 273, p. 723-741.
- Neathery, T.L., ed., 1975, Rock units in the high-rank belt of the northern Alabama Piedmont, Alabama Geological Society, Annual Field Trip Guidebook, no.13, Geologic profiles of the northern Alabama Piedmont, p. 9-48.
- Neathery, T.L., and Reynolds, J.W., 1975, Geology of the Lineville East, Ofelia, Wadley North and Mellow Valley quadrangles, Alabama: Geological Survey of Alabama Bulletin no. 109, 120 p.
- Neilson, M.J., and Stow, S.H., 1986, Geology and geochemistry of the mafic and ultramafic intrusive rocks, Dadeville belt, Alabama: *Geological Society of America Bulletin*, v. 97, p. 296-304.
- Nelson, K.D., Arnow, J.A., Giguere, M., and Schamel, S., 1987, Normal-fault boundary of an Appalachian basement massif: Results of COCORP profiling across the Pine Mountain belt in western Georgia: *Geology*, v. 15, p. 832-836.

- Osborne, W.E., Szabo, M.W., Neathery, T.L., and Copeland, C.W., Jr., compilers, 1988, Geologic map of Alabama, northeast sheet: Alabama Geological Survey Special Map 220, scale 1:250,000.
- Raymond, D.E., Osborne, W.E., Copeland, C.W., and Neathery, T.L., 1988, Alabama stratigraphy: Alabama Geological Survey Circular 140, 97 p.
- Renne, P.R., Swisher, C.C., Deino, A.L., Karner, D.B., Owens, T.L., and DePaolo, D.J., 1998, Intercalibration of standards, absolute ages and uncertainties in $^{40}\text{Ar}/^{39}\text{Ar}$ dating: *Chemical Geology*, v. 145, p. 117-152.
- Richardson, S.W., 1968, Staurolite stability in a part of the system Fe-Al-Si-O-H: *Journal of Petrology*, v. 9.3, p. 467-489.
- Robbins, G.A., 1972, Radiogenic argon diffusion in muscovite under hydrothermal conditions [M.S. thesis]: Providence, Rhode Island, Brown University, p. 189.
- Russell, G.S. 1987, U-Pb, Rb-Sr, and K-Ar isotopic studies bearing on the development of the southernmost Appalachian orogen, Alabama [Ph.D. thesis]: Tallahassee, Florida, Florida State University, p. 197.
- Schamel, S., Hanley, T.B., and Sears, J.W., 1980, Geology of the Pine Mountain Window and adjacent terranes in the Piedmont province of Alabama and Georgia: Southeastern Section of the Geological Society of America Field Trip Guidebook.
- Sears, J.W., Cook, R.B., and Brown, D.E., 1981, Tectonic evolution of the western part of the Pine Mountain window and adjacent Inner Piedmont Province, in Sears, J.W., ed., Contrasts in tectonic style between the Inner Piedmont terrane and the Pine Mountain window: Alabama Geological Society, 18th Annual Field Trip Guidebook, p. 1-13.
- Sibson, R. H., 1977, Fault rocks and fault mechanisms: *Geological Society of London Journal*, v. 133, p. 191-213.
- Steltenpohl, M.G., 1988, Kinematics of the Towaliga, Bartletts Ferry, and Goat Rock fault zones, Alabama: The late Paleozoic dextral shear system in the southernmost Appalachians: *Geology*, v. 16, p. 852-855.
- Steltenpohl, M.G., and Moore, W.B., 1988, Metamorphism in the Alabama Piedmont: Alabama Geological Survey Circular 138, 27 p.
- Steltenpohl, M.G., 1988, The Pine Mountain window of Alabama: Basement-cover evolution in the southernmost exposed Appalachians: *International Basement Tectonics Association Publication*, n. 8, p. 491-501.

- Steltenpohl, M.G., 1990, Structural development of the Opelika Complex, in Steltenpohl, M.G., et al., eds., *Geology of the southern Inner Piedmont terrane, Alabama and southwest Georgia: Southeastern Section of the Geological Society of America Field Trip Guidebook*, p. 29-42.
- Steltenpohl, M.G., Heatherington, A., Mueller, P., and Miller, B. V., 2005a, Tectonic implications of new isotopic dates on crystalline rocks from Alabama and Georgia, *in* Steltenpohl, M.G., Hanley T.B., and Cook R.B., ed., *New Perspectives on Southernmost Appalachian Terranes, Alabama and Georgia: Geological Society of Alabama 42nd Annual Field Trip Guidebook*, p. 51–69.
- Steltenpohl, M.G., 2005b, An introduction to the terranes of the southernmost Appalachians of Alabama and Georgia, *in* Steltenpohl, M.G., Hanley T.B., and Cook R.B., ed., *New perspectives on southernmost Appalachians terranes, Alabama and Georgia: Alabama Geological Society, 42nd Annual Field Trip Guidebook*, p. 3.
- Steltenpohl, M.G., Mueller, P.M., Heatherington, A.L., Hanley, T. B., and Wooden, J.L., 2008, Gondwanan/peri-Gondwanan origin for the Uchee terrane, Alabama and Georgia: Carolina zone or Suwannee terrane(?) and its suture with Grenvillian basement of the Pine Mountain window: *Geosphere*, v. 4, p. 131-144.
- Steltenpohl, M.G., Moecher, D., Andresen, A., Ball, J., Mager, S. & Hames, W.E., 2011, The Eidsfjord shear zone, Lofoten–Vesteralen, north Norway: an Early Devonian, paleoseismogenic low-angle normal fault. *Journal of Structural Geology*, 33, p. 1023–1043.
- Steltenpohl, M.G., Schwartz, J.J., Miller, B.V., 2013, Late to post-Appalachian strain partitioning and extension in the Blue Ridge of Alabama and Georgia: *Geosphere*, v. 9; n. 3, p. 647-666.
- Sterling, J.W., Steltenpohl, M.G., Cook, R.B., and Thomas B. Hanley, T.B., 2005, *Petrology and Geochemistry of Igneous Rocks in the Southernmost Brevard zone of Alabama and their Implications for Southern Appalachian Tectonic Evolution: Guidebook for the 42nd Annual Field Trip of the Alabama Geological Society*, p. 96-124.
- Sterling, J.W., 2006, *Geology of the southernmost exposures of the Brevard zone in the Red Hill Quadrangle, Alabama [M.S. thesis]: Auburn, Auburn University*, p. 118.
- Stow, S.H., Neilson, M.J., and Neathery, T.L., 1984, Petrography, geochemistry and tectonic significance of the amphibolites of the Alabama Piedmont: *American Journal of Science*, v. 284, nos. 4 and 5, p. 416-436.

- Thomas, W.A., 1977, Evolution of Appalachian-Ouachita salients and recesses from reentrants and promontories in the continental margin: *American Journal of Science*, v. 277, p. 1233–1278.
- Tull, J.F., 1978, Structural development of the Alabama Piedmont northwest of the Brevard zone: *American Journal of Science*, v. 278, p. 442-460.
- Tull, J.F., Barineau, C.I., Holm-Denoma, C.S., 2012, Characteristics, Extent, and Tectonic Significance of the Middle Ordovician Back-Arc Basin in the Southern Appalachian Blue Ridge, in Barineau, C.I., and Tull, J.F., *The Talledega Slate Belt and the eastern Blue Ridge: Laurentian plate passive margin to back-arc basin tectonics in the southern Appalachian orogen: Field Trip Guidebook for the Alabama Geological Society*, p. 12-26.
- Tull, J.F., Barineau, C.I., and Holm-Denoma, C.S., 2013, Characteristics, Extent, and Tectonic Significance of the Middle Ordovician Back-Arc Basin in the Southern Appalachian Blue Ridge, in Barineau, C.I., and Tull, J.F., *The Talladega Slate Belt and the eastern Blue Ridge: Laurentian plate passive margin to back-arc basin tectonics in the southern Appalachian orogen: Field Trip Guidebook for the Alabama Geological Society*, p. 12-26.
- Vauchez, A., 1987, Brevard fault zone, southern Appalachians: A medium-angle, dextral, Alleghanian shear zone: *Geology*, v. 15, p. 669–672.
- Vauchez, A., Babaie, H.A., and Babaei, A., 1993, Orogen-parallel tangential motion in the Late Devonian-Early Carboniferous southern Appalachians internides: *Canadian Journal of Earth Sciences*, v. 30, p. 1297–1305.
- Wagner, M.E., and Srogi, L., 1987, Early Paleozoic metamorphism at two crustal levels and a tectonic model for the Pennsylvania-Delaware Piedmont: *Geological Society of America Bulletin* v. 99, p. 113-126.
- White, T.W., 2008, *Geology of the 1:24,000 Tallassee, Alabama, Quadrangle, and its implications for southern Appalachian tectonics [M.S. thesis]: Auburn, Alabama, Auburn University*, p. 74.
- Wielchowsky, C.C., 1986, *The geology of the Brevard Zone and adjacent terranes in Alabama [Ph.D. dissertation]: Rice University, Houston, Texas*, 225 p.

II. GRAPHICAL TOOLS FOR TEACHING GEOMETRIES AND KINEMATICS OF FAULT ZONES

ABSTRACT

Two-dimensional graphical methods and a simple cut-and-staple paper model are described to help students visualize and understand three-dimensional fault-rock structures/fabrics and how to deduce from their movement sense. Lower hemisphere, equal-area, stereographic projections have long been used to help understand the geometry of geologic structures. This study sprung from our effort to resolve problems recognized while mapping oblique-slip shears in naturally deformed rocks (mylonites and phyllonites) from southern Appalachian fault zones. The technique enables one to stereographically solve the specific direction and sense of movement in both directions parallel to strike and to dip, hence, quantifying the oblique-sense of motion. It requires one to first understand the field relationships of the penetrative mylonitic fabrics in the rock, and second, to plot and analyze the measured data on a stereogram. The direction of the fault zone movement, either locally or regionally, may be determined using the relationships between the schistosity (S) and cisaillement (C) planes plotted as poles, and their relation to the each other along with the primitive and center of the stereonet. Our technique allows for solving of movement direction in the dip-slip (reverse/normal), strike-slip (dextral/sinistral), and oblique-slip motions from stereographic information.

Digital and physical models are provided to help advanced undergraduate and graduate students to better understand and grasp S-C fabrics and their applications for quantifying movement sense along natural faults.

INTRODUCTION

Schistosity (S) and Cisaillement (C) penetrative shear fabrics are tried-and-true indicators of movement along faults and shear zones (Berthé et al., 1979; Jegouzo, 1980; Lister and Snoke, 1984). The Brevard zone and Alexander City fault zone have well-developed S-C fabrics that make them easy to find and map. Careful mapping along strike of these zones indicate predominantly right-lateral S-C fabrics as had earlier been described, but persistent oblique components are also recognized. Potential explanations for oblique components are: 1.) multiple, diachronous movements; 2.) movements having occurred in distributed shears as well as singular, distinct faults; and 3.) porpoising of the plunge of movement along the primarily right-lateral strike-slip shear zones to either side of horizontal result in alternating oblique-normal-and-reverse motion along the same fault. During mapping we recognized that care had to be taken to define segments with slight-normal versus slight-reverse oblique components. We, therefore, explored methods to quantify the down-dip movement components of these faults for the various segments. The most practical method we find is the lower hemisphere stereographic projection, a powerful and field portable tool known to most all students of geology.

In this report we explain our semi quantitative method for characterizing fault movement that has general applicability. It is easily transportable and decipherable. In addition, electronic and physical models are presented that help to illustrate this method. The reader is assumed to have a basic background in S-C fabrics, and experience using stereographic projections, but if not, we recommend Simpson (1986) and Marshak and Mitra (1988).

S-C FABRICS AND THEIR GEOMETRIES

The impetus for this study comes from field/structural and petrographic studies of mylonites and phyllonites in east-central Alabama within and proximal to major southern Appalachian fault zones (Fig. 1). The outcrops studied lie within the retrogressive Brevard and Alexander City fault zones (Fig. 1) (Bentley and Neathery, 1970; Steltenpohl, 2005, 2013). The Brevard fault zone is a fundamental, polyphase shear zone separating Laurentian eastern Blue Ridge rocks from the Inner Piedmont suspect terranes and extends from Mt. Airy, North Carolina, southwest to the Coastal Plain onlap in Tallahassee, Alabama (Fig. 1). The Alexander City fault zone also contains polyphase structures and fabrics, but is internal to the eastern Blue Ridge terrane generally separating the structurally lower Wedowee Group from the Emuckfaw Group (Fig. 1) (Bentley and Neathery, 1970; Neathery and Reynolds, 1973, 1975; Osborne et al., 1988; Steltenpohl, 2005).

Higgins (1971), Bell and Etheridge (1973), Sibson (1977), and Wise et al. (1984) established early terminology and classification schemes for fault rocks. Mylonitic rocks are products of ductile flow and crystal plastic grain-size reduction due to deformation within or below the brittle-ductile transition (~7-15 km deep in average continental rocks) (Bell and Etheridge, 1973; Sibson, 1977; White et al., 1980; Wise et al., 1984; Poirier, 1985). Criteria used to determine the shear sense of movement in mylonitic rocks was first recognized by Berthé et al. (1979) and Jegouzo (1980) and these subsequently were refined by numerous other workers stated below. Generally, shear initiates at the crystal-lattice scale by the migration of point and line imperfections that propagate grain boundaries, resulting in a change in their shapes. This results in preferred orientations of grains (crystallographic, lattice, and grain-shape preferred orientation, mineral elongation or stretching lineations) providing strain markers in mylonites that can be used to glean a vector for material flow within a fault zone (Berthé et al., 1979; Lister and Snoke, 1984; Lister and Price, 1978; Garcia-Celma, 1982; Schmid, 1983; Simpson, 1986). Ideally the slip-line should parallel elongation lineations measured in the field. Although it can be argued that the overall slip-line (i.e., flow direction) can parallel the acute bisectrix of the intersection of an S-C pair, we follow the convention that the slip-line lies in the C-plane 90° from S-C plane's intersection in the direction of slip (e.g., Berthé et al., 1979; Lister and Snoke, 1984).

Berthé et al. (1979) and Jegouzo (1980) recognized composite planar fabrics, S- and C-planes, and asymmetrically rotated grains as indicators for rotational shear sense; we follow this terminology and convention. Simpson (1986) is a pedagogical approach that introduced the term “shear bands” in place of S-C unless synchronous timing of the

two fabrics can be demonstrated. S-planes are either relict or synchronous foliations at an inclined angle to the shear bands (C-plane equivalents), the latter being parallel to the shear-zone boundaries. S-planes tilt away from the direction of shear and curve asymptotically into the shear bands, creating sigmoidal shapes (Simpson, 1986).

Sheared pelitic rocks, phyllonites, tend to develop cleavages that allow for the determination of shear sense (Borradaile et al., 1982). These cleavages are equivalent to S-C fabrics (Berthé et al., 1979; Lister and Snoke, 1984) or normal slip crenulations (Dennis and Secor, 1987, 1990). Platt and Vissers (1980) and Bell (1981) described sigmoidal crenulation cleavages that may resemble shear bands but are inclined in an antithetic or sympathetic sense of shear to the main shear zone boundary. Use of the asymmetry of porphyroclast tails as a way to determine shear sense is described in Berthé et al. (1970), Simpson and Schmid (1983), Passchier and Simpson (1986), Simpson (1986), and Lumino (1987).

Other shear-sense indicators are commonly found in addition to S-C planes and shear bands. The history of the development of thought in analyzing the sense of movement in mylonitic zones is beyond the scope of this report, but the interested reader can find it in reports by Zwart (1962), Eisbacher (1970), Rosenfeld (1970), Roper (1972), Vernon (1976), Cosgrove (1976), Gray (1977), Powell and Vernon (1979), Gray and Durney (1979), White (1979), Cobbald and Quinquis (1980), Ramsay (1980), White et al. (1980), Gapais and White (1982), Simpson and Schmidt (1983), Malavielle and Cobb (1986), Ramsay and Huber (1987). Davis et al. (1987), Saltzer and Hodges (1988), Marshak and Mitra (1988), Krohe (1990), Toyoshima (1998), and Passchier and Trouw (2005).

Lister and Snoke (1984) stated that “The existence of a mylonite is itself not of great consequence, but it is important whether or not the mylonite marks the locus of a movement zone.” Rocks from the Brevard and Alexander City fault zones are characterized by mylonites and phyllonites containing abundant shear sense indicators including S-C composite planar foliations, mica fish, phacoids, asymmetric quartzo-feldspathic augens, broken-displaced grains, anastomosing foliations, rotated grains with recrystallized tails, and micro-and meso-sopic folds of the shear foliation. S-C fabrics form the basis of the current report.

Field-measured attitudes collected from S- and C-plane pairs can be analyzed by plotting their great circles or poles on a lower hemisphere, equal-area Schmidt stereographic projection. An arc connects the poles of the S-C pair’s planes. The S-C intercept is a point representing the line of intersection of a given S-C pair. The region in which the slip-line lies within the C-plane determines whether the motion is dip-slip, strike-slip, or oblique-slip. With regards to the S-C pair’s great circles and poles proximity to the center of the stereonet and relative clockwise motions, one can delineate the movement sense as dip-slip (normal or reverse), strike-slip (right- or left-lateral, herein referred to as dextral or sinistral, respectively, as viewed from above the fault), or oblique-slip, and also the relative angular shear strain. This follows the assumption that the attitudes and orientations of structural features have not been altered or deformed since the most recent shearing event. Studying the cross-section of the shear fabric in conjunction with the stereographic projection maximizes the effectiveness of the technique. The key to success of the method is first understanding the relationship of the

shear structures within the rock, and then plotting and analyzing the measured data on the stereogram.

DETERMINING DIRECTION OF MOVEMENT FROM STEREOGRAMS

The sense of rotation and direction of movement along a shear zone based on S-C fabrics can be determined from a stereoplot. Faults and shear zones are classified as dip-slip, strike-slip, or oblique-slip based on relative movement of blocks of rocks flanking the zone of movement, which on a stereoplot simply plots where the slip-line lies along the C-plane. If the slip-line lies in the in the maximum dip position of the C-plane's great circle, then the fault/shear zone's movement is purely dip-slip (Fig. 2). In this case, the S-C intercept plots at the stereonet's primitive, 90° away from the slip-line. If the slip-line lies at the intersection of the C-plane's great circle and the stereonet's primitive, then the fault/shear zone's movement is strike-slip (Fig. 2). The S-C intercept plots at the maximum dip of the C-plane's great circle, 90° away from the slip-line. If the slip-line lies along the C-plane's great circle in-between the maximum dip and the stereonet's primitive, the movement is oblique-slip (Fig. 2).

Since field measurements made at multiple exposures along a shear zone inherently contain room for a variety of potential errors (e.g., discrepancies in rock fabrics, inaccuracies in measurements, slumped or crept exposures in particularly saprolitized rocks, etc.). Our convention is that if the slip-line is plotted 10° in either direction of true dip-slip or true strike-slip within the C-plane, then the movement style

stands; if the slip-line lies outside of this margin of error, however, then the movement is considered to be oblique-slip (Fig. 2). Hence, the resulting stereoplot provides a simple but powerful 2-D representation for quick quantitative assessment of the movement sense, and classifying of the fault.

As shown below, much more information, including qualitative assessment of angular shear strains, is gleaned from our approach.

DIP-SLIP

In a dip-slip shear zone, the S- and C-planes share the same strike orientation, but differ in dip magnitudes (Figs. 3, 4, 5, 6, 7, and 8). The movement sense can be resolved based the poles-to-planes' proximity to the center of the stereonet (Figs. 3 and 4). If the pole of the S-plane is more proximal to the stereonet's center than that of the C-plane, then the movement sense is normal dip-slip (Figs. 3, 5, and 6). With normal dip-slip motion, the dip of the C-plane will be greater than that of the S-plane (Figs. 3, 5, and 6).

The same fundamentals apply for reverse dip-slip shear zones, except that the geometries are inverted. In a reverse dip-slip shear zone, the pole to the C-plane is more proximal to the center of the stereonet than that of the pole of the S-plane (Fig. 4). So, with reverse dip-slip motion, the dip of S-plane is greater than that of the C-plane (Figs. 4, 7, and 8).

STRIKE-SLIP

Similar fundamentals that allow for one to resolve the movement sense in a dip-slip setting allow for the understanding of strike-slip movement, only the frame of

reference is rotated 90° from a cross-sectional view to a map view. With pure strike-slip motion, the S- and C-planes differ in strike, but share the same dip magnitude. In a dextral strike-slip shear zone, the pole and the great circle of the C-plane will be more clockwise than that of the S-plane's pole and great circle (Figs. 9A, 10, and 11). The criteria for sinistral strike-slip motion are just the inverse. The pole and the great circle of the S-plane will be more clockwise than that of the C-plane's pole and great circle (Figs. 9B and 12).

OBLIQUE-SLIP

In an oblique-slip shear zone, the S- and C-planes will have both differing strikes and dip magnitudes (Figs. 13 and 14). The fundamentals and criteria used to resolve the movement sense for either dip-slip or strike-slip can be used in combination to evaluate for an oblique-slip movement sense (Figs. 13 and 14). In Figure 15, nine sets of S-C pairs measured from one outcrop along the Abanda fault of the Brevard zone are plotted. A visually estimated average C-plane great circle is plotted and slip-lines, determined geometrically, are plotted and contoured. The slip-lines neither plot near the maximum dip of the C-plane, nor do they plot near the intersection of the C-plane and the primitive. They plot in-between them, documenting oblique-slip motion (Figs. 2 and 15). Arcs connecting the poles of S-C pairs show oblique-dextral-normal-and-reverse movement. All of the C-planes' poles are more clockwise than that of the S-planes' poles, reflecting the dextral component. Proximity of these poles to the center of the stereonet, however, reveals both normal (S-planes' poles more proximal to stereonet's center) and reverse (C-planes' poles more proximal to stereonet's center) components (Fig. 15).

PROBLEMS WITH STEEP AND SHALLOW DIP ANGLES

In instances of steep (greater than 80°) and shallow (less than 10°) angles of dip, this method risks falls short of being useful. This is due generally to the phenomena that the relationships previously defined for understanding dip-slip faults/shear zones can flip in these cases and can actually be the opposite; for example, the C-plane may dip less than the S-plane in normal slip. However, this inhibitence at extreme dip angles cannot be directly quantifiable due to multiple factors, the most significant one being that the angle between and orientation of S-C planes varies due to relative degrees of angular shear strain.

ESTIMATING RELATIVE DEGREE OF SHEAR

The angle between the S-C planes is measurable as the arc angle on a stereoplot, or the angle between the poles of these planes (Fig. 16). This angle qualitatively correlates to the relative angular shear, and/or the relative degree of shear. An increase in the relative angular shear results in the decrease of the arc angle between S-C planes (Fig. 16). Conversely, a decrease in the relative angular shear corresponds to an increase of the arc angle between S-C planes. It is noted that the arc angle also is the difference in dip between the two planes for dip-slip motion or the difference in strike with strike-slip; this is found through equal-triangle identities (Fig. 16).

A THREE-DIMENSIONAL S-C MODEL

The three-dimensional perspective views (in Figs. 5, 7, 10, 12, 14, and 16) were designed in a computer-aided design (CAD) program as a model for S-C fabrics. This has advantages in that these models can be sent to a 3-D printer to produce a rigid S-C model. These models are rigid and are not able to demonstrate relative degrees of shear, but they are durable and multiple models can be produced at varying sizes to exhibit varying degrees of shear.

Some students struggle with envisioning three-dimensional structures and benefit from the kinesthetic aid of physical models to better grasp fundamental principles. Although digital models help to mitigate these mental hindrances, tangible three-dimensional models allow for the curious student to hold the feature in their hands to begin to better understand the geometries and spatial relationships of the related structures or fabrics. A simple three-dimensional model of S-C fabrics, constructed with basic office supplies, therefore, is suggested (Fig. 17).

A few sheets of paper can be stapled together to create a representative model for S-C fabric relationships. The sheets are stacked length-wise with approximately one and one-half inch offset (Figs. 17A and B). Each sheet is attached to the one below with staples (Figs. 17A and B). A sheet of paper is then rolled up length-wise with approximately one and one-half inch overlap and attached with staples to form a cylinder (Figs. 17C and D). These cylinders are then inserted in-between the stacked sheets of paper to form the archetypal phacoidal/sigmoidal S-C geometry; however, to be more

discrete, these cylinders can be cut in half (Fig. 17E, D, and I). Colored sheets of construction paper or cardstock can then be attached to the model to define the S-C planes. For example, an orange or red sheet of construction paper or cardstock can be attached to the top of the model with approximately one-inch of overhang, and attached with staples to the first sheet of stacked papers to define the C-plane (Fig. 17F). A blue sheet of construction paper or cardstock can be cut to square dimensions and attached to the back of the sigmoidal shape of the model with staples to define the S-plane (Fig. 17G and H). The model is then complete (Fig. 17H and I). The advantage is that a paper model is easily reproducible, rigid enough to hold its shape, but also pliable enough to manipulate and demonstrate the relative degree of shear strain. The model can be extended lengthwise to pull the S-C planes closer together and demonstrate an increase in relative shear, and also compressed to spread the S-C planes for decreased relative shear.

CONCLUSIONS

The principles established herein were developed to better aid in resolving fault/shear zone kinematics and to further upper-level students' understanding of S-C fabric geometries and relationships. We establish a set of criteria for the relationship of S-C planes when plotted on a stereogram, combined with field observations that can help delineate the movement sense as either reverse or normal dip-slip, dextral or sinistral strike-slip, or various combinations of oblique-slip, and also the relative angular shear strain. It is noted the shortcomings of this technique in occasions of steep and shallow

angles of dip. Construction of simple three-dimensional models is explained to help visualize S-C fabrics as they relate to our method. Below is an abbreviated listing of our principle findings as related to S- and C-plane geometries and shear/fault zone movements.

DIP-SLIP

- Same strikes, different dips
- Normal shear sense → S plane's pole more proximal to center than C-plane's
 - Normal fault = dip of C plane > dip of S plane
- Reverse shear sense → C plane's pole more proximal to center
 - Reverse fault = dip of C plane > dip of S plane

STRIKE-SLIP

- Different strike, same dip
- Dextral shear sense
 - C plane's great circle and pole more clockwise than S plane's
- Sinistral shear sense
 - S plane's great circle and pole more clockwise than C plane's

OBLIQUE-SLIP

- Combination of principles established
 - For example dextral-normal shear sense

- ◆ Normal component → pole to S plane more proximal to stereonet's center
- ◆ Dextral component → pole to C plane more clockwise along arc than pole to S plane

PROBLEMS WITH EXTREME DIP ANGLES

In instances of steep and shallow angles of dip this method falls short of being useful due to the phenomena that the S-C relationships can actually be the opposite in these scenarios; however, it cannot be directly quantifiable due to multiple factors, for example, the angle between and the orientation of S-C planes varies due to relative degrees of angular shear strain.

RELATIVE DEGREE OF SHEAR

- Smaller arc angle/angle between S-C planes = larger degree of angular shear
- Larger arc angle between S-C planes = smaller degree of angular shear

REFERENCES

- Bell, T.H., and Etheridge, M.A., 1973, Microstructures of mylonites and their descriptive terminology: *Lithos*, v. 6, p. 337-348.
- Bell, T.H., 1981, Foliation development: the contribution, geometry, and significance of progressive bulk inhomogeneous shortening: *Tectonophysics*, v. 75, p. 273-296.
- Bentley, R.D. and Neathery, T.L., 1970, Geology of the Brevard zone and Related Rocks of the Inner Piedmont of Alabama: Tuscaloosa, Alabama, Alabama Geological Society 8th Annual Field Trip Guidebook, 119 p.
- Berthé, D., Choukroune, P. & Jegouzo, P., 1979, Orthogneiss, mylonite and non coaxial deformation of granites: the example of the South Armorican shear zone: *Journal of Structural Geology*, v. 1, no. 1, p. 31-42.
- Borradaile, G.J., Bayly, M.B., and Powell, C.M.A., 1982, Atlas of deformational and metamorphic rock fabrics: Springer-Verlag, Berlin Heidelberg, New York, 551 p.
- Cobbold, P.R., and Quinquis, H., 1980, Development of sheath folds in shear regimes: *Journal of Structural Geology*, v. 2, no. 1-2, p. 39-47.
- Cosgrove, J.W., 1976, The formation of crenulation cleavage: *Journal of the Geological Society of London*, v. 132, p. 155-178.
- Davis, G.H., Gardulski, A.F., and Lister, G.S., 1987, Shear zone origin of quartzite mylonite and mylonitic pegmatite in the Coyote Mountains metamorphic core complex, Arizona: *Journal of Structural Geology*, v. 9, no. 7, p. 289-297.
- Dennis, A.J., and Secor, D.T., 1987, A model for the development of crenulations in shear zones with the applications from the southern Appalachian Piedmont: *Journal of Structural Geology*, v. 9, no. 7, p. 807-817.
- Dennis, A.J., and Secor, D.T., 1990, On resolving shear direction in foliated rocks deformed by simple shear: *Geological Society of America Bulletin*, v. 102, p. 1257-1267.

- Eibacher, G.H., 1970, Deformation mechanics of mylonitic rocks and fractured granites in Cobequid Mountains, Nova Scotia, Canada: Geological Society of America Bulletin, v. 81, p. 2009-2020.
- Higgins, M.W., 1971, Cataclastic rocks: U.S. Geological Survey Professional Paper 687, p. 97.
- Hobbs, B.E., Means, W.D., and Williams, P.F., 1976, An Outline of Structural Geology: John Wiley and Sons, New York, 571 p.
- Gapais, D., and White, S.H., 1982, Ductile shear bands in a naturally deformed quartzite: Textures and Microstructures, v. 5, p. 1-17.
- Garcia-Celma, A., 1982, Domainal and fabric heterogeneities in the Cap de Creus quartz mylonites: Journal of Structural Geology, v. 4, p. 443-455.
- Gray, D.R., 1977, Morphological classification of crenulation cleavage: Journal of Geology, v. 85, p. 229-235.
- Gray, D.R., and Durney, D.W., 1979, Investigations on the mechanical significance of crenulation cleavage: Tectonophysics, v. 58, p. 35-79.
- Jegouzo, P., 1980, The South Armorican shear zone: Journal of Structural Geology, v. 2, no. 1-2, 39-47.
- Krohe, A., 1990, Local variations in quartz (c)-axis orientations in non-coaxial regimes and their significance for the mechanics of S-C fabrics: Journal of Structural Geology, v. 12, p. 995-1004.
- Lister, G.S., and Price, G.P., 1978, Fabric development in a quartz-feldspar mylonite: Tectonophysics, v. 49, p. 37-78.
- Lister, G.S., and Snoke, A.W., 1984, S-C mylonites: Journal of Structural Geology, v. 6, no. 6, p. 617- 638.
- Lumino, K.M., 1987, Deformation within the Diana Complex along the Carthage-Colton mylonite zone: M.S. thesis, University of Rochester, Rochester, New York, 104 p.
- Malavieille J. et F. Cobb. 1986, Cinématique des déformations ductiles dans trois massifs métamorphiques de l'Ouest des Etats-Unis : Albion (Idaho), Raft River et Grouse Creek (Utah): Geological Society of France Bulletin, Numéro Spécial Cordillères Nord Américaines, t. 2, n. 6, p. 885-898.
- Marshak, S., and Mitra, G., 1988, Basic Methods of Structural Geology: Prentice Hill, Englewood Cliffs, New Jersey, 446 p.

- McClellan, E.A., Steltenpohl, M.G., Thomas, C., and Miller, C., 2007, Isotopic age constraints and metamorphic history of the Talladega belt: New evidence for timing of arc magmatism and terrane emplacement along the southern Laurentian margin: *Journal of Geology*, v. 115, p. 541–561.
- Neathery, T.L., and Reynolds, J.W., 1973, Stratigraphy and metamorphism of the Wedowee Group, a reconnaissance: *American Journal of Science*, v. 273, p. 723-741.
- Neathery, T.L., and Reynolds, J.W., 1975, Geology of the Lineville East, Ofelia, Wadley North and Mellow Valley quadrangles, Alabama: Geological Survey of Alabama Bulletin no. 109, 120 p.
- Osborne, W.E., Szabo, M.W., Neathery, T.L., and Copeland, C.W., Jr., compilers, 1988, Geologic map of Alabama, northeast sheet: Alabama Geological Survey Special Map 220, scale 1:250,000.
- Passchier, C.W., and Simpson, C., 1986, Porphyroclast systems as kinematic indicators: *Journal of Structural Geology*, v. 8, p. 831-843.
- Passchier, C.W., and Trouw, R.A.J., 2005, *Microtectonics*: Springer-Verlag, Berlin Heidelberg, Germany, ed. 2, 382 p.
- Platt, J.P., and Vissers, R.L.M., 1980, Extensional structures in anisotropic rocks: *Journal of Structural Geology*, v. 2, p. 397-410.
- Poirier, J.P., 1985, *Creep of Crystals*: Cambridge University Press, Cambridge, 260 p.
- Powell, C.M., and Vernon, R.H., 1979, Growth and rotation history of garnet porphyroblasts with inclusion spirals in a Karakoram schist: *Tectonophysics*, v. 54, p. 25-43.
- Ramsey, J.G., 1980, Shear zone geometry, a review: *Journal of Structural Geology*, v. 2, p. 83-89.
- Ramsey, J.G., and Huber, M.I., 1987, *The Techniques of Modern Structural Geology*, Volume 2, Folds and Fractures: Academic Press, London, p. 309-700.
- Roper, P.J., 1972, Structural significance of “button” or “fish scale” texture in the phyllonitic schist of the Brevard zone: *Geological Society of America Bulletin*, v. 83, p. 853-860.
- Rosenfeld, J.L., 1970, Rotated garnets in metamorphic rocks: *Geological Society of America Special Papers* 129, 105 p.

- Saltzer, S.D., and Hodges, K.V., 1988, The Middle Mountain shear zone, southern Idaho: kinematic analysis of an early Tertiary high-temperature detachment: *Geological Society of America Bulletin*, v. 100, p. 96-103.
- Schmid, S.M., 1983, Microfabric studies as indicators of deformation mechanisms and flow laws operative in mountain building: in Hsu, K.J., (ed.), *Mountain Building Processes*: Academic Press, London, p. 95-110.
- Sibson, R.H., 1977, Fault rocks and fault mechanisms: *Journal of the Geological Society of London*, v. 133, p. 191-213.
- Simpson, C., 1986, Determination of movement sense in mylonites: *Journal of Geological Education*, v. 34, p. 246-261.
- Simpson, C., and Schmid, S.M., 1983, An evaluation of criteria to deduce the sense of movement in sheared rocks: *Geological Society of America Bulletin*, v. 94, p. 1281-1288.
- Steltenpohl, M.G., 1988, Kinematics of the Towaliga, Bartletts Ferry, and Goat Rock fault zones, Alabama: The late Paleozoic dextral shear system in the southernmost Appalachians: *Geology*, v. 16, p. 852-855.
- Steltenpohl, M.G., Heatherington, A., Mueller, P., and Miller, B. V., 2005, Tectonic implications of new isotopic dates on crystalline rocks from Alabama and Georgia, in Steltenpohl, M.G., Hanley T.B., and Cook R.B., eds., *New Perspectives on Southernmost Appalachian Terranes, Alabama and Georgia: Geological Society of Alabama 42nd Annual Field Trip Guidebook*, p. 51–69.
- Steltenpohl, M.G., Mueller, P., Heatherington, A., Hanley, T.B., and Wooden, J.L., 2008, Gondwanan/Peri-Gondwanan origin for the Uchee terrane, Alabama and Georgia: Carolina zone or Suwannee terrane(?) and its suture with Grenvillian basement of the Pine Mountain window: *Geosphere*, v. 4, p. 131–144.
- Steltenpohl, M.G., Schwartz, J.J., and Miller, B.V., 2013, Late to post-Appalachian strain partitioning and extension in the Blue Ridge of Alabama and Georgia: *Geosphere*, v. 9; no. 3, p. 647-666.
- Suppe, J., 1985, *Principles of Structural Geology*: Prentice-Hall, Englewood Cliffs, New Jersey, 537 p.
- Thomas, W.A., Neathery, T.N., and Ferrill, B.A., 1989, Cross-section A-A', in Hatcher, R.D., Jr., et al., eds., *The Appalachian-Ouachita orogen in the United States*: Boulder, Colorado, Geological Society of America, *Geology of North America*, v. F-2.

- Thomas, W.A., 1991, The Appalachian–Ouachita rifted margin of southeastern North America: *Geological Society of America Bulletin*, v. 103, p. 415–431.
- Toyoshima, T., 1998, Gabbro mylonite developed along a crustal-scale décollement, in Snoke, A., Tullis, J., and Todd, V.R., (ed.) *Fault related rocks – a photographic atlas*: Princeton University Press, New Jersey, p. 426-427.
- Tull, J.F., 1984, Polyphase late Paleozoic deformation in the southeastern foreland and northwestern Piedmont of the Alabama Appalachians: *Journal of Structural Geology*, v. 6, p. 223–234.
- Vernon, R.H., 1976, *Metamorphic Processes. Reactions and Microstructure Development*: George Allen and Unwin, Boston, 247 p.
- White, S.H., 1979, Large strain deformation: report on a tectonic studies group discussion meeting held at Imperial College, London; introduction: *Journal of Structural Geology*, v. 4, p. 333-339.
- White, S.H., Burrows, S.E., Carreras, J., Shaw, N.D., and Humphreys, F.J., 1980, On mylonites in ductile shear zones: *Journal of Structural Geology*, v. 2, p. 175-187.
- Wise, D.U., Dunn, D.E, Engeldar, J.T., Geiser, P.A., Hatcher, R.D., Kish, S.A., Odom, A.L., and Schamel, S., 1984, Fault-related rocks: suggestions for terminology: *Geology*, v. 12, p. 391-394.
- Zwart, H.J., 1962, On the determination of polymetamorphic mineral associations and its application to the Busost area (central Pyrenees): *Geologische Rundschau*, v. 52, p. 38-65.

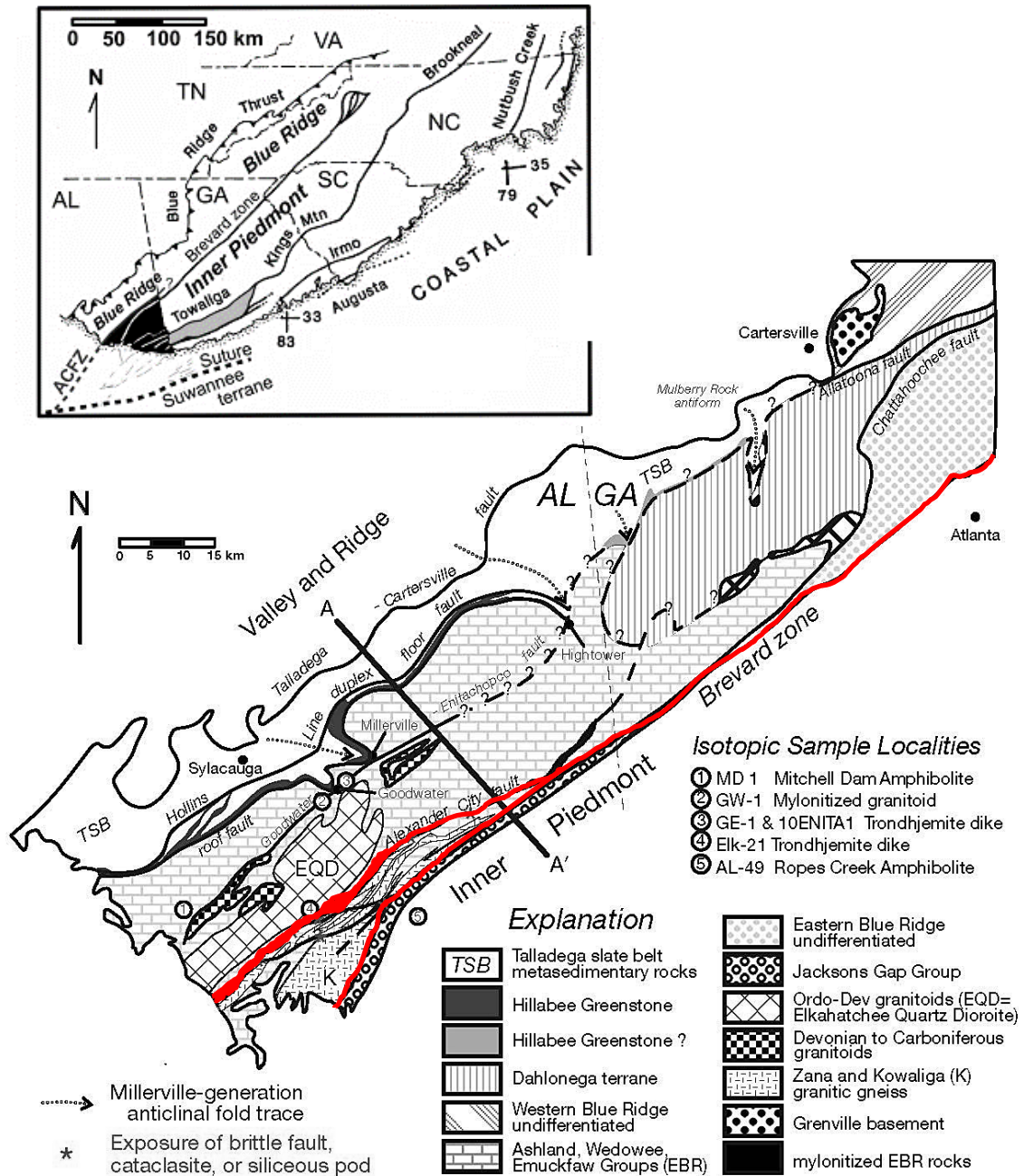


Figure 1. Tectonostratigraphic map of the Blue Ridge in east central Alabama (AL) and part of Georgia (GA) with major tectonic features, such as the ACF and the Abanda fault (in AL) of the BFZ, highlighted in red (modified after Tull, 1984; McClellan et al., 2007). (Cross section modified from Thomas et al., in Hatcher et al., 1989; Thomas, 1991; Steltenpohl, 2005; and Steltenpohl et al., 2008.) ACF—Alexander City fault; BFZ—Brevard fault zone; EBR—Eastern Blue Ridge; GEF—Goodwater-Enitachopco fault; HLF—Hollins Line fault; IP—Inner Piedmont; TFC Talladega Cartersville fault; TSB—Talladega slate belt; V&R—Valley and Ridge; Ordo-Dev—Ordovician–Devonian (modified from Steltenpohl, 2005; Steltenpohl et al., 2013).

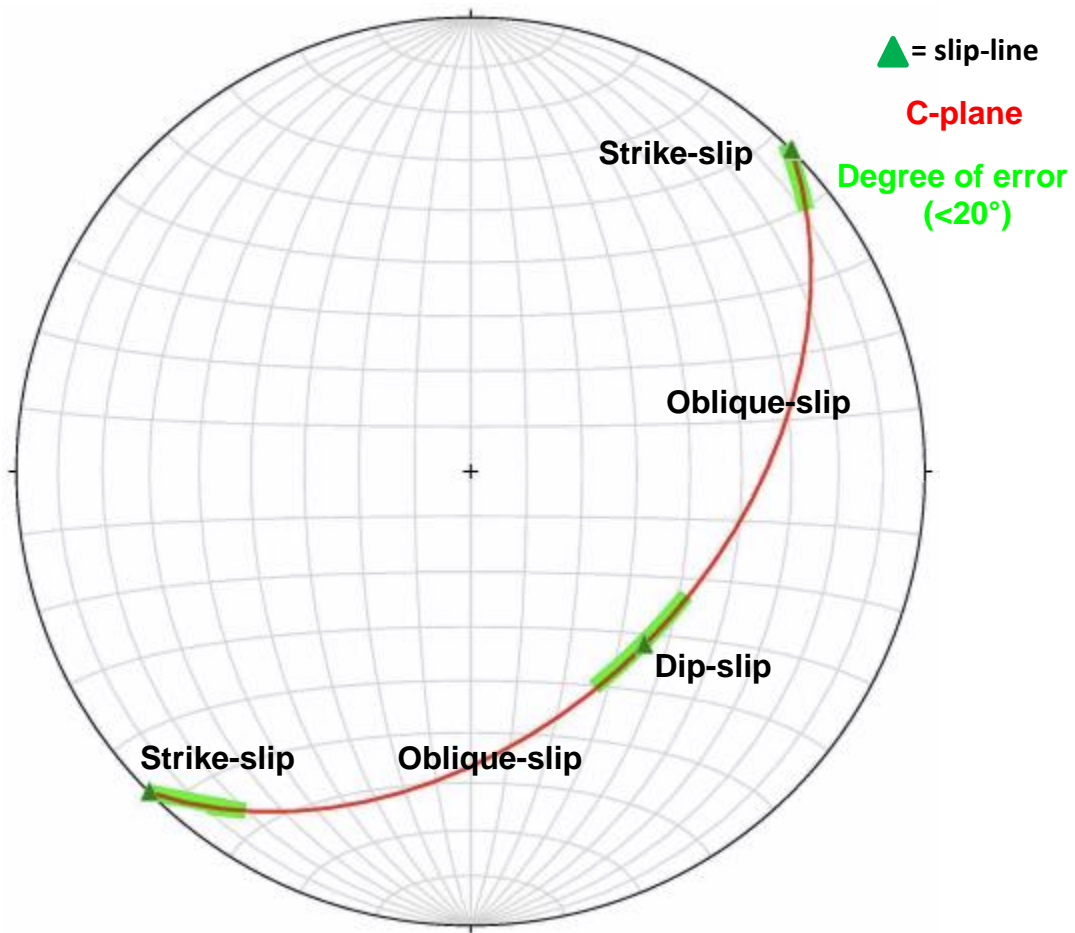


Figure 2. Stereonet showing slip-lines plotted on the C-plane's great circle representing dip-slip, strike-slip, and oblique-slip. Highlighted areas define degree of error.

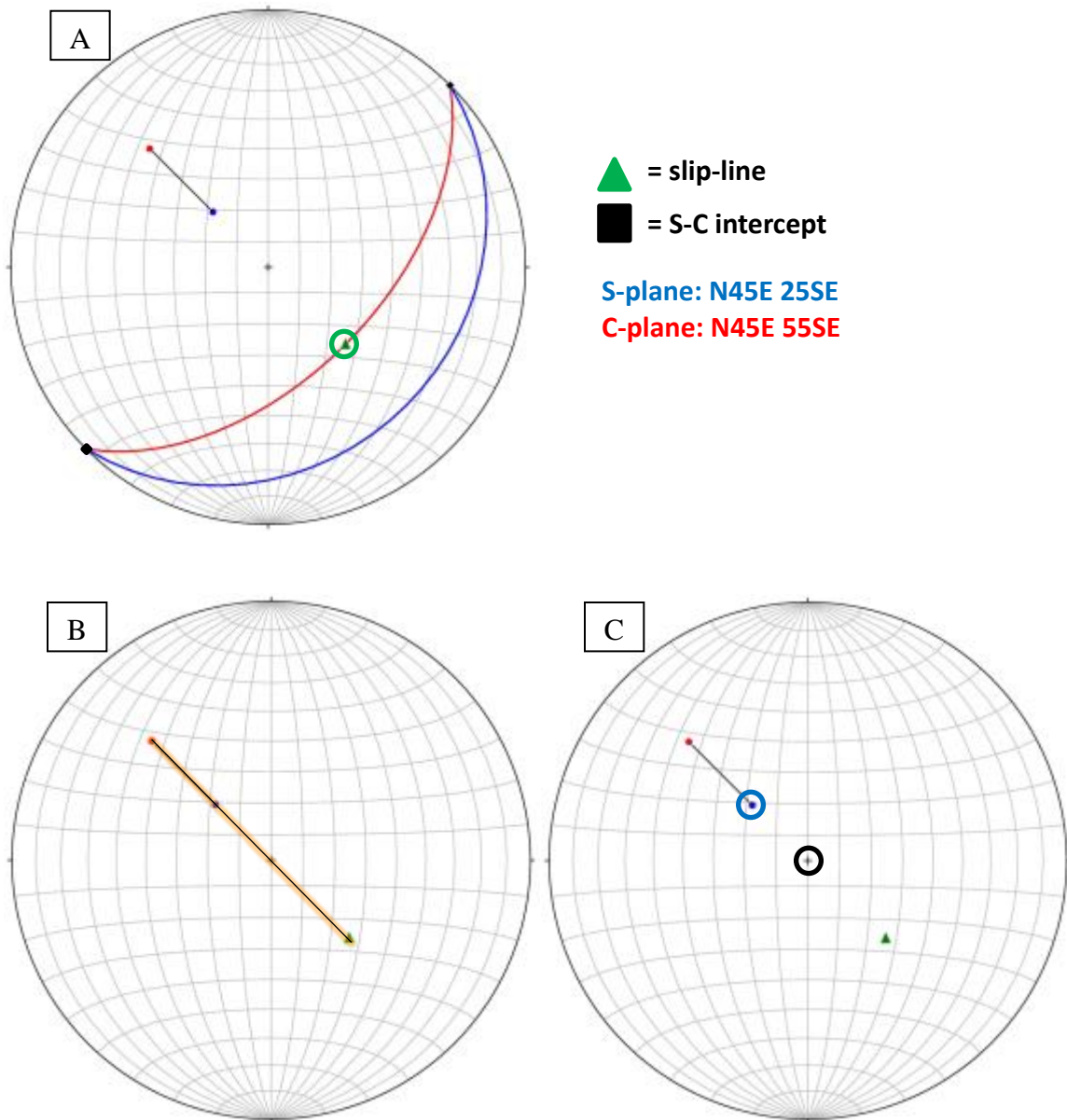


Figure 3. Dip-slip faults. A) S- and C-planes share the same strike but vary in dip magnitude. With true dip-slip, the slip-line lies at the maximum dip of the C-plane's great circle (green circle). B) Poles to S-C planes plot near the center of stereogram, and slip-line aligns along the same geometric line containing the arc angle (see text). S-C intercept lies along the primitive of the stereonet (see A.). C) Dip-slip motion is based on the poles of S-C planes' proximity to center of stereonet. S-plane's pole is more proximal to the center of the stereonet than is the C-plane's pole. Correspondingly, C-plane's dip > S-plane's dip = normal-slip.

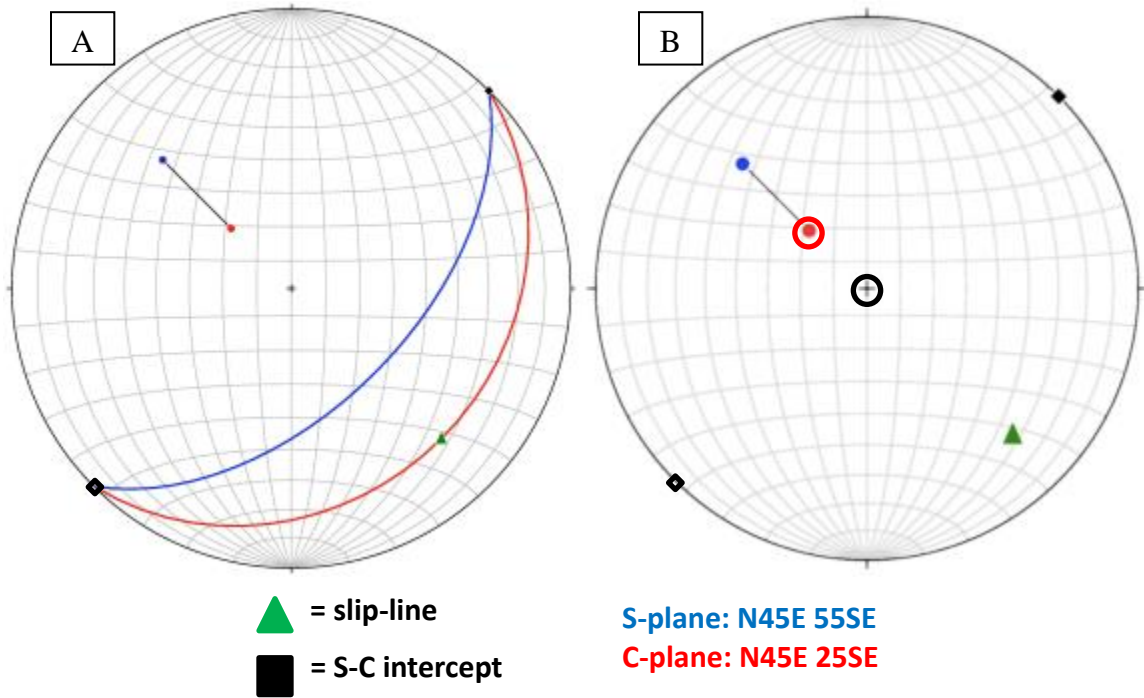


Figure 4. Reverse dip-slip faults. A) S- and C-planes share the same strike but vary in dip magnitude. B) Slip-line lies at the maximum dip of the C-plane's great circle and the poles to S-C planes, the center of stereonet, and slip-line aligns along the same line. The C-plane's pole is more proximal to the center of the stereonet than that of the S-plane. Correspondingly, C-plane's dip > S-plane's dip = reverse-slip.

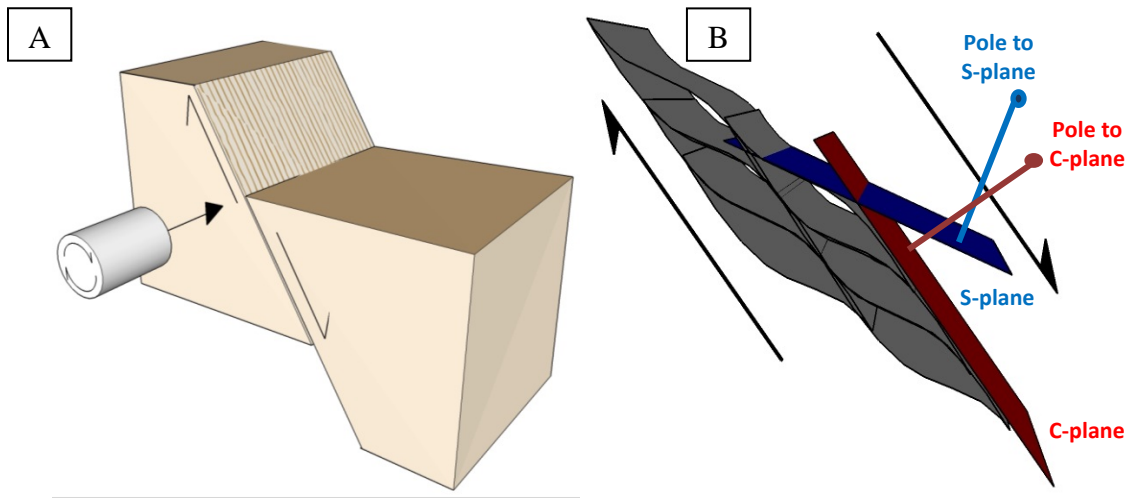


Figure 5. Normal dip-slip motion. A) Three-dimensional block diagram for normal dip-slip motion. B) Three-dimensional, cross-section perspective view (ideal view parallel to S-C intersections and along strike) of S-C fabrics illustrating normal dip-slip motion.

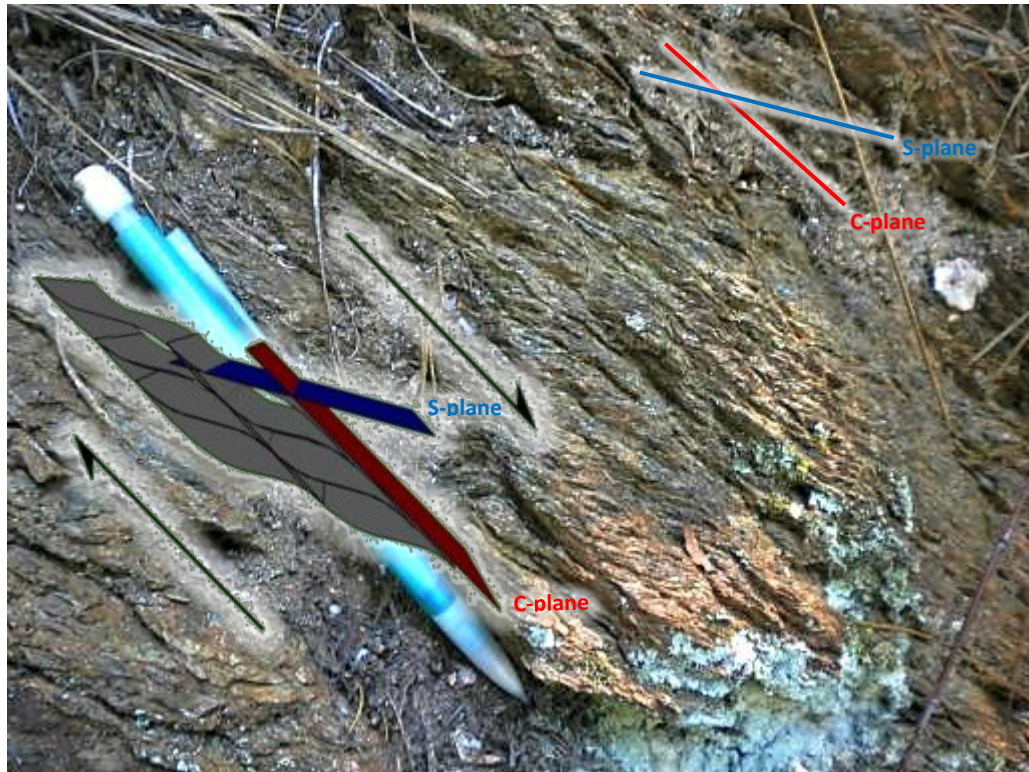


Figure 6. Outcrop photo looking parallel to the S-C planes' intersection, which is horizontal. Garnetiferous graphitic phyllonite/buton schist from the Jacksons Gap Group within the Abanda fault, the basal fault of the Brevard fault zone. C-plane's dip > S-plane's = normal-slip.

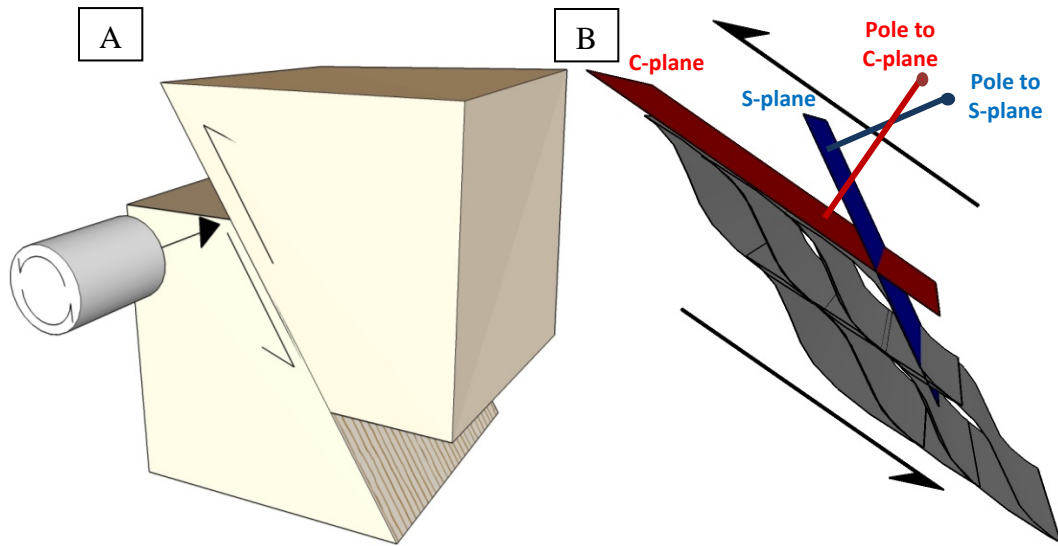


Figure 7. Reverse dip-slip motion. A) Three-dimensional block diagram for reverse dip-slip motion. B) Three-dimensional, cross-sectional perspective view (ideal view parallel to S-C intersections) of S-C fabrics showing reverse dip-slip motion.



Figure 8. Outcrop photo with view parallel to horizontal S-C intersection lineation within a graphitic phyllonite of the Jacksons Gap Group proximal to the Abanda fault. C-plane's dip < S-plane's = reverse-slip.

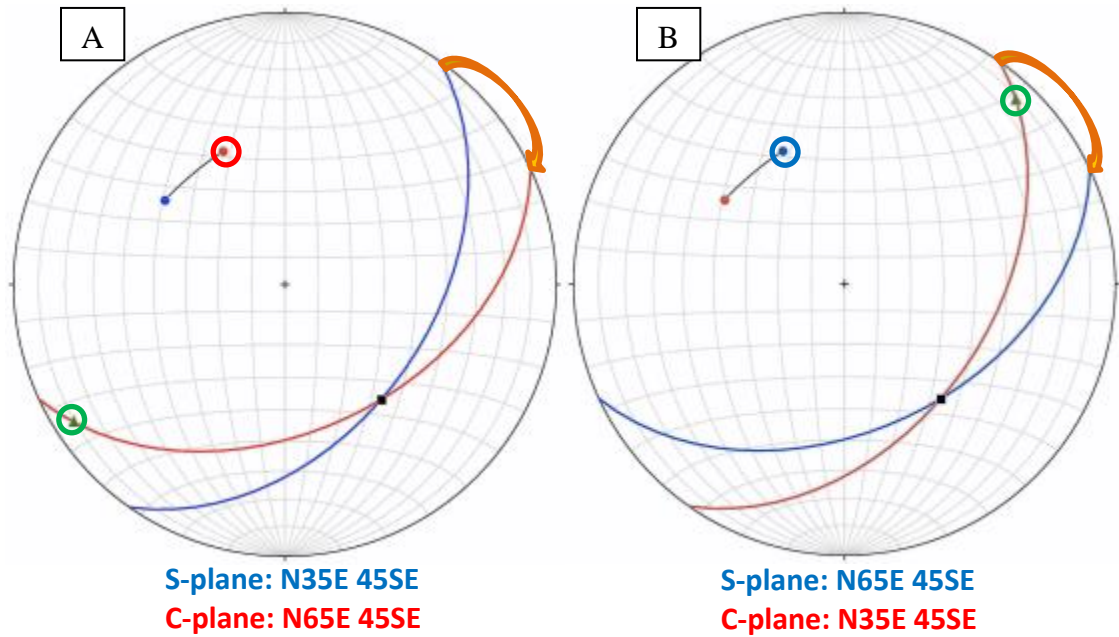


Figure 9. Strike-slip faults. S- and C-planes have different strikes but share the same strike dip magnitude. Slip-line (green circle) lies at the intersection of the C-plane's great circle and the primitive of the stereonet. S-C intercept lies near the maximum dip of the C-plane. A) C-plane's great circle and pole are more clockwise than that of the S-plane, indicative of dextral strike-slip motion. B) S-plane's great circle and pole are more clockwise than that of the C-plane, indicating sinistral strike-slip motion.

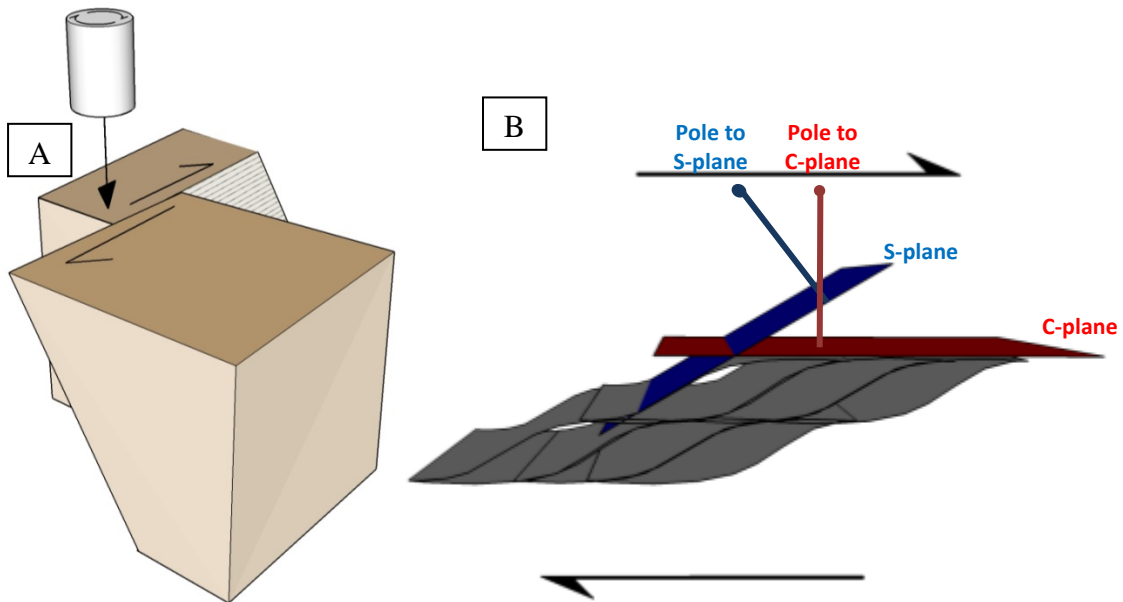


Figure 10. Dextral strike-slip motion. A) Three-dimensional block diagram illustrating dextral strike-slip motion. B) Three-dimensional, map-perspective view (ideal view parallel to S-C intersections) of S-C fabrics showing dextral strike-slip motion.

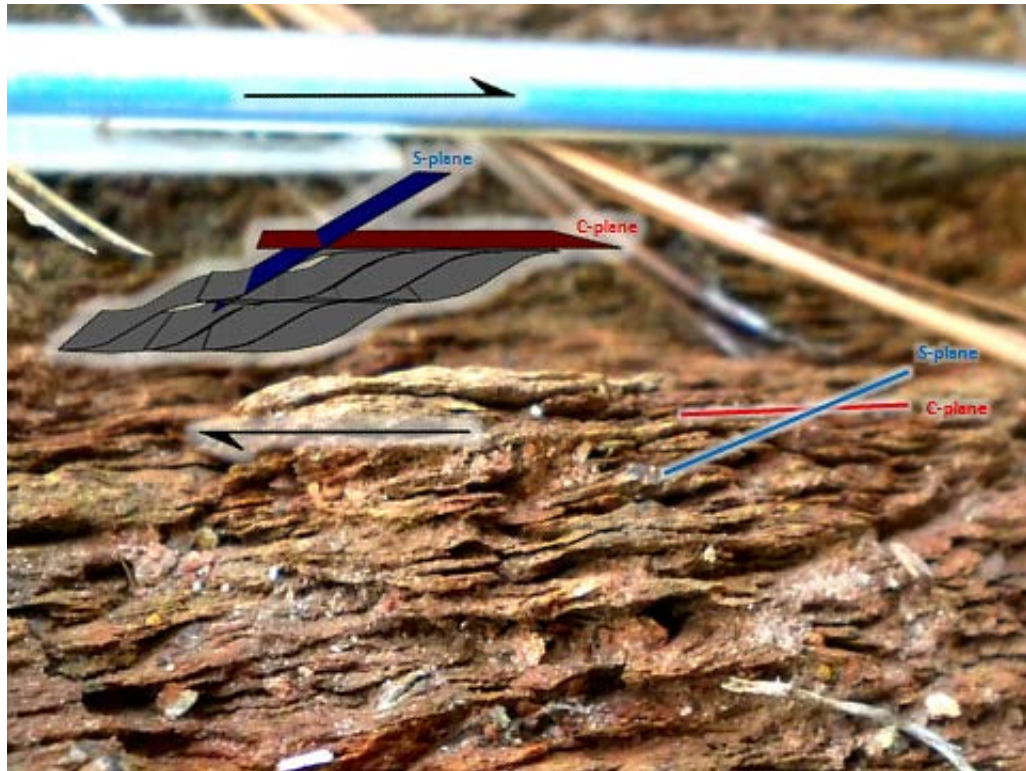


Figure 11. Outcrop photo looking down-dip of a button schist from the Jacksons Gap Group proximal to the Abanda fault. Viewed down-plunge of the S-C intersection with C-plane displaying a more clockwise orientation than that of the S-plane, demonstrating dextral slip.

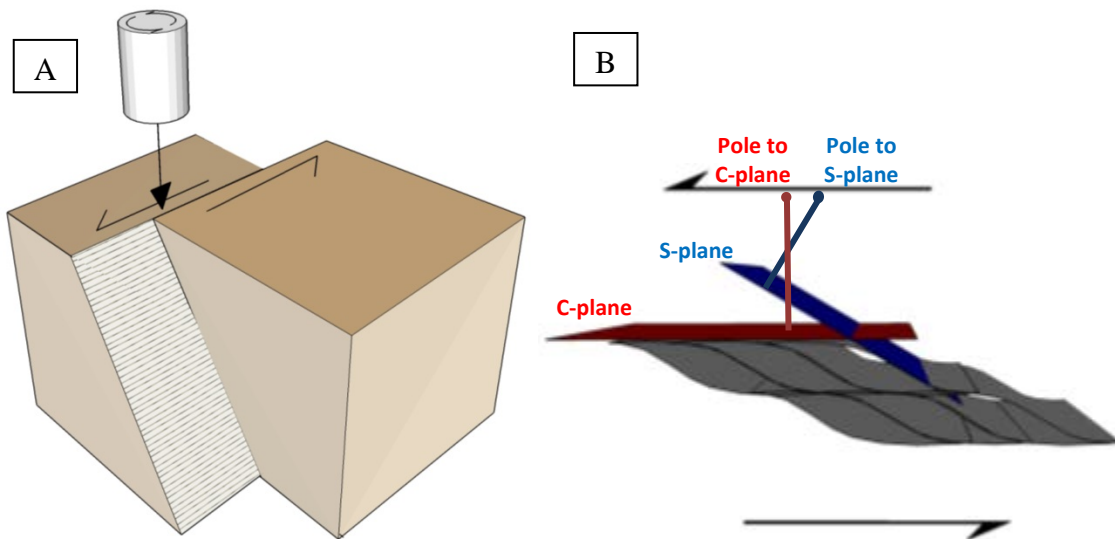


Figure 12. Sinistral strike-slip motion. A) Three-dimensional block diagram for sinistral strike-slip motion. B) Three-dimensional, map-perspective view (ideal view parallel to S-C intersections) of S-C fabrics showing sinistral strike-slip motion.

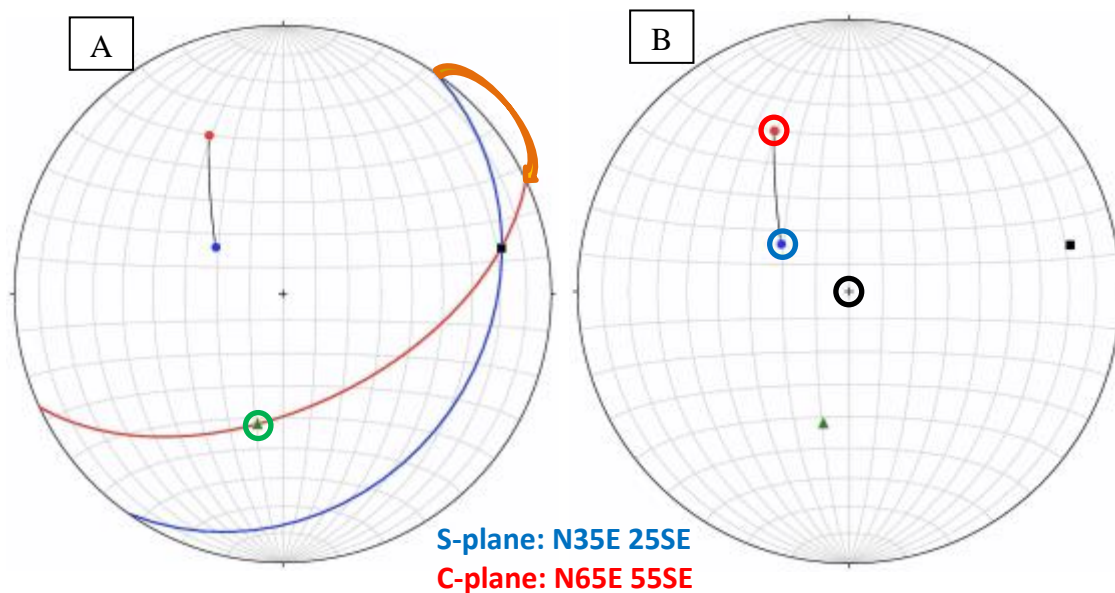


Figure 13. Dextral-normal-oblique-slip faults. A) S- and C-plane will have different strikes and dip magnitudes. Slip-line (green circle) does not lie near the maximum dip of the C-plane's great circle or at the intersection of the C-plane's great circle and the primitive, but somewhere in-between. B) Strike-slip is based on clockwise rotation of the S-C pair's great circles and poles relative to one another. C-plane's great circle and pole are more clockwise than that of the S-plane, indicating dextral strike-slip motion. The dip-slip component is based on the S-C planes' poles' proximity to center of stereonet. S-plane's pole is more proximal to the center of the stereonet than that of the C-plane, demonstrating normal slip (B.).

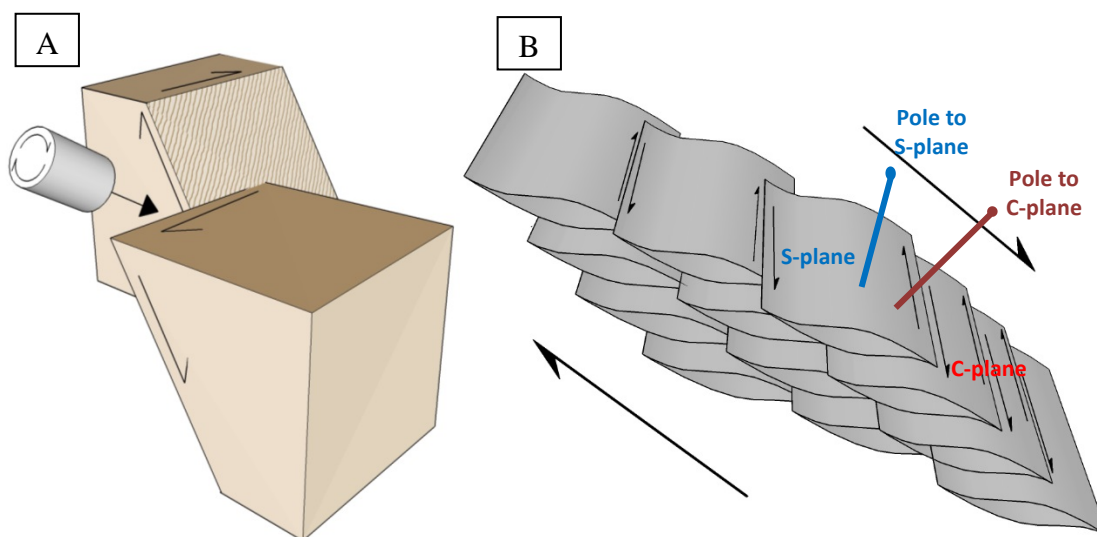


Figure 14. Dextral strike-slip motion. A) Three-dimensional block diagram showing oblique components of both a dextral strike-slip and normal dip-slip motion. B) Three-dimensional perspective view (ideal view parallel to S-C intersections) of S-C fabrics.

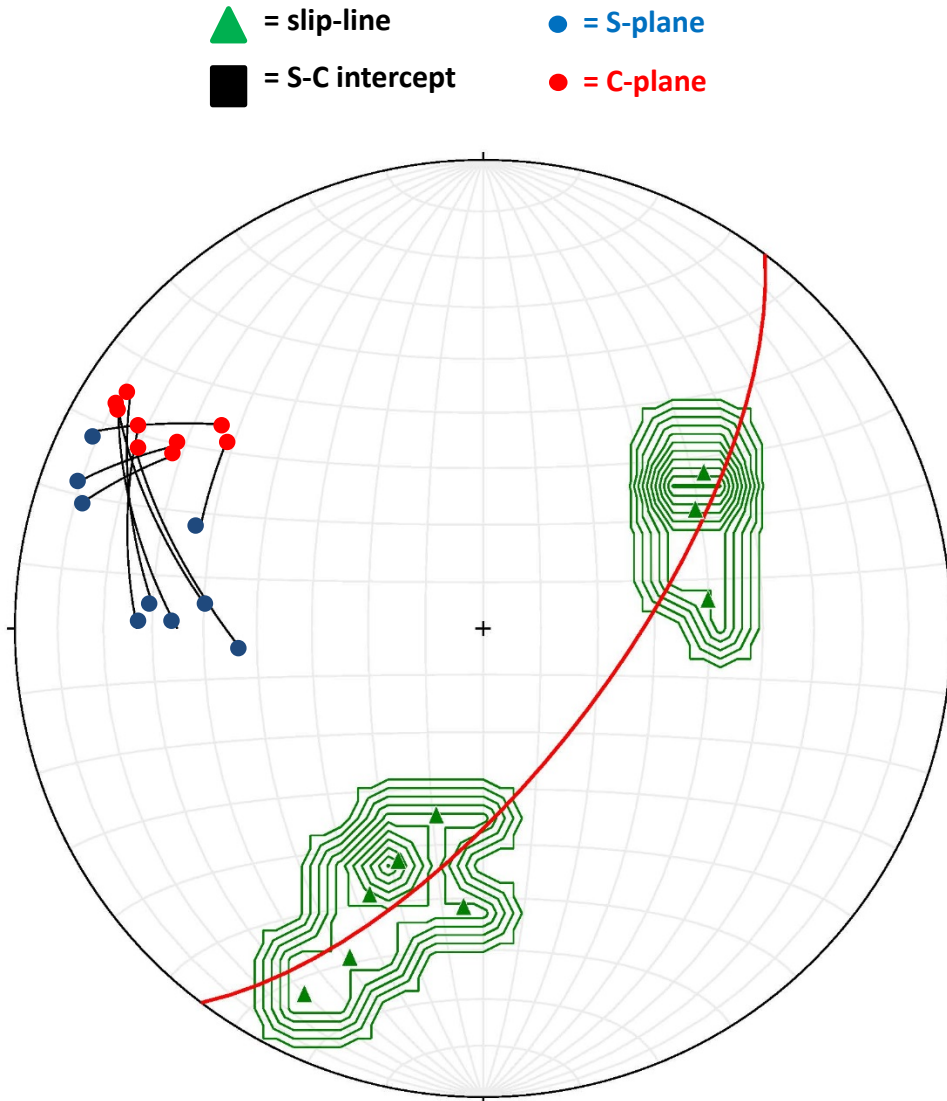


Figure 15. Countered lower hemisphere stereographic projection of slip vectors as determined from a set of paired S-C plane measurements made on the Abanda fault (n=9). The red great circle is best visual fit and represents the average C-plane orientation. Arcs connecting the poles of paired S-C planes indicate both oblique-dextral-normal- (southwest plunging maximum) -reverse-slip (northeast plunging maximum) movement. All of the C-planes' poles are more clockwise than that of the S-planes' poles, documenting the dextral component. Contour interval is 2% and counting area is 1% of net area.

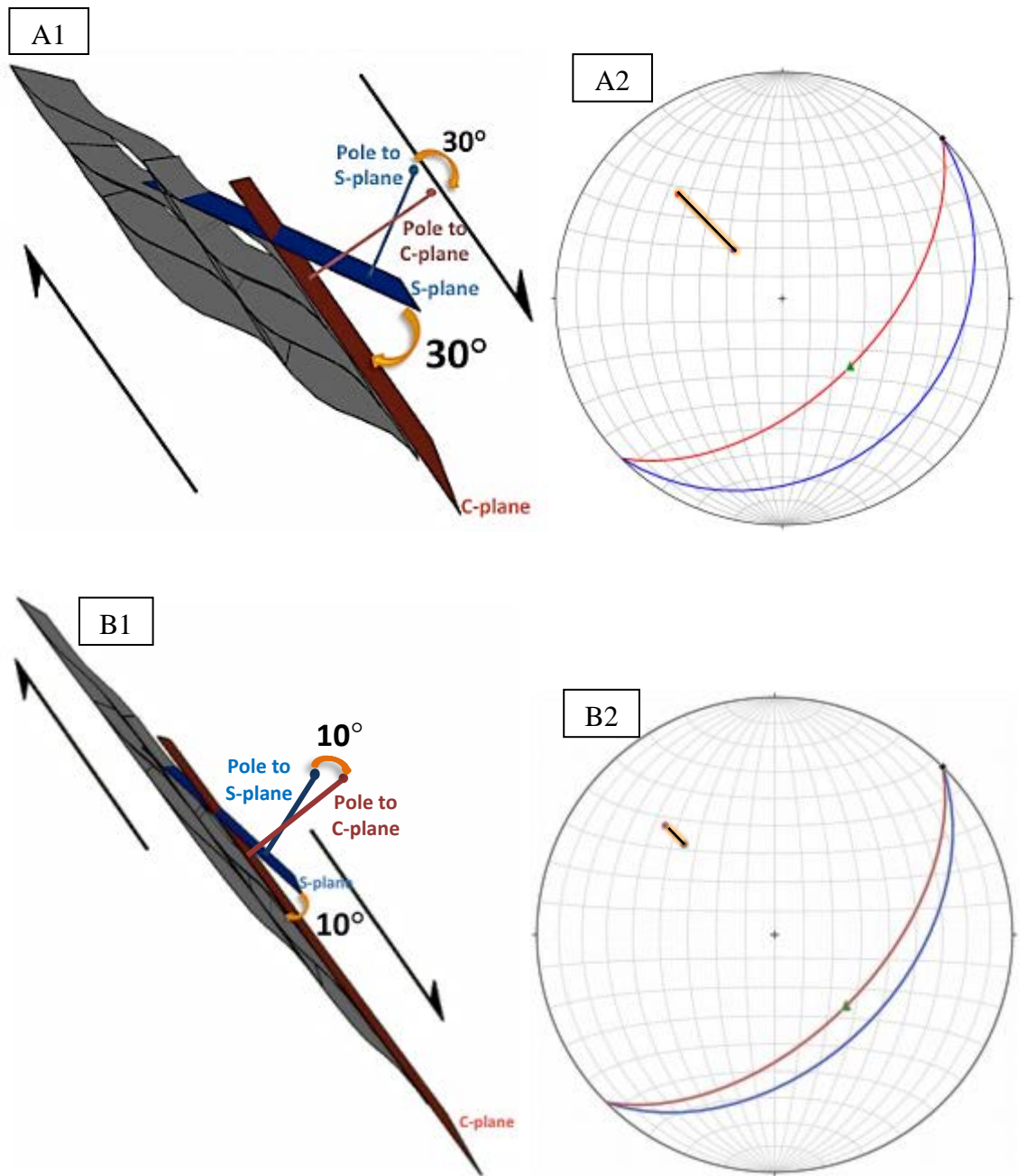


Figure 16. Arc-angle as a proxy for angular shear strains. A1. and A2) Lower magnitude of relative angular shear is reflected in a larger arc angle between S-C planes. B1. and B2) Smaller arc angles reflect higher degrees of angular shear strain.

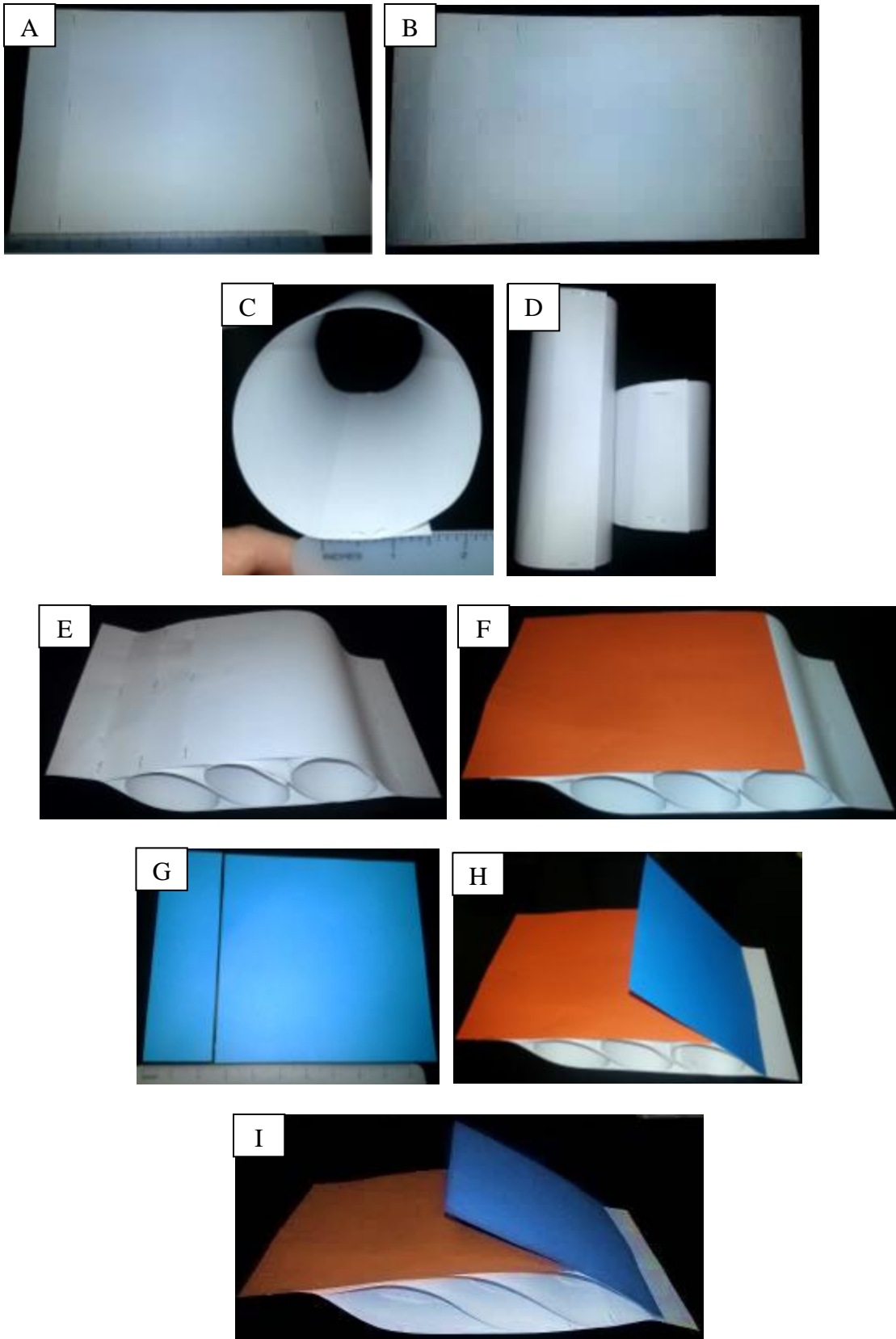


Figure 17. Constructing a three-dimensional S-C model out of basic office supplies. See text.

CONCLUSIONS

The first manuscript is a detailed geologic analysis of the Jacksons Gap, Alabama, 7.5-minute Quadrangle focusing on structures and lithologies related to the Brevard fault zone. This analysis included structural, kinematic, rheologic, petrographic, and isotopic analysis of three geologic terranes (eastern Blue Ridge, Jacksons Gap Group, and Dadeville Complex) and two fault zones (Abanda and Alexander City fault zones). Findings include the following.

- The eastern Blue Ridge likely is the oldest terrane based on the incorporation of xenoliths within the 440 Ma Kowaliga Gneiss that likely correlate to Early Ordovician volcanics elsewhere in the Blue Ridge.
- The eastern Blue Ridge may indicate evolution from the Laurentian slope-rise facies into a back-arc basin.
- The Jacksons Gap Group:
 - May mark the shallowing of the back-arc basin into a barrier island or submarine fan system with evidence for volcanic influence near the top, recording the encroaching Dadeville Complex island arc.
 - Contains lenses of lower-strained rocks with relict sedimentary structures indicating general stratigraphic right-way-up. These lenses are encapsulated by anastomosing shear zones. Internal shear zones exploited

soft graphitic units. Doubly-plunging tight to isoclinal folds are apparent at the scale of Plates 1 and 2.

- Contains greenschist to lower-amphibolite metamorphic rocks that are sandwiched between relatively higher-grade units of the eastern Blue Ridge and Dadeville Complex, with an apparent inverted metamorphic gradient spanning across the Katy Creek fault.
- The Abanda and Katy Creek fault bounding the Jacksons Gap group are temporally, kinematically, and rheologically different, whereas the Abanda and Alexander City faults are very similar in each regard.
- $^{40}\text{Ar}/^{39}\text{Ar}$ muscovite dating indicates that shearing and regional cooling are not synchronous due to faulting, with ages ranging from ~319-298 Ma, but are juxtaposed due to folding by the Tallassee synform. Dates of ~317 Ma are interpreted to represent the latest ductile movement along the Abanda and Alexander City fault zones and those between ~312 to 298 Ma are interpreted to reflect regional cooling.
- Cataclastic zones trending parallel to the Abanda fault and splaying off towards the Alexander City fault zone may record Mesozoic tensional relay zones between Triassic and Jurassic extensional faults.

The second manuscript was developed to aid in resolving fault/shear zone kinematics and furthering the understanding of upper-level geology students on S-C fabric geometries and fabric relationships. A set of criteria is established for S-C relationships plotted on a stereogram along with field observations to resolve movement

sense as reverse or normal dip-slip, dextral or sinistral strike-slip, or various combinations of oblique-slip, and also the relative angular shear strain. Shortcomings of this technique in occasions of steep and shallow angles of dip are noted. Instructions on constructing a simple three-dimensional model are provided to visualize S-C fabrics.

Below is an abbreviated listing of the main findings:

DIP-SLIP

- Same strikes, different dips
- Normal shear sense → S plane's pole more proximal to center than C-plane's
 - Normal fault = dip of C plane > dip of S plane
- Reverse shear sense → C plane's pole more proximal to center
 - Reverse fault = dip of C plane > dip of S plane

STRIKE-SLIP

- Different strike, same dip
- Dextral shear sense
 - C plane's great circle and pole more clockwise than S plane's
- Sinistral shear sense
 - S plane's great circle and pole more clockwise than C plane's

OBLIQUE-SLIP

- Combination of principles established

PROBLEMS WITH EXTREME DIP ANGLES

Steep and shallow angles of dip is a shortcoming of this method due to the phenomena that S-C relationships can be the opposite. This, however, cannot be directly quantifiable.

RELATIVE DEGREE OF SHEAR

- Smaller arc angle/angle between S-C planes = larger degree of angular shear
- Larger arc angle between S-C planes = smaller degree of angular shear

COMBINED REFERENCES

- Abrahams, J.B., 2014, Geology of the Dadeville Quadrangle and the Tallassee synform in characterizing the Dog River window, [unpublished M.S. thesis]: Auburn University, Auburn, Alabama, p. 126.
- Beiler, D.B., and Deininger, R.W., 1987, Geologic setting of the Kowaliga Augen Gneiss and the Zana Granite, northern Alabama Piedmont: in Drummond, M.S., and Green, N.L., eds., *Granites of Alabama: Geological Survey of Alabama*, p. 57-72.
- Bell, T.H., and Etheridge, M.A., 1973, Microstructures of mylonites and their descriptive terminology: *Lithos*, v. 6, p. 337-348.
- Bell, T.H., 1981, Foliation development: the contribution, geometry, and significance of progressive bulk inhomogeneous shortening: *Tectonophysics*, v. 75, p. 273-296.
- Bentley, R.D., and Neathery, T.L., 1970, Geology of the Brevard zone and Related Rocks of the Inner Piedmont of Alabama: Tuscaloosa, AL, Alabama Geological Society 8th Annual Field Trip Guidebook, 119 p.
- Berthé, D., Choukroune, P. & Jegouzo, P., 1979, Orthogneiss, mylonite and non coaxial deformation of granites: the example of the South Armorican shear zone: *Journal of Structural Geology*, v. 1, no. 1, p. 31-42.
- Bobyarchick, A.R., Edelman, S.H., and Horton, J.W., Jr., 1988, The role of dextral strike-slip in the displacement history of the Brevard fault zone, in Secor, D.T., Jr., ed., *Southeastern Geological Excursions: Geological Society of America 1988 Annual Meeting Field Trip Guidebook*, p. 53-104.
- Bobyarchick, A.R., 1999, The history of investigation of the Brevard fault zone and evolving concepts in tectonics: *Southeastern Geology*, v. 38, no. 3, p. 223-238.
- Borradaile, G.J., Bayly, M.B., and Powell, C.M.A., 1982, *Atlas of deformational and metamorphic rock fabrics*: Springer-Verlag, Berlin Heidelberg, New York, 551 p.
- Cobbold, P.R., and Quinquis, H., 1980, Development of sheath folds in shear regimes: *Journal of Structural Geology*, v. 2, no. 1-2, p. 39-47.

- Coker-Dewey, J., Steltenpohl, M.G., and Andresen, A., 2000, Geology of western Ullfjord, North Norway, with emphasis on the development of an inverted metamorphic gradient at the Top of the Lyngen Nappe Complex: *Norsk Geologisk Tidsskrift*, v. 80.2, p. 111-127.
- Cook, F.A., Albuagh, D.S., Brown, L.D., Kaufman, S., Oliver, J.E., and Hatcher, R.D., Jr., 1979, Thin-skinned tectonics in the crystalline southern Appalachians; COCORP seismic-reflection profiling of the Blue Ridge and Piedmont: *Geology*, v. 7, p. 563-567.
- Cosgrove, J.W., 1976, The formation of crenulation cleavage: *Journal of the Geological Society of London*, v. 132, p. 155-178.
- Davis, G.H., Gardulski, A.F., and Lister, G.S., 1987, Shear zone origin of quartzite mylonite and mylonitic pegmatite in the Coyote Mountains metamorphic core complex, Arizona: *Journal of Structural Geology*, v. 9, no. 7, p. 289-297.
- Davis, T.L., 1993, Lithostratigraphy, structure, and metamorphism of a crystalline thrust terrane, western Inner Piedmont, North Carolina [PhD dissertation]: University of Tennessee, 245 p.
- Dennis, A.J., and Secor, D.T., 1987, A model for the development of crenulations in shear zones with the applications from the southern Appalachian Piedmont: *Journal of Structural Geology*, v. 9, no. 7, p. 807-817.
- Dennis, A.J., and Secor, D.T., 1990, On resolving shear direction in foliated rocks deformed by simple shear: *Geological Society of America Bulletin*, v. 102, p. 1257-1267.
- Dodson, M.H., and McClelland-Brown, E., 1985, Isotopic and palaeomagnetic evidence for rates of cooling, uplift, and erosion, *in* Snelling, N.J., ed., *The chronology of the geologic record*: Geological Society of London Memoir 10, p. 315-325.
- Drummond, M.S., Allison, D.T., and Wesolowski, D.J., 1994, Igneous petrogenesis and tectonic setting of the Elkahatchee Quartz Diorite, Alabama Appalachians: Implications for the Penobscotian Magmatism in the eastern Blue Ridge: *American Journal of Science*, v. 294, p.173-236.
- Duebendorfer, E.M., 1988, Evidence for an inverted metamorphic gradient associated with a Precambrian suture, southern Wyoming: *Journal of Metamorphic Geology*, v. 6, p. 41-63.
- Dunlap, W.J., Teyssier, C., McDougall, I., and Balwin, S., 1991, Ages of deformation from K/Ar and $^{40}\text{Ar}/^{39}\text{Ar}$ dating of white micas: *Geology*, v. 19, p. 1213-1216.

- Eibacher, G.H., 1970, Deformation mechanics of mylonitic rocks and fractured granites in Cobequid Mountains, Nova Scotia, Canada: Geological Society of America Bulletin, v. 81, p. 2009-2020.
- Etheridge, M.A., and Hobbs, B.E., 1974, Chemical and deformational controls on recrystallization of mica: Contributions to Mineralogy and Petrology, v. 43, p. 111-124.
- Gapais, D., and White, S.H., 1982, Ductile shear bands in a naturally deformed quartzite: Textures and Microstructures, v. 5, p. 1-17.
- Garcia-Celma, A., 1982, Domainal and fabric heterogeneities in the Cap de Creus quartz mylonites: Journal of Structural Geology, v. 4, p. 443-455.
- Gray, D.R., 1977, Morphological classification of crenulation cleavage: Journal of Geology, v. 85, p. 229-235.
- Gray, D.R., and Durney, D.W., 1979, Investigations on the mechanical significance of crenulation cleavage: Tectonophysics, v. 58, p. 35-79.
- Hames W.E., and Hodges K. V., 1993, Laser $^{40}\text{Ar}/^{39}\text{Ar}$ evaluation of slow cooling and episodic loss of ^{40}Ar from a sample of polymetamorphic muscovite: Science 261, p.1721-1723.
- Harrison T.M., and McDougall I., 1981, Excess ^{40}Ar in metamorphic rocks from Broken Hill, New South Wales: Implications for $^{40}\text{Ar}/^{39}\text{Ar}$ age spectra and the thermal history of the region; Earth and Planetary Science Letters, v. 55, p.123-149
- Hatcher, R.D., Jr., 1972, Developmental model for the southern Appalachians: Geological Society of America Bulletin, v. 83, p. 2735-2760.
- Hatcher, R.D., Jr., 1987, Tectonics of the southern and central Appalachian internides: Annual Review of Earth and Planetary Sciences, v. 15, p. 337-362.
- Hatcher, R.D., Jr., Osberg, P.H., Drake, A.A., Jr., Robinson, P., and Thomas, W.A., 1990, Tectonic Map of the U.S. Appalachians: The Appalachian-Ouachita Orogen in the United States, v. F-2 of The Geology of North America (GNA-F2).
- Hatcher, R.D., Jr., 2001, Rheological partitioning during multiple reactivation of the Paleozoic Brevard fault zone, southern Appalachians, USA, *in* Holdsworth, R.E., et al., eds., The Nature and Tectonic Significance of Fault Zone Weakening: Geological Society of London Special Publication 186, p. 255-269.

- Hatcher, R.D., Jr., and Merschat, A.J., 2006, The Appalachian Inner Piedmont: An exhumed strike-parallel, tectonically forced orogenic channel, *in* Law, R.D., Searle, M.P., and Godin, L., eds., Channel Flow, Ductile Extrusion and Exhumation in Continental Collision Zones: Geological Society of London Special Paper 268, p. 517–541.
- Hatcher, R.D., Jr., 2010, The Appalachian orogen: A brief summary, in Tollo, R.P., Bartholomew, M.J., Hibbard, J.P., and Karabinos, P.M., eds., From Rodina to Pangea: The Lithotectonic Record of the Appalachian Region: Geological Society of America Memoir 206, p. 1-19.
- Hawkins, J.F., Steltenpohl, M.G., Zou, H., Mueller, P.A., and Schwartz, J.J., 2013, New constraints on Ordovician magmatism in the southernmost exposures of the eastern Blue Ridge in Alabama: Geological Society of America Abstracts with Programs, v. 45, p. 62.
- Hawkins, J.F., 2013, Geology, petrology, and geochronology of rock in Our Town, Alabama quadrangle [M.S. thesis]: Auburn, Auburn University, 118p.
- Higgins, M.W., 1971, Cataclastic rocks: U.S. Geological Survey Professional Paper 687, p. 97.
- Hirth, G., and Tullis, J., 1992, Dislocation Creep Regimes in Quartz Aggregates: Journal of Structural Geology, v. 14.2, p. 145-59.
- Hobbs, B.E., Means, W.D., and Williams, P.F., 1976, An Outline of Structural Geology: John Wiley and Sons, New York, 571 p.
- Hodges, K.V. 1991, Pressure-temperature-time paths: Annual Review of Earth and Planetary Sciences, v. 19, p. 207-236.
- Holdaway, M.J., 1971, Stability of andalusite and the aluminosilicate phase diagram: American Journal of Science, v. 271, p. 97-131.
- Hopson, J.L. and Hatcher, R.D., Jr., 1988, Structural and stratigraphic setting of the Alto allochthon, northeast Georgia: Geological Society of America Bulletin, v. 100, p. 339-350.
- Horton, J.W., Jr., Avery, A.D., Jr., and Rankin, D.W., 1989, Tectonostratigraphic terranes and their Paleozoic boundaries in the central and southern Appalachians: Geological Society of America Special Paper 230, p. 213-245.
- Hoschek, G., 1969, The Stability of Staurolite and Chloritoid and their Significance in Metamorphism of Pelitic Rocks: Contributions to Mineralogy and Petrology, v. 22.3, p. 208-32.

- Hubbard, M.S., 1989, thermobarometric constraints on the thermal history of the Main Central Thrust zone and Tibetan Slab, eastern Nepal Himalaya: *Journal of Metamorphic Geology* 7, p. 19-30.
- Jegouzo, P., 1980, The South Armorican shear zone: *Journal of Structural Geology*, v. 2, no. 1-2, 39-47.
- Johnson, M.J., 1988, Geology of the gold occurrences near Jackson's Gap, Tallapoosa County, Alabama, [M.S. thesis]: Auburn University, Auburn, Alabama, 156 p.
- Keefer, W.D., 1992, Geology of the Tallassee Synform hinge zone and its relationship to the Brevard zone, Tallapoosa and Elmore Counties, Alabama [M.S. thesis]: Auburn, Auburn University, 195 p.
- Krohe, A., 1990, Local variations in quartz (c)-axis orientations in non-coaxial regimes and their significance for the mechanics of S-C fabrics: *Journal of Structural Geology*, v. 12, p. 995-1004.
- Lister, G.S., and Price, G.P., 1978, Fabric development in a quartz-feldspar mylonite: *Tectonophysics*, v. 49, p. 37-78.
- Lister, G.S., and Snoke, A.W., 1984, S-C mylonites: *Journal of Structural Geology*, v. 6, no. 6, p. 617- 638.
- Lumino, K.M., 1987, Deformation within the Diana Complex along the Carthage-Colton mylonite zone: M.S. thesis, University of Rochester, Rochester, New York, 104 p.
- Malavielle J. et F. Cobb. 1986, Cinématique des déformations ductiles dans trois massifs métamorphiques de l'Ouest des Etats-Unis : Albion (Idaho), Raft River et Grouse Creek (Utah): *Geological Society of France Bulletin, Numéro Spécial Cordillères Nord Américaines*, t. 2, n. 6, p. 885-898.
- Marshak, S., and Mitra, G., 1988, *Basic Methods of Structural Geology*: Prentice Hall, Engelwood Cliffs, New Jersey, 446 p.
- McClellan, E.A., Steltenpohl, M.G., Thomas, C., and Miller, C.F., 2007, Isotopic Constraints and Metamorphic History of the Talladega Belt: New Evidence for Timing of Arc Magmatism and Terrane Emplacement Along the Southern Laurentian Margin: *The Journal of Geology*, v. 115, p. 541-561.
- Medlin, J.H., and Crawford, T.J., 1973, Stratigraphy and structure along the Brevard fault zone in western Georgia and Alabama: *American Journal of Science*, v. 273-A, p. 89-104.

- Merschat, A.H., Hatcher, R.D., Jr., and Davis, T.L., 2005, The northern Inner Piedmont, southern Appalachians, USA: Kinematics of transpression and SW-directed mid-crustal flow: *Journal of Structural Geology*, v. 27, p. 1252–1281.
- Muangnoicharoen, N., 1975, The geology and structure of a portion of the northern piedmont, east-central Alabama [M.S. thesis]: Tuscaloosa, University of Alabama, p. 72.
- Mueller, P. A., Wooden, J.L., Mogk, D.W., and Foster, D.A., 2011, Paleoproterozoic evolution of the Farmington zone: Implications for terrane accretion in southwestern Laurentia: *Lithosphere*, v. 3, p. 401-408.
- Neathery, T.L., and Reynolds, J.W., 1973, Stratigraphy and metamorphism of the Wedowee Group, a reconnaissance: *American Journal of Science Alabama*, v. 273, p. 723-741.
- Neathery, T.L., ed., 1975, Rock units in the high-rank belt of the northern Alabama Piedmont, Alabama Geological Society, Annual Field Trip Guidebook, no.13, Geologic profiles of the northern Alabama Piedmont, p. 9-48.
- Neathery, T.L., and Reynolds, J.W., 1975, Geology of the Lineville East, Ofelia, Wadley North and Mellow Valley quadrangles, Alabama: Geological Survey of Alabama Bulletin no. 109, 120 p.
- Neilson, M.J., and Stow, S.H., 1986, Geology and geochemistry of the mafic and ultramafic intrusive rocks, Dadeville belt, Alabama: *Geological Society of America Bulletin*, v. 97, p. 296-304.
- Nelson, K.D., Arnou, J.A., Giguere, M., and Schamel, S., 1987, Normal-fault boundary of an Appalachian basement massif: Results of COCORP profiling across the Pine Mountain belt in western Georgia: *Geology*, v. 15, p. 832-836.
- Osborne, W.E., Szabo, M.W., Neathery, T.L., and Copeland, C.W., Jr., compilers, 1988, Geologic map of Alabama, northeast sheet: Alabama Geological Survey Special Map 220, scale 1:250,000.
- Passchier, C.W., and Simpson, C., 1986, Porphyroclast systems as kinematic indicators: *Journal of Structural Geology*, v. 8, p. 831-843.
- Passchier, C.W., and Trouw, R.A.J., 2005, *Microtectonics*: Springer-Verlag, Berlin Heidelberg, Germany, ed. 2, 382 p.
- Platt, J.P., and Vissers, R.L.M., 1980, Extensional structures in anisotropic rocks: *Journal of Structural Geology*, v. 2, p. 397-410.
- Poirier, J.P., 1985, *Creep of Crystals*: Cambridge University Press, Cambridge, 260 p.

- Powell, C.M., and Vernon, R.H., 1979, Growth and rotation history of garnet porphyroblasts with inclusion spirals in a Karakoram schist: *Tectonophysics*, v. 54, p. 25-43.
- Ramsey, J.G., 1980, Shear zone geometry, a review: *Journal of Structural Geology*, v. 2, p. 83-89.
- Ramsey, J.G., and Huber, M.I., 1987, *The Techniques of Modern Structural Geology*, Volume 2, Folds and Fractures: Academic Press, London, p. 309-700.
- Raymond, D.E., Osborne, W.E., Copeland, C.W., and Neathery, T.L., 1988, Alabama stratigraphy: Alabama Geological Survey Circular 140, 97 p.
- Richardson, S.W., 1968, Staurolite stability in a part of the system Fe-Al-Si-O-H: *Journal of Petrology*, v. 9.3, p. 467-489.
- Renne, P.R., Swisher, C.C., Deino, A.L., Karner, D.B., Owens, T.L., and DePaolo, D.J., 1998, Intercalibration of standards, absolute ages and uncertainties in $^{40}\text{Ar}/^{39}\text{Ar}$ dating: *Chemical Geology*, v. 145, p. 117-152.
- Robbins, G.A., 1972, Radiogenic argon diffusion in muscovite under hydrothermal conditions [M.S. thesis]: Providence, Rhode Island, Brown University, p. 189.
- Roper, P.J., 1972, Structural significance of "button" or "fish scale" texture in the phyllonitic schist of the Brevard zone: *Geological Society of America Bulletin*, v. 83, p. 853-860.
- Rosenfeld, J.L., 1970, Rotated garnets in metamorphic rocks: *Geological Society of America Special Papers* 129, 105 p.
- Russell, G.S. 1987, U-Pb, Rb-Sr, and K-Ar isotopic studies bearing on the development of the southernmost Appalachian orogen, Alabama [Ph.D. thesis]: Tallahassee, Florida, Florida State University, p. 197.
- Saltzer, S.D., and Hodges, K.V., 1988, The Middle Mountain shear zone, southern Idaho: kinematic analysis of an early Tertiary high-temperature detachment: *Geological Society of America Bulletin*, v. 100, p. 96-103.
- Schamel, S., Hanley, T.B., and Sears, J.W., 1980, Geology of the Pine Mountain Window and adjacent terranes in the Piedmont province of Alabama and Georgia: Southeastern Section of the Geological Society of America Field Trip Guidebook.
- Schmid, S.M., 1983, Microfabric studies as indicators of deformation mechanisms and flow laws operative in mountain building: in Hsu, K.J., (ed.), *Mountain Building Processes*: Academic Press, London, p. 95-110.

- Sears, J.W., Cook, R.B., and Brown, D.E., 1981, Tectonic evolution of the western part of the Pine Mountain window and adjacent Inner Piedmont Province, in Sears, J.W., ed., Contrasts in tectonic style between the Inner Piedmont terrane and the Pine Mountain window: Alabama Geological Society, 18th Annual Field Trip Guidebook, p. 1-13.
- Sibson, R. H., 1977, Fault rocks and fault mechanisms: Geological Society of London Journal, v. 133, p. 191-213.
- Simpson, C., 1986, Determination of movement sense in mylonites: Journal of Geological Education, v. 34, p. 246-261.
- Simpson, C., and Schmid, S.M, 1983, An evaluation of criteria to deduce the sense of movement in sheared rocks: Geological Society of America Bulletin, v. 94, p. 1281-1288.
- Steltenpohl, M.G., 1988, Kinematics of the Towaliga, Bartletts Ferry, and Goat Rock fault zones, Alabama: The late Paleozoic dextral shear system in the southernmost Appalachians: Geology, v. 16, p. 852-855.
- Steltenpohl, M.G., and Moore, W.B., 1988, Metamorphism in the Alabama Piedmont: Alabama Geological Survey Circular 138, 27 p.
- Steltenpohl, M.G., 1988, The Pine Mountain window of Alabama: Basement-cover evolution in the southernmost exposed Appalachians: International Basement Tectonics Association Publication, n. 8, p. 491-501.
- Steltenpohl, M.G., 1990, Structural development of the Opelika Complex, in Steltenpohl, M.G., et al., eds., Geology of the southern Inner Piedmont terrane, Alabama and southwest Georgia: Southeastern Section of the Geological Society of America Field Trip Guidebook, p. 29-42.
- Steltenpohl, M.G., Heatherington, A., Mueller, P., and Miller, B. V., 2005, Tectonic implications of new isotopic dates on crystalline rocks from Alabama and Georgia, in Steltenpohl, M.G., Hanley T.B., and Cook R.B., ed., New Perspectives on Southernmost Appalachian Terranes, Alabama and Georgia: Geological Society of Alabama 42nd Annual Field Trip Guidebook, p. 51-69.
- Steltenpohl, M.G., 2005, An introduction to the terranes of the southernmost Appalachians of Alabama and Georgia, in Steltenpohl, M.G., Hanley T.B., and Cook R.B., ed., New perspectives on southernmost Appalachians terranes, Alabama and Georgia: Alabama Geological Society, 42nd Annual Field Trip Guidebook, p. 3.

- Steltenpohl, M.G., Mueller, P.M., Heatherington, A.L., Hanley, T. B., and Wooden, J.L., 2008, Gondwanan/peri-Gondwanan origin for the Uchee terrane, Alabama and Georgia: Carolina zone or Suwannee terrane(?) and its suture with Grenvillian basement of the Pine Mountain window: *Geosphere*, v. 4, p. 131-144.
- Steltenpohl, M.G., Moecher, D., Andresen, A., Ball, J., Mager, S. & Hames, W.E., 2011, The Eidsfjord shear zone, Lofoten–Vesteralen, north Norway: an Early Devonian, paleoseismogenic low-angle normal fault. *Journal of Structural Geology*, 33, p. 1023–1043.
- Steltenpohl, M.G., Schwartz, J.J., Miller, B.V., 2013, Late to post-Appalachian strain partitioning and extension in the Blue Ridge of Alabama and Georgia: *Geosphere*, v. 9; n. 3, p. 647-666.
- Sterling, J.W., Steltenpohl, M.G., Cook, R.B., and Thomas B. Hanley, T.B., 2005, Petrology and Geochemistry of Igneous Rocks in the Southernmost Brevard zone of Alabama and their Implications for Southern Appalachian Tectonic Evolution: Guidebook for the 42nd Annual Field Trip of the Alabama Geological Society, p. 96-124.
- Sterling, J.W., 2006, Geology of the southernmost exposures of the Brevard zone in the Red Hill Quadrangle, Alabama [M.S. thesis]: Auburn, Auburn University, p. 118.
- Stow, S.H., Neilson, M.J., and Neathery, T.L., 1984, Petrography, geochemistry and tectonic significance of the amphibolites of the Alabama Piedmont: *American Journal of Science*, v. 284, nos. 4 and 5, p. 416-436.
- Suppe, J., 1985, *Principles of Structural Geology*: Prentice-Hall, Englewood Cliffs, New Jersey, 537 p.
- Thomas, W.A., 1977, Evolution of Appalachian-Ouachita salients and recesses from reentrants and promontories in the continental margin: *American Journal of Science*, v. 277, p. 1233–1278.
- Thomas, W.A., Neathery, T.N., and Ferrill, B.A., 1989, Cross-section A-A', *in* Hatcher, R.D., Jr., et al., eds., *The Appalachian-Ouachita orogen in the United States*: Boulder, Colorado, Geological Society of America, *Geology of North America*, v. F-2.
- Thomas, W.A., 1991, The Appalachian–Ouachita rifted margin of southeastern North America: *Geological Society of America Bulletin*, v. 103, p. 415–431.
- Toyoshima, T., 1998, Gabbro mylonite developed along a crustal-scale décollement, in Snoke, A., Tullis, J., and Todd, V.R., (ed.) *Fault related rocks – a photographic atlas*: Princeton University Press, New Jersey, p. 426-427.

- Tull, J.F., 1978, Structural development of the Alabama Piedmont northwest of the Brevard zone: *American Journal of Science*, v. 278, p. 442-460.
- Tull, J.F., 1984, Polyphase late Paleozoic deformation in the southeastern foreland and northwestern Piedmont of the Alabama Appalachians: *Journal of Structural Geology*, v. 6, p. 223–234.
- Tull, J.F., Barineau, C.I., Holm-Denoma, C.S., 2012, Characteristics, Extent, and Tectonic Significance of the Middle Ordovician Back-Arc Basin in the Southern Appalachian Blue Ridge, in Barineau, C.I., and Tull, J.F., *The Talledega Slate Belt and the eastern Blue Ridge: Laurentian plate passive margin to back-arc basin tectonics in the southern Appalachian orogen: Field Trip Guidebook for the Alabama Geological Society*, p. 12-26.
- Tull, J.F., Barineau, C.I., and Holm-Denoma, C.S., 2013, Characteristics, Extent, and Tectonic Significance of the Middle Ordovician Back-Arc Basin in the Southern Appalachian Blue Ridge, in Barineau, C.I., and Tull, J.F., *The Talladega Slate Belt and the eastern Blue Ridge: Laurentian plate passive margin to back-arc basin tectonics in the southern Appalachian orogen: Field Trip Guidebook for the Alabama Geological Society*, p. 12-26.
- Vauchez, A., 1987, Brevard fault zone, southern Appalachians: A medium-angle, dextral, Alleghanian shear zone: *Geology*, v. 15, p. 669–672.
- Vauchez, A., Babaie, H.A., and Babaei, A., 1993, Orogen-parallel tangential motion in the Late Devonian-Early Carboniferous southern Appalachians internides: *Canadian Journal of Earth Sciences*, v. 30, p. 1297–1305.
- Vernon, R.H., 1976, *Metamorphic Processes. Reactions and Microstructure Development*: George Allen and Unwin, Boston, 247 p.
- Wagner, M.E., and Srogi, L., 1987, Early Paleozoic metamorphism at two crustal levels and a tectonic model for the Pennsylvania-Delaware Piedmont: *Geological Society of America Bulletin* v. 99, p. 113-126.
- White, S.H., 1979, Large strain deformation: report on a tectonic studies group discussion meeting held at Imperial College, London; introduction: *Journal of Structural Geology*, v. 4, p. 333-339.
- White, S.H., Burrows, S.E., Carreras, J., Shaw, N.D., and Humphreys, F.J., 1980, On mylonites in ductile shear zones: *Journal of Structural Geology*, v. 2, p. 175-187.
- White, T.W., 2008, *Geology of the 1:24,000 Tallassee, Alabama, Quadrangle, and its implications for southern Appalachian tectonics [M.S. thesis]*: Auburn, Alabama, Auburn University, p. 74.

Wise, D.U., Dunn, D.E, Engeldar, J.T., Geiser, P.A., Hatcher, R.D., Kish, S.A., Odom, A.L., and Schamel, S., 1984, Fault-related rocks: suggestions for terminology: *Geology*, v. 12, p. 391-394.

Wielchowsky, C.C., 1986, The geology of the Brevard Zone and adjacent terranes in Alabama [Ph.D. dissertation]: Rice University, Houston, Texas, 225 p.

Zwart, H.J., 1962, On the determination of polymetamorphic mineral associations and its application to the Busost area (central Pyrenees): *Geologische Rundschau*, v. 52, p. 38-65.

APPENDIX

$^{40}\text{Ar}/^{39}\text{Ar}$ ISOTOPIC DATA

Single Crystal Analyses

Sensivity (Moles/vol):	1.62E-14 2E-16
J-Value:	28020000 112080
Measured 40/36 of Air:	290 1.5
Mass Discrimination (% per amu):	-0.00215059 0.001015228
(36/37)Ca:	0.0002900 0.0000110
(39/37)Ca:	0.0006800 0.0001100
(40/39)K:	0 4E-04
(38/39)Cl:	0.01 0.01
% of Sample in Split	0.58
Date of Irradiation:	9/9/2013
Date of Analysis:	4/6/2014

FCS monitor age

Representative Analyses of "blank" and air.

All data are in volts, with standard deviation, unless indicated otherwise.

Air	P	t	40 V	39 V	38 V	37 V	36 V	Moles 40Ar*	40/36	40/38	M. Fract	Date
air.4.2.14.a.txt	0	0	23.57225 ± 0.01316	0.00025 ± 0.00016	0.01572 ± 0.00010	0.00041 ± 0.00003	0.0808418 ± 0.0002738	3.83E-13	291.6	1500	0.996687832	4/2/14 12:37
blank.4.6.14.p.txt	0	0	0.00940 ± 0.000099	0.00119 ± 0.000073	0.00027 ± 0.000012	0.00048 ± 0.000015	0.0000796 ± 0.000016	1.53E-16	118	22.3	14.8	4/6/14 22:43

Neutron Flux Standards (J-values)

Monitor	P	t	40	39	38	37	36	Moles 40Ar*	% Rad	R	J-value	%-sd
au24.5a.bio.100a.txt	2.2	10	2.11926 ± 0.002137	0.59142 ± 0.001064	0.05246 ± 0.000185	0.00133 ± 0.000327	0.000393 ± 0.000034	3.44E-14	94.52%	3.38718	0.01661744 ± 0.000090	0.545%
au24.5a.bio.102a.txt	2.2	10	8.62283 ± 0.003010	2.44335 ± 0.001887	0.22055 ± 0.000377	0.01087 ± 0.000251	0.001413 ± 0.000052	1.40E-13	95.16%	3.35866	0.01675855 ± 0.000035	0.208%
au24.5a.bio.101a.txt	2.2	10	1.55015 ± 0.002052	0.43990 ± 0.000898	0.02831 ± 0.000217	0.00055 ± 0.000185	0.000204 ± 0.000035	2.52E-14	96.12%	3.38705	0.01661810 ± 0.000123	0.742%
au24.5a.bio.103a.txt	2.2	10	2.75224 ± 0.002125	0.74630 ± 0.000975	0.06401 ± 0.000236	0.00209 ± 0.000283	0.000789 ± 0.000034	4.47E-14	91.52%	3.37551	0.01667493 ± 0.000073	0.436%
au24.5a.bio.104a.txt	2.2	10	3.29943 ± 0.002136	0.87342 ± 0.000842	0.07468 ± 0.000390	0.02235 ± 0.000267	0.001167 ± 0.000033	5.36E-14	89.55%	3.38518	0.01662727 ± 0.000060	0.359%
au24.5e.bio.105a.txt	2.2	10	1.15338 ± 0.001981	0.29622 ± 0.000697	0.02601 ± 0.000200	0.00581 ± 0.000262	0.000542 ± 0.000021	1.87E-14	86.10%	3.35441	0.01677983 ± 0.000118	0.705%
au24.5e.bio.106a.txt	2.2	10	0.76258 ± 0.000979	0.21920 ± 0.000456	0.01749 ± 0.000102	0.01699 ± 0.000344	0.000080 ± 0.000031	1.24E-14	96.88%	3.37772	0.01666402 ± 0.000212	1.272%
au24.5e.bio.107a.txt	2.2	10	4.99597 ± 0.001555	1.40821 ± 0.001749	0.12358 ± 0.000408	0.01392 ± 0.000289	0.000907 ± 0.000036	8.11E-14	94.63%	3.35834	0.01676019 ± 0.000044	0.261%
au24.5e.bio.108a.txt	2.2	10	9.98755 ± 0.010176	2.75893 ± 0.002354	0.24778 ± 0.000432	0.00553 ± 0.000376	0.002444 ± 0.000039	1.62E-13	92.77%	3.35851	0.01675931 ± 0.000032	0.190%
au24.5e.bio.109a.txt	2.2	10	1.29015 ± 0.001434	0.36245 ± 0.000691	0.03270 ± 0.000129	0.00226 ± 0.000259	0.000267 ± 0.000031	2.09E-14	93.89%	3.34244	0.01683991 ± 0.000135	0.802%
au24.5i.bio.113a.txt	2.2	10	9.13191 ± 0.005637	2.33289 ± 0.001821	0.20144 ± 0.000558	0.00529 ± 0.000264	0.004209 ± 0.000070	1.48E-13	86.38%	3.38155	0.01664514 ± 0.000048	0.287%
au24.5i.bio.114a.txt	2.2	10	3.51219 ± 0.002511	0.95267 ± 0.001751	0.08188 ± 0.000424	0.00089 ± 0.000188	0.001016 ± 0.000025	5.70E-14	91.45%	3.37152	0.01669462 ± 0.000053	0.319%
au24.5i.bio.115a.txt	2.2	10	7.62654 ± 0.008831	2.14795 ± 0.002633	0.19610 ± 0.000616	0.09376 ± 0.000690	0.001322 ± 0.000027	1.24E-13	94.88%	3.37283	0.01668818 ± 0.000035	0.208%
au24.5i.bio.116a.txt	2.2	10	1.15305 ± 0.001089	0.32873 ± 0.000772	0.02714 ± 0.000186	0.00108 ± 0.000245	0.000125 ± 0.000034	1.87E-14	96.79%	3.39536	0.01657744 ± 0.000155	0.936%
au24.5s.bio.117a.txt	2.2	10	6.62169 ± 0.005302	1.89933 ± 0.002516	0.15245 ± 0.000639	0.08265 ± 0.000395	0.000790 ± 0.000020	1.08E-13	96.47%	3.36751	0.01671453 ± 0.000031	0.185%
au24.5s.bio.118a.txt	2.2	10	3.72763 ± 0.003196	1.03708 ± 0.001313	0.08811 ± 0.000374	0.00124 ± 0.000294	0.000776 ± 0.000023	6.05E-14	93.85%	3.37335	0.01668561 ± 0.000042	0.251%
au25.5s.bio.23a.txt	2	10	7.07297 ± 0.006441	1.99499 ± 0.001661	0.16722 ± 0.000699	0.00238 ± 0.000333	0.001210 ± 0.000021	1.15E-13	94.94%	3.36626	0.01672075 ± 0.000027	0.160%
au25.5s.san.26a.txt	1.8	10	4.19454 ± 0.001985	4.42625 ± 0.002627	0.05703 ± 0.000277	0.02586 ± 0.000352	0.000058 ± 0.000023	6.81E-14	99.59%	0.94430	0.01657596 ± 0.000030	0.182%
au25.5s.san.27a.txt	2	10	6.83508 ± 0.005169	6.99901 ± 0.006072	0.09072 ± 0.000160	0.08198 ± 0.000472	0.000856 ± 0.000022	1.11E-13	96.30%	0.94151	0.01662509 ± 0.000026	0.156%
au25.5s.san.24a.txt	2	10	4.00002 ± 0.004956	4.24844 ± 0.002854	0.05490 ± 0.000310	0.02531 ± 0.000280	0.000048 ± 0.000022	6.49E-14	99.65%	0.93874	0.01667420 ± 0.000036	0.214%
au25.5s.san.25a.txt	2	10	5.69988 ± 0.007080	6.00755 ± 0.004491	0.07819 ± 0.000257	0.03417 ± 0.000440	0.000079 ± 0.000039	9.25E-14	99.59%	0.94542	0.01655632 ± 0.000041	0.249%

Layer 5 all (preferred):
 Mean = 0.016721 ± 0.000021 [0.12%] 95% conf.
 Wtd by data-pt errs only, 0 of 22 rej.
 MSWD = 0.97, probability = 0.50

Layer 5 Perimeter
 Mean = 0.016714 ± 0.000029 [0.17%] 2σ
 Wtd by data-pt errs only, 0 of 14 rej.
 MSWD = 1.05, probability = 0.40

Mean = 317.35 ± 0.27 [0.084%] 95% conf.
 Wtd by data-pt errs only, 6 of 97 rej.
 MSWD = 1.4, probability = 0.007

Single Crystal Total-Fusion Analyses

JP-ACF-1 (32° 59' 5.61" N, 85° 51' 35.90" W), 40-60 mesh sieve, Wedowee Group from Alexander City fault/shear zone

Sample Number	P	t	40	39	38	37	36	Moles 40Ar*	% Rad	R	Age (Ma)	% -sd
au25.5c.mus.6a.txt	1.8	10	3.20699 ± 0.001775	0.27605 ± 0.000542	0.00352 ± 0.000043	-0.00017 ± 0.000622	0.000101 ± 0.000016	5.21E-14	99.1%	11.5099	317.39 ± 0.81	0.255%
au25.5c.mus.7a.txt	1.8	10	2.51105 ± 0.002841	0.20898 ± 0.000498	0.00268 ± 0.000028	0.00027 ± 0.001004	0.000369 ± 0.000017	4.08E-14	95.7%	11.4936	316.98 ± 1.11	0.349%
au25.5c.mus.8a.txt	1.8	10	1.61035 ± 0.002315	0.12908 ± 0.000467	0.00170 ± 0.000020	0.00132 ± 0.000673	0.000488 ± 0.000018	2.61E-14	91.0%	11.3596	313.58 ± 1.77	0.564%
au25.5c.mus.11a.txt	1.8	10	6.05869 ± 0.004940	0.50448 ± 0.000834	0.00685 ± 0.000099	-0.00314 ± 0.001088	0.000670 ± 0.000016	9.84E-14	96.7%	11.6168	320.09 ± 0.67	0.208%
au25.5c.mus.12a.txt	1.8	10	1.56405 ± 0.002433	0.13434 ± 0.000356	0.00172 ± 0.000030	0.00069 ± 0.000778	0.000120 ± 0.000016	2.54E-14	97.7%	11.3792	314.08 ± 1.38	0.438%
au25.5c.mus.13a.txt	1.8	10	2.69585 ± 0.001371	0.23135 ± 0.000586	0.00289 ± 0.000029	0.00029 ± 0.001114	0.000146 ± 0.000015	4.38E-14	98.4%	11.4657	316.27 ± 0.99	0.313%
au25.5c.mus.14a.txt	1.8	10	1.20812 ± 0.001038	0.10233 ± 0.000521	0.00137 ± 0.000025	0.00064 ± 0.000650	0.000133 ± 0.000017	1.96E-14	96.7%	11.4217	315.16 ± 2.15	0.682%
au25.5c.mus.15a.txt	1.8	10	2.16306 ± 0.002537	0.18596 ± 0.000467	0.00236 ± 0.000034	-0.00003 ± 0.000835	0.000081 ± 0.000022	3.51E-14	98.9%	11.5038	317.24 ± 1.30	0.410%
au25.5c.mus.16a.txt	1.8	10	0.98872 ± 0.001735	0.08488 ± 0.000289	0.00114 ± 0.000035	0.00191 ± 0.000827	0.000076 ± 0.000016	1.61E-14	97.7%	11.3864	314.26 ± 1.99	0.634%
au25.5c.mus.17a.txt	1.8	10	5.37361 ± 0.003347	0.45666 ± 0.000889	0.00577 ± 0.000068	0.00406 ± 0.001445	0.000403 ± 0.000017	8.72E-14	97.8%	11.5076	317.33 ± 0.73	0.230%
au25.5c.mus.18a.txt	1.8	10	1.43036 ± 0.001194	0.12264 ± 0.000384	0.00170 ± 0.000042	0.00104 ± 0.000983	0.000114 ± 0.000016	2.32E-14	97.6%	11.3892	314.33 ± 1.48	0.471%
au25.5c.mus.19a.txt	1.8	10	3.16510 ± 0.003144	0.26765 ± 0.000406	0.00338 ± 0.000032	0.00114 ± 0.000325	0.000330 ± 0.000017	5.14E-14	96.9%	11.4617	316.17 ± 0.79	0.250%
au25.5c.mus.21a.txt	1.8	10	3.21876 ± 0.001333	0.26704 ± 0.000541	0.00345 ± 0.000047	0.00226 ± 0.000777	0.000445 ± 0.000018	5.23E-14	95.9%	11.5622	318.71 ± 0.88	0.275%
au25.5c.mus.22a.txt	1.8	10	2.97174 ± 0.003558	0.25428 ± 0.000471	0.00326 ± 0.000029	0.00206 ± 0.000721	0.000124 ± 0.000016	4.82E-14	98.8%	11.5442	318.26 ± 0.88	0.276%
au25.5c.mus.23a.txt	1.8	10	2.78405 ± 0.003849	0.23673 ± 0.000588	0.00301 ± 0.000041	-0.00007 ± 0.000788	0.000158 ± 0.000012	4.52E-14	98.3%	11.5626	318.72 ± 1.01	0.317%
au25.5c.mus.24a.txt	1.8	10	2.54334 ± 0.002185	0.21469 ± 0.000411	0.00269 ± 0.000036	-0.00045 ± 0.000745	0.000232 ± 0.000012	4.13E-14	97.3%	11.5266	317.81 ± 0.82	0.257%
au25.5c.mus.25a.txt	1.8	10	1.58259 ± 0.001697	0.13242 ± 0.000429	0.00166 ± 0.000037	0.00009 ± 0.000733	0.000187 ± 0.000011	2.57E-14	96.5%	11.5338	317.99 ± 1.31	0.411%
au25.5c.mus.26a.txt	1.8	10	2.75560 ± 0.005710	0.23558 ± 0.000841	0.00301 ± 0.000061	-0.00145 ± 0.000824	0.000122 ± 0.000020	4.47E-14	98.7%	11.5434	318.24 ± 1.50	0.473%
au25.5c.mus.27a.txt	1.8	10	0.88976 ± 0.000892	0.07580 ± 0.000523	0.00097 ± 0.000027	-0.00024 ± 0.000843	0.000061 ± 0.000010	1.44E-14	98.0%	11.4998	317.14 ± 2.52	0.794%
au25.5c.mus.28a.txt	1.8	10	2.04361 ± 0.002780	0.17579 ± 0.000412	0.00223 ± 0.000036	-0.00038 ± 0.000926	0.000040 ± 0.000012	3.32E-14	99.4%	11.5572	318.58 ± 1.02	0.321%
au25.5c.mus.29a.txt	1.8	10	2.44249 ± 0.002414	0.20518 ± 0.000429	0.00269 ± 0.000034	0.00202 ± 0.000616	0.000249 ± 0.000018	3.97E-14	97.0%	11.5472	318.33 ± 1.04	0.326%
au25.5c.mus.30a.txt	1.8	10	1.70367 ± 0.001263	0.14849 ± 0.000537	0.00183 ± 0.000028	0.00186 ± 0.000806	0.000032 ± 0.000009	2.77E-14	99.4%	11.4101	314.86 ± 1.27	0.403%
au25.5c.mus.31a.txt	1.8	10	1.44822 ± 0.000678	0.12426 ± 0.000467	0.00155 ± 0.000029	-0.00064 ± 0.000752	0.000023 ± 0.000016	2.35E-14	99.5%	11.6001	319.67 ± 1.59	0.496%
au25.5c.mus.32a.txt	1.8	10	2.08014 ± 0.002257	0.18102 ± 0.000570	0.00220 ± 0.000023	0.00022 ± 0.000446	0.000016 ± 0.000010	3.38E-14	99.8%	11.4652	316.26 ± 1.15	0.363%

n= 24

Mean = 317.22±0.61 [0.19%] 95% conf.
 Wtd by data-pt errs only, 1 of 24 rej.
 MSWD = 1.7, probability = 0.027

Single Crvstal Total-Fusion Analyses

JP-ACF-2 (32° 52' 27.70" N, 85° 57' 57.56" W), 40-60 mesh sieve, Wedowee Group from Alexander City fault/shear zone

Sample Number	P	t	40	39	38	37	36	Moles 40Ar*	% Rad	R	Age (Ma)	% -s.d
au25.5d.mus.36a.txt	1.8	10	5.78777 ± 0.002648	0.49933 ± 0.000904	0.00635 ± 0.000059	-0.00077 ± 0.000394	0.000182 ± 0.000016	9.40E-14	99.1%	11.4831	316.71 ± 0.65	0.205%
au25.5d.mus.37a.txt	1.8	10	4.41001 ± 0.003089	0.38316 ± 0.000647	0.00516 ± 0.000137	-0.00017 ± 0.000722	0.000009 ± 0.000019	7.16E-14	99.9%	11.5024	317.20 ± 0.70	0.222%
au25.5d.mus.38a.txt	1.8	10	2.51208 ± 0.003331	0.21691 ± 0.000566	0.00271 ± 0.000022	-0.00253 ± 0.000629	-0.000013 ± 0.000019	4.08E-14	100.1%	11.5802	319.17 ± 1.17	0.368%
au25.5d.mus.39a.txt	1.8	10	1.52422 ± 0.002728	0.13157 ± 0.000339	0.00164 ± 0.000036	-0.00149 ± 0.000560	-0.000041 ± 0.000021	2.47E-14	100.8%	11.5836	319.25 ± 1.64	0.514%
au25.5d.mus.39a.txt	1.8	10	1.52422 ± 0.002728	0.13157 ± 0.000339	0.00164 ± 0.000036	-0.00149 ± 0.000560	-0.000041 ± 0.000021	2.47E-14	100.8%	11.5836	319.25 ± 1.64	0.514%
au25.5d.mus.40a.txt	1.8	10	1.39787 ± 0.001667	0.12046 ± 0.000446	0.00147 ± 0.000021	-0.00140 ± 0.000736	-0.000018 ± 0.000022	2.27E-14	100.4%	11.6034	319.75 ± 1.94	0.606%
au25.5d.mus.41a.txt	1.8	10	2.97331 ± 0.002723	0.25544 ± 0.000785	0.00335 ± 0.000059	0.00033 ± 0.000909	0.000135 ± 0.000019	4.83E-14	98.7%	11.4838	316.73 ± 1.19	0.375%
au25.5d.mus.42a.txt	1.8	10	2.73469 ± 0.003239	0.23420 ± 0.000769	0.00295 ± 0.000041	-0.00133 ± 0.000530	0.000141 ± 0.000018	4.44E-14	98.5%	11.4983	317.10 ± 1.29	0.406%
au25.5d.mus.44a.txt	1.8	10	1.88770 ± 0.001184	0.16284 ± 0.000367	0.00202 ± 0.000047	-0.00390 ± 0.000741	0.000074 ± 0.000018	3.06E-14	98.8%	11.4553	316.01 ± 1.19	0.376%
au25.5d.mus.45a.txt	1.8	10	2.19390 ± 0.002031	0.18891 ± 0.000740	0.00235 ± 0.000027	-0.00006 ± 0.001029	0.000054 ± 0.000018	3.56E-14	99.3%	11.5284	317.86 ± 1.50	0.473%
au25.5d.mus.46a.txt	1.8	10	3.07367 ± 0.001843	0.26797 ± 0.000669	0.00360 ± 0.000079	0.00086 ± 0.000718	0.000032 ± 0.000010	4.99E-14	99.7%	11.4356	315.51 ± 0.87	0.276%
au25.5d.mus.47a.txt	1.8	10	1.53121 ± 0.002572	0.13252 ± 0.000437	0.00171 ± 0.000030	0.00068 ± 0.000722	-0.000007 ± 0.000011	2.49E-14	100.1%	11.5549	318.53 ± 1.36	0.428%
au25.5d.mus.48a.txt	1.8	10	2.32552 ± 0.002362	0.20117 ± 0.000527	0.00259 ± 0.000037	0.00179 ± 0.000885	-0.000028 ± 0.000016	3.78E-14	100.4%	11.5608	318.68 ± 1.11	0.347%
au25.5d.mus.49a.txt	1.8	10	0.95892 ± 0.001180	0.08301 ± 0.000234	0.00104 ± 0.000021	0.00126 ± 0.000620	0.000009 ± 0.000012	1.56E-14	99.7%	11.5218	317.69 ± 1.53	0.481%
au25.5d.mus.50a.txt	1.8	10	0.74523 ± 0.002406	0.06489 ± 0.000215	0.00083 ± 0.000029	0.00030 ± 0.000411	0.000003 ± 0.000011	1.21E-14	99.9%	11.4715	316.42 ± 2.06	0.650%
au25.5d.mus.51a.txt	1.8	10	1.02544 ± 0.000912	0.08841 ± 0.000230	0.00114 ± 0.000030	-0.00195 ± 0.000750	0.000022 ± 0.000012	1.66E-14	99.4%	11.5213	317.68 ± 1.38	0.435%
au25.5d.mus.52a.txt	1.8	10	0.75150 ± 0.001012	0.06545 ± 0.000378	0.00083 ± 0.000040	-0.00502 ± 0.000888	0.000006 ± 0.000011	1.22E-14	99.8%	11.4480	315.82 ± 2.35	0.744%
au25.5d.mus.53a.txt	1.8	10	1.94639 ± 0.002314	0.16923 ± 0.000483	0.00213 ± 0.000052	0.00085 ± 0.000869	-0.000040 ± 0.000018	3.16E-14	100.6%	11.5018	317.18 ± 1.31	0.413%
au25.5d.mus.54a.txt	1.8	10	1.14479 ± 0.001320	0.09924 ± 0.000193	0.00123 ± 0.000037	-0.00004 ± 0.000781	-0.000002 ± 0.000011	1.86E-14	100.1%	11.5355	318.04 ± 1.18	0.371%
au25.5d.mus.55a.txt	1.8	10	1.73813 ± 0.002050	0.15160 ± 0.000584	0.00191 ± 0.000027	0.00012 ± 0.000856	0.000016 ± 0.000011	2.82E-14	99.7%	11.4340	315.47 ± 1.41	0.447%
au25.5d.mus.56a.txt	1.8	10	1.59249 ± 0.001420	0.13841 ± 0.000700	0.00178 ± 0.000025	-0.00347 ± 0.001287	-0.000002 ± 0.000010	2.59E-14	100.0%	11.5029	317.21 ± 1.74	0.548%
au25.5d.mus.57a.txt	1.8	10	2.30342 ± 0.001534	0.19933 ± 0.000596	0.00251 ± 0.000041	-0.00050 ± 0.000546	0.000047 ± 0.000011	3.74E-14	99.4%	11.4865	316.80 ± 1.07	0.338%
au25.5d.mus.58a.txt	1.8	10	1.70959 ± 0.002073	0.14580 ± 0.000438	0.00188 ± 0.000028	-0.00068 ± 0.000811	0.000077 ± 0.000010	2.78E-14	98.7%	11.5693	318.89 ± 1.19	0.374%
au25.5d.mus.59a.txt	1.8	10	2.78180 ± 0.003428	0.24083 ± 0.000407	0.00320 ± 0.000049	-0.00059 ± 0.000958	0.000024 ± 0.000019	4.52E-14	99.7%	11.5214	317.68 ± 0.92	0.288%
au25.5d.mus.60a.txt	1.8	10	2.16540 ± 0.001493	0.18838 ± 0.000452	0.00243 ± 0.000037	-0.00083 ± 0.001011	-0.000003 ± 0.000010	3.52E-14	100.0%	11.4942	316.99 ± 0.91	0.288%

n= 25

Mean = 317.31±0.45 [0.14%] 95% conf.
 Wtd by data-pt errs only, 0 of 25 rej.
 MSWD = 0.88, probability = 0.64

Single Crystal Total-Fusion Analyses

JP-KG (32° 58' 24.51" N, 85° 51' 1.59" W), 40-60 mesh sieve, Kowaliga Gneiss

Sample Number	P	t	40	39	38	37	36	Moles 40Ar*	% Rad	R	Age (Ma)	% -s.d
au25.5e.mus.92a.txt	1.8	10	3.16663 ± 0.003233	0.26398 ± 0.000780	0.00346 ± 0.000051	0.00127 ± 0.000721	0.000439 ± 0.000010	5.14E-14	95.9%	11.5052	317.27 ± 1.08	0.341%
au25.5e.mus.93a.txt	1.8	10	1.57742 ± 0.001549	0.13648 ± 0.000413	0.00179 ± 0.000036	0.00134 ± 0.000744	-0.000010 ± 0.000015	2.56E-14	100.2%	11.5592	318.64 ± 1.33	0.418%
au25.5e.mus.94a.txt	1.8	10	2.30194 ± 0.001852	0.19497 ± 0.000394	0.00271 ± 0.000046	-0.00038 ± 0.000647	0.000163 ± 0.000010	3.74E-14	97.9%	11.5592	318.64 ± 0.82	0.257%
au25.5e.mus.95a.txt	1.8	10	3.29015 ± 0.002778	0.27181 ± 0.001022	0.00387 ± 0.000048	0.00171 ± 0.000590	0.000515 ± 0.000010	5.34E-14	95.4%	11.5455	318.29 ± 1.32	0.416%
au25.5e.mus.96a.txt	1.8	10	1.32074 ± 0.001835	0.11390 ± 0.000265	0.00162 ± 0.000031	-0.00012 ± 0.000578	0.000045 ± 0.000011	2.14E-14	99.0%	11.4777	316.57 ± 1.16	0.365%
au25.5e.mus.97a.txt	1.8	10	4.17554 ± 0.004363	0.35876 ± 0.000679	0.00484 ± 0.000053	-0.00018 ± 0.000458	0.000176 ± 0.000011	6.78E-14	98.8%	11.4938	316.98 ± 0.74	0.233%
au25.5e.mus.98a.txt	1.8	10	7.43380 ± 0.005584	0.63110 ± 0.000932	0.00882 ± 0.000113	0.00162 ± 0.000896	0.000550 ± 0.000022	1.21E-13	97.8%	11.5220	317.70 ± 0.61	0.192%
au25.5e.mus.99a.txt	1.8	10	2.25902 ± 0.002633	0.19263 ± 0.000505	0.00255 ± 0.000035	-0.00063 ± 0.000608	0.000130 ± 0.000011	3.67E-14	98.3%	11.5276	317.84 ± 1.03	0.324%
au25.5e.mus.100a.txt	1.8	10	4.97496 ± 0.004729	0.42523 ± 0.000606	0.00569 ± 0.000054	0.00157 ± 0.000518	0.000321 ± 0.000013	8.08E-14	98.1%	11.4769	316.55 ± 0.61	0.192%
au25.5e.mus.101a.txt	1.8	10	2.49170 ± 0.003290	0.21655 ± 0.000421	0.00290 ± 0.000037	-0.00038 ± 0.000632	0.000100 ± 0.000009	4.05E-14	98.8%	11.3692	313.83 ± 0.83	0.264%
au25.5e.mus.102a.txt	1.8	10	1.87407 ± 0.002678	0.16271 ± 0.000550	0.00217 ± 0.000042	0.00066 ± 0.001008	0.000080 ± 0.000014	3.04E-14	98.7%	11.3730	313.92 ± 1.37	0.436%
au25.5e.mus.103a.txt	1.8	10	3.27619 ± 0.002929	0.28101 ± 0.000637	0.00369 ± 0.000048	-0.00062 ± 0.000899	0.000136 ± 0.000013	5.32E-14	98.8%	11.5154	317.53 ± 0.87	0.273%
au25.5e.mus.104a.txt	1.8	10	5.58050 ± 0.002955	0.48209 ± 0.001201	0.00655 ± 0.000096	0.00382 ± 0.000724	0.000176 ± 0.000012	9.06E-14	99.1%	11.4687	316.35 ± 0.84	0.265%
au25.5e.mus.105a.txt	1.8	10	2.44827 ± 0.003297	0.20793 ± 0.000321	0.00281 ± 0.000039	0.00247 ± 0.000807	0.000177 ± 0.000012	3.97E-14	97.9%	11.5246	317.76 ± 0.82	0.257%
au25.5e.mus.106a.txt	1.8	10	8.01070 ± 0.009527	0.69107 ± 0.001112	0.00939 ± 0.000105	0.00273 ± 0.000765	0.000045 ± 0.000018	1.30E-13	99.8%	11.5730	318.98 ± 0.67	0.211%
au25.5e.mus.107a.txt	1.8	10	1.72184 ± 0.001281	0.14969 ± 0.000475	0.00208 ± 0.000044	0.00030 ± 0.000462	0.000011 ± 0.000017	2.80E-14	99.8%	11.4816	316.67 ± 1.39	0.438%
au25.5e.mus.108a.txt	1.8	10	3.65589 ± 0.002847	0.31439 ± 0.000894	0.00445 ± 0.000085	0.00170 ± 0.000699	0.000048 ± 0.000011	5.94E-14	99.6%	11.5842	319.27 ± 0.99	0.309%
au25.5e.mus.109a.txt	1.8	10	2.22615 ± 0.001843	0.18729 ± 0.000379	0.00246 ± 0.000034	-0.00035 ± 0.000639	0.000280 ± 0.000013	3.61E-14	96.3%	11.4442	315.73 ± 0.91	0.287%
au25.5e.mus.110a.txt	1.8	10	3.59459 ± 0.002106	0.31162 ± 0.001066	0.00416 ± 0.000044	-0.00010 ± 0.000918	0.000045 ± 0.000017	5.84E-14	99.6%	11.4928	316.96 ± 1.19	0.377%
au25.5e.mus.113a.txt	1.8	10	3.46099 ± 0.001793	0.29958 ± 0.000730	0.00405 ± 0.000032	0.00089 ± 0.000636	0.000016 ± 0.000022	5.62E-14	99.9%	11.5375	318.09 ± 1.00	0.313%
au25.5e.mus.114a.txt	1.8	10	5.11257 ± 0.005191	0.43897 ± 0.000821	0.00573 ± 0.000045	0.00071 ± 0.000998	0.000292 ± 0.000011	8.30E-14	98.3%	11.4504	315.88 ± 0.72	0.226%
au25.5e.mus.115a.txt	1.8	10	0.68483 ± 0.000969	0.05798 ± 0.000158	0.00076 ± 0.000028	0.00023 ± 0.001034	0.000066 ± 0.000012	1.11E-14	97.2%	11.4764	316.54 ± 1.91	0.602%
au25.5e.mus.116a.txt	1.8	10	4.23631 ± 0.003804	0.36593 ± 0.000953	0.00517 ± 0.000078	-0.00066 ± 0.000720	0.000156 ± 0.000010	6.88E-14	98.9%	11.4502	315.88 ± 0.91	0.287%
au25.5e.mus.117a.txt	1.8	10	2.55341 ± 0.001723	0.21594 ± 0.000411	0.00298 ± 0.000059	-0.00064 ± 0.001039	0.000199 ± 0.000020	4.15E-14	97.7%	11.5519	318.45 ± 0.99	0.312%
au25.5e.mus.118a.txt	1.8	10	2.75956 ± 0.002732	0.23295 ± 0.000426	0.00318 ± 0.000039	-0.00232 ± 0.000724	0.000224 ± 0.000012	4.48E-14	97.6%	11.5612	318.69 ± 0.79	0.248%

n= 25

Mean = 317.38±0.50 [0.16%] 95% conf.
 Wtd by data-pt errs only, 1 of 25 rej.
 MSWD = 1.7, probability = 0.017

Single Crystal Total-Fusion Analyses

JP-AF-1 (32° 45' 13.45" N, 85° 53' 17.00" W), 40-60 mesh sieve, Jacksons Gap Group from Abanda fault/shear zone (Brevard fault/shear zone)

Sample Number	P	t	40	39	38	37	36	Moles 40Ar*	% Rad	R	Age (Ma)	% -s.d
au25.5f.mus.64a.txt	1.8	10	1.01898 ± 0.001187	0.08754 ± 0.000430	0.00107 ± 0.000029	0.00033 ± 0.000709	0.000054 ± 0.000022	1.65E-14	98.4%	11.4572	316.06 ± 2.59	0.819%
au25.5f.mus.65a.txt	1.8	10	0.88615 ± 0.001243	0.07602 ± 0.000221	0.00096 ± 0.000044	0.00084 ± 0.000932	0.000039 ± 0.000023	1.44E-14	98.7%	11.5078	317.34 ± 2.68	0.845%
au25.5f.mus.66a.txt	1.8	10	0.42078 ± 0.000951	0.03547 ± 0.000108	0.00043 ± 0.000026	-0.00075 ± 0.000525	0.000021 ± 0.000011	6.83E-15	98.6%	11.6892	321.92 ± 2.89	0.899%
au25.5f.mus.67a.txt	1.8	10	2.39590 ± 0.001708	0.20679 ± 0.000327	0.00264 ± 0.000041	0.00130 ± 0.000501	0.000067 ± 0.000017	3.89E-14	99.2%	11.4907	316.90 ± 0.88	0.279%
au25.5f.mus.68a.txt	1.8	10	2.15619 ± 0.001922	0.18374 ± 0.000448	0.00231 ± 0.000031	-0.00179 ± 0.001113	0.000184 ± 0.000018	3.50E-14	97.5%	11.4383	315.58 ± 1.16	0.368%
au25.5f.mus.70a.txt	1.8	10	2.39600 ± 0.001366	0.20216 ± 0.000655	0.00266 ± 0.000065	0.00005 ± 0.000734	0.000173 ± 0.000013	3.89E-14	97.9%	11.5987	319.63 ± 1.19	0.372%
au25.5f.mus.71a.txt	1.8	10	1.50950 ± 0.001156	0.13316 ± 0.000338	0.00168 ± 0.000033	0.00081 ± 0.000736	-0.000012 ± 0.000018	2.45E-14	100.2%	11.3366	313.00 ± 1.38	0.440%
au25.5f.mus.72a.txt	1.8	10	1.99308 ± 0.001983	0.17291 ± 0.000446	0.00219 ± 0.000031	0.00074 ± 0.000739	0.000033 ± 0.000011	3.24E-14	99.5%	11.4710	316.40 ± 1.01	0.320%
au25.5f.mus.73a.txt	1.8	10	0.89771 ± 0.000509	0.07778 ± 0.000238	0.00097 ± 0.000025	0.00033 ± 0.000927	0.000026 ± 0.000011	1.46E-14	99.1%	11.4425	315.68 ± 1.56	0.493%
au25.5f.mus.74a.txt	1.8	10	1.46449 ± 0.001181	0.12624 ± 0.000553	0.00161 ± 0.000044	0.00000 ± 0.000460	0.000022 ± 0.000011	2.38E-14	99.6%	11.5493	318.38 ± 1.59	0.499%
au25.5f.mus.75a.txt	1.8	10	0.77090 ± 0.001111	0.06694 ± 0.000335	0.00083 ± 0.000031	0.00041 ± 0.000655	0.000022 ± 0.000011	1.25E-14	99.2%	11.4212	315.15 ± 2.12	0.674%
au25.5f.mus.76a.txt	1.8	10	0.68969 ± 0.000871	0.05861 ± 0.000293	0.00074 ± 0.000024	0.00093 ± 0.000652	0.000015 ± 0.000012	1.12E-14	99.4%	11.6965	322.10 ± 2.33	0.722%
au25.5f.mus.77a.txt	1.8	10	2.17016 ± 0.001545	0.18453 ± 0.000571	0.00234 ± 0.000034	0.00000 ± 0.000704	0.000104 ± 0.000011	3.52E-14	98.6%	11.5945	319.53 ± 1.14	0.357%
au25.5f.mus.78a.txt	1.8	10	4.19814 ± 0.004155	0.36081 ± 0.001054	0.00471 ± 0.000065	0.00208 ± 0.000593	0.000105 ± 0.000012	6.82E-14	99.3%	11.5503	318.41 ± 1.03	0.322%
au25.5f.mus.79a.txt	1.8	10	1.06308 ± 0.001336	0.09176 ± 0.000331	0.00121 ± 0.000030	0.00148 ± 0.000896	0.000011 ± 0.000012	1.73E-14	99.7%	11.5524	318.46 ± 1.63	0.511%
au25.5f.mus.80a.txt	1.8	10	0.59256 ± 0.001147	0.05083 ± 0.000158	0.00064 ± 0.000034	0.00089 ± 0.000433	0.000029 ± 0.000011	9.62E-15	98.6%	11.4932	316.97 ± 2.13	0.673%
au25.5f.mus.82a.txt	1.8	10	0.79460 ± 0.000832	0.06780 ± 0.000260	0.00087 ± 0.000023	0.00054 ± 0.000562	-0.000020 ± 0.000016	1.29E-14	100.8%	11.7199	322.69 ± 2.31	0.715%
au25.5f.mus.83a.txt	1.8	10	2.03322 ± 0.001794	0.17438 ± 0.000539	0.00234 ± 0.000066	0.00260 ± 0.000582	-0.000007 ± 0.000016	3.30E-14	100.1%	11.6611	321.21 ± 1.28	0.398%
au25.5f.mus.84a.txt	1.8	10	1.63110 ± 0.002087	0.13724 ± 0.000271	0.00175 ± 0.000036	0.00107 ± 0.000546	0.000119 ± 0.000011	2.65E-14	97.8%	11.6291	320.40 ± 1.01	0.316%
au25.5f.mus.85a.txt	1.8	10	2.08104 ± 0.002346	0.17755 ± 0.000677	0.00220 ± 0.000049	0.00068 ± 0.000561	0.000079 ± 0.000010	3.38E-14	98.9%	11.5908	319.43 ± 1.37	0.428%
au25.5f.mus.86a.txt	1.8	10	0.88500 ± 0.000909	0.07687 ± 0.000308	0.00096 ± 0.000039	0.00092 ± 0.001037	0.000029 ± 0.000011	1.44E-14	99.0%	11.4029	314.68 ± 1.76	0.559%
au25.5f.mus.87a.txt	1.8	10	0.70213 ± 0.000904	0.06010 ± 0.000291	0.00072 ± 0.000024	0.00073 ± 0.001150	0.000015 ± 0.000011	1.14E-14	99.4%	11.6110	319.94 ± 2.17	0.679%
au25.5f.mus.88a.txt	1.8	10	1.58358 ± 0.002224	0.13635 ± 0.000300	0.00175 ± 0.000040	0.00031 ± 0.000606	0.000068 ± 0.000011	2.57E-14	98.7%	11.4663	316.29 ± 1.05	0.334%

n= 23

Mean = 318.09±0.91 [0.29%] 95% conf.
 Wtd by data-pt errs only, 1 of 23 rej.
 MSWD = 2.2, probability = 0.001

Single Crvstal Incremental-Heating Analyses

JP-KG (32° 58' 24.51" N, 85° 51' 1.59" W), 30-40 mesh sieve, Kowaliga Gneiss

Sample Number	P	t	40	39	38	37	36	Moles 40Ar*	% Rad	R	Age (Ma)	% -sd
au25.5e.mus.89a.txt	0.35	15	0.00008 ± 0.000202	-0.00007 ± 0.000073	-0.00002 ± 0.000021	-0.00103 ± 0.000830	0.000009 ± 0.000017	1.30E-18	-3278.8%	38.1442	889.68 ± 1829.07	205.588%
au25.5e.mus.89b.txt	0.4	10	0.04125 ± 0.000470	0.00303 ± 0.000114	0.00003 ± 0.000024	0.00061 ± 0.000788	0.000004 ± 0.000010	6.70E-16	97.1%	13.2194	360.11 ± 31.16	8.654%
au25.5e.mus.89c.txt	0.45	10	0.25668 ± 0.000249	0.01974 ± 0.000096	0.00025 ± 0.000019	-0.00097 ± 0.000785	0.000074 ± 0.000012	4.17E-15	91.4%	11.8832	326.81 ± 5.11	1.563%
au25.5e.mus.89d.txt	0.5	10	1.04470 ± 0.001344	0.08001 ± 0.000369	0.00110 ± 0.000033	0.00097 ± 0.000922	0.000398 ± 0.000012	1.70E-14	88.7%	11.5898	319.41 ± 2.13	0.668%
au25.5e.mus.89e.txt	0.6	10	10.27175 ± 0.009344	0.88213 ± 0.001645	0.01246 ± 0.000136	0.00136 ± 0.000443	0.000267 ± 0.000013	1.67E-13	99.2%	11.5550	318.53 ± 0.68	0.212%
au25.5e.mus.89f.txt	0.64	10	1.90937 ± 0.001630	0.16417 ± 0.000564	0.00216 ± 0.000028	0.00027 ± 0.000633	-0.000010 ± 0.000014	3.10E-14	100.2%	11.6306	320.44 ± 1.34	0.417%
au25.5e.mus.89g.txt	0.68	10	0.14091 ± 0.000466	0.01211 ± 0.000125	0.00012 ± 0.000021	-0.00153 ± 0.000502	0.000012 ± 0.000010	2.29E-15	97.4%	11.3197	312.57 ± 7.82	2.502%
au25.5e.mus.89h.txt	0.8	10	0.23553 ± 0.000475	0.02050 ± 0.000108	0.00026 ± 0.000027	-0.00227 ± 0.000637	0.000000 ± 0.000011	3.82E-15	100.0%	11.4766	316.55 ± 4.60	1.453%
au25.5e.mus.89i.txt	0.9	10	0.12858 ± 0.000325	0.01095 ± 0.000121	0.00016 ± 0.000023	-0.00087 ± 0.000750	-0.000002 ± 0.000010	2.09E-15	100.4%	11.7375	323.14 ± 8.35	2.584%

Plateau age = 319.01±0.57 Ma (1σ)
MSWD = 0.99, probability=0.43
Includes 100% of the ³⁹Ar

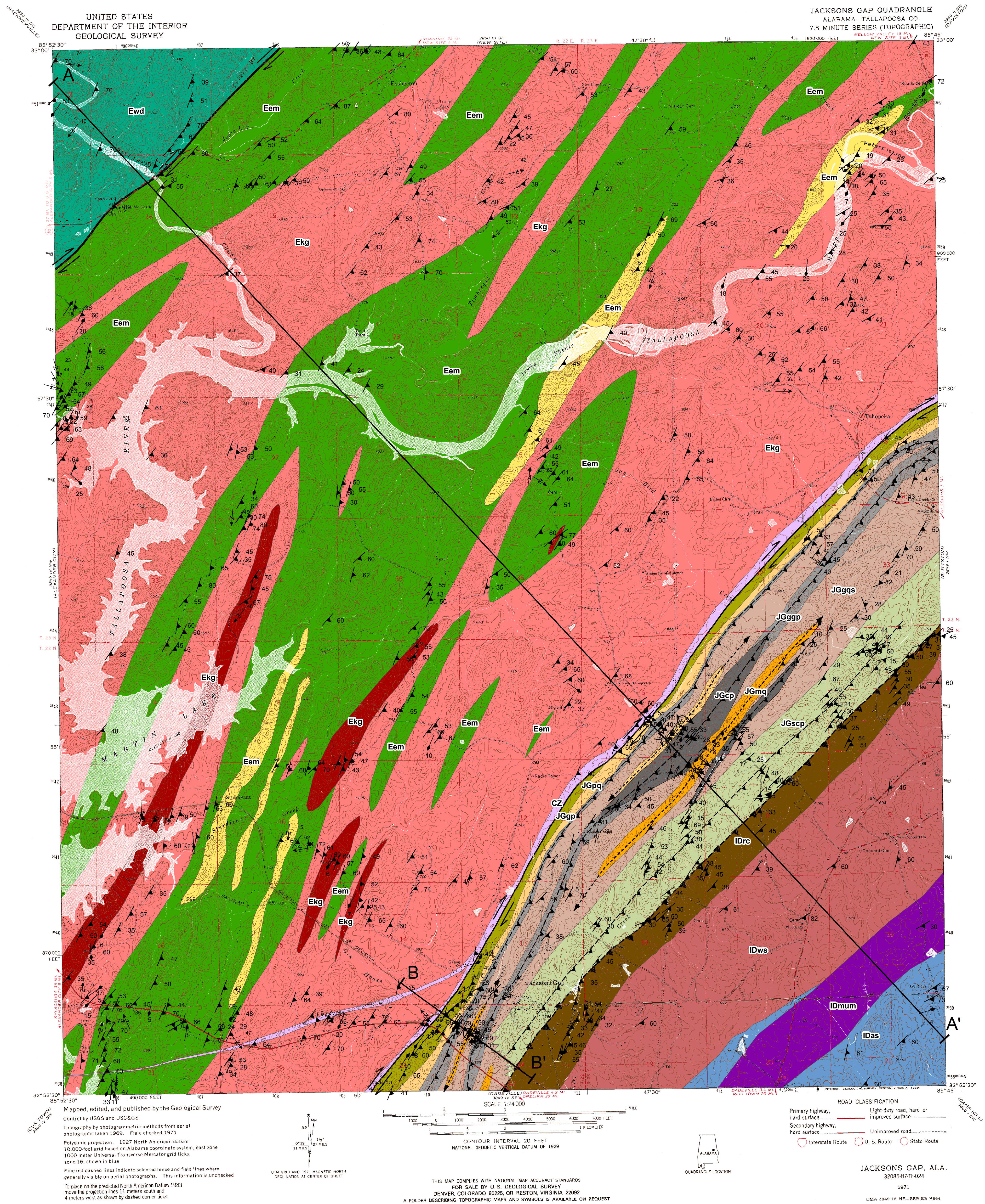
Single Crvstal Incremental-Heating Analyses

JP-KG (32° 58' 24.51" N, 85° 51' 1.59" W), 30-40 mesh sieve, Kowaliga Gneiss

Sample Number	P	t	40	39	38	37	36	Moles 40Ar*	% Rad	R	Age (Ma)	% -sd
au25.5e.mus.90c.txt	0.45	20	0.00097 ± 0.000169	0.00027 ± 0.000064	0.00003 ± 0.000021	-0.00101 ± 0.000385	0.000023 ± 0.000013	1.57E-17	-616.6%	-22.2834	-840.44 ± 573.63	68.253%
au25.5e.mus.90d.txt	0.5	20	0.02039 ± 0.000208	0.00195 ± 0.000100	0.00005 ± 0.000022	-0.00011 ± 0.000775	0.000017 ± 0.000012	3.31E-16	75.9%	7.9381	224.74 ± 52.06	23.165%
au25.5e.mus.90e.txt	0.55	20	0.06988 ± 0.000511	0.00556 ± 0.000104	0.00009 ± 0.000023	0.00414 ± 0.000567	0.000021 ± 0.000010	1.13E-15	91.3%	11.5542	318.51 ± 16.29	5.114%
au25.5e.mus.90f.txt	0.6	20	0.07866 ± 0.000391	0.00614 ± 0.000113	0.00009 ± 0.000024	0.00135 ± 0.000871	0.000006 ± 0.000021	1.28E-15	97.8%	12.5616	343.79 ± 28.08	8.167%
au25.5e.mus.90g.txt	0.65	20	0.12835 ± 0.000394	0.01004 ± 0.000144	0.00018 ± 0.000025	0.00263 ± 0.000733	0.000007 ± 0.000022	2.08E-15	98.4%	12.5995	344.73 ± 18.24	5.290%
au25.5e.mus.90h.txt	0.7	20	0.33752 ± 0.000838	0.02788 ± 0.000251	0.00033 ± 0.000028	0.00069 ± 0.001273	0.000093 ± 0.000015	5.48E-15	91.9%	11.1267	307.67 ± 5.47	1.777%
au25.5e.mus.90i.txt	0.75	20	3.66168 ± 0.001882	0.31557 ± 0.000803	0.00434 ± 0.000073	0.00317 ± 0.001161	0.000174 ± 0.000017	5.94E-14	98.6%	11.4414	315.66 ± 0.94	0.297%
au25.5e.mus.90j.txt	0.8	20	2.20376 ± 0.001741	0.19098 ± 0.000479	0.00259 ± 0.000054	0.00220 ± 0.000892	0.000046 ± 0.000015	3.58E-14	99.4%	11.4689	316.35 ± 1.07	0.337%
au25.5e.mus.90k.txt	0.85	20	3.97761 ± 0.002744	0.34677 ± 0.000508	0.00456 ± 0.000043	0.00074 ± 0.000519	0.000054 ± 0.000018	6.46E-14	99.6%	11.4244	315.23 ± 0.67	0.212%
au25.5e.mus.90l.txt	0.9	20	6.10184 ± 0.005122	0.53087 ± 0.000999	0.00729 ± 0.000092	0.00985 ± 0.000633	0.000052 ± 0.000025	9.91E-14	99.7%	11.4667	316.30 ± 0.76	0.241%
au25.5e.mus.90m.txt	0.95	20	2.84032 ± 0.003963	0.24611 ± 0.000942	0.00326 ± 0.000038	0.00419 ± 0.000730	0.000072 ± 0.000017	4.61E-14	99.3%	11.4566	316.04 ± 1.42	0.448%
au25.5e.mus.90n.txt	1	10	0.13266 ± 0.000370	0.01157 ± 0.000167	0.00017 ± 0.000020	0.00067 ± 0.000674	0.000012 ± 0.000010	2.15E-15	97.3%	11.1604	308.53 ± 8.74	2.831%
au25.5e.mus.90o.txt	1.1	10	0.18949 ± 0.000548	0.01573 ± 0.000137	0.00021 ± 0.000020	0.00133 ± 0.000291	0.000040 ± 0.000018	3.08E-15	93.8%	11.3045	312.19 ± 10.02	3.209%
au25.5e.mus.90p.txt	1.2	10	0.20914 ± 0.000581	0.01762 ± 0.000114	0.00025 ± 0.000018	0.00132 ± 0.000615	0.000028 ± 0.000017	3.40E-15	96.1%	11.4120	314.91 ± 8.18	2.597%
au25.5e.mus.90q.txt	1.3	10	0.42301 ± 0.000660	0.03604 ± 0.000162	0.00047 ± 0.000027	0.00208 ± 0.000922	0.000036 ± 0.000018	6.87E-15	97.5%	11.4531	315.95 ± 4.36	1.379%
au25.5e.mus.90r.txt	1.45	10	0.77706 ± 0.000740	0.06716 ± 0.000239	0.00089 ± 0.000035	0.00094 ± 0.000884	-0.000001 ± 0.000022	1.26E-14	100.0%	11.5720	318.96 ± 2.96	0.928%
au25.5e.mus.90s.txt	1.6	10	0.56115 ± 0.000896	0.04800 ± 0.000230	0.00065 ± 0.000022	0.00178 ± 0.001050	0.000051 ± 0.000018	9.11E-15	97.3%	11.3772	314.03 ± 3.42	1.088%
au25.5e.mus.90t.txt	1.75	10	0.03251 ± 0.000294	0.00286 ± 0.000120	-0.00001 ± 0.000026	-0.00061 ± 0.000549	0.000022 ± 0.000020	5.28E-16	79.6%	9.0272	253.49 ± 60.61	23.908%
au25.5e.mus.90u.txt	1.9	10	0.03708 ± 0.000269	0.00317 ± 0.000102	0.00007 ± 0.000036	0.00001 ± 0.000641	0.000030 ± 0.000017	6.02E-16	75.8%	8.8790	249.61 ± 46.08	18.460%
au25.5e.mus.90v.txt	2	10	0.03354 ± 0.000332	0.00293 ± 0.000129	0.00003 ± 0.000023	-0.00024 ± 0.001035	-0.000051 ± 0.000018	5.45E-16	145.0%	11.4272	315.30 ± 52.07	16.513%
au25.5e.mus.90w.txt	2.1	10	0.06295 ± 0.000313	0.00541 ± 0.000067	0.00010 ± 0.000024	-0.00097 ± 0.000903	-0.000005 ± 0.000010	1.02E-15	102.3%	11.6216	320.21 ± 16.15	5.044%
au25.5e.mus.90x.txt	2.2	10	0.17440 ± 0.000502	0.01521 ± 0.000103	0.00024 ± 0.000026	-0.00064 ± 0.000742	-0.000026 ± 0.000015	2.83E-15	104.5%	11.4626	316.19 ± 8.59	2.717%

Plateau age = 315.79±0.38 Ma (1σ)
MSWD = 0.84, probability=0.64
Includes 100% of the ³⁹Ar

Plate 1. Detailed Geologic Map of the Jacksons Gap, AL, 7.5-Minute Quadrangle Josh Poole







LEGEND

Lithologic Units

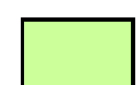







Inner Piedmont

Dadeville Complex

	IDas	Agricola Schist
	IDmum	Mafic/Ultramafic
	IDws	Wareville Schist
	IDrc	Ropes Creek Amphibolite





Brevard Zone

Jacksons Gap Group


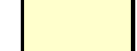
	JGscp	Sericite-Chlorite Phyllite
	JGgqs	Garnetiferous Quartz Schist
	JGmq	Massive Quartzite
	JGcp	Carbonaceous Phyllite
	JGggp	Garnetiferous Graphitic Phyllite
	JGpq	Phyllitic Quartzite
	JGgp	Garnetiferous Phyllite
	CZ	Cataclastic Zone

Eastern Blue Ridge

Emuckfaw Group

	Eems	Emuckfaw Schist 1
	Eemq	Emuckfaw Schist 2
	Egg	Granitic Gneiss
	Ekg	Kowaliga Gneiss

Wedowee Group

	Ewd	Wedowee Phyllite
	Eeqd	Eikahatchee Quartz-Diorite Gneiss

Structural Symbols








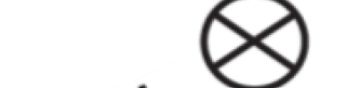

	Cryptic Syn-Metamorphic Thrust Fault
	Right-Lateral Oblique-Slip Fault
	Doubly Plunging Overturned Antiform
	10 Mineral Elongation Lineation
	45 Hinge Line of Asymmetric Fold
	60 Strike and Dip
	Strike-Slip Motion Towards
	Strike-Slip Motion Away
	Reverse Fault

Plate 2. Cross-Sections Dissecting the Jacksons Gap, AL, 7.5-Minute Quadrangle
Josh Poole

